Ice Growth Inhibition by Synthetic Macromolecules

By

Thomas Richard Congdon

A thesis submitted to The University of Warwick

for the degree of

Doctor of Philosophy

University of Warwick, Department of Chemistry

May 2015

Table of Contents

2. Synthesis and Ice Recrystallisation Inhibition Activity of PVA and PVA Co-polymers

3. Synthesis and Ice Recrystallisation Inhibition Activity of PVA-*block*-PVP Co-polymers

4. Synthesis and Ice Recrystallisation Inhibition Activity of Three-Arm Star-PVA

5. Synthesis and Cloud Point Behaviour of Thermoresponsive PVA Co-polymers

List of Figures

Chapter 1. Introduction

2. Synthesis and Ice Recrystallisation Inhibition Activity of PVA and PVA Co-polymers

3. Synthesis and Ice Recrystallisation Inhibition Activity of PVA-*block*-PVP Co-polymers

4. Synthesis and Ice Recrystallisation Inhibition Activity of Three-Arm Star-PVA

5. Synthesis and Cloud Point Behaviour of Thermoresponsive PVA Co-polymers

List of Schemes

Chapter 1. Introduction

2. Synthesis and Ice Recrystallisation Inhibition Activity of PVA and PVA Co-polymers

3. Synthesis and Ice Recrystallisation Inhibition Activity of PVA-*block*-PVP Co-polymers

4. Synthesis and Ice Recrystallisation Inhibition Activity of Three-Arm Star-PVA

5. Synthesis and Cloud Point Behaviour of Thermoresponsive PVA Co-polymers

List of Tables

Chapter 1. Introduction

2. Synthesis and Ice Recrystallisation Inhibition Activity of PVA and PVA Co-polymers

3. Synthesis and Ice Recrystallisation Inhibition Activity of PVA-*block*-PVP Co-polymers

4. Synthesis and Ice Recrystallisation Inhibition Activity of Three-Arm Star-PVA

5. Synthesis and Cloud Point Behaviour of Thermoresponsive PVA Co-polymers

List of Equations

Chapter 1. Introduction

5. Synthesis and Cloud Point Behaviour of Thermoresponsive PVA Co-polymers

Abbreviations

°C	Degrees Centigrade
µ	micro ($\times 10^{-6}$)
Ac	Acetate
ACVA	Azo-bis-cyanovaleric acid
AFGP	Antifreeze Glycoprotein
AFM	Atomic Force Microscopy
AFP	Antifreeze Protein
AIBN	Azo-bis-isobutyronitrile
Ala	Alanine
ATRP	Atom-Transfer Radical Polymerisation
CP	Cloud Point
CRP	Controlled Radical Polymerisation
CTA	Chain-Transfer Agent
Đ	Dispersity Index = M_w/M_n
Da	Daltons
DCM	Dichloromethane
DIS	Dynamic Ice Shaping
dm	decimetre
DMF	Dimethylformamide
DMSO	Dimethyl sulfoxide
DNA	Deoxyribonucleic acid
DP_n	Number-average Degree of Polymerisation

ESI-MS	Electrospray Ionisation Mass Spectrometry
FDA	United States of America Food and Drug Administration
g	Gram
INI	Initiator
iPA	Isopropenyl Acetate
IR	Infrared Spectroscopy
IRI	Ice Recrystallisation Inhibition
ITP	Iodine-Transfer Polymerisation
kDa	kilo-Daltons (1×10^3) Daltons
LAM	Less-Activated Monomer
LCST	Lower-Critical Solution Temperature
m	metre
MADIX	"Macromolecular Design *via* the Interchange of Xanthates"
MAM	More-Activated Monomer
mCTA	Macro Chain-Transfer Agent
MD	Molecular Dynamics
mg	milligram
min	minute
mL	millilitre
MLGS	Mean Largest Grain Size
M_n	Number-Average Molecular Weight
Mol	Moles
M_w	Weight-Average Molecular Weight
ɳ	"Blockiness Index"
nm	nanometre ($\times 10^{-9}$ meters)

NMP	Nitroxide-Mediated Radical Polymerisation
NMR	Nuclear Magnetic Resonance
OH	Hydroxyl
OMRP	Organoheteroatom-Mediated Radical Polymerisation
PBS	Phosphate-Buffered Saline
PEG	Poly(ethylene glycol)
PiPA	Poly(isopropenyl alcohol)
PiPAc	Poly(isopropenyl acetate)
pNIPAM	Poly(*N*-isopropyl acrylamide)
Pro	Proline
PVA	Poly(vinyl alcohol)
PVAc	Poly(vinyl acetate)
PVP	Poly(vinyl pyrrolidone)
QCM	Quartz Crystal Microbalance
QLL	Quasi-Liquid Layer
RAFT	Reversible Addition-Fragmentation Transfer Radical Polymerisation
SEC	Size Exclusion Chromatography
synAFGP	Synthetic-Antifreeze Glycoprotein
TH	Thermal Hysteresis
THF	Tetrahydrofuran
Thr	Threonine
TPH	Triphenyl Hexatriene
UCST	Upper Critical Solution Temperature
UV/Vis	Ultraviolet/Visible

Acknowledgements

This thesis wouldn't exist without the help and support of a lot people. A huge thank you to Dr Matthew Gibson and Dr Rebecca Notman for giving me this brilliant opportunity, and for their support. Matt is unrelentingly enthusiastic and allowed me to pursue my own ideas, which more often than not didn't work out, but has helped me come into my own as a researcher. I am grateful for the generous funding provided by the Leverhulme Foundation, who have supported my time here and allowed me to travel to conferences, and purchase chemicals and equipment. Thank you to the MIG group; Gemma, Dan, Caroline, Sarah-Jane, Lucienne, Dan, Ben, Rick, Lewis, Sang Ho and Rob for making my time here a lot of fun, I'm going to miss you guys. Team Ice also deserve a special mention – Rob, Dan, Alaina, Bethany and Jamie. During my PhD I had the pleasure of supervising Masters, URSS and Erasmus project students. This was the most fun, valuable and enriching aspect of my time here and I am indebted to you all for your hard work. Charlene, Becky, Abdul, Mary, Julia, Matt, Rob and Bethany - you're the best! A big thank you Peter Shaw at Synthomer for valuable discussions about PVA, and to my supervisory committee, Professor Haddleton and Professor Rodger, for their timely advice.

A huge thank you is due to the University of Warwick and the Department of Chemistry. I've been here almost eight years and the people to whom I am indebted are almost too numerous to count. On the technical side, a big thank you to Dr Ivan Prokes for the NMR, Ant and Kay for the SEC, Dr Lijiang Song and Phil Aston for the mass spec, and Ben Douglas for pretty much every other machine in the department! A huge thank you to Olvi, Sam and Sukhjit for their accounting wizardry and for bailing me out when I ordered all that equipment by accident. Finally, I am

really grateful to Nick Barker for all the school's outreach sessions, which has been one of the highlights of my time here.

On a personal note there I several people who kept me going and enriched my time here no end. I am incredibly lucky to have a great group of friends that I can share my life with, both the awesome and the naff. In no particular order: Luke and Lauren, who came up with the working title 'watery glue, what does it do?' which sadly did not make the final cut of this thesis. Caroline, Dan and Sarah-Jane, for the unforgettable conference experiences, and for making my time here, especially the day to day, infinitely more awesome. I will always remember our time here with happiness, from all the fun we got up to in the lab, to the impromptu group therapy sessions during the Summer of Discontent. To Helen, Cat and Rob, Sandy and Ben, Sherine, Andy, Nick Mike, Paul, Anish, Danielle and Bethany, a huge thank you for all the great times outside of work.

My family have been incredibly supportive and caring. Thank you Mum, Dad, Ben and Sam for being there, for your love and support, and for helping me make a life up here in the barren midlands. And extra thanks for all the proof reading Dad! I promise we will be able to get some more golf in now.

Declaration

This thesis is submitted to the University of Warwick in support of my application for the degree of Doctor of Philosophy. It has been composed by myself and has not been submitted in any previous form for any degree at any other University. The work presented was carried out by the author alone.

Sections of this thesis have been published or have been submitted for publication as follows:

- **Chapter 2**: Congdon, T., Notman, R., Gibson, M. I., Antifreeze (Glyco)Protein Mimetic Behaviour of Poly(vinyl alcohol): Detailed Structure-Ice Recrystallisation Inhibition Activity Study *Biomacromolecules*, 2013, **14**, 1578 – 1586
- **Chapter 5**: Congdon, T., Shaw P., Gibson, M.I., Thermoresponsive, Well-defined, poly(vinyl alcohol) co-polymers. Precision control of transition temperature and enzyme switchability. *In Revision*.

Abstract

Animals, plants and bacteria can survive sub-zero environments by using specialist proteins that inhibit ice growth. There has been a great deal of work into trying to understand and exploit these proteins for use in cryopreservation, but several strategies fail as the protein's mechanism for ice growth inhibition causes ice to grow into needle-like crystals, which cause mechanical damage to the cryopreserved material. A range of studies have shown that this shaping can be removed, without affecting ice growth inhibition activity. Synthetic mimics exist, the most interesting being the simple polymer, poly(vinyl alcohol), which alone amongst other synthetic macromolecules displays ice growth inhibition behaviour. The scientific principles behind ice growth, and the molecules that can inhibit this, are detailed in **Chapter 1.**

Chapter 2 examines how the molecular weight of poly(vinyl alcohol) affects ice recrystallisation inhibition activity, and the importance of hydroxyl sequence, using post-polymerisation modification and co-polymerisation. **Chapter 3** details the preparation of well-defined block co-polymers of poly(vinyl alcohol), and confirms the importance of the hydroxyl sequence. These polymers maintained their ice recrystallisation inhibition activity despite the addition of large non-active blocks. **Chapter 4** demonstrates the synthesis and utility of a novel multifunctional chain transfer agent, which is used to prepare star polymers. The resultant *star*-poly(vinyl alcohol) was highly active, and activity profiles of these polymers provided further evidence that the mechanism of ice recrystallisation inhibition by poly(vinyl alcohol) does not involve direct binding to ice. **Chapter 5** uses the techniques and methodologies developed in Chapter 2 and applies them to another lesser-known ability of poly(vinyl alcohol); thermoresponsivity.

In summary, controlled radical polymerisation of vinyl acetate was employed in a range of different ways to prepare poly(vinyl alcohol) and its various co-polymers. These polymers were then tested for ice recrystallisation inhibition. Due to their well-defined physical properties, and advanced architectures, new insights into the nature and mechanisms of their activity were available. This mechanistic understanding, and the materials developed for this thesis, display a great deal of potential in expanding the field of cryopreservation.

Chapter 1

Introduction

One of the most difficult things to reconcile in Nature is both the resilience and fragility of life. Examining cells under a microscope, it is difficult to fathom how these precisely formed and arranged clusters of protein chains, carbohydrates and fatty acids can possibly survive outside of their thermo-regulated and pH controlled agar plates. Even more so billions of them thriving and forming living organisms, at the whim of everything the world can throw at them. But they do. Microorganisms are found in the mouths of sulfur dioxide-belching, 450 °C undersea thermal vents, and in the abyssal waters 4000 m deep where no sunlight can penetrate. The humbly named tardigrades (Italian for ‘slow stepper’) have, in the name of science, been boiled, frozen, squeezed with 6000 bar pressure, blasted with hundreds of times the human lethal dose of radiation, starved for a decade, and on one occasion launched into the vacuum of outer space, all without suffering any ill effects. (I like to think that all this happened to the same batch of the little guys).

Extreme survival seems to be all in a day’s work for microorganisms, but as size increases so do the demands and environmental constraints on the creature. Some species of frog will replace the water in their bodies with a glucose-rich syrup allowing them to overwinter, but what about Arctic and Antarctic fish, animals that need to keep moving to push water through their gills, to keep blood moving to muscles, so they can keep swimming in - 2 °C waters that in minutes would freeze most other organisms solid? How do you even start to sort out that?

1.1 Antifreeze Glycoproteins

Antifreeze (glyco)proteins (AFGPs) were discovered shortly after biologists and zoologists began to study how fish could survive in water with temperatures of - 1.7 °C to - 1.9 °C. The first report of this being investigated was by Scholander *et al.*, who after an abortive expedition to northern Canada (one of the three fish caught over *a two week* period was eaten by a dog) discovered that few fish could survive being directly seeded with ice but were unperturbed when subjected to supercooled water. This was attributed to abnormalities in body fluids, and not entirely to NaCl concentration in the blood, suggesting that this was due to a metastable state in the fish, and posited that spontaneous freezing (homogeneous ice formation) in supercooled solution occurs too rarely to affect the fish.[1, 2]

DeVries and Wohlschlag were the first to report glycoproteins isolated from Antarctic fish.[3] They later noted that these proteins accounted for around a third of the observable freezing point depression, far greater than expected given their concentration in solution. Several different sizes of AFGP were discovered,[4] and their composition found to be a tripeptide repeat unit composed of one threonine residue and two alanine residues, with the disaccharide β-D-galactosyl-(1,3)-α-D-*N*-acetylgalactosamine linked to each threonine, (Figure 1.1).[5]

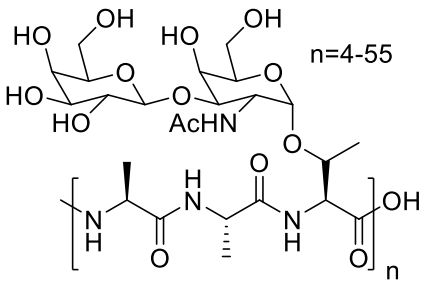

Figure 1.1 Structure of a typical Antifreeze Glycoprotein.

The structures of AFGPs are highly conserved, with little structural variation beyond (Ala-Ala-Thr) residues being replaced with (Pro-Ala-Thr) tripeptide sequences, but this is rare and is only seen in ~ 5 % of AFGPs.[6] Peptide sequence length tends to be between four and fifty tripeptide repeat units depending on the species, with longer sequences exhibiting greater antifreeze activity.[7] Interestingly it appears that both Arctic and Antarctic fish evolved AFGPs independently of each other, in response to ancient climate change.[8, 9]

The secondary structure and conformation that these glycoproteins adopt has been the topic of some debate. Most reports agree that AFGPs exist as 3-fold helices.[10] Through nuclear magnetic resonance (NMR) spectroscopic analysis, it also appears that the disaccharide is held against the backbone *via* amine hydrogen bonding to the threonine residue, stabilising the structure and affording a stationary binding surface.[11] However the AFGP structure is highly flexible,[12] and a recent report using Molecular Dynamics (MD) simulations showed that while a helical conformer is preferable, there are a number of similarly accessible conformations.[13] The disaccharide moiety has been identified as greatly affecting the structure and efficacy of antifreeze glycoproteins, and modifications to this will completely remove antifreeze activity.[14, 15] Almost all freeze tolerant fish have been found with internalised ice crystals sequestered in macrophages in the spleen, and it appears that once an AFGP has bound to ice it is adsorbed onto the surface of spleen cells to reduce the amount of ice circulating in the fish's bloodstream. Due to the difficulty associated with finding and purifying AFGPs this mechanism has yet to be proven.[16]

1.2 Antifreeze Proteins

There exists a class of biological antifreeze agents which also display antifreeze activity but contain structural features seen in traditional globular proteins. These antifreeze proteins (AFPs) were discovered soon after AFGPs[17] and despite having similar antifreeze effects, the range of structures and sources is huge. As well as dozens of examples in fish species,[11] AFPs have been isolated from insects,[18] plants,[19] trees,[20] grasses,[21] fungi and bacteria.[22] Recently many of these AFPs have been structurally resolved and most interestingly these proteins display hydrophobic and hydrophilic faces, similar to AFGPs. The general structure of AFPs can be described as a large mixed hydrophobic/hydrophilic cluster presenting a hydrophobic face, across which is presented a highly ordered array of hydrophilic moieties (Figure 1.2).

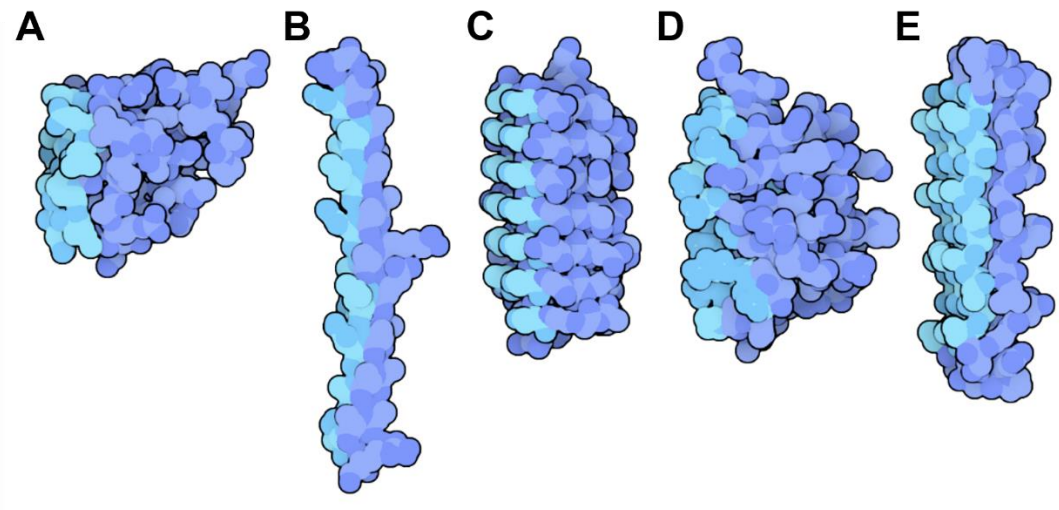

Figure 1.2 Graphical representations of a selection of Antifreeze Proteins prepared by Goodsell.[23] Light blue denotes a threonine rich surface responsible for binding to a growing ice crystal. AFP sources: **A** Ocean Pout.[24] **B** Winter Flounder.[25] **C** Yellow Mealworm Beetle.[26] **D** Spruce Budworm Moth.[27] **E** Snow Flea.[28]

The secondary structures of the AFPs are highly diverse. The Snow Flea AFP is composed of six stacked helices, the Ocean Pout AFP is a globular protein composed

of beta sheets, the Winter Flounder AFP is a single alpha helix, and the structure of the Spruce Budworm Moth AFP appears to have a structure similar to the one adopted by AFGPs (Figure 1.3). Despite this, the antifreeze mechanism is essentially the same (*vide infra*). However, the Spruce Budworm Moth and Snow Flea AFPs display a greater degree of thermal hysteresis (see page 10 for more details on TH).

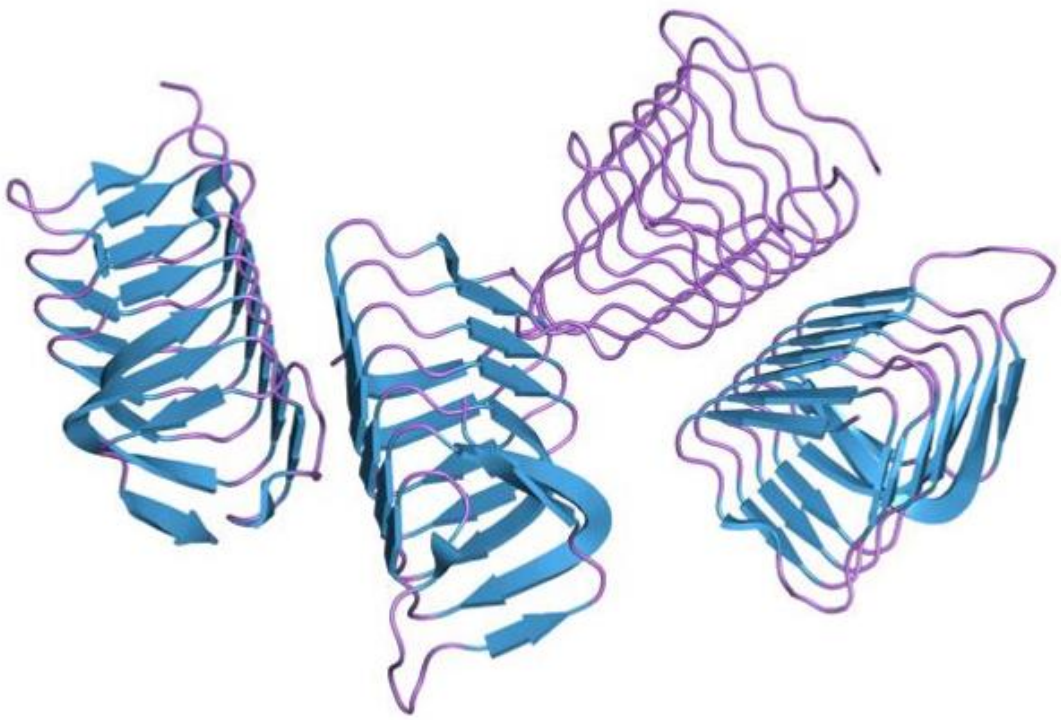

Figure 1.3 The Structure of *Choristoneura fumiferana* (Spruce Budworm Moth) beta-helical antifreeze protein, at various orientations.[29]

Historically it has been difficult to obtain accurate crystal structures of these proteins and elucidate the ice binding mechanism.[30] Davies and co-workers showed that *Marinomonas primoryensis*, an Antarctic bacterium, produces a large antifreeze protein that absorbs clathrate waters onto the protein surface to act as a binding motif, aiding the protein adsorption onto growing ice crystals and inhibiting ice growth.[31] This is not the only case, and some AFPs may include more than four hundred clathrate waters in their folded structure,[32] where usually proteins will exclude water upon

folding. AFP from the Antarctic bacterium *Marinomonas primoryensis* will also incorporate Ca^{2+} ions to create a rigid structure (Figure 1.4).

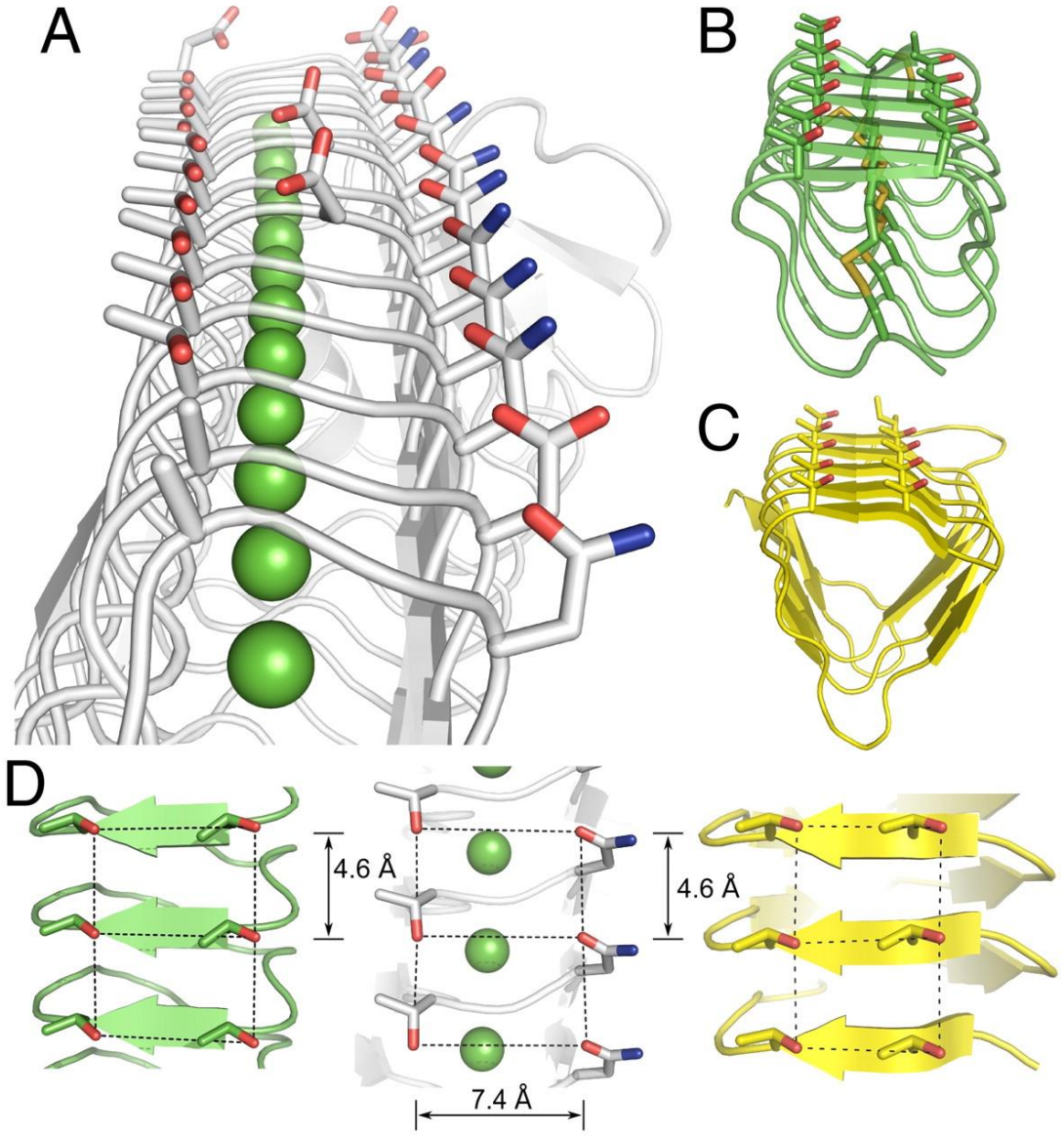

Figure 1.4 Crystal structures showing the ice binding surface of some highly active AFPs. **A** Crystal structure of AFP from the Antarctic bacterium *Marinomonas primoryensis,* Ca^{2+} ions in green. **B** AFP from the beetle T. molitor. Green = carbon, red = oxygen, and orange = sulfur. **C** AFP from Spruce Budworm Moth (Choristoneura fumiferana). Yellow = carbon and red = oxygen. **D** Comparison of the ice binding structural geometry between **A**, **B** and **C.**[31]

This water-like surface presented by AFPs is an example of nature adapting to an uncommon problem; most proteins function through chemical detection, but how can a protein chemically detect the difference between water and ice? This is solved by a defined secondary structure holding hydrophilic amino acids on a predominantly hydrophobic surface, binding waters to form a *pseudo* ice-face, enabling the protein to interact and bind to an ice crystal. As with AFGPs, modification of the proteins has been shown to dramatically reduce the activity, but has aided mechanistic understanding.[33] AFPs have not been widely exploited due to the difficulties associated with their isolation from natural sources and the challenges of total synthesis, and their adverse effects when used in cryopreservation strategies.[34]

1.3 Antifreeze Mechanisms

The term antifreeze activity is used to describe the overall effect of a range of different phenomena that change the properties of water in its liquid or solid state, and depend on whether the induced effect is colligative (based on the number of solvent to solute particles, not on the nature of the particles) or non-colligative (based on some other property of the chemical species introduced into the solvent). The most well-known and popular antifreezes are all colligative (Table 1.1).

The effect of colligate freezing point depression can be highly potent. NaCl (used for gritting icy roads) at 23.3 % w/v will depress the freezing point of water to - 21 °C, and ethylene glycol at 60.0 % w/v will depress the freezing point to - 60 °C. This is achieved by interfering with the ordering of water in such a way that it becomes more energetically unfavourable to nucleate and form ice, but very high concentrations of solute are required. Many salt-based antifreezes are not suitable for machinery or

engines due to the dangers of corrosion. The popular alternative is ethylene glycol, which is toxic. Propylene glycol is far less toxic but a large weight % of the antifreeze is still required to stop ice formation (Table 1.1).

All AFPs and AFGPs have been shown to prevent ice formation and growth in a non-colligative fashion. This is essential as most organisms cannot employ colligative methods due to the level of osmotic stress involved. The only real example of colligative antifreeze strategies in Nature is the Wood Frog, *Lithobates sylvaticus.* This animal can overwinter by first accumulating urea in their tissues and producing large amounts of glucose in the liver and blood stream, allowing survive freezing temperatures – so long as no more than 65 % of their water content freezes.[35]

Table 1.1 The Eutectic Point of some common antifreezes

Name	Formula	Eutectic Point/ °C [a]	Eutectic Composition/ % w/w [b]
Urea	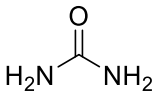	- 11.9	32.0
Sodium Chloride	NaCl	- 21.0	23.3
Calcium Magnesium Acetate	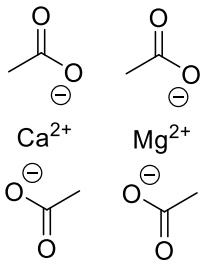	- 27.5	32.5
Magnesium Chloride	$MgCl_2$	- 33.0	21.6
Glycerol	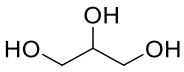	- 37.8	70.0
Ethylene Glycol	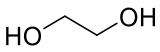	- 50.0	60.0
Calcium Chloride	$CaCl_2$	- 51.0	29.8
Potassium Acetate	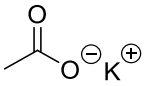	- 60.0	49.0
Propylene Glycol	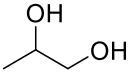	- 60.0	60.0

A Colligative freezing point depression; the difference between the freezing point of pure water and the freezing point with the additive. Eutectic point is the maximum freezing point depression possible. **B** Concentration at which the maximum freezing point depression occurs.

1.4 Thermal Hysteresis

Thermal Hysteresis (TH) is a kinetic effect that creates a difference between the freezing and melting points of water. The difference between these two points is known as the thermal hysteresis gap, and nucleated ice crystals within this temperature range will neither melt nor grow (Figure 1.5). This effect is only seen in non-colligative systems; AFPs, AFGPs and some polymers. (*vide infra*)

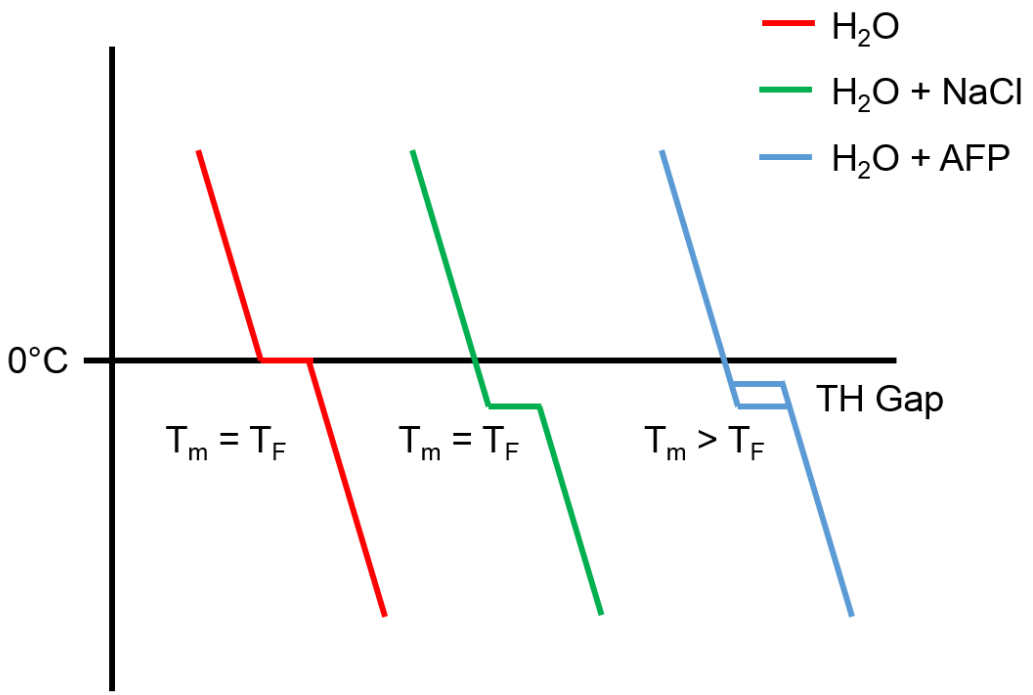

Figure 1.5 Illustration of Thermal Hysteresis activity and the TH Gap; crystal freezing point depression relative to the melting point. T_m = melting point, T_F = freezing point.

The reason for the huge interest in AFPs and AFGPs is that observed thermal hysteresis cannot be attributed to concentration; the effect is much greater than predicted by Blagden's Law, (Equation 1.1), which states that thermal hysteresis is dependent on the concertation of ions in the solvent. For Blagden's Law, $\Delta T_F = T_F(\text{Pure Solvent}) - T_F(\text{Solution})$, K_F = the cryoscopic constant of the solvent (K_F(pure water) = 1.853 K.kg.mol^{-1}, b = molality (moles of solute per kg of solvent), i = Van 't Hoff factor (number of ion particles per molecule of solute). In fact, AFGPs and AFPs

can depress the freezing temperature of water by ~ 500 times the amount expected on a purely colligative basis.[36]

$$\Delta T_F = K_F . b . i$$

Equation 1.1 Blagden's Law.

TH is commonly observed with AFPs, but the exact mechanism remains unresolved. It is accepted knowledge that AFPs and AFGPs will bind to growing ice crystals, but beyond that mechanisms are somewhat speculative. Most AFPs exhibit a specific ice-binding face mimicking that of the hexagonal crystal face of ice, which can bind onto the growing crystal surface, causing the pattern of ice growth to be changed and making it less favourable for ice to grow.[37] Adsorption has been reported using femtosecond laser spectroscopy,[38] computational simulation[39] and *via* direct observation of single crystal growth using a nanolitre osmometer.[40] AFP binding has been shown to be essentially irreversible[41] and inhibits local addition of water molecules to the ice crystal face causing the ice to grow in convex ridges (Figure 1.6).

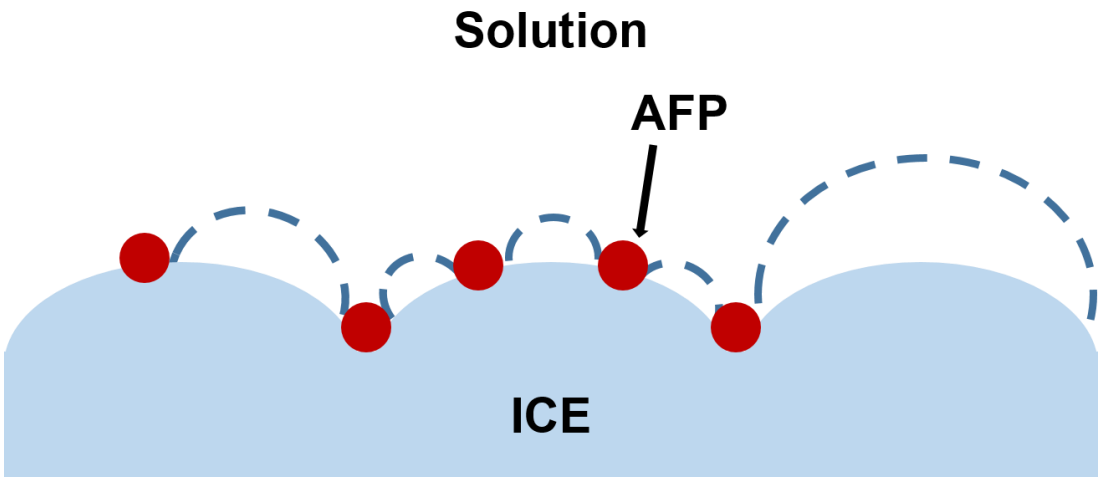

Figure 1.6 Illustration showing the formation of convex ridges growing between adsorbed antifreeze proteins, known as the step-pinning model.

It is postulated that this increase in surface area either i) causes an equilibrium between growth and melting over the TH gap, or ii) that the heat of fusion of water is linked to the radius of the convex ridges, as shown by the Gibbs-Thompson effect, where , where γ = interfacial energy of the ice-water interface, Ω = molar volume of ice, ρ = radius of the convex surface (and 2ρ being the average spacing of adsorbed AFP on the ice crystal surface), and ΔH = heat of fusion of water. ΔT is the theoretical value of TH (Equation 1.2). This would increase the energetic cost of adding water molecules to this curved surface and would cause local depression of the freezing point across the convex ridge. Binding to ice occurs in both AFPs and AFGPs. Protein solubility is also a factor and each protein will be tailored to the specific native environment of the animal. More concentrated solutions of AFPs and AFGPs will bind in greater density to the ice crystal face. This makes it much less favourable for the addition of more water molecules, and stops the growth of the ice crystal at a very small size. When the AFP is diluted this effect is diminished as the percentage of AFP bound to the ice crystal is reduced.[42]

$$\Delta T = \frac{2\gamma \Omega T m}{\rho \Delta H}$$

Equation 1.2 The Gibbs-Thomson effect

1.5 Dynamic Ice Shaping

Hexagonal ice (Ice 1h) is the most predominant form of ice, due to the pressure and temperature at which ice most commonly forms on Earth (Figure 1.7). Dynamic Ice Shaping (DIS) arises due to solute molecules directly interacting with the specific crystallographic faces of these ice crystals, causing the growth of the crystal in certain dimensions to be hindered (Figure 1.8).

AFPs display strong DIS properties and will selectively bind to the prism planes of ice (the 'a axis') (Figure 1.9). Below the TH point this will cause the growth of needle-like crystals when the AFP is present in high enough concentration. DIS and TH are somewhat interlinked as they are both caused by direct binding to the ice crystal surface. DIS is unfavourable due to the mechanical damage that the needle-like crystals will cause to cells and tissues.[43]

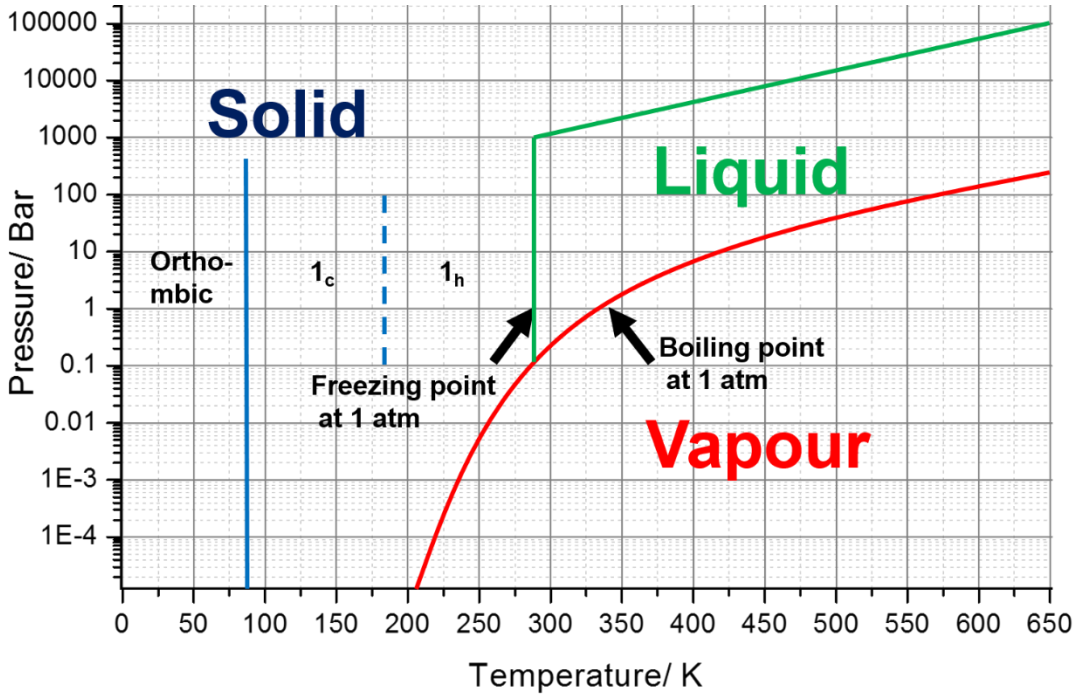

Figure 1.7 Graph showing the effect of pressure and temperature on ice crystal structure. Several other crystal forms are possible at higher pressures but have been excluded for clarity.

It can be imagined that, for fish and animals, the primary mechanism of survival is to rely on the TH effect stopping ice growth over an ambient temperature range, as DIS only occurs below the TH gap. Hyperactive AFPs expressed by some insects and plants will also adsorb to the basal plane, which could explain their superior TH activity.[27]

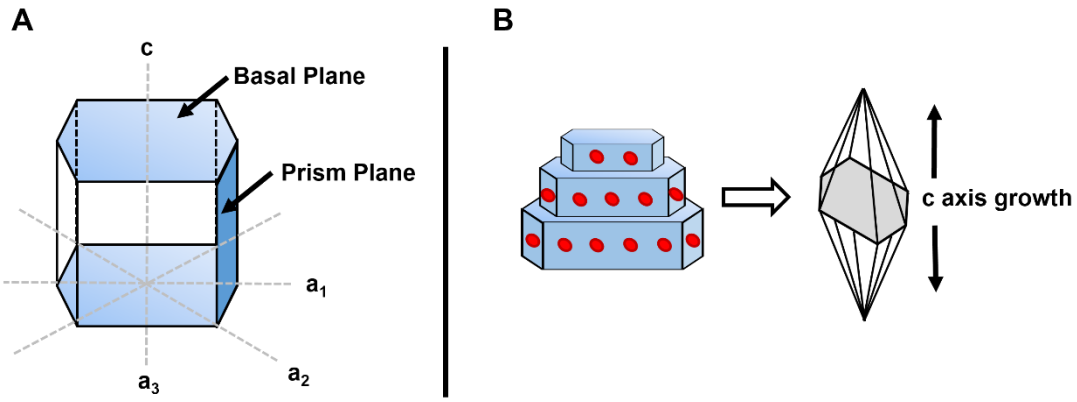

Figure 1.8 A Schematic of the planes of hexagonal ice (Ice 1h). **B** Schematic of the adsorption of AFPs onto the hexagonal prism planes, leading to needle-like crystals.

Frivik and co-workers have examined adsorption-induced DIS using osmometry and atomic force microscopy (AFM).[44] DeVries showed that AFGPs with four and five tripeptide repeat units will display specific ice face binding through several hydrogen bonds.[45]

Figure 1.9 Single ice crystals grown in increasingly concentrated AFP solution.[19]

Williams *et al.* modulated ice crystal growth morphology using AFGP analogues, and showed that there was an important link between hydrophobic and hydrophilic groups and their ice binding activity.[46] Specifically, the *N*-acetyl group at the *C2* position of the galactosamine, the α-configuration of the glycosidic bond, and the methyl group of the threonine residue are all essential for TH and DIS activity.[15]

1.6 Ice Recrystallisation Inhibition

Ice Recrystallisation Inhibition (IRI) is the term used to describe the growth of ice crystals over time; an Ostwald-Ripening type process where larger crystals grow at the expense of smaller crystals to minimise the energy of the system.[47] Knight *et al.* are attributed with one of the first reports demonstrating the IRI activity of AFPs and some synthetic macromolecules, and pioneered an assay derived from a method used to test alloy formation in metals – the 'splat' test.[48]

Briefly, the splat test consists of dropping a single droplet of water onto an aluminium plate held at - 78 °C using dry ice. Saline solution or some other additive is used as it is essential for determining IRI activity; a solute promotes liquid channels at the interface between ice crystals. On impact the droplet instantly freezes and forms a very thin (approximately 10 μm) wafer of polynucleated ice, formed of 6 μm wide ice crystals. The crystals are allowed to anneal below freezing (generally - 6 to - 8 °C) and, using a microscope, the crystal sizes can be recorded as they grow over time.

The term 'recrystallisation' comes from a very similar process used in metallurgy. It describes the phenomenon where upon heating, deformed grains are replaced by a new set of non-deformed grains. Grains in this case are defined as discrete microstructures that constitute metals and alloys. Boundaries between grains have poor alignment with neighbouring grains and decrease packing efficiency, leading to regions of higher

internal energy.[49] In metallurgy smaller grains with poor alignment are desirable as they increase the hardness and brittleness of the metal; the popular image of a blacksmith quenching a piece of worked metal quickly to trap small grains in a highly disordered state. Through grain boundary migration, boundary regions and smaller grain microstructures are subsumed into larger grains, lowering internal energy and creating a larger, more uniform crystal structure.

Recrystallisation in ice can be seen to work in a very similar way. Rapidly frozen ice exists not as a continuous plane but as many small nucleated ice crystals with boundary regions separating each crystal (Figure 1.10).

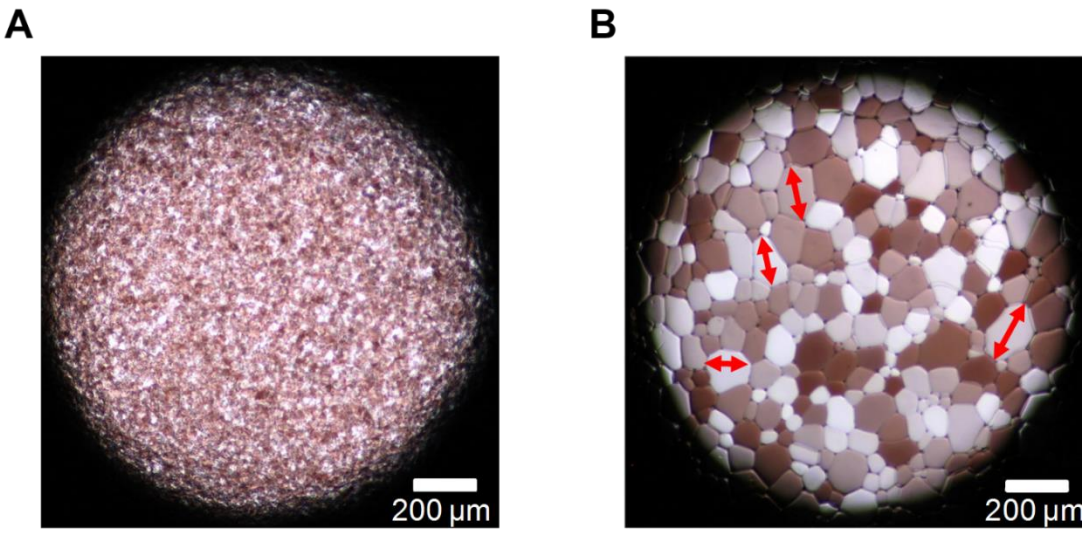

Figure 1.10 Representative ice crystal micrographs of Phosphate Buffered Saline (PBS) solution. **A** After nucleation. **B** After annealing for 30 minutes at - 8 °C.

These boundary regions are caused by solutes in the solution being forced out of the pure ice crystals upon nucleation and forming highly concentrated regions that will not freeze. Each boundary region is made up of a liquid layer and a layer adjacent to the ice crystal, where water appears to be in a semi ordered but non solid state, (Figure 1.11). Fletcher was the first to examine this 'quasi-liquid layer (QLL).[50] Since then many studies have examined whether the QLL is more 'water-like' or 'ice-like'.[51]

Optical,[52] QCM[53] and MD simulations show what appeared to be a temperature dependent thickness, with the size range from 15 nm at - 0.01 °C to 0.3 nm at -10 °C; almost a monolayer of water molecules surrounding each ice crystal.[54] Light scattering studies have shown that ice crystals can only grow into the QLL and not directly into the bulk water layer, i.e. ice can only grow into the semi-ordered state.[55]

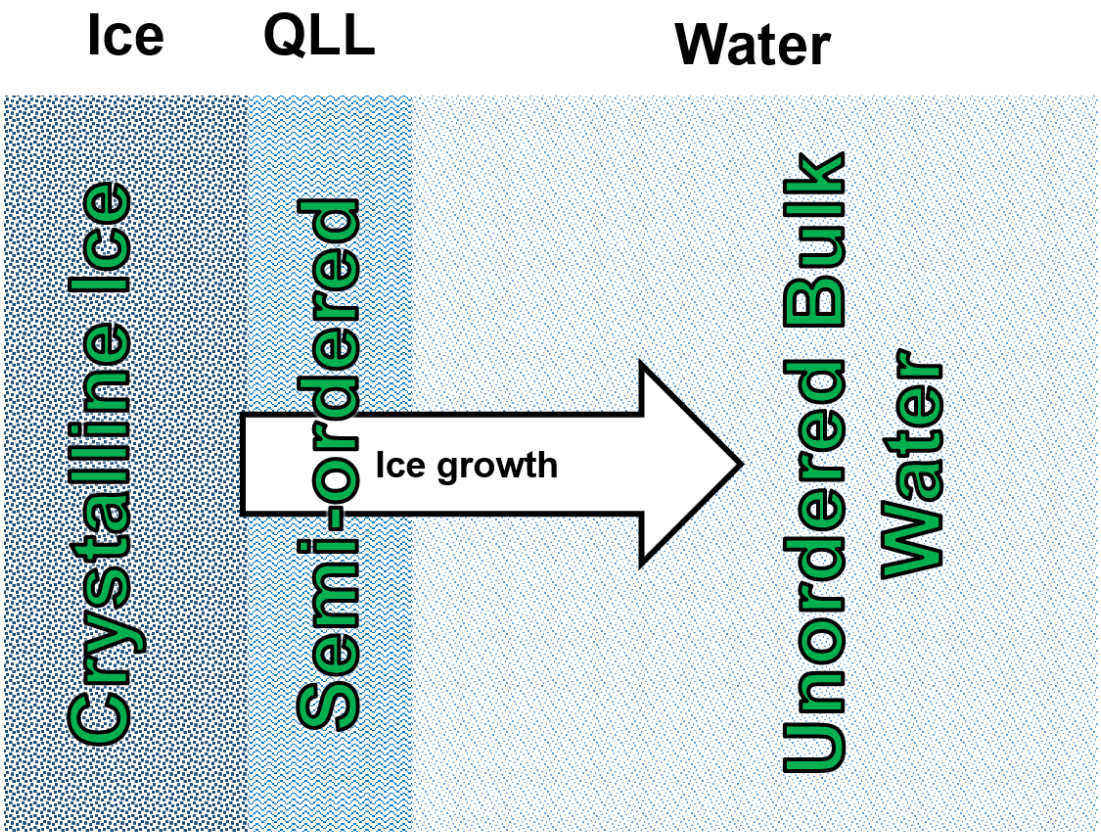

Figure 1.11 Schematic of ice in solution and the QLL.

Ice recrystallisation is postulated to occur through either Ostwald-Ripening or Grain-Boundary Migration. Of the two, Ostwald-Ripening is the more plausible mechanism as it considers the whole ice crystal system, and describes recrystallisation through the minimisation of energy to create as small a surface area to volume ratio as possible.

It can be seen that the surface of the ice crystal, the QLL, and the bulk water layer are in a constant state of molecular interchange (flux), but the molecules trapped in the

crystalline ice lattice are not subject to change. Over the same period of time, a large crystal will lose less of its total water molecules to the QLL interface as a smaller ice crystal. This affects the equilibrium of ice loss/ ice addition and leads to Ostwald-Ripening through the growth of large crystals at the expense of the smaller.[56]

As stated before, biological antifreezes like AFPs and AFGPs are excellent inhibitors of ice recrystallisation at low (< 1 $mg.mL^{-1}$) concentration.[48] Some AFPs are so IRI active that they can effectively inhibit ice growth at concentrations lower than 0.01 $mg.mL^{-1}$.[57, 37] In the case of the AFP of Perennial Rye-Grass, *Lolium perenne*, juxtaposition of imperfect ice-binding surfaces affords weak TH but the protein maintains potent IRI activity, suggesting that these two forms of antifreeze activity are mechanistically removed from each other.[21, 58] However, cost and the DIS displayed by AFPs prohibits their use as effective cryoprotectants. AFGPs display less DIS but they are much harder to access naturally than AFPs and cannot be easily synthesised due to the carbohydrate component.

DIS is problematic in cryostorage as the needle-like crystals formed will cause mechanical damage by puncturing the cells. This side-effect is predominantly caused by TH active molecules, this precludes a lot of antifreeze agents from being exploited in cryopreservation. Colligative agents such as ethylene glycol or dimethyl sulfoxide (DMSO) are currently used as they vitrify the frozen solution, forming the solid in a glassy state where no crystal growth can occur. The volume required to achieve this means that whatever has been stored needs to be purified, as these agents are extremely toxic. This is accepted in vital procedures such as bone marrow transplants for leukaemia, where the amount of DMSO required to store the bone marrow effectively poisons the patient necessitating weeks of recovery. However for more routine

procedures or uses, such as blood storage or improving the quality of frozen food, highly toxic colligative antifreeze agents are useless.

Compared to thermal hysteresis and dynamic ice shaping, ice recrystallisation inhibition is the most useful aspect of non-colligative antifreeze agents, in terms of cryopreservation. TH is only strongly displayed by AFPs, and while this has been commercially exploited for food products,[59, 60] there has been little success in applying the technology to the cryostorage of blood,[61] cells,[62] and organs[43, 63] for substantial time periods. Many cellular processes will also continue below typical TH gap temperatures, meaning that cells will still be capable of degradation or apoptosis.[47]

On the other hand, IRI activity is an extremely desirable property. While blood and organs can be frozen and stored at very low temperatures where there is no ice growth, thawing prior to use leads to rapid ice crystal growth causing mechanical damage to the cells.[64] For this reason, any cell recovery from cryopreservation protocols depend on specific thawing rates for different cell types.[65] This is a problem compounded by complex tissues during thawing, such as hearts and kidneys, which will be fully defrosted on the outside but could have ice growing and causing cryo-injury internally.

In this respect, IRI is far more desirable as it can effectively bypass mechanical cell damage by stopping the growth of nucleated ice during thawing. Reviews of the literature have concluded that cell death occurs not from the initial nucleation of ice but due to an alternate process during thawing, as a result of ice recrystallisation.[66]

It cannot be stressed how important practical advances and new antifreeze technologies could be in fields as diverse as anti-icing/frost protection for aircraft, vehicles and engines, food storage,[59] cryosurgery,[67, 68] cryostorage of biological

samples and tissues,[69, 70] and perhaps even suspended animation of critically ill patients.

1.7 Synthetic AFP and AFGP Mimics

Biological antifreeze agents (AFPs and AFGPs) will always display IRI and TH and until recently it was believed that these properties were linked and derived from their ice-binding ability.[71, 72] However, some plant[73] and insect[57] AFPs exhibit low TH but potent IRI. Unfortunately neither of the above reports employed the splat test to examine this activity, or even used the same assay, so it is difficult to draw conclusions from this alone as to whether IRI and TH are linked.

Payne and co-workers showed that although being extremely synthetically challenging, it was possible to prepare synthetic analogues of AFGPs, and gain some insight into the required functionality for potent IRI activity.[34] This inspired attempts to create synthetic mimics. The most extensive work in this area has been conducted by Ben *et al.*[74] Their first generation AFGP mimics showed some IRI activity despite significant structural differences from the original proteins. The synthesis of these mimics requires significant modification to the sugar, involving benzene, Gringard reagents and Grubbs catalyst over nine reaction steps in order to prepare the peptide analogue in low overall yield.[75]

Payne prepared a monomeric form of the tripeptide repeat unit of an AFGP, and then polymerised this to form synthetic AFGPs (*syn*AFGP) with masses between 1.2 - 19.5 kDa (2-32 tripeptide repeat units) (Figure 1.12).[34] *syn*AFGP$_8$ and *syn*AFGP$_{12}$ showed strong TH and IRI activities. Increasing this length to 16 repeat units weakened activity, but the largest *syn*AFGP prepared, with 32 repeat units, displayed equivalent

IRI activity as *syn*AFGP$_{16}$ and a 4 times greater TH gap. These results, while somewhat inconclusive, showed that IRI and TH activity can be decoupled.

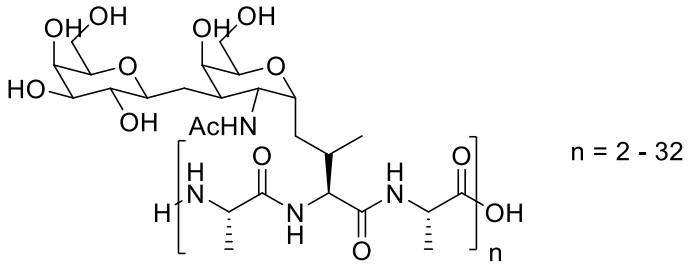

Figure 1.12 *syn*AFGPs prepared by Ben *et al.*[34]

Eniade *et al.* attempted to simplify the synthesis by using a tripeptide monomer with a longer amide linker derived from lysine (Figure 1.13). These glyco-peptides were moderately IRI active at degrees of polymerisation greater than six, and showed no activity below this. There were also signs of DIS, and a TH gap of 0.06 °C.[76]

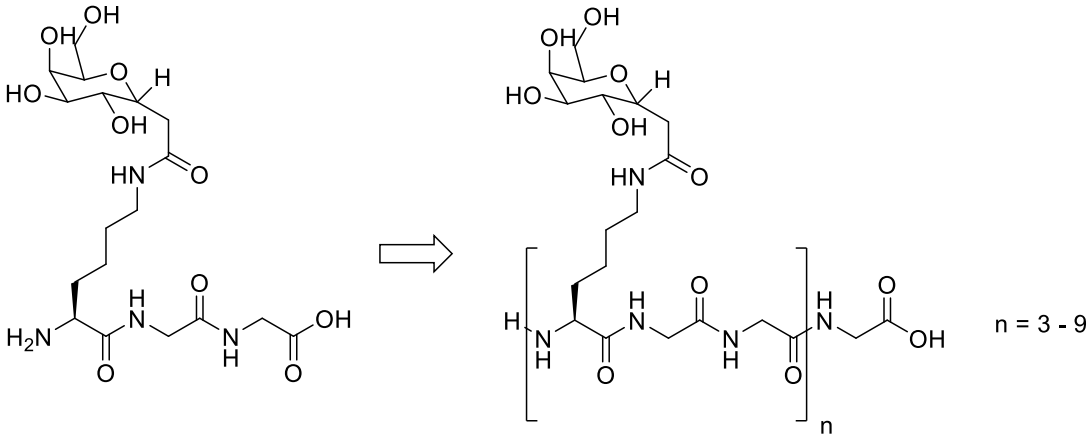

Figure 1.13 1st generation glyco-peptide AFGP analogues prepared by Ben *et al.*[76]

Ben and co-workers went on to prepare *syn*AFGPs that displayed only IRI activity, with no TH or DIS observed (Figure 1.14).[75] Reducing the length of the carbon chain linker afforded an increase in IRI activity, and TH and DIS were no longer observed for the short chain alkyl linked analogue. Very weak TH and DIS was observed in the

longer amide linked analogue, the first example of decoupling TH and IRI in structural AFGP mimics. Replacing galactose with glucose substantially reduced IRI activity, and mannose and talose substitution saw a complete dissappearance.[77]

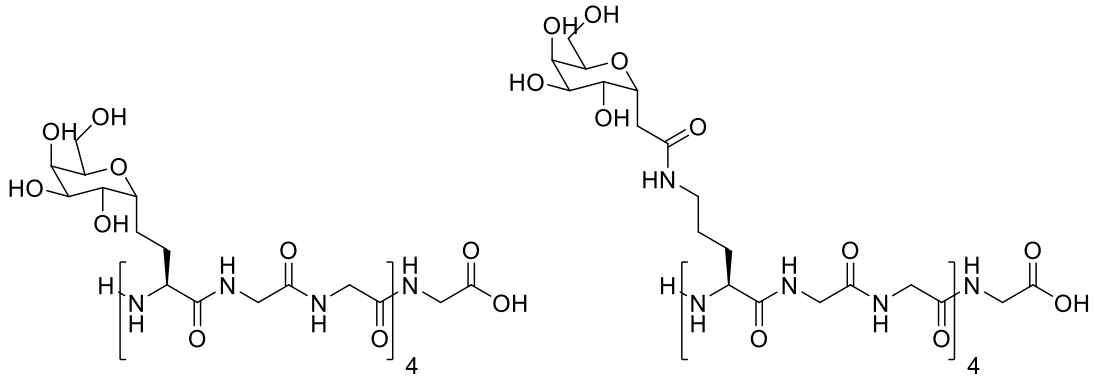

Figure 1.14 2nd generation AFGP mimics with shorter glyosidic linkages and more potent IRI. The galactose unit is essential for potent IRI activity.[75]

Reduction in IRI activity caused by different monosaccharides was attributed to sugar hydration; or more accurately the ability of sugars to bind and order water around themselves.[78] Of the monosaccharides tested, galactose has the highest hydration number and talose the lowest, meaning galactose will bind the most water molecules and will disrupt the H-bonded network of water the most, introducing disorder into the system, which Ben *et al.* put forward as the mechanism behind AFGP IRI activity.[79]

This is logical, since it is known that ice will only grow into the QLL, which contains more ordered water molecules than bulk water. The nature of the interface between the QLL and bulk water (or even if there is an interface) is less well understood, but it is safe to assume that introducing disorder into the bulk water system will increase the energetic cost of ordering water into the QLL layer, and hence decrease the rate of recrystallisation.

Further modification to the linker length failed to produce more active AFGP mimics, and the ideal lengths appear to be the ones initially prepared (2 atoms for the *c*-linked

analogues, 6 atoms for the amide, (Figure 1.14). This is attributed to the unique conformation adopted by the peptide in solution. MD simulations (Figure 1.15) showed that longer linkers were extended in solution, whereas the IRI active species were capable of folding back on themselves to form hydrophobic pockets – which the smaller linkers were unable to do (Figure 1.16).[80]

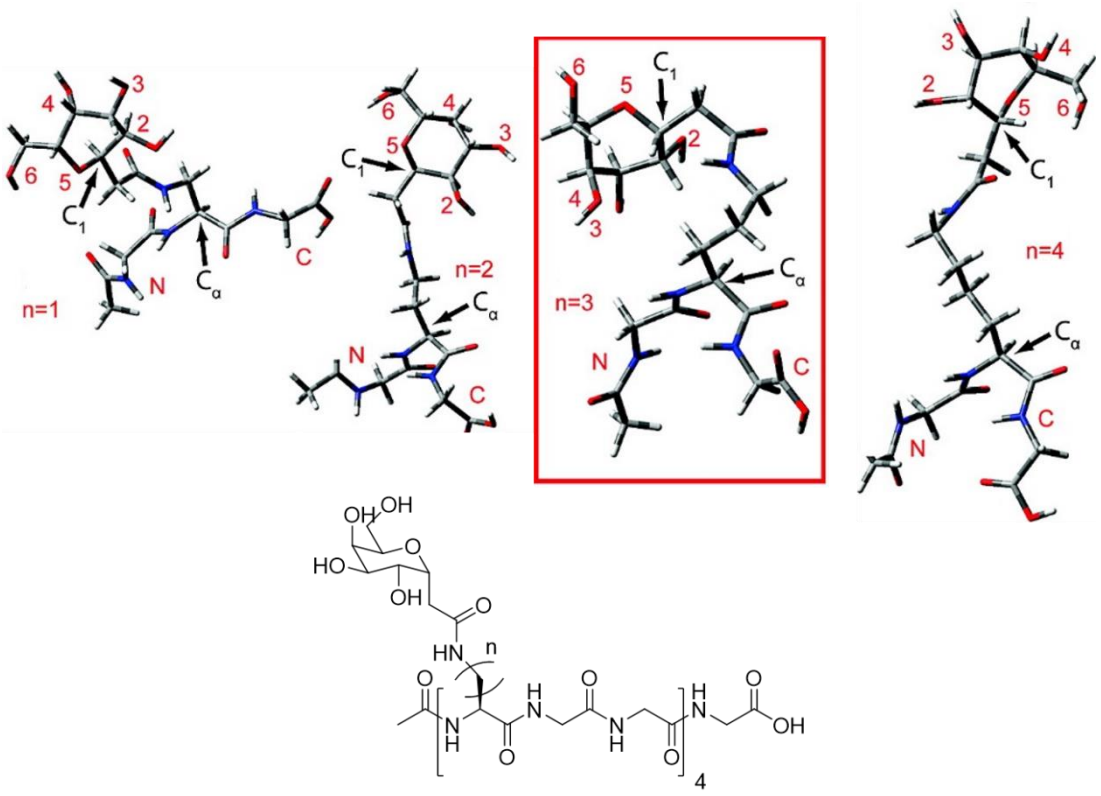

Figure 1.15 Energy minimised MD simulations of the 2nd Generation AFGP analogues designed by Ben *et al.*[80]

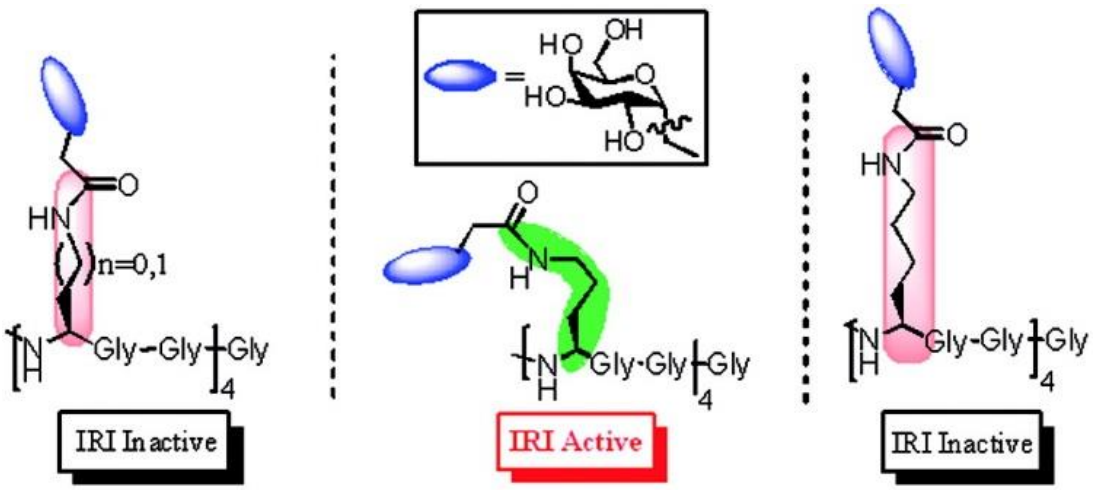

Figure 1.16 Illustration from Ben *et al.* summarising the conformers of different linker lengths.[80]

Other structural mimics of AFGPs exist but are not as effective IRI agents. Attempts to simply the synthesis of these mimics using click chemistry in order to make them feasible for more mainstream use were not successful. Cu(I) catalysed Huisgen azide-alkyne cycloadditions of alkyne sugars onto azide functionalised peptides introduced too much steric bulk. Brimble,[81] Sewald[82] and Ben[83] reported no IRI, TH or DIS activity from these mimics (Figure 1.17).

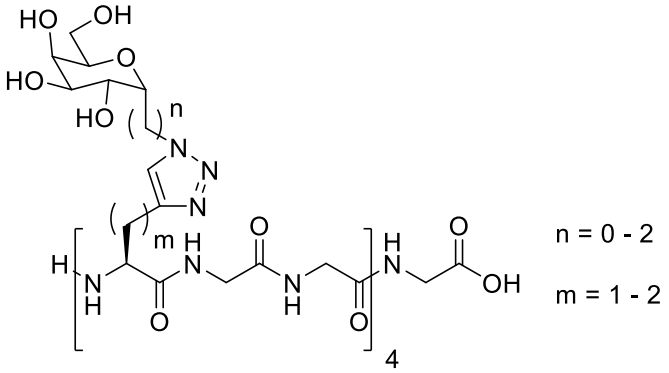

Figure 1.17 The Structure of triazole-containing AFGP analogues reported by Ben *et al.*[83]

Noting the importance of the sugar sub-unit, and presumably wishing to do away with the long multi-step synthetic protocols required to prepare AFGP analogues, Tam *et al.* tested a range of monosaccharides with known hydration parameters.[79] Only galactose showed any appreciable IRI, with no TH or DIS – indicating no direct interaction with the growing ice crystal. Linking hydration with IRI activity did not hold when disaccharides were tested; melibiose has a hydration number of 15.5, yet had a similar IRI to galactose (hydration number 8.7). However at high concentrations (220 mM) disaccharides displayed higher IRI activity than monosaccharides. Somewhat surprisingly the activity 'per OH group' was not examined, although there was some attempt to normalise the data by employing a hydration index (hydration

number/partial molar volume). This is unfortunate as a 'per OH' scale would allow the effect of different configurations to be examined. Alkylation and allylation of these sugars reduced activity, in a somewhat contradictory result to Deller *et al.* who showed that IRI activity slightly increased when galactose and glucose were *O*-alkylated.[84]

Most recently Capicciotti *et al.* reported on the potent IRI activity of a range of carbohydrate-based surfactants and hydrogelators.[85, 86] It was hoped that hydrogelators and surfactants would display IRI activity as they should disrupt the H-bond network of bulk water. This supposition was correct and several of these saccharides displayed high IRI activity. In particular *N*-octyl-D-gluconamide displayed IRI activity as low as 0.5 mM; far more potent than anything else reported by Ben and co-workers. Gel formation was not necessary for IRI activity but amide functionality was a must, with activity dependent on the presence of a secondary amide, and the configuration of the sugar. (Figure 1.18). Interestingly galactopyranoside is the more potent IRI agent compared to glucopyranoside, but in their open chain forms (**D** and **E**) *N*-octyl-D-gluconamide is more active.

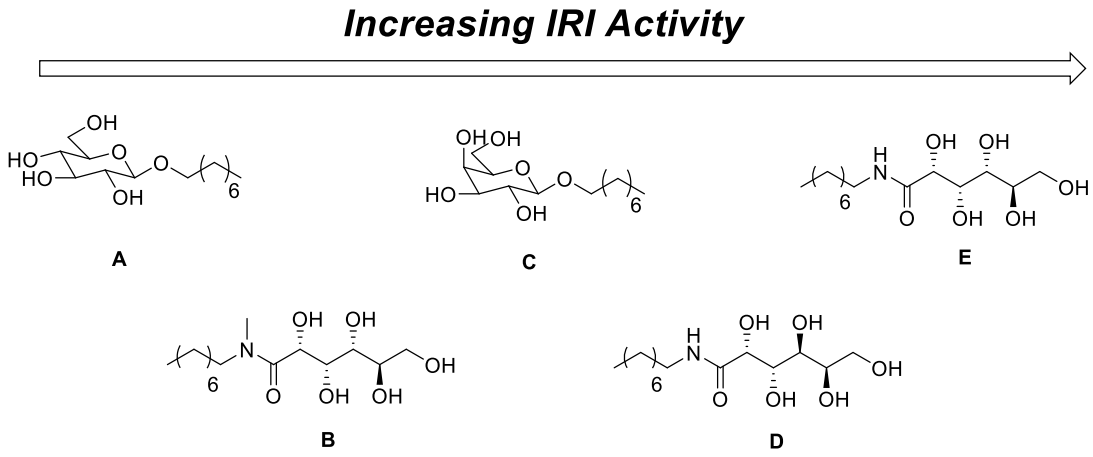

Figure 1.18 IRI active small molecules, arranged in order of increasing potency. **A** *N*-octyl-β-D-glucopyranoside. **B** methylated *N*-octyl-D-gluconamide. **C** *n*-octyl-β-D-galactopyranoside. **D** *N*-octyl-D-galactonamide. **E** *N*-octyl-D-gluconamide.

1.8 Synthetic Macromolecular AFGP Mimics

There is a simpler way to access highly active IRI agents that do not display TH or DIS. As well as being the first report on the IRI activity of AFPs, Knight *et al*. reported that several polymers could also inhibit ice growth.[48] Four polypeptides and three vinyl-polymers were tested for IRI activity. In particular Knight showed that poly(L-histidine), poly(L-hydroxyproline) and poly(vinyl alcohol) all displayed IRI activity in the dilute (< 1 $mg.mL^{-1}$) concentration range while poly(acrylic acid), poly(L-aspartic acid), poly(vinyl pyrrolidone) and poly(L-asparagine) were inactive (Figure 1.19). The section concerning PVA is directly quoted below, as it presciently sets out the question that has been puzzling scientists examining this ever since:

"However, polyvinyl alcohol, My, from 14,000 to 100,000 and with degree of hydrolysis varying from 86 to 98%, is a strong recrystallization inhibitor both before and after thorough dialysis...the difference between its behaviour and that of the other two polyolefins is puzzling. Unless poly(vinyl alcohol) is compact or aggregated in solution rather than extended, we see no ready explanation why the dialyzed solutions still have strong recrystallization-inhibiting properties"

- Knight, Wen and Laursen Cryobiology **1995** *32, 23-34*

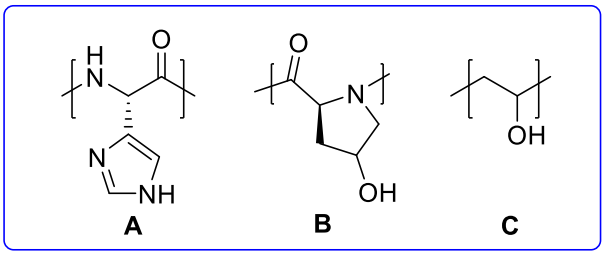

ACTIVE

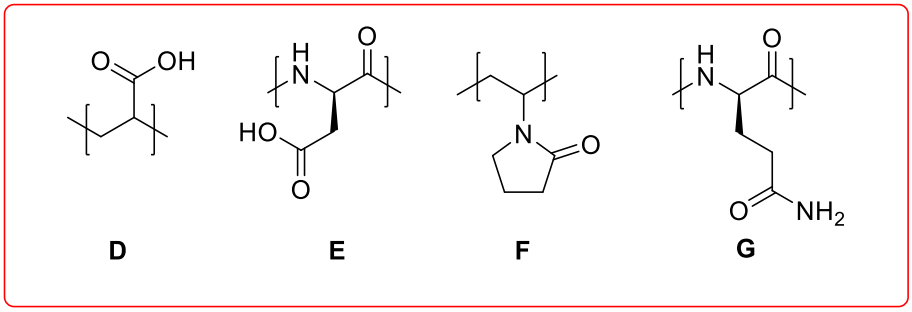

INACTIVE

Figure 1.19 IRI active and IRI inactive polymers. **A** poly(L-histidine). **B** poly(L-hydroxyproline). **C** poly(vinyl alcohol). **D** poly(acrylic acid). **E** poly(L-aspartic acid). **F** poly(vinyl pyrrolidone). **G** poly(L-asparagine).

These results are remarkable considering the significant structural difference between each of these polymers and native AFGPs. For example poly(L-hydroxyproline) displays a helical structure like many AFPs, but it is not facially amphiphillic – the hydroxyl groups are distributed regularly along the backbone. Poly(L-histidine) is an interesting exception as all other AFGPs and IRI active polymers contain hydroxyl groups. Gibson and co-workers showed that poly(L-glutamic acid) and poly(L-lysine), which have helical structures at physiological pH, displayed no IRI activity (Figure 1.20).[87] They concluded that charged side-chains do not interfere with the growing ice crystals correctly to induce Thermal Hysteresis (TH). It seems that the side chain must be able to both donate and accept hydrogen bonds, explaining why polymers such as PEG (polyethylene glycol) do not show significant IRI activity.

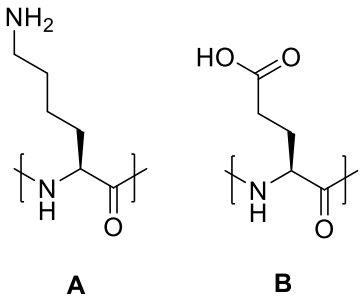

Figure 1.20 A poly(L-glutamic acid). **B** poly(L-lysine).

There have been several papers testing different types of commercially available PVA for IRI activity. The most extensive study was conducted by Inada *et al.* who showed that the activity is molecular weight dependent.[88] Inada also showed that mixing PVA with AFP improved IRI activity,[89, 90] and assessed the very weak TH activity of PVA at 50 mg.mL^{-1}.[91] Gibson *et al.* assayed a library of structurally diverse polymers and showed that PVA was by far the most IRI active, the other polymers showing little or no IRI activity even in concentrated solution.[87] In 2010, Gibson reviewed all antifreeze active synthetic macromolecules reported so far and rationalised this activity with respect to AFGPs and their mimics, and the different assays used to test activity.[92] This work was followed up by examining a range of poly-ols; polymers and small molecules that present a range of hydroxyl groups. When compared on a *per –OH* concentration basis it appeared that the activity of PVA is independent of its hydroxyl group concentration, (Figure 1.21) indicating that its conformation in solution is playing an important role in its IRI activity.[84]

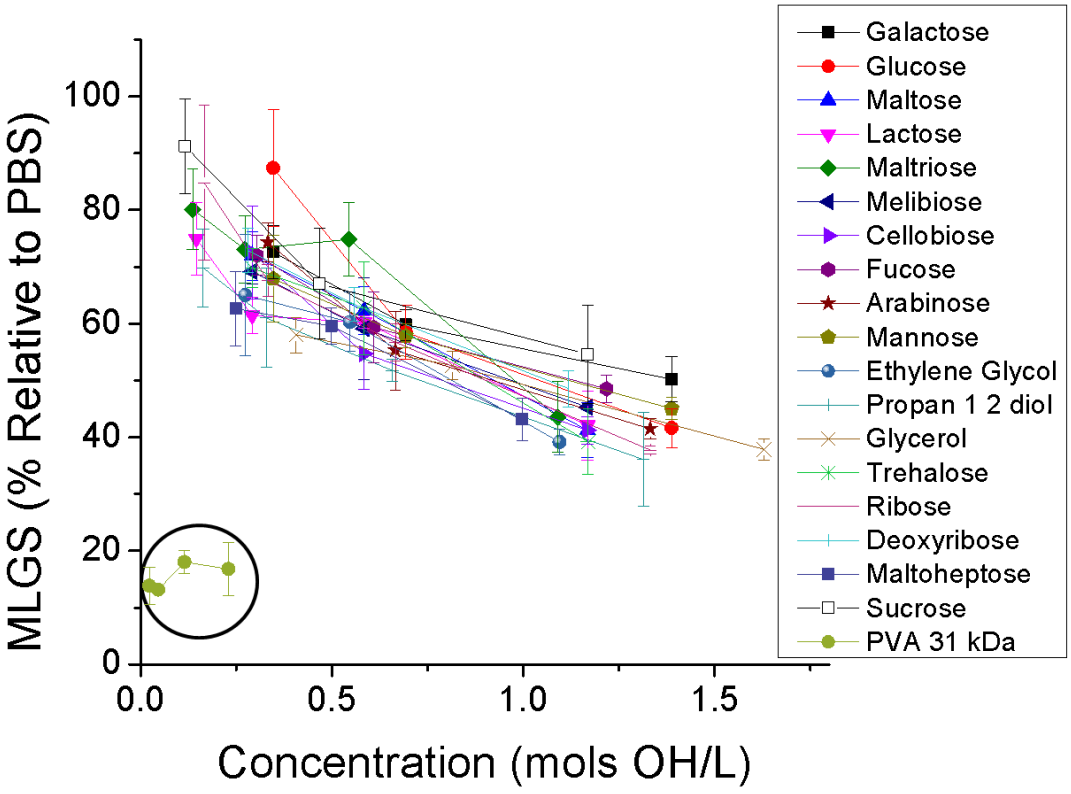

Figure 1.21 Comparison of PVA and other polyols on a hydroxyl group concentration basis, as reported by Deller.[84]

Detailed mechanistic studies on PVA conducted by Budke and Koop suggested that the spacing of hydroxyl groups in PVA are closely matched to that of the prism planes of hexagonal ice, with three PVA units (7.56 Å) having a similar spacing to every second oxygen atom (7.36 Å) in the ice unit cell.[93] This is somewhat at odds with the theory that direct interaction with ice crystal faces will lead to TH and DIS. The most remarkable feature however is the lack of a secondary structure in PVA, which was previously thought to be a requirement for binding to ice crystals. PVA probably exists as a multiple H-bonded random coil in aqueous solution[94] or as a pseudo-micelle if the residual acetate functionality is sufficient.[95] Inada reported the effectiveness of PVA when used as an additive in vitrified solutions, reporting that PVA inhibited nucleation and growth of ice crystals at low temperatures.[96] Recently Deller *et al.* reported that PVA can be used to efficiently cryopreserve blood, reporting exceptionally high

recovery of up to 80 %.[97] There are several other real world applications that would benefit from a commodity product that displays strong, non-colligative antifreeze activity.[98]

Other antifreeze polymers have been reported. Mitchell *et al.* reported that alternately charged zwitterionic polyampholytes were effective IRI agents.[99] Miyata and co-workers showed that ammonium polyacrylate displayed a weak TH effect and DIS in the form of reduced growth in the c-axis direction, the opposite of DIS in AFPs.[100] Baruch and Mastai reported that PEG-polyethyleneimine and PEG-poly(glycidol) may display thermal hysteresis (0.83 °C and 0.69 °C respectively, at 1 $mg.mL^{-1}$),[101] but the assay used was most likely measuring IRI instead of TH. Antonietti *et al.* reported that partially phosphorylated poly(ethylene-oxide)-*block*-poly[2-(2-hydroxyethyl) ethylene)] could inhibit ice growth at high concentrations. Activity was dependent on the degree of phosphorylation, with higher degrees removing IRI activity.[102] Zirconium acetate can exist in a H-bonded polymeric form and displays ice shaping properties, although the assay used by Guizard and co-workers was decidedly non-standard.[103]

Commercially available PVA is neither well defined nor fully hydrolysed from its poly(vinyl acetate) precursor - vinyl alcohol cannot be directly polymerised. The high molecular weight fractions also reduce solubility of the polymer in water and therefore the accuracy of the measurements.

1.9 Controlled Radical Polymerisation of Vinyl Acetate

Controlling the addition of monomers to a polymeric chain is something Nature can achieve with total accuracy, producing proteins and DNA with perfect control of sequence. The preparation of synthetic polymers with the same level of precision is currently not possible, but thanks to controlled polymerisation techniques there are certain strategies available to prepare more precise structures.

Anionic and cationic polymerisation is widely used industrially to prepare polymers, and were the first techniques to be adapted for living polymerisation. Polymers with narrow molecular weight distributions and predictable molecular weights were accessible.[104, 105, 106] However, the preparation of these polymers was frustrating due to the need for the complete removal of oxygen and water, and extremely pure monomer and solvent, if the living polymers with narrow dispersities were to be prepared. There were also very few compatible monomers, which severely limited the scope of these techniques.

These issues have been overcome by recent efforts to control radical polymerisation reactions. The free radical polymerisation of vinyl monomers is an extremely efficient reaction, but there is little control available over the propagation rate, causing a rapid conversion of monomer to polymer and a broad range of molecular weights. With controlled radical polymerisation (CRP), the range of compatible monomers is far greater and the reaction conditions more tolerant towards impurities. Nitroxide-mediated polymerisation (NMP),[107] atom-transfer radical polymerisation (ATRP)[108] and reversible addition-fragmentation chain transfer (RAFT)[109, 110] are the three most

successful techniques in use today, and all share the same mechanistic principle (Scheme 1.1).

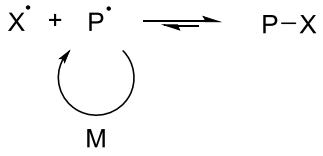

Scheme 1.1 The basic principle of controlled radical polymerisation. The active species (**P·**) is in equilibrium with the dormant species (**P-X**). Addition of monomer (**M**) only occurs with the active species. [**P-X**] > [**P·**], meaning that radical activity is very low and rate of propagation is controlled.

All controlled radical techniques function by minimising the radical concentration present in the reaction at any time, through exploiting the equilibrium position in Scheme 1.1. CRP techniques will also ensure that the radical concentration is constant throughout the reaction, giving linear growth of polymers over time, which is essential for predictable molecular weights and narrow molecular weight dispersity.

Of these controlled radical techniques. RAFT and ATRP have seen the most use due to their simplicity of use and applicability to the largest range of monomers. NMP is more limited in the number of compatible monomers and polymer purification, requires high reaction temperatures, and the overall control of the polymerisation is less efficient than ATRP or RAFT.[111]

RAFT agents, based on either a dithioester or trithiocarbonate core, can modulate the observed propagation kinetics to such a degree that molecular weight increases linearly with monomer conversion, in stark contrast to free radical polymerisation, allowing the targeting of specific molecular weights. Concentration of propagating radicals is kept very low and constant throughout the polymerisation, causing all chains to grow at the same rate. This furnishes polymers with narrow molecular weight

ranges. Through extensive chain transfer, polymerisation is controlled to the degree that multi-arm star polymers can be prepared,[112, 113] as well as a range of other architectures.[114] In addition to this, polymer chains are functionalised at the alpha and omega chain ends with the corresponding components of the RAFT agent (Figure 1.22), a highly desirable outcome. This means the polymer can be further chemically modified at the chain end,[115] or grafted onto surfaces[116] and particles,[117] for example.

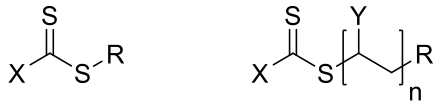

A **B**

Figure 1.22 A General structure of a RAFT agent with notation used to describe functionality. X groups are attributed with the ability to mediate radical stability in the molecule, R groups are the radical chain transfer group, which primarily affects the rate at which the RAFT agent is consumed. **B** Components of the RAFT agent in the resultant polymer.

The major issue is that the RAFT agent needs to be specifically tailored to the monomer in order to ensure fast propagation and the best control over molecular weight distribution (Figure 1.23). This is less of an issue recently due to extensive research into the preparation or RAFT agents, and nowadays most RAFT agents can be prepared with relative ease.[118]

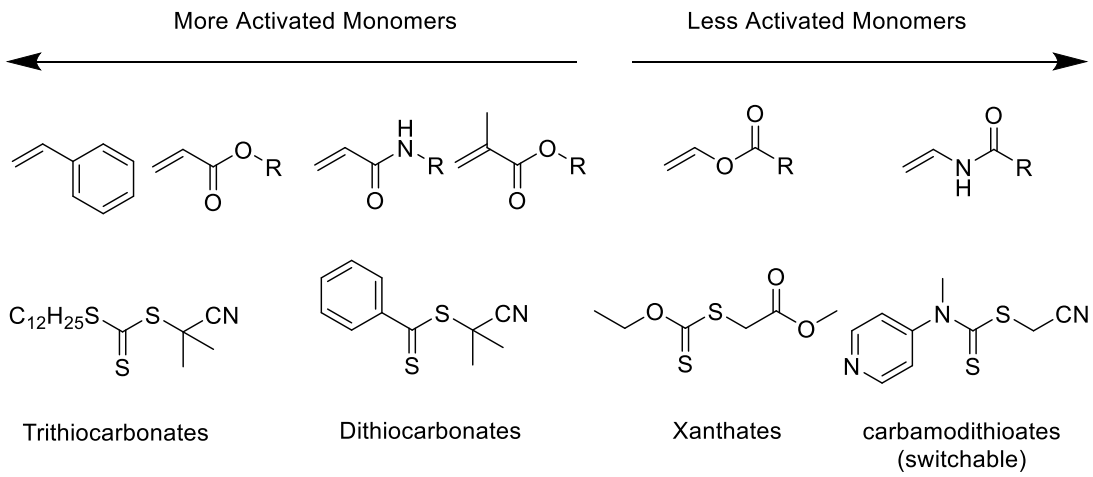

Figure 1.23 A range of monomers and their suitable RAFT agents. Carbamodithioates can switch between efficiently mediating the polymerisation of LAMs and MAMs depending on the alkalinity of the reaction mixture.[119]

The exact mechanism of RAFT polymerisation is complex,[120] with several phenomena yet to be explained,[121] but the mechanism below is currently accepted to be the best description of what is occurring during the reaction (Scheme 1.2).[122] In order for this mechanism to hold, RAFT agents must be tailored to promote fragmentation and propagation, but still maintain control over the concentration of radicals in the system.

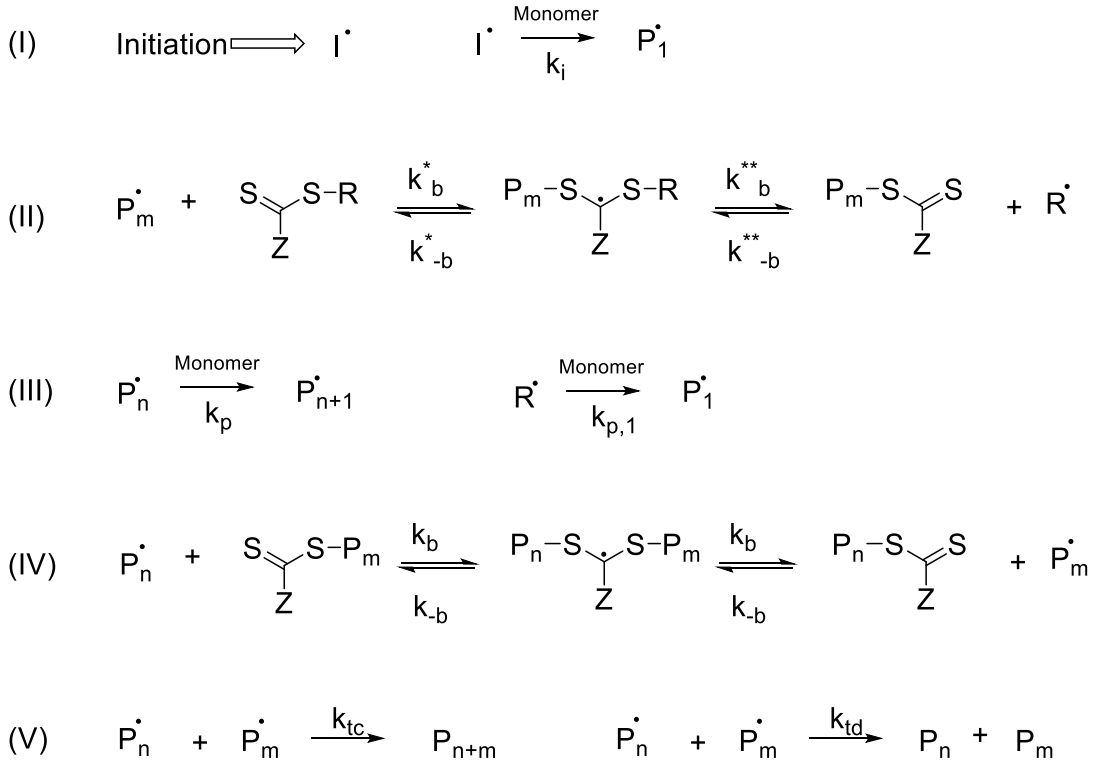

Scheme 1.2 Reaction scheme detailing the various reactions occurring in a RAFT mediated controlled radical polymerisation.

While RAFT agents are adept at controlling the radical polymerisation of styrene and acrylate type monomers, the polymerisation of vinyl acetate and vinyl esters in general has always been more challenging. Less known techniques such organo-cobalt mediated radical polymerisation,[123, 124] iodine-transfer polymerisation (ITP)[125] and organoheteroatom-mediated polymerisation (OMRP)[126] have been shown to be effective. NMP and ATRP have yet to be of any use in controlling vinyl acetate polymerisation.[127]

While the terms 'less activated' and 'more activated' find regular use in the literature, a complete definition is harder to come by. A review of the RAFT polymerisation of vinyl esters by Destarac provides a complete picture.[128] Less activated monomers form very stable intermediates with the RAFT agent so Z groups that stabilise the intermediate radical adduct (Scheme 1.2 II) will cause retardation of the vinyl ester polymerisation. This is because if the RAFT adduct is stabilised then fragmentation is

discouraged, leading to termination events dominating the reaction kinetics. Therefore a RAFT agent must be selected that is both susceptible to radical attack by propagating chains, but be capable of destabilising the intermediate radical.

If the reinitiating rate (fragmentation) is lower, then an inhibition time is observed. This inhibition time arises after azo initiation, initial propagation and chain transfer occurs. The R group radical fragment is not effective at reinitiation, the system becomes effectively dormant for up to several hours and no propagation is observed. A specific example is the use of 2-cyanoisopropyl R groups in a MADIX mediated radical polymerisation of vinyl acetate; at 315 K this radical fragment will add to sulfur (MADIX agent) with a rate constant of 2410 $L.mol^{-1}s^{-1}$, but will add to VAc at only 41 $L.mol^{-1}s^{-1}$.[129]

Vinyl acetate is a very attractive target for controlled radical polymerisation due to its uses in adhesives, emulsions and additives, but also because it is a precursor for PVA, which in addition to displaying exceptional IRI activity, is essentially non-toxic (LD_{50} = 5000 mg/kg in rats).[130] PVA has FDA approval for use in food products and as a medical suture, and is an important industrial polymer additive and coating. Changing the tacticity of PVA dramatically changes the solubility and gelation character of the polymer.[131]

The controlled radical polymerisation of vinyl acetate also poses some interesting challenges for the polymer chemist. As well as a propensity for chain transfer to solvent,[132] PVAc will also display head-to-head addition (generally 1.23 % of the polymer)[133] and will readily transfer radical activity to the methyl group of the acetate, causing branching (Scheme 1.3).[134]

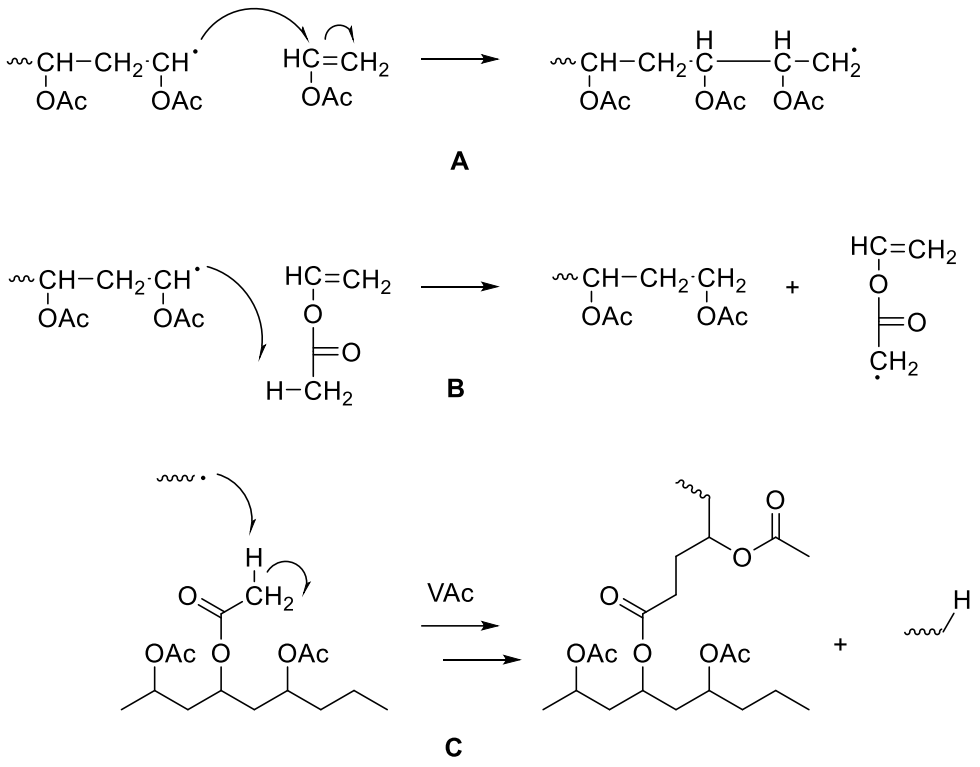

Scheme 1.3 The various chain transfer reactions that can occur during the polymerisation of vinyl acetate.[134]

Since these events are dependent on radical concentration and temperature, controlled polymerisation seems to be capable of reducing these by limiting radical concentration. When using RAFT agents, dormant chains can form from head-to-head or head-to-tail propagating chain ends adding to RAFT agents (Figure 1.24), and it can be assumed that the difference in fragmentation/reactivity contributes to the increase of Đ at high molecular weights.[135] For this reason RAFT is not suitable for the polymerisation of high molecular weight PVAc (> 10^5 g.mol^{-1}) with low dispersities (Đ < 1.2).[136]

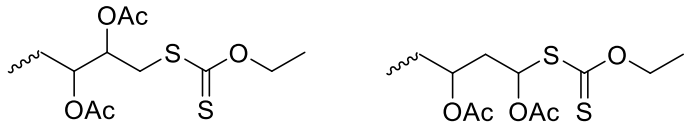

Figure 1.24 Various addition pathways that result in dormant chain, caused by head-to-head or head-to-tail addition to a RAFT agent.

Stenzel *et al.* showed that RAFT agents (strictly MADIX agents) containing *o*-ethoxy Z groups are the most efficient mediators for the controlled polymerisation of vinyl acetate, so long as the R-group is more labile than the poly(vinyl acetate) chain, and can reinitiate polymerisation at a comparable rate to that of propagation (Figure 1.25).[137] This *O*ethoxy xanthate-based strategy was then applied to multifunctional MADIX agents,[138, 139] polymer combs,[140] and block copolymers.[141] Shim *et al.* reported control of tacticity using a MADIX agents and fluoroalcohols,[142] but Smith *et al.* reported that the syndiotactic component of the polymer could be increased, reporting the synthesis PVAc with the highest ever degree of syndiotacticity.[143]

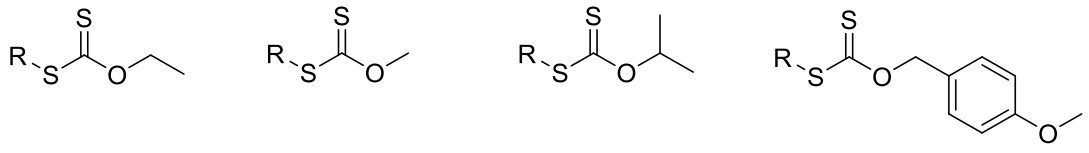

t_{inh} = 0.32	t_{inh} = 0.34	t_{inh} = 2.1	t_{inh} = 1.6
R_p = 6.4	R_p = 6.2	R_p = 1.8	R_p = 2.5
M_w/M_n = 1.18	M_w/M_n = 1.25	M_w/M_n = 1.19	M_w/M_n = 1.2

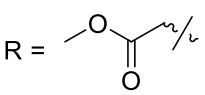

Figure 1.25 MADIX agents reported by Stenzel *et al.* capable of controlling the radical polymerisation of VAc, and the inhibition times /h, conversion rates / 10^4 mol.L^{-1}.s^{-1}, and M_w/M_n (at ~25 % conversion) of the resultant polymers.[137]

Despite the issues highlighted, a RAFT/MADIX strategy is the best tool for preparing PVAc and PVA to probe the structure-property relationships that afford such anomalously high IRI activity. Not only does it provide the best control over the molecular weight, but it can be used to incorporate other less-activated monomers for the preparation of blocks, and the ease of chain transfer agent (CTA) synthesis affords access to higher-order structures.

1.10 Summary

While micro-organisms can survive well below the freezing point of water due to resilient and simple evolutionary design, larger organisms have come to rely on preventing damage due to ice through hindering ice growth *via* specialist ice-binding and ice-structuring proteins. These proteins are highly efficient at lowering the freezing point of ice through thermal hysteresis, and then inhibiting the growth of any nucleated ice crystals. However, the unfortunate side effect of ice shaping caused by direct binding of the proteins to specific ice faces prohibits their use in cryopreserving organs, tissues and blood. Efforts to prepare mimics that avoid DIS have been successful but the complex multistep synthesis precludes widespread use. Structural similarities between AFGPs and polymers, and a fortuitous discovery by Knight *et al.*, inspired research into the antifreeze activity of a range of polymers. PVA was found to be far and away the most effective inhibitor of ice growth, and showed no thermal hysteresis or ice shaping.

Further insight into why PVA is such a potent inhibitor, and why other poly-ols are not, is complicated by the difficulties in preparing well-defined PVA. Currently the effect on IRI activity of molecular weight, residual acetate content, hydroxyl group sequence, and morphological effects afforded by blocks and stars are unknown.

Controlled radical polymerisation has made great strides in preparing polymers with predictable, controlled molecular weight and narrow molecular weight distributions, and considerable work has gone into trying to control the polymerisation of vinyl esters, namely vinyl acetate; the precursor to PVA. Herein these controlled radical techniques have been employed to prepare well-defined PVA, in order to gain insight into the structure-property relationships highlighted above.

1.11 Project Aims and Overview

Using controlled radical polymerisation techniques, a range of polymers will be prepared and their IRI activity quantitatively and systemically assayed using the splat assay. This will afford a previously unavailable level of molecular weight resolution of the IRI activity of PVA. New insights on the IRI mechanism of PVA will be shown using the advanced structures available *via* the exploitation of living polymerisation.

1.12 Thesis Summary

Chapter 2 examines the role molecular weight plays on IRI activity, and then examines the importance of hydroxyl sequence using post-polymerisation modification and copolymerisation with other less activated monomers. **Chapter 3** details the ability of CRP and MADIX to produce well defined block co-polymers of PVA, and confirms the importance of the hydroxyl sequence. These polymers maintained their IRI activity despite large non-active blocks, showing that there is potential to add secondary functionality without sacrificing IRI activity. **Chapter 4** demonstrates the synthesis and utility of a novel multifunctional MADIX agent, which is used to prepare *Star*-PVAs at high conversion and narrow MWD. The resultant star polymers were highly IRI active, and activity profiles of these polymers provides further evidence that the mechanism of PVA IRI does not involve direct binding to ice. **Chapter 5** uses the techniques and methodologies developed in Chapter 2 and applies them to another lesser-known ability of PVA; thermoresponsivity. The cloud point behaviour of PVA was examined for the first time using a controlled radical polymerisation methodology, and through simple post polymerisation modification PVA.Alkyl random co-polymers were prepared. These polymers were shown to display highly tuneable, thermoresponsive polymers capable of enzymatically-triggered isothermal phase changes.

1.13 References

1. Scholander, P. F.; van Dam, L.; Kanwisher, J. W.; Hammel, H. T.; Gordon, M. S., Supercooling and osmoregulation in arctic fish. *Journal of Cellular and Comparative Physiology* **1957,** *49* (1), 5-24.

2. Gordon, M. S.; Amdur, B. H.; Scholander, P. F., Freezing Resistance in Some Northern Fishes. *The Biological Bulletin* **1962,** *122* (1), 52-62.

3. DeVries, A. L.; Wohlschlag, D. E., Freezing Resistance in Some Antarctic Fishes. *Science* **1969,** *163* (3871), 1073-1075.

4. DeVries, A. L.; Komatsu, S. K.; Feeney, R. E., Chemical and Physical Properties of Freezing Point-depressing Glycoproteins from Antarctic Fishes. *Journal of Biological Chemistry* **1970,** *245* (11), 2901-2908.

5. Shier, W. T.; Lin, Y.; De Vries, A. L., Structure and mode of action of glycoproteins from an antarctic fish. *Biochimica et Biophysica Acta (BBA) - Protein Structure* **1972,** *263* (2), 406-413.

6. Harding, M. M.; Anderberg, P. I.; Haymet, A. D. J., 'Antifreeze' glycoproteins from polar fish. *European Journal of Biochemistry* **2003,** *270* (7), 1381-1392.

7. Bouvet, V.; Ben, R., Antifreeze glycoproteins. *Cell Biochemistry and Biophysics* **2003,** *39* (2), 133-144.

8. Chen, L.; DeVries, A. L.; Cheng, C.-H. C., Convergent evolution of antifreeze glycoproteins in Antarctic notothenioid fish and Arctic cod. *Proceedings of the National Academy of Sciences* **1997,** *94* (8), 3817-3822.

9. Near, T. J.; Dornburg, A.; Kuhn, K. L.; Eastman, J. T.; Pennington, J. N.; Patarnello, T.; Zane, L.; Fernández, D. A.; Jones, C. D., Ancient climate change, antifreeze, and the evolutionary diversification of Antarctic fishes. *Proceedings of the National Academy of Sciences* **2012,** *109* (9), 3434-3439.

10. Lane, A. N.; Hays, L. M.; Feeney, R. E.; Crowe, L. M.; Crowe, J. H., Conformational and dynamic properties of a 14 residue antifreeze glycopeptide from

Antarctic cod. *Protein Science : A Publication of the Protein Society* **1998,** *7* (7), 1555-1563.

11. Yeh, Y.; Feeney, R. E., Antifreeze proteins: Structures and mechanisms of function. *Chemical Reviews* **1996,** *96* (2).

12. Tsvetkova, N. M.; Phillips, B. L.; Krishnan, V. V.; Feeney, R. E.; Fink, W. H.; Crowe, J. H.; Risbud, S. H.; Tablin, F.; Yeh, Y., Dynamics of antifreeze glycoproteins in the presence of ice. *Biophysical Journal* **2002,** *82* (1), 464-473.

13. Nguyen, D. H.; Colvin, M. E.; Yeh, Y.; Feeney, R. E.; Fink, W. H., The dynamics, structure, and conformational free energy of proline-containing antifreeze glycoprotein. *Biophysical Journal* **2002,** *82* (6), 2892-2905.

14. Ahmed, A. I.; Osuga, D. T.; Feeney, R. E., Antifreeze Glycoprotein from an Antarctic Fish: Effects of Chemical Modifications of Carbohydrate Residues on Antifreeze and Antilectin Activities. *Journal of Biological Chemistry* **1973,** *248* (24), 8524-8527.

15. Tachibana, Y.; Fletcher, G. L.; Fujitani, N.; Tsuda, S.; Monde, K.; Nishimura, S.-I., Antifreeze Glycoproteins: Elucidation of the Structural Motifs That Are Essential for Antifreeze Activity. *Angewandte Chemie* **2004,** *116* (7), 874-880.

16. Yang, S.-H.; Wojnar, J. M.; Harris, P. W. R.; DeVries, A. L.; Evans, C. W.; Brimble, M. A., Chemical synthesis of a masked analogue of the fish antifreeze potentiating protein (AFPP). *Organic & Biomolecular Chemistry* **2013,** *11* (30), 4935-4942.

17. Duman, J. G.; Devries, A. L., Freezing resistance in winter flounder Pseudopleuronectes americanus. *Nature* **1974,** *247* (5438), 237-238.

18. Clark, M.; Worland, M. R., How insects survive the cold: molecular mechanisms—a review. *Journal of Comparative Physiology B* **2008,** *178* (8), 917-933.

19. Griffith, M.; Yaish, M. W. F., Antifreeze proteins in overwintering plants: a tale of two activities. *Trends in Plant Science* **2004,** *9* (8), 399-405.

20. Jarząbek, M.; Pukacki, P. M.; Nuc, K., Cold-regulated proteins with potent antifreeze and cryoprotective activities in spruces (Picea spp.). *Cryobiology* **2009,** *58* (3), 268-274.

21. Lauersen, K. J.; Brown, A.; Middleton, A.; Davies, P. L.; Walker, V. K., Expression and characterization of an antifreeze protein from the perennial rye grass, Lolium perenne. *Cryobiology* **2011,** *62* (3), 194-201.

22. Duman, J. G.; Olsen, T. M., Thermal Hysteresis Protein Activity in Bacteria, Fungi, and Phylogenetically Diverse Plants. *Cryobiology* **1993,** *30* (3), 322-328.

23. Goodsell, D. Antifreeze Proteins 10.2210/rcsb_pdb/mom_2009_12 *Molecule of the Month* [Online], 2009.

24. Sönnichsen, F. D.; DeLuca, C. I.; Davies, P. L.; Sykes, B. D., Refined solution structure of type III antifreeze protein: hydrophobic groups may be involved in the energetics of the protein–ice interaction. *Structure* **1996,** *4* (11), 1325-1337.

25. Sicheri, F.; Yang, D. S. C., Ice-Binding Structure and Mechanism of an Antifreeze Protein from Winter Flounder. *Nature* **1995,** *375* (6530), 427-431.

26. Liou, Y.-C.; Tocilj, A.; Davies, P. L.; Jia, Z., Mimicry of ice structure by surface hydroxyls and water of a [beta]-helix antifreeze protein. *Nature* **2000,** *406* (6793), 322-324.

27. Graether, S. P.; Kuiper, M. J.; Gagne, S. M.; Walker, V. K.; Jia, Z.; Sykes, B. D.; Davies, P. L., [beta]-Helix structure and ice-binding properties of a hyperactive antifreeze protein from an insect. *Nature* **2000,** *406* (6793), 325-328.

28. Pentelute, B. L.; Gates, Z. P.; Tereshko, V.; Dashnau, J. L.; Vanderkooi, J. M.; Kossiakoff, A. A.; Kent, S. B. H., X-ray Structure of Snow Flea Antifreeze Protein Determined by Racemic Crystallization of Synthetic Protein Enantiomers. *Journal of the American Chemical Society* **2008,** *130* (30), 9695-9701.

29. Leinala, E. K.; Davies, P. L.; Doucet, D.; Tyshenko, M. G.; Walker, V. K.; Jia, Z., A beta-helical antifreeze protein isoform with increased activity. Structural and functional insights. *Journal of Biological Chemistry* **2002,** *277* (36), 33349-33352.

30. Sharp, K. A., A peek at ice binding by antifreeze proteins. *Proceedings of the National Academy of Sciences* **2011,** *108* (18), 7281-7282.

31. Garnham, C. P.; Campbell, R. L.; Davies, P. L., Anchored clathrate waters bind antifreeze proteins to ice. *Proceedings of the National Academy of Sciences* **2011,** *108* (18), 7363-7367.

32. Sun, T.; Lin, F.-H.; Campbell, R. L.; Allingham, J. S.; Davies, P. L., An Antifreeze Protein Folds with an Interior Network of More Than 400 Semi-Clathrate Waters. *Science* **2014,** *343* (6172), 795-798.

33. Garnham, C. P.; Natarajan, A.; Middleton, A. J.; Kuiper, M. J.; Braslavsky, I.; Davies, P. L., Compound Ice-Binding Site of an Antifreeze Protein Revealed by Mutagenesis and Fluorescent Tagging. *Biochemistry* **2010,** *49* (42), 9063-9071.

34. Wilkinson, B. L.; Stone, R. S.; Capicciotti, C. J.; Thaysen-Andersen, M.; Matthews, J. M.; Packer, N. H.; Ben, R. N.; Payne, R. J., Total Synthesis of Homogeneous Antifreeze Glycopeptides and Glycoproteins. *Angewandte Chemie-International Edition* **2012,** *51* (15), 3606-3610.

35. Costanzo, J. P.; Lee, R. E.; DeVries, A. L.; Wang, T.; Layne, J. R., Survival mechanisms of vertebrate ectotherms at subfreezing temperatures: applications in cryomedicine. *The FASEB Journal* **1995,** *9* (5), 351-358.

36. Burcham, T. S.; Osuga, D. T.; Yeh, Y.; Feeney, R. E., A Kinetic Description of Antifreeze Glycoprotein Activity. *Journal of Biological Chemistry* **1986,** *261* (14), 6390-6397.

37. Davies, P. L.; Baardsnes, J.; Kuiper, M. J.; Walker, V. K., Structure and function of antifreeze proteins. *Philosophical Transactions of the Royal Society of London B: Biological Sciences* **2002,** *357* (1423), 927-935.

38. Meister, K.; Strazdaite, S.; DeVries, A. L.; Lotze, S.; Olijve, L. L. C.; Voets, I. K.; Bakker, H. J., Observation of ice-like water layers at an aqueous protein surface. *Proceedings of the National Academy of Sciences* **2014,** *111* (50), 17732-17736.

39. Cheng, A.; Merz, K. M., Ice-binding mechanism of winter flounder antifreeze proteins. *Biophysical Journal* **1997,** *73* (6), 2851-2873.

40. Drori, R.; Celik, Y.; Davies, P. L.; Braslavsky, I., Ice-binding proteins that accumulate on different ice crystal planes produce distinct thermal hysteresis dynamics. *Journal of The Royal Society Interface* **2014,** *11* (98), DOI: 10.1098/rsif.2014.0526.

41. Celik, Y.; Drori, R.; Pertaya-Braun, N.; Altan, A.; Barton, T.; Bar-Dolev, M.; Groisman, A.; Davies, P. L.; Braslavsky, I., Microfluidic experiments reveal that antifreeze proteins bound to ice crystals suffice to prevent their growth. *Proceedings of the National Academy of Sciences* **2013,** *110* (4), 1309-1314.

42. Kristiansen, E.; Zachariassen, K. E., The mechanism by which fish antifreeze proteins cause thermal hysteresis. *Cryobiology* **2005,** *51* (3), 262-280.

43. Amir, G.; Rubinsky, B.; Kassif, Y.; Horowitz, L.; Smolinsky, A. K.; Lavee, J., Preservation of myocyte structure and mitochondrial integrity in subzero cryopreservation of mammalian hearts for transplantation using antifreeze proteins—an electron microscopy study. *European journal of cardio-thoracic surgery* **2003,** *24* (2), 292-297.

44. Grandum, S.; Yabe, A.; Nakagomi, K.; Tanaka, M.; Fumio, T.; Kobayashi, Y.; Frivik, P.-E., Analysis of ice crystal growth for a crystal surface containing adsorbed antifreeze proteins. *Journal of Crystal Growth* **1999,** *205* (3), 382-390.

45. Knight, C. A.; Driggers, E.; DeVries, A. L., Adsorption to ice of fish antifreeze glycopeptides 7 and 8. *Biophysical Journal* **1993,** *64* (1), 252-259.

46. Peltier, R.; Evans, C. W.; DeVries, A. L.; Brimble, M. A.; Dingley, A. J.; Williams, D. E., Growth Habit Modification of Ice Crystals Using Antifreeze Glycoprotein (AFGP) Analogues. *Crystal Growth & Design* **2010,** *10* (12), 5066-5077.

47. Capicciotti, C. J.; Doshi, M.; Ben, R. N., *Ice Recrystallization Inhibitors: From Biological Antifreezes to Small Molecules*. 2013.

48. Knight, C. A.; Wen, D.; Laursen, R. A., Nonequilibrium Antifreeze Peptides and the Recrystallization of Ice. *Cryobiology* **1995,** *32* (1), 23-34.

49. Doherty, R. D.; Hughes, D. A.; Humphreys, F. J.; Jonas, J. J.; Jensen, D. J.; Kassner, M. E.; King, W. E.; McNelley, T. R.; McQueen, H. J.; Rollett, A. D., Current issues in recrystallization: a review. *Materials Science and Engineering: A* **1997,** *238* (2), 219-274.

50. Fletcher, N. H., Surface structure of water and ice. *Philosophical Magazine* **1968,** *18* (156), 1287-1300.

51. Döppenschmidt, A.; Butt, H.-J., Measuring the Thickness of the Liquid-like Layer on Ice Surfaces with Atomic Force Microscopy. *Langmuir* **2000,** *16* (16), 6709-6714.

52. Elbaum, M.; Lipson, S. G.; Dash, J. G., Optical study of surface melting on ice. *Journal of Crystal Growth* **1993,** *129* (3–4), 491-505.

53. Karim, O. A.; Kay, P. A.; Haymet, A. D. J., The ice/water interface: A molecular dynamics simulation using the simple point charge model. *The Journal of Chemical Physics* **1990,** *92* (7), 4634-4635.

54. Bilgram, J. H., The structure and properties of melt and concentrated solutions. *Progress in Crystal Growth and Characterization of Materials* **1993,** *26*, 99-119.

55. Budke, C.; Heggemann, C.; Koch, M.; Sewald, N.; Koop, T., Ice Recrystallization Kinetics in the Presence of Synthetic Antifreeze Glycoprotein Analogues Using the Framework of LSW Theory. *Journal of Physical Chemistry B* **2009,** *113* (9), 2865–2873.

56. Budke, C.; Heggemann, C.; Koch, M.; Sewald, N.; Koop, T., Ice Recrystallization Kinetics in the Presence of Synthetic Antifreeze Glycoprotein Analogues Using the Framework of LSW Theory. *Journal of Physical Chemistry B* **2009,** *113* (9).

57. Yu, S. O.; Brown, A.; Middleton, A. J.; Tomczak, M. M.; Walker, V. K.; Davies, P. L., Ice restructuring inhibition activities in antifreeze proteins with distinct differences in thermal hysteresis. *Cryobiology* **2010,** *61* (3), 327-334.

58. Kuiper, M. J.; Davies, P. L.; Walker, V. K., A Theoretical Model of a Plant Antifreeze Protein from Lolium perenne. *Biophysical Journal* **2001,** *81* (6), 3560-3565.

59. Li, B.; Sun, D.-W., Novel methods for rapid freezing and thawing of foods – a review. *Journal of Food Engineering* **2002,** *54* (3), 175-182.

60. Petzold, G.; Aguilera, J., Ice Morphology: Fundamentals and Technological Applications in Foods. *Food Biophysics* **2009,** *4* (4), 378-396.

61. Chao, H.; Davies, P. L.; Carpenter, J. F., Effects of antifreeze proteins on red blood cell survival during cryopreservation. *The Journal of experimental biology* **1996,** *199* (9), 2071-2076.

62. Chaytor, J. L.; Tokarew, J. M.; Wu, L. K.; Leclère, M.; Tam, R. Y.; Capicciotti, C. J.; Guolla, L.; von Moos, E.; Findlay, C. S.; Allan, D. S.; Ben, R. N., Inhibiting ice recrystallization and optimization of cell viability after cryopreservation. *Glycobiology* **2012,** *22* (1), 123-133.

63. Soltys, K. A.; Batta, A. K.; Koneru, B., Successful Nonfreezing, Subzero Preservation of Rat Liver with 2,3-Butanediol and Type I Antifreeze Protein. *Journal of Surgical Research* **2001,** *96* (1), 30-34.

64. Baust, J. M., Molecular mechanisms of cellular demise associated with cryopreservation failure. *Cell Preservation Technology* **2002,** *1* (1), 17-31.

65. Fowler, A.; Toner, M., Cryo-Injury and Biopreservation. *Annals of the New York Academy of Sciences* **2006,** *1066* (1), 119-135.

66. Acker, J. P.; McGann, L. E., Innocuous Intracellular Ice Improves Survival of Frozen Cells. *Cell transplantation* **2002,** *11* (6), 563-571.

67. Gage, A. A.; Baust, J. M.; Baust, J. G., Experimental Cryosurgery Investigations In Vivo. *Cryobiology* **2009,** *59* (3), 229.

68. Alam, H. B.; Bowyer, M. W.; Koustova, E.; Gushchin, V.; Anderson, D.; Stanton, K.; Kreishman, P.; Cryer, C. M. T.; Hancock, T.; Rhee, P., Learning and memory is preserved after induced asanguineous hyperkalemic hypothermic arrest in a swine model of traumatic exsanguination. *Surgery* **2002,** *132* (2), 278-288.

69. Scott, C. T.; Caulfield, T.; Borgelt, E.; Illes, J., Personal medicine - the new banking crisis. *Nature Biotechnology* **2012,** *30* (2), 141-147.

70. Opar, A., As demand for organs expands, so does transplant technology. *Nature Medicine* **2008,** *14* (3), 225-225.

71. Knight, C. A.; Hallett, J.; DeVries, A. L., Solute effects on ice recrystallization: An assessment technique. *Cryobiology* **1988,** *25* (1), 55-60.

72. Hall, D. G.; Lips, A., Phenomenology and Mechanism of Antifreeze Peptide Activity. *Langmuir* **1999,** *15* (6), 1905-1912.

73. Sidebottom, C.; Buckley, S.; Pudney, P.; Twigg, S.; Jarman, C.; Holt, C.; Telford, J.; McArthur, A.; Worrall, D.; Hubbard, R.; Lillford, P., Phytochemistry - Heat-stable antifreeze protein from grass. *Nature* **2000,** *406* (6793), 256-256.

74. Balcerzak, A. K.; Capicciotti, C. J.; Briard, J. G.; Ben, R. N., Designing ice recrystallization inhibitors: from antifreeze (glyco)proteins to small molecules. *RSC Advances* **2014,** *4* (80), 42682-42696.

75. Liu, S. H.; Ben, R. N., C-linked galactosyl serine AFGP analogues as potent recrystallization inhibitors. *Organic Letters* **2005,** *7* (12), 2385-2388.

76. Eniade, A.; Purushotham, M.; Ben, R. N.; Wang, J. B.; Horwath, K., A serendipitous discovery of antifreeze protein-specific activity in C-linked antifreeze glycoprotein analogs. *Cell Biochemistry and Biophysics* **2003,** *38* (2), 115-124.

77. Czechura, P.; Tam, R. Y.; Dimitrijevic, E.; Murphy, A. V.; Ben, R. N., The Importance of Hydration for Inhibiting Ice Recrystallization with C-Linked Antifreeze Glycoproteins. *Journal of the American Chemical Society* **2008,** *130* (10), 2928-2929.

78. Galema, S. A.; Engberts, J. B. F. N.; Hoeiland, H.; Foerland, G. M., Informative thermodynamic properties of the effect of stereochemistry on carbohydrate hydration. *The Journal of Physical Chemistry* **1993,** *97* (26), 6885-6889.

79. Tam, R. Y.; Ferreira, S. S.; Czechura, P.; Chaytor, J. L.; Ben, R. N., Hydration Index—A Better Parameter for Explaining Small Molecule Hydration in Inhibition of Ice Recrystallization. *Journal of the American Chemical Society* **2008,** *130* (51), 17494-17501.

80. Tam, R. Y.; Rowley, C. N.; Petrov, I.; Zhang, T.; Afagh, N. A.; Woo, T. K.; Ben, R. N., Solution Conformation of C-Linked Antifreeze Glycoprotein Analogues and Modulation of Ice Recrystallization. *Journal of the American Chemical Society* **2009,** *131* (43), 15745-15753.

81. Miller, N.; Williams, G. M.; Brimble, M. A., Synthesis of Fish Antifreeze Neoglycopeptides Using Microwave-Assisted "Click Chemistry". *Organic Letters* **2010,** *12* (6), 1375-1376.

82. Norgren, A. S.; Budke, C.; Majer, Z.; Heggemann, C.; Koop, T.; Sewald, N., On-Resin Click-Glycoconjugation of Peptoids. *Synthesis-Stuttgart* **2009,** (3), 488-494.

83. Capicciotti, C. J.; Trant, J. F.; Leclère, M.; Ben, R. N., Synthesis of C-Linked Triazole-Containing AFGP Analogues and Their Ability to Inhibit Ice Recrystallization. *Bioconjugate Chemistry* **2011,** *22* (4), 605-616.

84. Deller, R. C.; Congdon, T.; Sahid, M. A.; Morgan, M.; Vatish, M.; Mitchell, D. A.; Notman, R.; Gibson, M. I., Ice recrystallisation inhibition by polyols: comparison of molecular and macromolecular inhibitors and role of hydrophobic units. *Biomaterials Science* **2013,** *1* (5), 478-485.

85. Capicciotti, C. J.; Leclere, M.; Perras, F. A.; Bryce, D. L.; Paulin, H.; Harden, J.; Liu, Y.; Ben, R. N., Potent inhibition of ice recrystallization by low molecular weight carbohydrate-based surfactants and hydrogelators. *Chemical Science* **2012,** *3* (5), 1408-1416.

86. Trant, J. F.; Biggs, R. A.; Capicciotti, C. J.; Ben, R. N., Developing highly active small molecule ice recrystallization inhibitors based upon C-linked antifreeze glycoprotein analogues. *RSC Advances* **2013,** *3* (48), 26005-26009.

87. Gibson, M. I.; Barker, C. A.; Spain, S. G.; Albertin, L.; Cameron, N. R., Inhibition of Ice Crystal Growth by Synthetic Glycopolymers: Implications for the Rational Design of Antifreeze Glycoprotein Mimics. *Biomacromolecules* **2009,** *10* (2), 328-333.

88. Inada, T.; Lu, S. S., Inhibition of recrystallization of ice grains by adsorption of poly(vinyl alcohol) onto ice surfaces. *Crystal Growth & Design* **2003,** *3* (5), 747-752; Lu, S. S.; Inada, T.; Yabe, A.; Zhang, X.; Grandum, S., Microscale study of poly(vinyl alcohol) as an effective additive for inhibiting recrystallization in ice slurries. *International Journal of Refrigeration-Revue Internationale Du Froid* **2002,** *25* (5), 562-568.

89. Inada, T.; Modak, P. R., Growth control of ice crystals by poly(vinyl alcohol) and antifreeze protein in ice slurries. *Chemical Engineering Science* **2006,** *61* (10), 3149-3158.

90. Inada, T.; Koyama, T.; Goto, F.; Seto, T., Ice Nucleation in Emulsified Aqueous Solutions of Antifreeze Protein Type III and Poly(vinyl alcohol). *Journal of Physical Chemistry B* **2011,** *115* (24), 7914-7922.

91. Inada, T.; Lu, S. S., Thermal hysteresis caused by non-equilibrium antifreeze activity of poly(vinyl alcohol). *Chemical Physics Letters* **2004,** *394* (4-6), 361-365.

92. Gibson, M. I., Slowing the growth of ice with synthetic macromolecules: beyond antifreeze(glyco) proteins. *Polymer Chemistry* **2010,** *1* (8), 1141-1152.

93. Budke, C.; Koop, T., Ice recrystallization inhibition and molecular recognition of ice faces by poly(vinyl alcohol). *Chemphyschem* **2006,** *7* (12), 2601-2606.

94. Li, H.; Zhang, W.; Xu, W.; Zhang, X., Hydrogen Bonding Governs the Elastic Properties of Poly(vinyl alcohol) in Water: Single-Molecule Force Spectroscopic Studies of PVA by AFM. *Macromolecules* **2000,** *33* (2), 465-469.

95. Atanase, L. I.; Riess, G., Thermal Cloud Point Fractionation of Poly (vinyl alcohol-co-vinyl acetate): Partition of Nanogels in the Fractions. *Polymers* **2011,** *3* (3), 1065-1075.

96. Wang, H.-Y.; Inada, T.; Funakoshi, K.; Lu, S.-S., Inhibition of nucleation and growth of ice by poly(vinyl alcohol) in vitrification solution. *Cryobiology* **2009,** *59* (1), 83-89.

97. Deller, R. C.; Vatish, M.; Mitchell, D. A.; Gibson, M. I., Synthetic polymers enable non-vitreous cellular cryopreservation by reducing ice crystal growth during thawing. *Nature Communications* **2014,** *5*, DOI:10.1038/ncomms4244.

98. Lv, J.; Song, Y.; Jiang, L.; Wang, J., Bio-Inspired Strategies for Anti-Icing. *ACS Nano* **2014,** *8* (4), 3152-3169.

99. .

100. Funakoshi, K.; Inada, T.; Tomita, T.; Kawahara, H.; Miyata, T., Thermal hysteresis induced by ammonium polyacrylate as antifreeze polymer. *Journal of Crystal Growth* **2008,** *310* (14), 3342-3347.

101. Baruch, E.; Mastai, Y., Antifreeze Properties of Polyglycidol Block Copolymers. *Macromolecular Rapid Communications* **2007,** *28* (23), 2256-2261.

102. Mastai, Y.; Rudloff, J.; Cölfen, H.; Antonietti, M., Control over the Structure of Ice and Water by Block Copolymer Additives. *ChemPhysChem* **2002,** *3* (1), 119-123.

103. Deville, S.; Viazzi, C.; Guizard, C., Ice-Structuring Mechanism for Zirconium Acetate. *Langmuir* **2012,** *28* (42), 14892-14898.

104. Szwarc, M.; Levy, M.; Milkovich, R., Polymerization Initiated by Electron Transfer to Monomer. A New Method of Formation of Block Polymers. *Journal of the American Chemical Society* **1956,** *78* (11), 2656-2657.

105. Szwarc, M., `Living' Polymers. *Nature* **1956,** *178* (4543), 1168-1169.

106. Higashimura, T.; Kishiro, O., Possible Formation of Living Polymers of p-Methoxystyrene by Iodine. *Polymer Journal* **1977,** *9* (1), 87-93.

107. Hawker, C. J., Molecular Weight Control by a "Living" Free-Radical Polymerization Process. *Journal of the American Chemical Society* **1994,** *116* (24), 11185-11186.

108. Matyjaszewski, K.; Gaynor, S.; Wang, J.-S., Controlled Radical Polymerizations: The Use of Alkyl Iodides in Degenerative Transfer. *Macromolecules* **1995,** *28* (6), 2093-2095.

109. Chiefari, J.; Chong, Y. K.; Ercole, F.; Krstina, J.; Jeffery, J.; Le, T. P. T.; Mayadunne, R. T. A.; Meijs, G. F.; Moad, C. L.; Moad, G.; Rizzardo, E.; Thang, S. H., Living free-radical polymerization by reversible addition-fragmentation chain transfer: The RAFT process. *Macromolecules* **1998,** *31* (16), 5559-5562.

110. Moad, G.; Chiefari, J.; Chong, Y. K.; Krstina, J.; Mayadunne, R. T. A.; Postma, A.; Rizzardo, E.; Thang, S. H., Living free radical polymerization with reversible addition-fragmentation chain transfer (the life of RAFT). *Polymer International* **2000,** *49* (9), 993-1001.

111. Nicolas, J.; Guillaneuf, Y.; Lefay, C.; Bertin, D.; Gigmes, D.; Charleux, B., Nitroxide-mediated polymerization. *Progress in Polymer Science* **2013,** *38* (1), 63-235.

112. Barner-Kowollik, C.; Davis, T. P.; Stenzel, M. H., Synthesis of Star Polymers using RAFT Polymerization: What is Possible? *Australian Journal of Chemistry* **2006,** *59* (10), 719-727.

113. Nguyen, T. L. U.; Eagles, K.; Davis, T. P.; Barner-Kowollik, C.; Stenzel, M. H., Investigation of the influence of the architectures of poly(vinyl pyrrolidone) polymers made via the reversible addition–fragmentation chain transfer/macromolecular design via the interchange of xanthates mechanism on the stabilization of suspension polymerizations. *Journal of Polymer Science Part A: Polymer Chemistry* **2006,** *44* (15), 4372-4383.

114. Barner, L.; Davis, T. P.; Stenzel, M. H.; Barner-Kowollik, C., Complex Macromolecular Architectures by Reversible Addition Fragmentation Chain Transfer Chemistry: Theory and Practice. *Macromolecular Rapid Communications* **2007,** *28* (5), 539-559.

115. Tong, Y.-Y.; Wang, R.; Xu, N.; Du, F.-S.; Li, Z.-C., Synthesis of Well-Defined Azide-Terminated Poly(vinyl alcohol) and Their Subsequent Modification via Click Chemistry. *Journal of Polymer Science Part a-Polymer Chemistry* **2009,** *47* (18), 4494-4504.

116. Biggs, C. I.; Edmondson, S.; Gibson, M. I., Thiol-ene immobilisation of carbohydrates onto glass slides as a simple alternative to gold-thiol monolayers, amines or lipid binding. *Biomaterials Science* **2015,** *3* (1), 175-181.

117. Phillips, D. J.; Davies, G.-L.; Gibson, M. I., Siderophore-inspired nanoparticle-based biosensor for the selective detection of Fe3+. *Journal of Materials Chemistry B* **2015,** *3* (2), 270-275.

118. Skey, J.; O'Reilly, R. K., Facile one pot synthesis of a range of reversible addition-fragmentation chain transfer (RAFT) agents. *Chemical Communications* **2008,** (35), 4183-4185.

119. Benaglia, M.; Chiefari, J.; Chong, Y. K.; Moad, G.; Rizzardo, E.; Thang, S. H., Universal (Switchable) RAFT Agents. *Journal of the American Chemical Society* **2009,** *131* (20), 6914-6915.

120. Perrier, S.; Takolpuckdee, P., Macromolecular design via reversible addition–fragmentation chain transfer (RAFT)/xanthates (MADIX) polymerization. *Journal of Polymer Science Part A: Polymer Chemistry* **2005,** *43* (22), 5347-5393.

121. Klumperman, B.; van den Dungen, E. T. A.; Heuts, J. P. A.; Monteiro, M. J., RAFT-Mediated Polymerization—A Story of Incompatible Data? *Macromolecular Rapid Communications* **2010,** *31* (21), 1846-1862.

122. Moad, G.; Rizzardo, E.; Thang, S. H., Living radical polymerization by the RAFT process. *Australian Journal of Chemistry* **2005,** *58* (6), 379-410.

123. Peng, C.-H.; Scricco, J.; Li, S.; Fryd, M.; Wayland, B. B., Organo-Cobalt Mediated Living Radical Polymerization of Vinyl Acetate. *Macromolecules* **2008,** *41* (7), 2368-2373.

124. Debuigne, A.; Caille, J.-R.; Willet, N.; Jérôme, R., Synthesis of Poly(vinyl acetate) and Poly(vinyl alcohol) Containing Block Copolymers by Combination of Cobalt-Mediated Radical Polymerization and ATRP. *Macromolecules* **2005,** *38* (23), 9488-9496.

125. David, G.; Boyer, C.; Tonnar, J.; Ameduri, B.; Lacroix-Desmazes, P.; Boutevin, B., Use of Iodocompounds in Radical Polymerization. *Chemical Reviews* **2006,** *106* (9), 3936-3962.

126. Yamago, S.; Ray, B.; Iida, K.; Yoshida, J.-i.; Tada, T.; Yoshizawa, K.; Kwak, Y.; Goto, A.; Fukuda, T., Highly Versatile Organostibine Mediators for Living Radical Polymerization. *Journal of the American Chemical Society* **2004,** *126* (43), 13908-13909.

127. Paik, H.-j.; Teodorescu, M.; Xia, J.; Matyjaszewski, K., Block Copolymerizations of Vinyl Acetate by Combination of Conventional and Atom Transfer Radical Polymerization. *Macromolecules* **1999,** *32* (21), 7023-7031.

128. Harrisson, S.; Liu, X.; Ollagnier, J.-N.; Coutelier, O.; Marty, J.-D.; Destarac, M., RAFT Polymerization of Vinyl Esters: Synthesis and Applications. *Polymers* **2014,** *6* (5), 1437-1488.

129. Fischer, H.; Radom, L., Factors Controlling the Addition of Carbon-Centered Radicals to Alkenes—An Experimental and Theoretical Perspective. *Angewandte Chemie International Edition* **2001,** *40* (8), 1340-1371.

130. DeMerlis, C. C.; Schoneker, D. R., Review of the oral toxicity of polyvinyl alcohol (PVA). *Food and Chemical Toxicology* **2003,** *41* (3), 319-326.

131. Nagara, Y.; Nakano, T.; Okamoto, Y.; Gotoh, Y.; Nagura, M., Properties of highly syndiotactic poly(vinyl alcohol). *Polymer* **2001,** *42* (24), 9679-9686.

132. Moad, G.; Solomon, D. H., 6 - Chain Transfer. In *The Chemistry of Radical Polymerization (Second Edition)*, Solomon, D. H., Ed. Elsevier Science Ltd: Amsterdam, 2005; pp 279-331.

133. Flory, P. J.; Leutner, F. S., Occurrence of head-to-head arrangements of structural units in polyvinyl alcohol. *Journal of Polymer Science* **1948,** *3* (6), 880-890.

134. Britton, D.; Heatley, F.; Lovell, P. A., Chain Transfer to Polymer in Free-Radical Bulk and Emulsion Polymerization of Vinyl Acetate Studied by NMR Spectroscopy. *Macromolecules* **1998,** *31* (9), 2828-2837.

135. Dufils, P. E.; David, G.; Boutevin, B.; Woodward, G.; Otter, G.; Guinaudeau, A.; Mazières, S.; Destarac, M., Phosphonate-terminated poly(vinyl acetate) synthesized by RAFT/MADIX polymerization. *Journal of Polymer Science Part A: Polymer Chemistry* **2012,** *50* (10), 1997-2007.

136. Zhao, F.; Mahdavian, A.; Teimouri, M.; Daniels, E.; Klein, A.; El-Aasser, M., RAFT-mediated emulsion polymerization of vinyl acetate: a challenge towards producing high molecular weight poly(vinyl acetate). *Colloid and Polymer Science* **2012,** *290* (13), 1247-1255.

137. Stenzel, M. H.; Cummins, L.; Roberts, G. E.; Davis, T. P.; Vana, P.; Barner-Kowollik, C., Xanthate mediated living polymerization of vinyl acetate: A systematic variation in MADIX/RAFT agent structure. *Macromolecular Chemistry and Physics* **2003,** *204* (9), 1160-1168.

138. Stenzel, M. H.; Davis, T. P.; Barner-Kowollik, C., Poly(vinyl alcohol) star polymers prepared via MADIX/RAFT polymerisation. *Chemical Communications* **2004,** (13), 1546-1547.

139. Bernard, J.; Favier, A.; Zhang, L.; Nilasaroya, A.; Davis, T. P.; Barner-Kowollik, C.; Stenzel, M. H., Poly(vinyl ester) star polymers via xanthate-mediated living radical polymerization: From poly(vinyl alcohol) to glycopolymer stars. *Macromolecules* **2005,** *38* (13), 5475-5484.

140. Bernard, J.; Favier, A.; Davis, T. P.; Barner-Kowollik, C.; Stenzel, M. H., Synthesis of poly(vinyl alcohol) combs via MADIX/RAFT polymerization. *Polymer* **2006,** *47* (4), 1073-1080.

141. Bailly, N.; Pound-Lana, G.; Klumperman, B., Synthesis, Characterization, and Self-Assembly of Poly(N-vinylpyrrolidone)-block-poly(vinyl acetate). *Australian Journal of Chemistry* **2012,** *65* (8), 1124-1131.

142. Shim, S.-H.; Ham, M.-k.; Huh, J.; Kwon, Y.-K.; Kwark, Y.-J., Simultaneous control over the molecular weight and tacticity of poly(vinyl acetate) using a low-temperature photoinitiated RAFT process in fluoroalcohols. *Polymer Chemistry* **2013,** *4* (21), 5449-5455.

143. Smith, A. A. A.; Hussmann, T.; Elich, J.; Postma, A.; Alves, M.-H.; Zelikin, A. N., Macromolecular design of poly(vinyl alcohol) by RAFT polymerization. *Polymer Chemistry* **2012,** *3* (1), 85-88.

Chapter 2

Synthesis and Ice Recrystallisation Inhibition Activity of PVA and PVA Co-polymers

---

2.1 Chapter Overview

This chapter describes a detailed study into the structural basis of the inhibition of ice crystal growth by poly(vinyl alcohol). A brief review of the literature is presented, highlighting the key points and difficulties with analysing the IRI activity of PVA. To obtain quantitative structure–activity relationships it is necessary to use a controlled polymerisation technique which ensures polymers with predictable molecular weights and narrow Đ are obtained. To ensure homogeneity a method that achieves quantitative hydrolysis of the acetate groups must also be employed. The results section details the preparation of a range of RAFT/MADIX chain transfer agents known for their ability to mediate vinyl acetate polymerisations were tested and the agent which best afforded control over the molecular weight, dispersity, and with the lowest inhibition time was selected. Using this optimised synthetic protocol a library of polymers was prepared and IRI activity was tested using the 'splat' assay. The results showed that, for high molecular weight polymers, the IRI activity was very high; in line with previous reports. Additionally, low molecular weight polymers and PVA oligomers displayed surprisingly similar IRI activity to the high molecular weight polymers. Most interestingly, it was observed that the IRI of PVA with 20 repeat units is highly active, whereas PVA with 10 repeat units displays

almost no activity. The effect of residual acetate functionality was also examined, as this has not been previously explored systematically. High molecular weight PVA was prepared and from this exemplar polymer a range of acetate functionalised polymers was prepared *via* acid catalysis. It was discovered that a sharp decrease in activity occurs when acetate functionality exceeds 20 mol %. Using the same RAFT/MADIX scheme, *N*-vinyl pyrrolidone (NVP) was polymerised first as a homopolymer and then as a co-polymer with PVA. There were conflicting reports on the IRI activity of poly(vinyl pyrrolidone) (PVP), but testing confirmed that PVP does have an effect on crystal morphology in the splat assay, but no IRI activity. From these results it was postulated that hydroxyl groups are essential for potent IRI activity. To this end, isopropenyl acetate was polymerised as a homopolymer and co-polymer. This monomer would afford an unbroken sequence of hydroxyl groups, but with an increased hydrophobic component from the methyl group. Preparation and solubility issues meant that only a few examples could be tested. Despite this, comparable activity to homo-PVA was observed. This results show that the IRI activity of PVA is dependent on molecular weight, and intolerance to functional group changes, but when the hydroxyl sequence is maintained activity is preserved.

2.2 Chapter Introduction

Controlling ice growth in frozen media would open up many applications for the long term storage of biological material,[1] and would address the issue of unwanted ice growth for a number of additional real world problems.[2] Currently poly(vinyl alcohol) (PVA) has been shown to be the most potent synthetic macromolecule capable of inhibiting ice growth.[3, 4] Antifreeze proteins and antifreeze glycoproteins display strong ice shaping ability - a detrimental effect causing needle-like ice growth that has been shown to increase cryoinjury,[5] but PVA only affects ice growth; it displays no dynamic ice shaping or thermal hysteresis.[6] PVA is a commodity material manufactured on the multi tonne scale, allowing easy access to a range of different formulations. In addition, PVA also has FDA approval for use in many *in vivo* applications; one of the first applications of PVA finds use as an emergency suture, and it is currently used in a range of medical devices.[7, 8]

However the underlying mechanisms that govern the anomalously high activity of PVA are unknown. Deller *et al.* showed that hydroxyl group concentration is not a factor in activity.[9] Polymer size correlates roughly with an increase in activity,[10] but this is far from proven, and the role (if any) of residual acetate functionality on the polymer is not understood.[11] This is in part due to previous studies using poorly defined materials; commercially available PVA is a highly disperse material comprising of a huge range of molecular weights.

Controlled radical polymerisation, where the random radical propagation reactions of vinyl monomers is controlled by a range of additives, has seen huge progress in terms of understanding and new technologies being designed and discovered. Using this, a truly systematic analysis of the various physical properties of PVA can be

conducted, but due to the nature of vinyl acetate (the monomeric precursor of PVA) as a lesser activated monomer (LAM), comparatively little research has been done into its controlled radical polymerisation. Nevertheless, a range of viable technologies exist, namely MADIX agents; xanthates that are similar in structure to the more well-known RAFT agents. Stenzel and co-workers have published a number of reports on the most efficient MADIX agents to use to control the polymerisation of vinyl acetate.[12] This system has so far been shown to be the best for controlling the radical polymerisation of vinyl acetate, with other popular systems producing inferior polymers,[13] or requiring very long polymerisation times.[14] For this reason it was decided to use MADIX to produce a library of well-defined polymers and then subsequently test their IRI activities. This approach would afford some insight into the mechanisms that govern the anomalously high IRI activity of PVA.

2.3 Results

2.3i The Synthesis of PVA Homopolymers

In order to gain greater insight into the structure-property relationships that govern the IRI activity of PVA, the effect of molecular weight needed to be examined in greater detail. Controlled radical polymerisation techniques allow access to predictable molecular weights with narrow dispersity. Of all the techniques currently available, a RAFT/MADIX system has been shown to be the most efficient mediator of the radical polymerisation of vinyl acetate. Stenzel and co-workers tested a range of MADIX agents and determined that an *o*-ethoxy functional MADIX agent was the most suitable, with an *o*-isopropoxy functional agent a close second in terms of rate

of conversion and control of dispersity of the resultant polymer.[12] The *o*-isopropoxy MADIX agent was trialled as a potentially more suitable mediator for the polymerisation of low molecular weight polymers, but this was unsuccessful due to long inhibition times. For vinyl acetate, radical chain transfer ('R'-group) functionality does not seem to affect polymerisation kinetics. After initially using a methyl ethanoate 'R' group a second agent was prepared using a benzyl 'R 'group, (Figure 2.1) as this is easily distinguished in ^{1}H NMR spectra and can be used for end-group analysis.

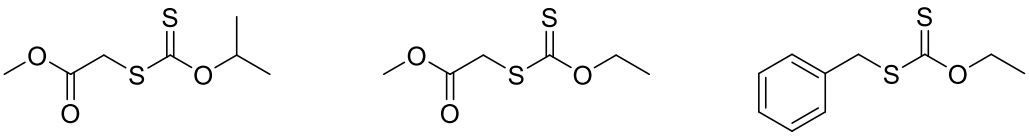

Figure 2.1 MADIX agents synthesised.

Synthesis of these MADIX agents was very straightforward. Potassium ethyl xanthate can be prepared *in situ via* the reaction of ethanol with carbon disulfide to form potassium ethyl xanthate, followed by the nucleophilic attack on either benzyl bromide or methyl bromoacetate. This forms the desired chain transfer agent (CTA) in good yield, typically 40 - 50 % after purification. (Scheme 2.1). Alternatively, potassium ethyl xanthate can be purchased and used directly instead of generating the xanthate *in situ*, which improved the yield by 10 %.

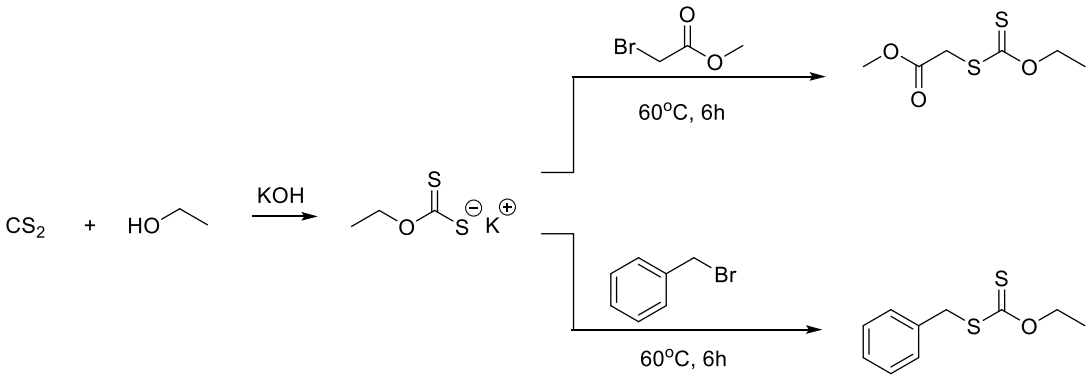

Scheme 2.1 Synthesis of MADIX agents.

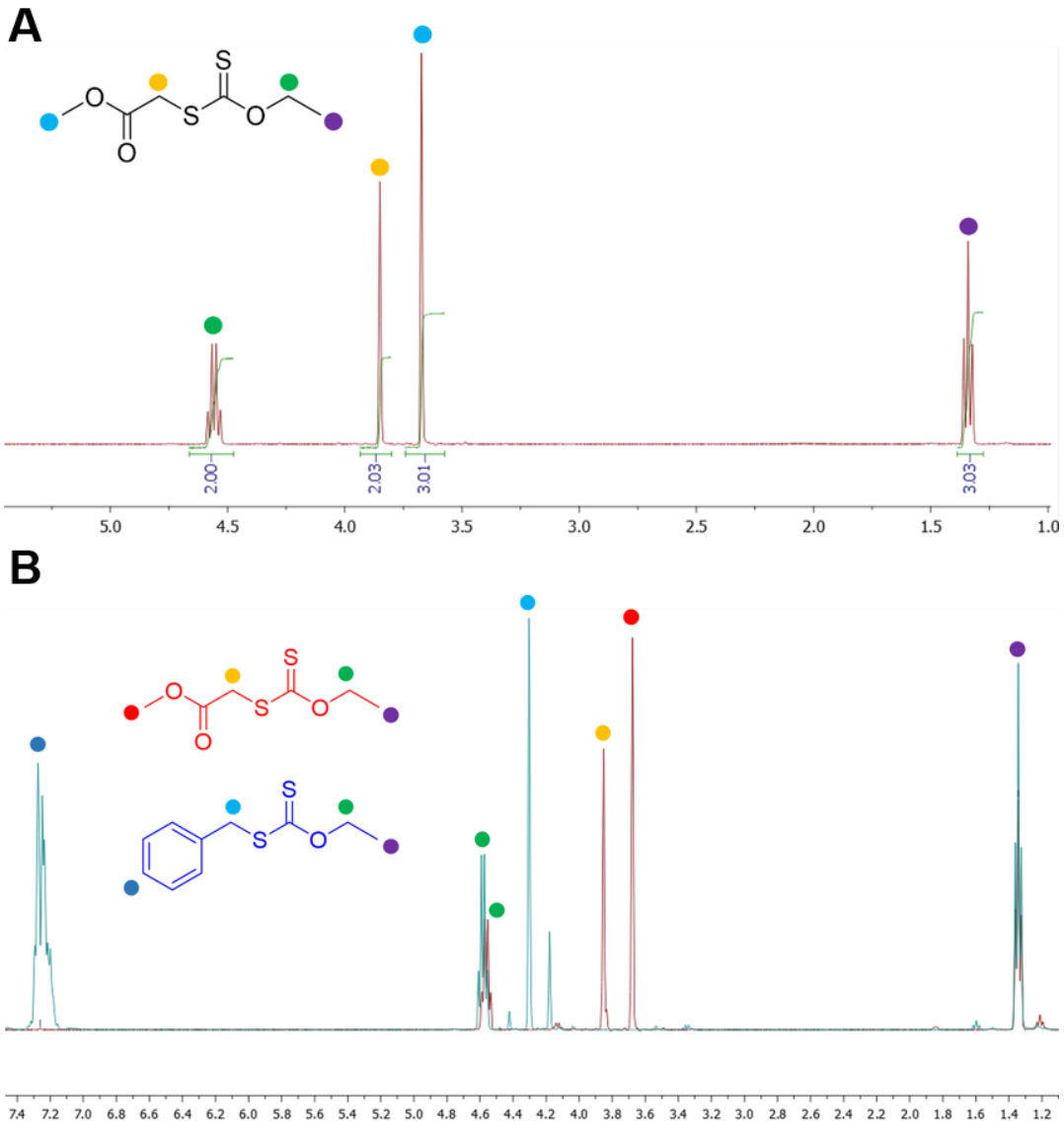

Figure 2.2 A ^{1}H NMR spectrum of **MADIX 2 B** Comparison ^{1}H NMR spectra of **MADIX 2** and **MADIX 3**.

MADIX agents could be isolated by first removing the reaction solvent *in vacuo* then dissolving the residue in dichloromethane (DCM) and washing with water and brine, and then by column chromatography using a small plug of silica and eluting with hexane:methanol 99:1. If commercial potassium ethyl xanthate was used then further purification using column chromatography was rarely necessary (Figure 2.2). Purity of the compound was confirmed by a single spot on the TLC plate.

Trial polymerisations did not start to propagate until several hours after initiation. This behaviour initially thwarted attempts to gather kinetic data or quench reactions at lower conversions to access low molecular weight polymers. Stenzel and co-workers also reported inhibition times; a period of time after initiation where no polymer growth was observed. The inhibition time was proportional to both the concentration of the MADIX agent and the type of MADIX agent used, and was not linked to the 'R' group, ruling out differences in reinitiation kinetics.

It was found that agents which afforded lower rates of propagation tended to have longer inhibition times. The *type* of MADIX agent used affects inhibition time, which suggests that this might not be caused by an unknown impurity in the MADIX agent. The radical initiator could be forming a pre-initiation, stable intermediate with the MADIX agent that needs to re-fragment before propagation can occur. However, recently in the work it was found that when the MADIX agent was passed through a plug of basic alumina immediately prior to use, no inhibition time is observed at any concentration of CTA.

The reasons for this are still not entirely clear. When left in the fridge for extended periods of time (several months) a slight precipitate forms. Even more confusingly, when the filtered MADIX agent is left, the inhibition period is again observed, and

previously successful polymerisation reaction procedures no longer produce polymer on the same timescales. All these results suggest that a small percentage of the MADIX agent is slowly degrading over time into something that inhibits radical activity in the system. This, however, proved not to be too much of an issue. Targeting specific molecular weights by varying the monomer/MADIX agent ratio, and allowing the polymerisations to run to 80 % conversion led to a library of linear PVAc polymers with the desired narrow molecular weight ranges being prepared (Scheme 2.2).

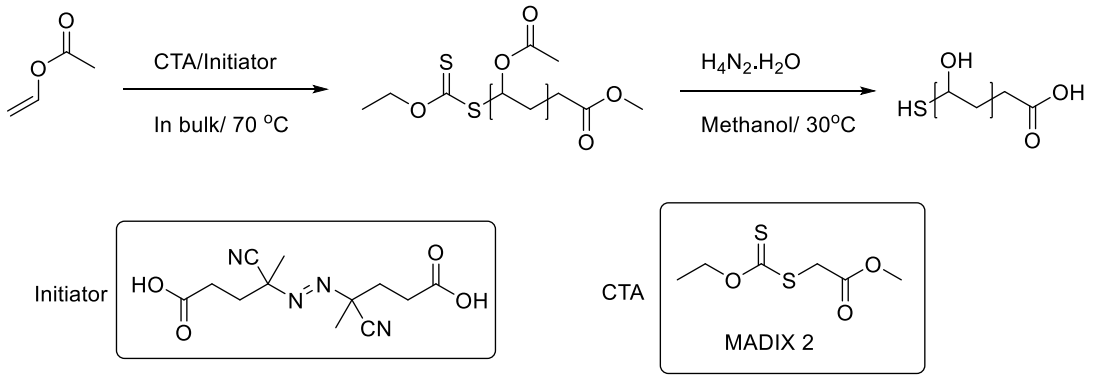

Scheme 2.2 MADIX mediated polymerisation of vinyl acetate to poly(vinyl acetate), and the subsequent conversion to poly(vinyl alcohol) using hydrazine hydrate solution.

Polymerisations were conducted either in bulk or in solution providing that 1,4-dioxane is used as a solvent. The reduced monomer concentration for polymerisation conducted in solutions slowed the propagation of the reaction, so unless it was necessary all polymerisations were conducted in bulk.

The kinetics of the reaction were determined by setting up a standard azo-initiated radical polymerisation of vinyl acetate, with [VAc]:[**MADIX 2**] in a 100:1 molar ratio and initiator in a [VAc]:[ACVA] 1000:1 molar ratio. The solution was de-gassed for 10 minutes by bubbling through N_2, and was then allowed to polymerise

at 68 °C. Aliquots were taken at various time intervals. The aliquots were then quenched using liquid nitrogen, conversion determined by ^{1}H NMR spectroscopy, and then the polymer isolated and analysed using size exclusion chromatography (SEC) in tetrahydrofuran (THF). As expected with a controlled radical process, conversion was high, polydispersity was low, and first-order kinetics were observed (Figure 2.3) with an increase in molecular weight proceeding linearly with conversion (Figure 2.4). First-order kinetic plots and a linear increase in $Ln([M]_0/[M])$ indicate that radical concentration did not fluctuate during the polymerisation, showing that the MADIX agent was effectively meditating the polymerisation reaction.

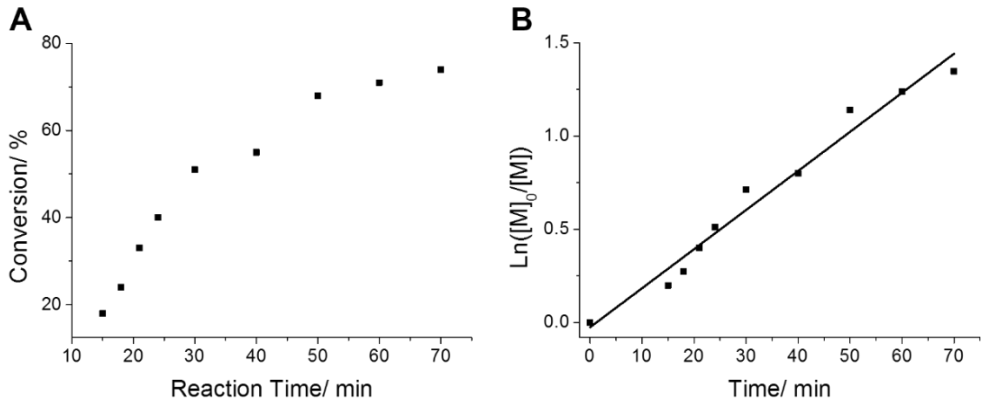

Figure 2.3 A Time dependent monomer conversion of the polymerisation of vinyl acetate mediated by MADIX 2. **B** Pseudo first order kinetic plot.

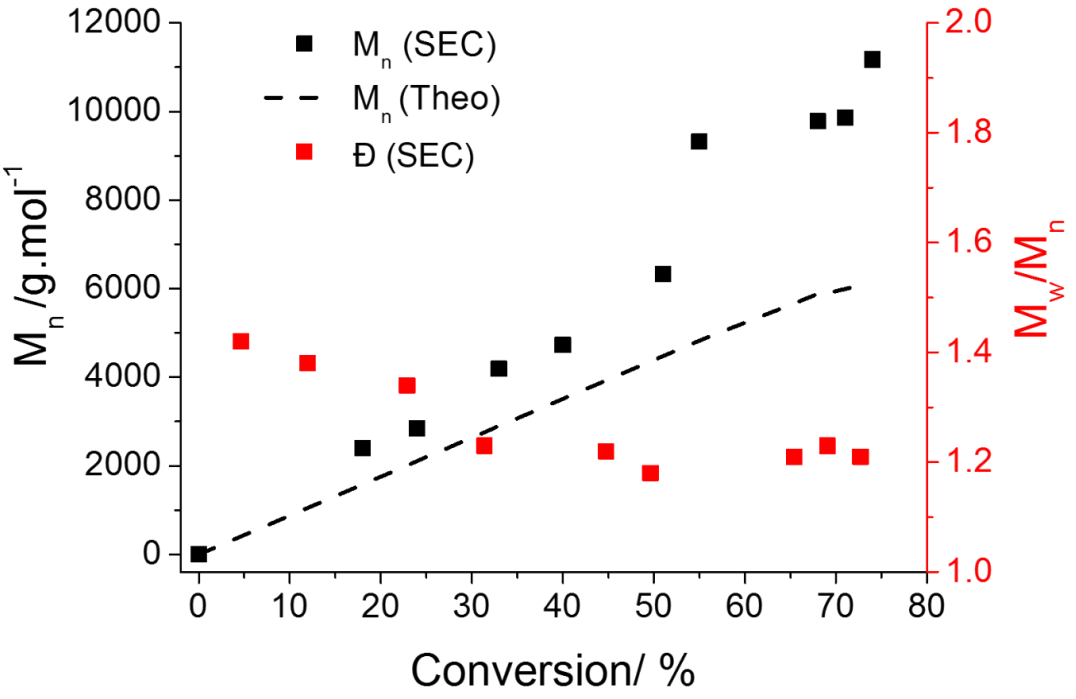

Figure 2.4 Polymerisation of vinyl acetate mediated by **MADIX 2**. M_n (Theo) determined from conversion by ^{1}H NMR spectroscopy.

Conversion of monomer to polymer generally ceased after approximately 80 % conversion. At this stage the viscosity of the solution increases to the point where the kinetic assumptions about reactions in solution break down, and the polymerisation can auto-accelerate; also known as the Trommsford-Norrish effect, this arrises due to the increase in viscosity. The rate of termination is lowered, causing a rapid increase in the rate of propagation. In the case of vinyl acetate it appears that when the bulk viscosity reached this point, all radical activity ceased. Allowing polymerisations to proceed to high conversion is generally unfavourable as it causes a loss of end-group fidelity, which is most observable in the discrepancy between the perceived molecular weight by ^{1}H NMR spectroscopic analysis and SEC.

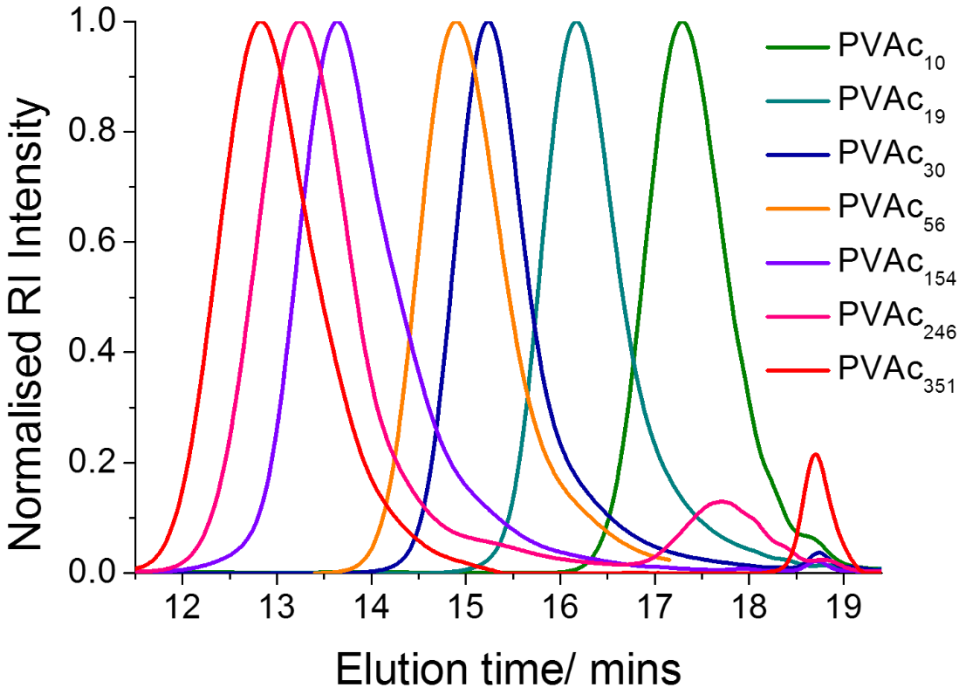

Figure 2.5 A selection of SEC traces for poly(vinyl acetate) samples in THF prepared in this study.

Resulting polymers were then isolated by removal of monomer *in vacuo* or by evaporation of the residual monomer with compressed air followed by precipitation in hexane. Molecular weight distributions were subsequently determined by SEC in THF (Figure 2.5). Poly(vinyl acetate) samples prepared for this study are detailed below (Table 2.1). These polymers were hydrolysed and their IRI activity tested (*vide infra*).

Table 2.1 PVAc homopolymers prepared for this study, and the corresponding PVA.

Entry	[M]/ [CTA][a]	Conv[b] %	$M_{n,}$[theo c] $g.mol^{-1}$	$M_{n,}$[NMR d] $g.mol^{-1}$	$M_{n,}$[SEC e] $g.mol^{-1}$	M_w/M_n [e]	DP_n[f]	PVA [g]
$PVAc_{10}$	10	83.2	716	900	870	1.18	10	**PVA_{10}**
$PVAc_{19}$	20	95.3	1640	1640	1700	1.18	19	**PVA_{19}**
$PVAc_{25}$	30	85.2	2200	2200	2320	1.21	25	**PVA_{25}**
$PVAc_{30}$	50	60.0	2582	2580	2700	1.45	30	**PVA_{30}**
$PVAc_{56}$	100	54.7	4709	4700	5100	1.23	56	**PVA_{56}**
$PVAc_{154}$	200	73.8	12706	12700	13800	1.45	154	**PVA_{154}**
$PVAc_{246}$	300	80.1	25687	20660	21700	1.39	246	**PVA_{246}**
$PVAc_{351}$	500	68.8	29615	29600	30900	1.28	351	**PVA_{351}**

A Monomer to RAFT agent ratio. **B** Determined by ^{1}H NMR spectroscopy. **C** Theoretical M_n determined from monomer to RAFT agent ratio. **D** Determined by ^{1}H NMR spectroscopy. **E** Determined by SEC in THF using PMMA standards. **F** Number-average degree of polymerisation determined by SEC. **G** Corresponding PVA prepared by hydrazinolysis of the respective PVAc precursor.

Procedures to hydrolyse PVAc to PVA are well known. Convention in the literature tends to favour basic hydrolysis, either using concentrated potassium hydroxide solution, or hydrazine hydrate solution. In theory, utilising potassium hydroxide solution might seem ideal, however in practice hydrazine hydrate solution proved to be better as the hydrolysis is more efficient, taking as little as an hour at 60 °C. Concentrated hydrazine hydrate solutions are very safe to use, especially on the

small scale required by these reactions. In all cases of hydrazinolysis using hydrazine hydrate, complete removal of acetate groups is seen (Figure 2.6, Figure 2.7).

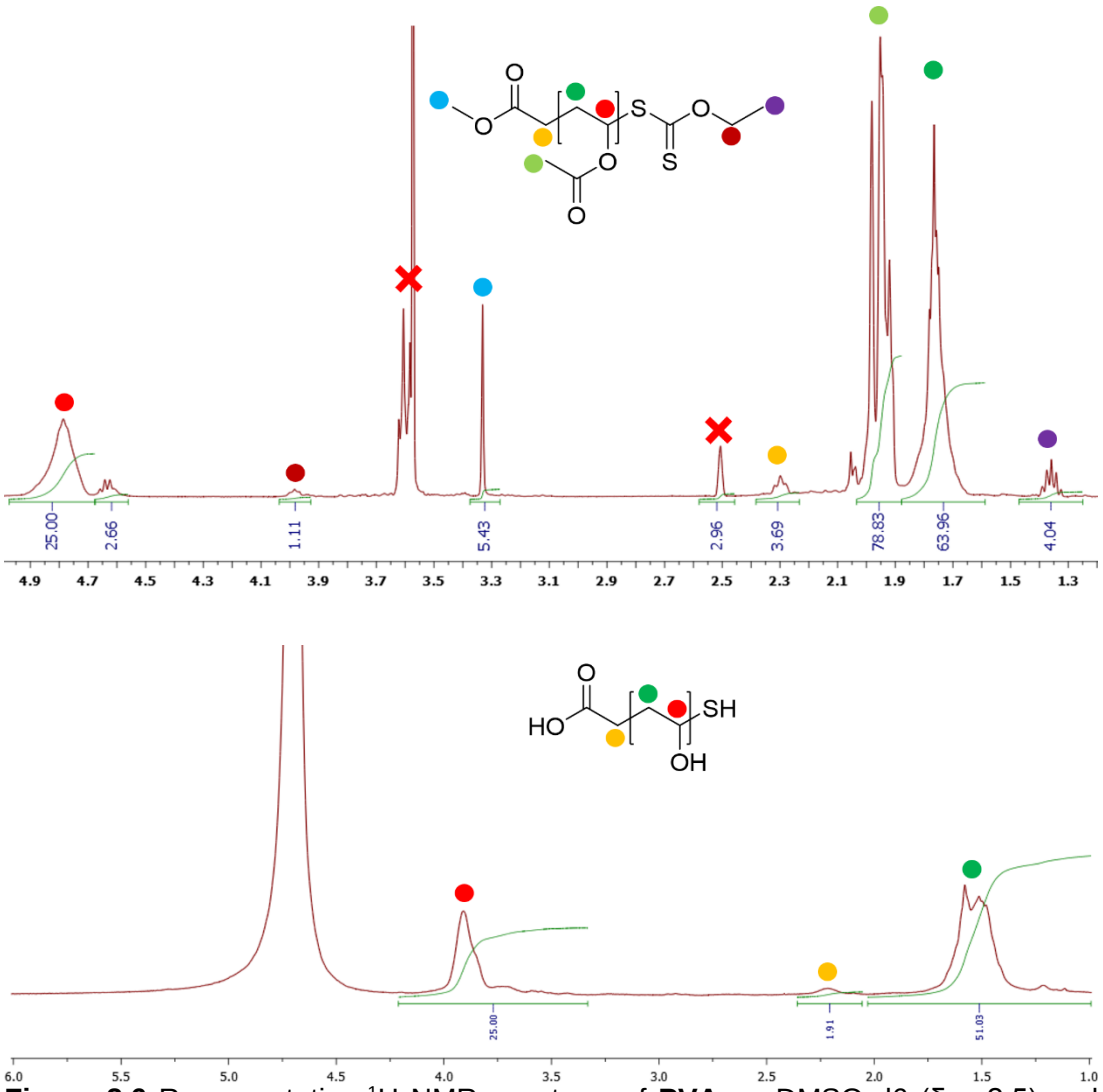

Figure 2.6 Representative ^{1}H NMR spectrum of **PVAc$_{25}$**. DMSO d6 (δ = 2.5) and residual THF and 1,4-dioxane (δ = 3.6-3.7) are marked with crosses. Representative ^{1}H NMR spectra of **PVA$_{25}$** in D_2O.

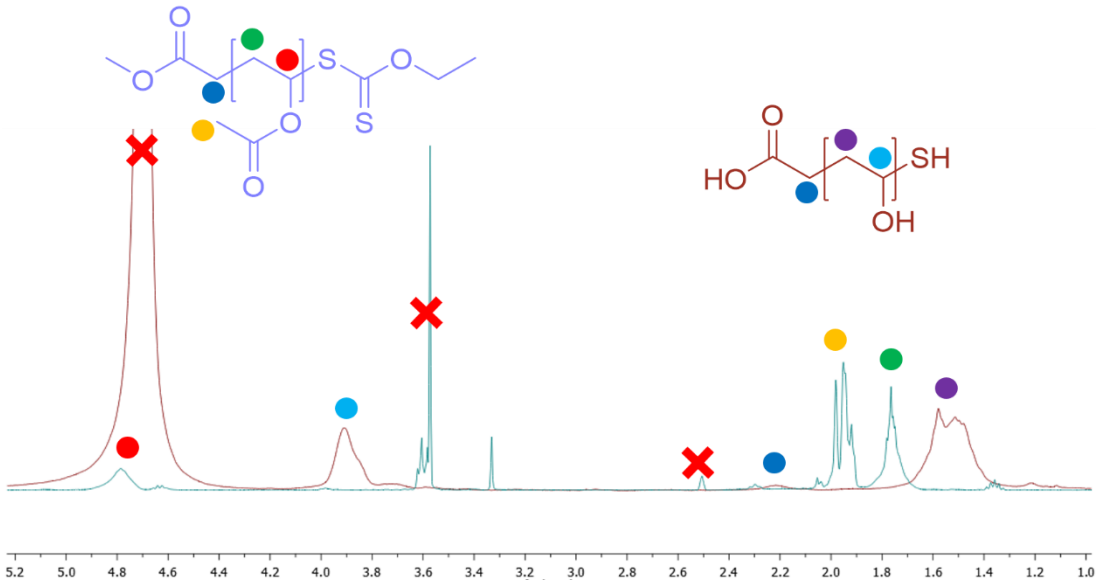

Figure 2.7 Comparison ^{1}H NMR showing conversion of PVAc to PVA.

2.3ii The IRI Activity of PVA Homopolymers

With fully hydrolysed, well defined PVAs in hand, the IRI activity of the polymers could be assessed. Knight *et al.* pioneered the use of the splat assay to measure the recrystallisation of ice in a range of solutions, and a modified version was employed in this study. In this assay a droplet of polymer-containing PBS solution is dropped from 1.4 m onto a glass microscope coverslip, which is on top of an aluminium plate cooled to -78 °C using dry ice. The droplet freezes instantly upon impact with the plate, spreading out and forming a thin wafer of ice. This wafer is then placed on a liquid nitrogen cooled cryostage held at - 8 °C. Photographs of the wafer at 20× zoom under cross polarisers are taken and then the wafer is left to anneal for 30 minutes at - 8 °C. Three photographs are taken of the wafer and a final photograph at 4× zoom is taken. These photographs are then analysed using ImageJ, a free image analysis software program, to determine crystal size, using a standard of 100 µm wide gold tracks printed on a glass slide. The largest 4 crystals from three 20×

photographs are measured and then averaged, and this average is then divided by the MLGS for PBS solution (138 µm). This gives as a percentage of growth compared to PBS, or the % MLGS.

The IRI 'splat' assay was carried out on the synthesised PVAs (see Table 2.1) over a range of concentrations (Figure 2.8, Figure 2.9). IRI activity was assayed at increasing dilutions until the % MLGS equalled that of PBS solution. This concentration dependent behaviour is shown in (Figure 2.10).

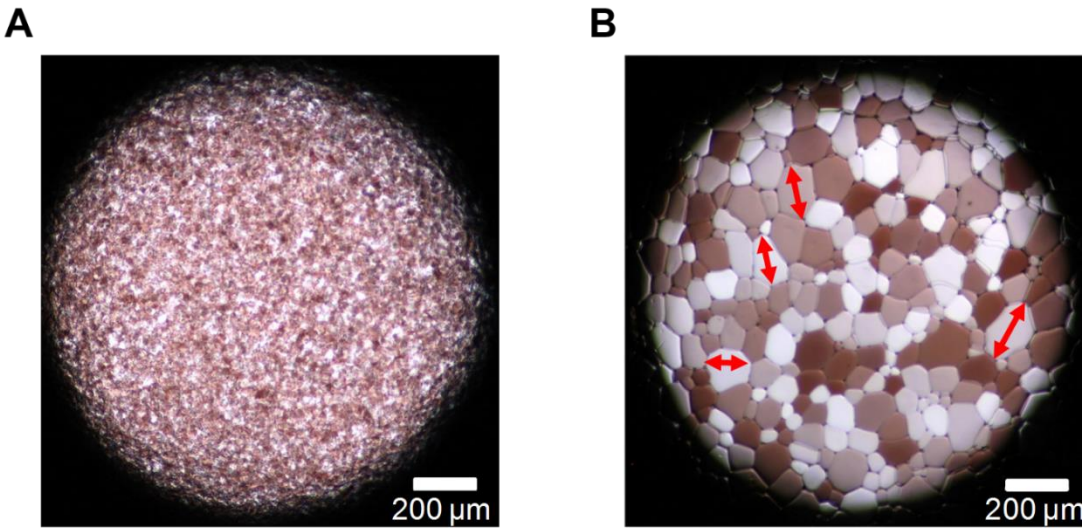

Figure 2.8 Representative Ice crystal micrographs of PBS solution. **A** After nucleation **B** After annealing for 30 minutes at - 8 °C.

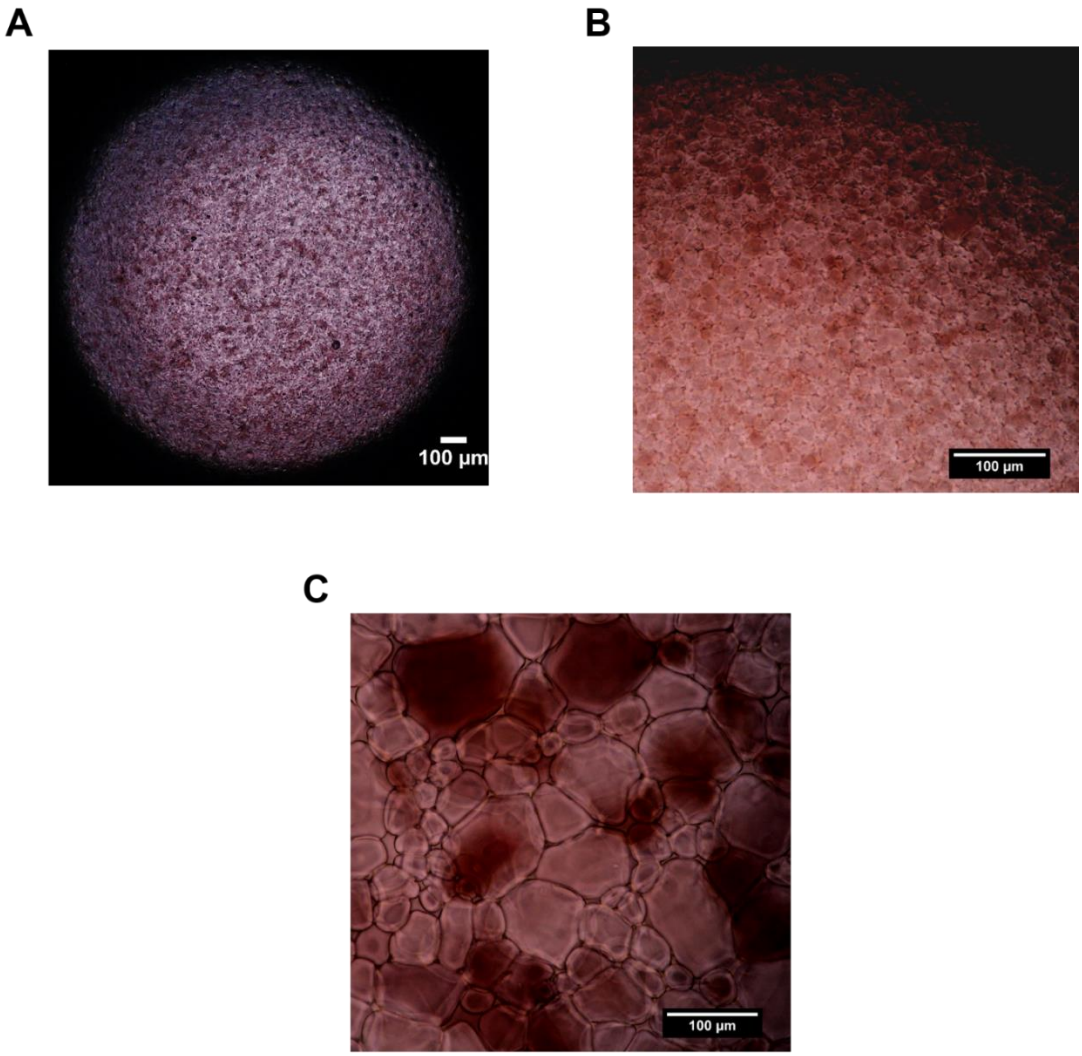

Figure 2.9 Representative Ice crystal micrographs of 1 mg.mL^{-1} **PVA_{20}** in PBS solution. **A** After annealing for 30 minutes at - 8 °C. **B** After annealing for 30 minutes at - 8 °C, at 20× magnification. **C** 0.25 mg.mL^{-1}. **PVA_{20}** in PBS solution, after annealing for 30 minutes at - 8 °C.

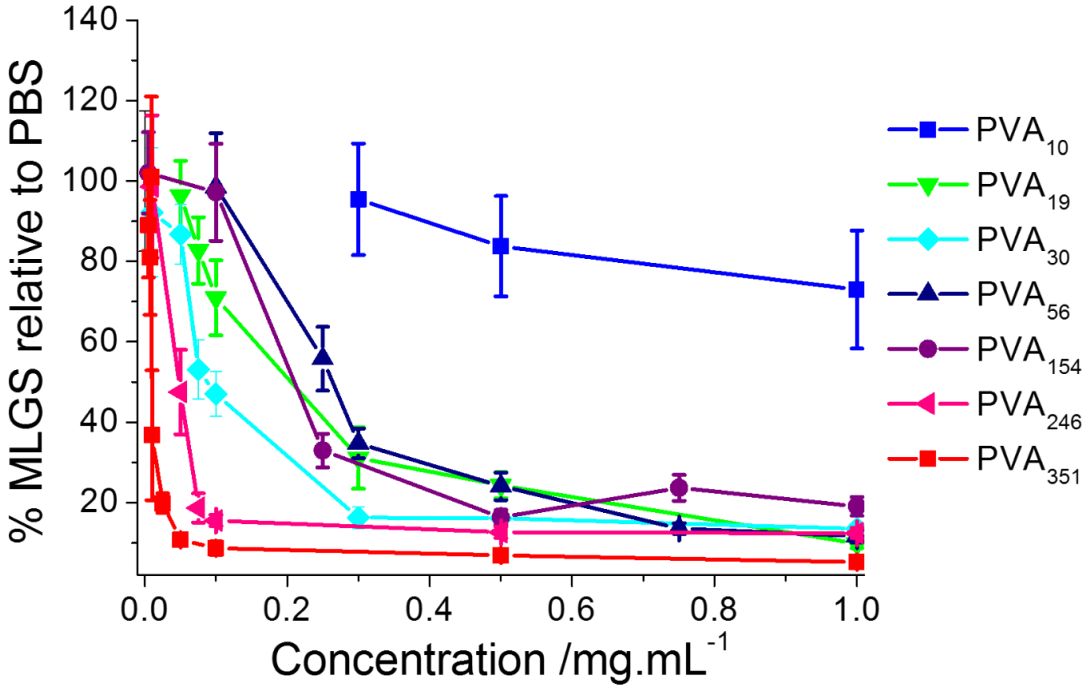

Figure 2.10 Ice recrystallisation inhibition activity of PVA homopolymers as measured by the splat assay. IRI activity as a function of polymer concentration. MLGS = mean largest grain size relative to a PBS control, expressed as %. Error bars represent the standard deviation from the 12 largest crystals.

As previously reported by Inada *et al.* there was a clear molecular weight dependence on the observed IRI activity, with the highest molecular weight polymers giving the most activity.[6] It can clearly be seen that as the degree of polymerisation of PVA increases from 10 to 19 units there is a significant increase in activity in the dilute concentration range assayed (see Figure 2.10). At 1.0 $mg.mL^{-1}$, **PVA_{10}** gives a MLGS of 80 % (relative to PBS), whereas **PVA_{19}** gives an MLGS of 20 %. Further increases in molecular weight display a steady increase in IRI activity, with PVA_{351} maintaining IRI activity at concentrations as low as 0.05 $mg.mL^{-1}$. On a molar basis, this is approximately 3.2 μM; this is comparable to the IRI activity of peptide-based AFGP analogues of Ben *et al.*, which typically retain IRI activity at μM concentrations.[15,16] Budke and Koop have stated that at least 6 to 8

units of PVA are necessary to bind to ice,[17] but this was only speculation. These results suggest that longer sequences are essential for activity, which itself may not be directly linked to ice-binding, but rather disruption of the quasi liquid layer at the ice/water interface or a combination of the two.[18] Larger polymers were not tested due to the limits of RAFT/MADIX polymerisation of deactivated monomers such as vinyl acetate,[19] and these results suggest that at high molecular weights activity has begun to plateau; there is little difference in the IRI activity of **PVA_{246}** compared to **PVA_{351}**.

Two major observations arose from this detailed examination of the effect of molecular weight on IRI activity. First was the 'cut off' concentration seen with the larger polymers; where over a small concentration range activity rapidly dropped off. The most striking observation was the difference in IRI activity between the **PVA_{10}** and **PVA_{19}**. Numerous small molecule poly-ols have been examined for IRI activity, many with a similar or greater number of hydroxyl groups to the oligomers tested here, but no activity change similar to the one in Figure 2.10 has been seen before. This result does lend credence to the theory behind a minimum hydroxyl sequence being an intrinsic factor in explaining the anomalously high IRI activity of PVA, compared to other poly-ols.

2.3iii The Synthesis of PVA-*rand*-PVAc Co-polymers

The results above reinforce the idea that a there is a minimum amount of hydroxyl functional groups required for PVA to display strong IRI activity. This could be due to one of two factors; (i) a minimum molecular weight (from these results, 840 $g.mol^{-1}$) is required before PVA displays high IRI activity; suggesting that activity is due to a conformation of the polymer in solution, only achievable above a specific

molecular weight. Or (ii) an uninterrupted sequence of hydroxyl groups is required before substantial IRI activity is displayed. This would suggest a direct interaction with a growing ice crystal face similar to antifreeze proteins, and reinforces the theories of Budke and Koop.[17]

In order to gain insight into this it was proposed that highly active PVA could be modified through post polymerisation modification to randomly 'block' hydroxyl groups, thereby disrupting the sequence of uninterrupted hydroxyl groups. This was achievable by simply reintroducing acetate groups.

As stated before, previous studies of the IRI activity of PVA have focused on using commercially available samples which, in addition to being highly disperse, also have varying degrees of acetate hydrolysis - typically from 80 % to 95 % of the repeat units. A truly systematic study of the effect of degree of acetate functionality has never been reported. The presence of residual acetate groups could have one of two contradictory effects: (i) acetate groups break the continuous series of regularly spaced hydroxyl groups, which may be binding to the ice surface and thus reduce IRI activity; (ii) recent observations of IRI active compounds have indicated hydrophobicity plays a key role in IRI,[20, 4] and as acetates are more hydrophobic than hydroxyls, they may attenuate activity. Separate studies on small molecule IRIs have revealed that sequentially longer alkyl chains enhance activity, rather than acetate groups.[21] To probe the role of additional hydrophobic units, well-defined polymer **PVA$_{351}$** (Table 2.1) was acetylated in a controlled fashion by esterification with acetic acid/HCl to provide a library of PVA-*co*-PVAc with variable densities of acetate groups (Scheme 2.3, Table 2.2). PVA can be functionalised in a range of ways, but this somewhat unconventional approach was chosen as the acid-catalysed

reaction is inherently reversible, which over time leads to a random distribution of acetate groups across the polymer chain.

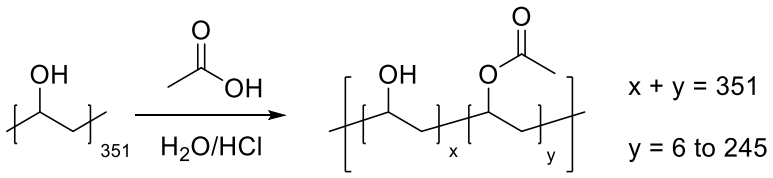

Scheme 2.3 Reaction scheme showing how **PVA$_{351}$** was partially reacetylated to varying degrees using acetic acid/water mixtures and the reversible acid catalysed esterification reaction.

Briefly, 1 g of **PVA$_{351}$** was dissolved in a mixture of glacial acetic acid and water in a vial. 3 M Hydrochloric acid solution was added, either 0.1 mL or 1 mL depending on the approximate degree of acetylation desired – higher degrees of acetylation could be accessed more easily when a higher volume of acid was added, but this was not explored in detail. After 4 days of vigorous stirring at 40 °C the contents of the vial was dialysed and freeze dried, and the polymer characterised by ^{1}H NMR spectroscopy. This was used to characterise the resultant polymers and, by examining the integrals of the backbone -C*H*OH proton and the –C*H*$_3$ protons, the degree of acetylation was determined (Figure 2.11).

Table 2.2 PVA.PVAc co-polymers prepared from **PVA_{351}**

Polymer	[water]/[acetic acid] (−)	Degree of acetylation (^{1}H NMR %)[c]
$PVA(Ac)_1$	85:15[a]	1.7
$PVA(Ac)_2$	76:24[a]	3.9
$PVA(Ac)_3$	68:32[a]	4.2
$PVA(Ac)_4$	60:40[a]	7.4
$PVA(Ac)_5$	44:56[b]	19.0
$PVA(Ac)_6$	41:59[b]	19.9
$PVA(Ac)_7$	45:55[b]	22.0
$PVA(Ac)_8$	48:52[b]	23.7
$PVA(Ac)_9$	50:50[b]	26.8
$PVA(Ac)_{10}$	32:68[b]	44.4
$PVA(Ac)_{11}$	24:76[b]	69.5
$PVA(Ac)_{12}$	17:83[b]	70.3

A 0.10 mL of 3 M HCl solution added to reaction mixture. **B** 1.00 mL of 3 M HCl solution added to reaction mixture. **C** Determined by ^{1}H NMR spectroscopy, by comparing the integrals of the integrals of the PVA α-H (δ = 4.10 – 3.30 ppm), PVAc α-H (δ = 5.50 - 4.80), and PVAc–CH_3 (δ = 2.10 ppm) shifts of the purified co-polymer.

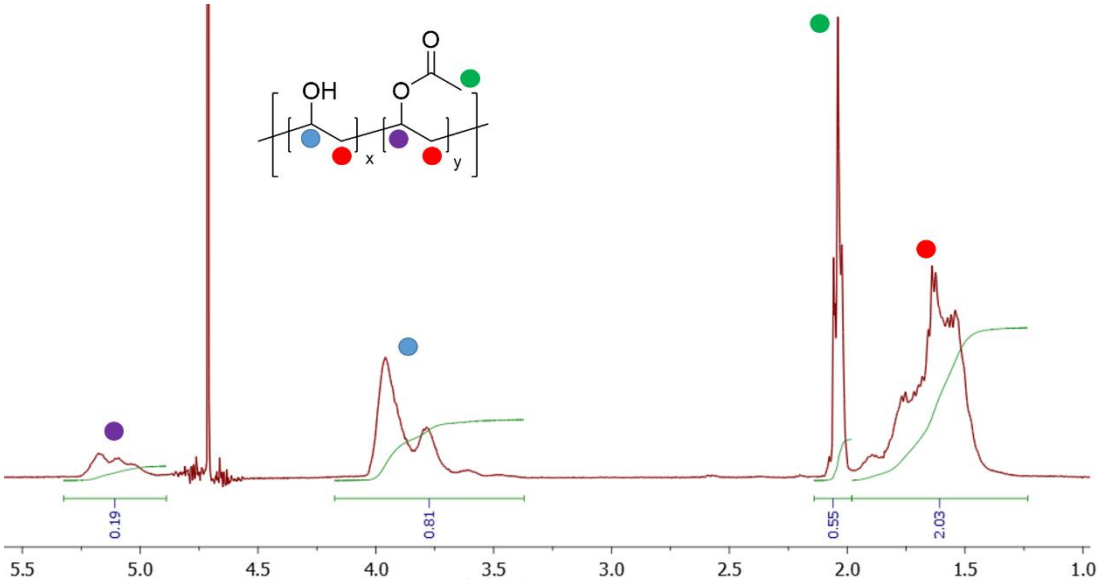

Figure 2.11 Representative ^{1}H NMR spectra of **PVA(Ac)$_5$**. Degree of reacetylation determined by ^{1}H NMR, by comparing the integrals of the PVA α-H (δ = 4.10 – 3.30 ppm), PVAc α-H (δ = 5.50 - 4.80), and PVAc–CH_3 (δ = 2.10 ppm) shifts of the purified co-polymer.

Analysis and the effects of the arrangement of functionality, known as PVA 'blockiness' (the microstructure of PVA.PVAc co-polymers), has been widely studied. Here it was assumed that the co-polymers prepared contained a random distribution of acetate and hydroxyl groups. Experimental evidence later confirmed this – see Chapter 5 for more detail

2.3iv The IRI Activity of PVA-*rand*-PVAc Co-polymers

IRI activity of these polymers was determined using the same protocol as the PVA homopolymers (Figure. 2.12). All experiments were conducted at 2 $mg.mL^{-1}$ to ensure sufficient activity.

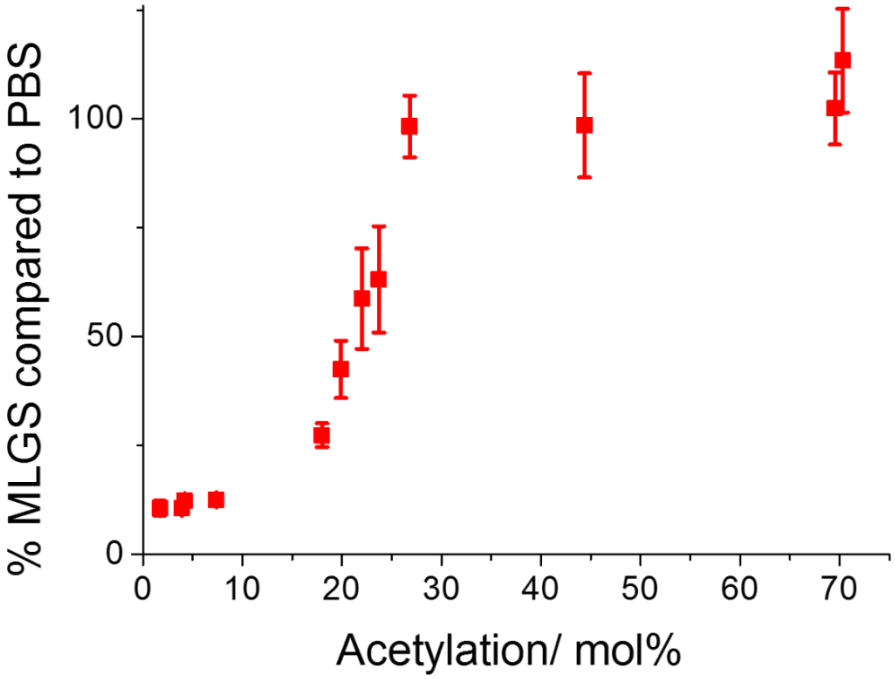

Figure 2.12 Ice recrystallisation inhibition activity of PVA/PVAc statistical co-polymers, as measured by the splat assay at 2 mg.mL^{-1}. All polymers have DP_n = 351; Errors bars represent the standard deviation from at least 12 measurements; % acetylation is the mol % of repeat units which are functionalised with an acetate group, as determined by ^{1}H NMR spectroscopy of the polymers.

Inclusion of acetate groups above 10 mol % leads to a significant decrease in the IRI activity of PVA, and demonstrates the need for well-defined polymers, unlike those used in previous studies.[22] The reason for the decrease in activity could be disruption of the hydrogen bonding interactions between PVA/ice, preventing 'pattern matching'.[17] Indeed, modification of the hydroxyl groups on the carbohydrate portion of antifreeze glycoproteins has been shown to remove antifreeze activity.[23] *Ben et al.* have shown that *N*-octyl galactoside has significantly higher IRI activity than galactose alone.[24] The controlled addition of acetate groups to PVA could therefore be expected to enhance the IRI activity, which is the opposite of what is reported here. Moreover, PVA is well-known as a colloidal stabiliser due to its

surfactant-like properties,[25] and ability to present a hydrophobic face, which might be disrupted by the addition of the acetate groups, altering its solution conformation.

2.3v The Synthesis and IRI Activity of PVP, and PVA-*rand*-PVP Co-polymers

Given the results presented above regarding the loss of activity upon addition of hydrophobic acetate groups, it was also important to evaluate the effect of hydrophilic co-monomers. Due to vinyl acetate being a less activated monomer, there are few monomers which can be efficiently co-polymerised with it using a compatible MADIX agent. Fortunately, *N*-vinyl pyrrolidone is one of the few monomers that can be polymerised, due to it also falling under the category of a less activated monomer (LAM). The first step was to evaluate if the homopolymer of poly(*N*-vinyl pyrrolidone), (PVP) has any IRI activity. There is some debate in the literature as to whether PVP displays IRI activity, and it was necessary to determine if any change in crystal growth occurs using our specific conditions for the splat assay.

PVP can be prepared using the same MADIX agent as for vinyl acetate. In the case of *N*-vinyl pyrrolidone, the R-group on the MADIX agent affects the polymerisation kinetics more than with vinyl acetate. A benzyl R-group has been shown to be best for ensuring an efficient polymerisation and high conversion.[26] The polymerisation protocol is otherwise very similar to the one used for vinyl acetate, the main exception being the higher reaction temperature and the necessity of a solvent, as the monomer is too viscous to be polymerised in bulk (Scheme 2.4) and characterised by ^{1}H NMR and SEC (Table 2.3).

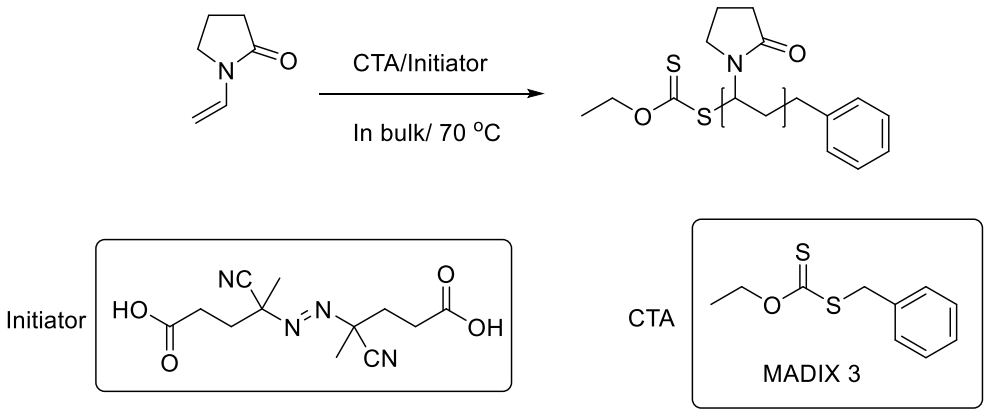

Scheme 2.4 Reaction Scheme for the MADIX-mediated polymerisation of *N*-vinyl pyrrolidone.

The molecular weights obtained by ^{1}H NMR spectroscopic end-group analysis were in close agreement with those expected from the feed ratio. The molecular weight values obtained by SEC were, however, significantly lower than expected, with wide reported molecular weight dispersity. This is a known problem with PVP molecular weight analysis[27] and there are only a few solutions available. O'Reilly and co-workers demonstrated that when hexafluoroisopropanol was used as the solvent, SEC calculated values for PVP were in agreement with the theoretical and end-group values.[28,29] This solvent system was unavailable. Initial assays were conducted showing that these PVP polymers and a range of commercial high molecular weight PVP polymers exhibited no activity at all (Figure 2.13, Figure 2.14).

Table 2.3 PVP polymers prepared for this study

PVP	[M]/ [CTA][a]	conv.[d] %	$M_{n,theo}$[e] g.mol^{-1}	$M_{n,NMR}$[f] g.mol^{-1}	$M_{n,GPC}$[g] g.mol^{-1}	M_w/M_n [g]	DP_n[h] (−)
PVP$_{30}$	25[b]	64.7	2800	3900	1800	1.35	30
PVP$_{48}$	50[b]	44.9	5600	5100	2500	1.58	48
PVP$_{62}$	50[c]	48.5	5600	5900	2700	1.59	62
PVP$_{87}$	100[c]	26.1	11100	6000	2900	1.65	87
PVP$_{140}$	100[c]	50.4	11100	10100	5600	1.73	140

A Monomer to RAFT agent ratio. **B** Polymerisation conducted in a 2 M solution of monomer in 1,4-dioxane. **C** Polymerisation conducted in bulk. **D** Determined by ^{1}H NMR spectroscopy. **E** Theoretical M_n determined from [M]/[CTA] and conversion. **F** Determined by ^{1}H NMR of PVP after precipitation and drying. **G** Determined by SEC in DMF using PMMA standards. **H** Number-average degree of polymerisation.

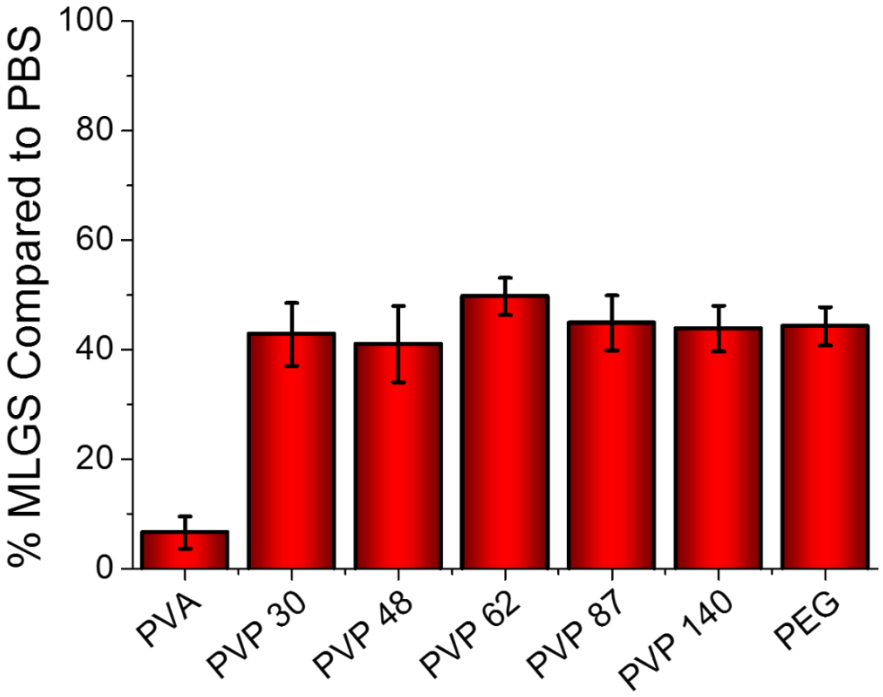

Figure 2.13 IRI activity of PVP at 50 mg.mL^{-1}. PVA and PEG have been included as positive and negative controls respectively. PVA = **PVA$_{351}$**, PEG = 2000 Da.

These results confirm that poly(vinyl pyrrolidone) has no IRI activity in the low concentration range (< 1 mg.mL^{-1}). An initial screen of the IRI activity of PVP (using commercially available higher molecular weight samples of 10 and 40 kDa to maximise any activity) was undertaken showing IRI activity was only observable at very high concentrations (Figure 2.14). Even at 50 mg.mL^{-1} PVP led to an MLGS of only 40 %, significantly less active than any of the PVAs tested. Comparison of all the synthesised PVPs at 50 mg.mL^{-1} revealed no strong relationship between IRI activity and molecular weight. Overall activity was similar to that of poly(ethylene glycol), which is included as a negative control due to it being well established as having no specific IRI behaviour.[3, 4] Both the PEG and PVP samples are weaker than some synthetic glyco-polymers, which also have limited IRI activity.[4,30]

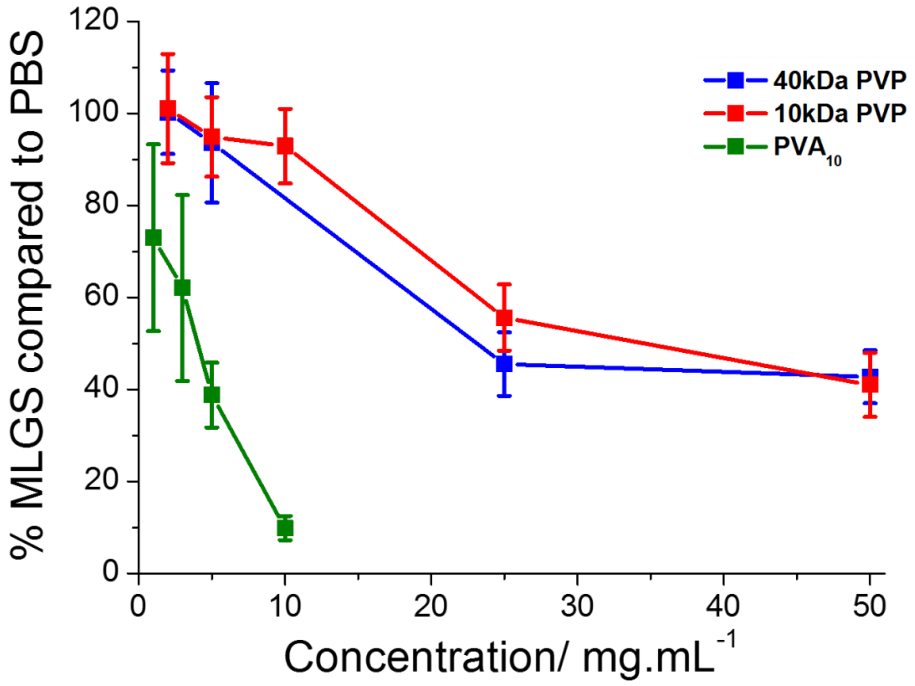

Figure 2.14 IRI activity of commercially available poly(vinyl pyrrolidone). PVA_{10} has been included for reference.

The above results demonstrate that PVP is not an IRI active polymer, but its high solubility, hydrophilicity, and compatibility with the MADIX agent used to polymerise vinyl acetate make it a viable candidate for random inclusion into PVA to 'block' hydroxyl groups, but without introducing hydrophobic groups into the polymer, which could affect the overall solubility. Addition of PVP would also determine how the IRI is affected by increasing the hydrophilicity of the resultant polymer. Vinyl acetate and *N*-vinyl pyrrolidone were co-polymerised in dioxane *via* MADIX with vinyl acetate content varying between 10 and 80 mol% of the monomer mixture, (Scheme 2.5).

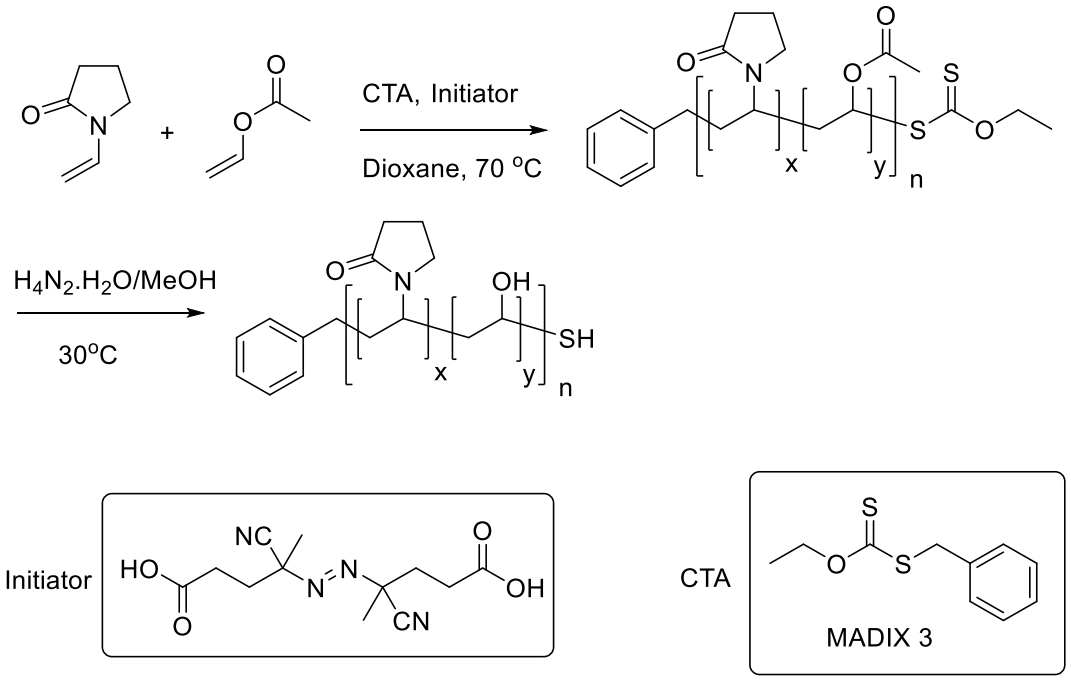

Scheme 2.5 Co-polymerisation of vinyl acetate and *N*-vinyl pyrrolidone, and their subsequent hydrazinolysis to form PVA.PVP co-polymers.

Polymerisation reactions were quenched at approximately 50 % conversion. These monomers do not have identical reactivity ratios (in free radical polymerisation), so in all likelihood these polymers are not fully random and there will be a degree of gradation.[31] Following isolation, the polymers were hydrolysed using hydrazine hydrate solution, dialysed and then freeze-dried, (Table 2.4).

Table 2.4 PVA-*co*-PVP random co-polymers prepared for this study.

Polymer	VAc[a]	VP[a]	conv.[b]	$M_{n,NMR}$[d]	$M_{n,SEC}$[e]	M_w/M_n[e]	PVP[f]
	mmol	mmol	%	g·mol^{-1}	g·mol^{-1}		mol %
PVA(PVP)$_1$	1.7	15.3	48.9	5300	2400	1.48	81.0
PVA(PVP)$_2$	4.2	12.8	38.2	4000	2500	1.41	64.9
PVA(PVP)$_3$	8.5	8.5	38.5	3800	2600	1.41	64.8
PVA(PVP)$_4$	15.3	5.4	36.3	3500	800	1.39	39.9
PVA(PVP)$_5$	17.4	3.7	46.2	4300	3000	1.33	28.6
PVA(PVP)$_6$	19.6	1.8	23.0	2000	1900	1.21	12.3

A [total monomer]/[RAFT agent] ratio = 100:1; Polymerisations conducted in 2 M monomer solutions in dioxane. **B** Determined by ^{1}H NMR spectroscopy. **C** Theoretical M_n determined from monomer to RAFT agent ratio. **D** Determined by ^{1}H NMR spectroscopy of co-polymers after precipitation and drying. **E** Determined by SEC in DMF using PMMA standards. **F** Determined by ^{1}H NMR spectroscopy.

The composition of the polymers was determined by ^{1}H NMR spectroscopy by comparing the integrals of the unique peaks associated with each monomer type (Figure 2.15). The benzyl end group proton shift can be observed between 7.2 and 7.4 ppm, and integration of the α protons of the hydroxyl and pyrrolidinone functionalities at 4.0 ppm and 3.6 ppm respectively can be used to determine polymer composition. Due to the aforementioned difficulties associated with SEC analysis of PVP, molecular weights as determined by SEC appear to deviate significantly from those predicted by the monomer ratio and end-group analysis. End-group analysis indicated that all the co-polymers had similar chain lengths (approximately $DP_n = 50$), which is essential when comparing their IRI activity.

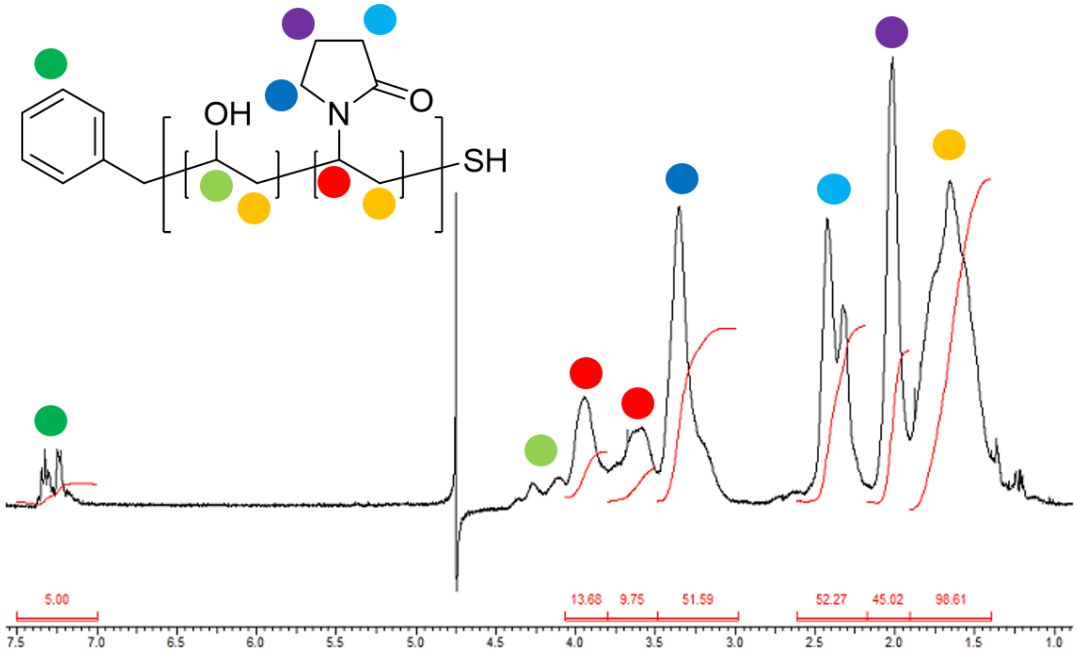

Figure 2.15 ^{1}H NMR spectrum of **PVA-(PVP)$_{1}$**, a random co-polymer of poly(vinyl alcohol) and poly(vinyl pyrrolidone) in D_2O, prepared *via* MADIX polymerisation.

High concentrations of 50 mg.mL^{-1} of polymer were required before relative IRI activities of these hydrophilically doped PVA co-polymers could be assessed relative to another (Figure 2.16). As all the polymers had similar degrees of polymerisation (DP $\simeq$ 50), it is assumed that any differences must be due to the change in composition of the polymers. Interestingly, a similar trend was seen as for the hydrophobic co-polymers.

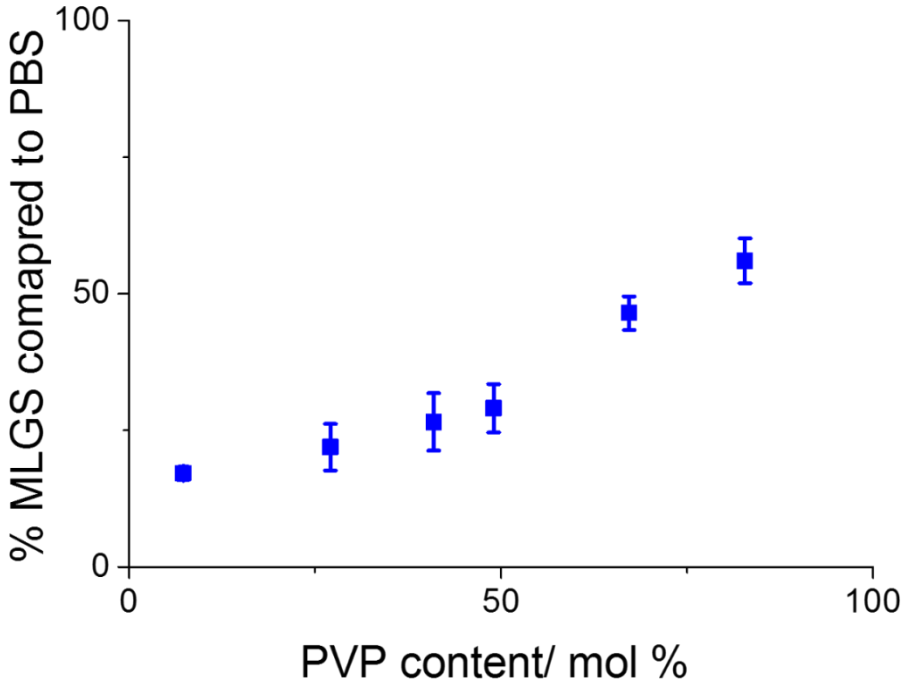

Figure 2.16 Ice recrystallisation activity of statistical co-polymers of PVA-*co*-PVP at 50 mg.mL^{-1}. Mol % PVA is the molar ratio of repeat units of the total polymer.

Above 20 % PVP content (i.e., 80 % PVA), the observed MLGS began to gradually increase, indicating a reduction in activity. Increasing the PVP content further gave rise to a significant decrease in activity (increased MLGS), even at the high concentrations used here (50 mg.mL^{-1}). The polymer with 40 % PVA had essentially no residual activity, giving similar results to homo-PVP. The co-polymer **PVA(PVP)$_5$** (mol % PVP = 28.6, M_w/M_n = 1.33) was also tested for concentration-dependent IRI activity and compared to homo-PVA of similar molecular weight. The co-polymer was significantly less active across all concentrations, (Figure 2.17).

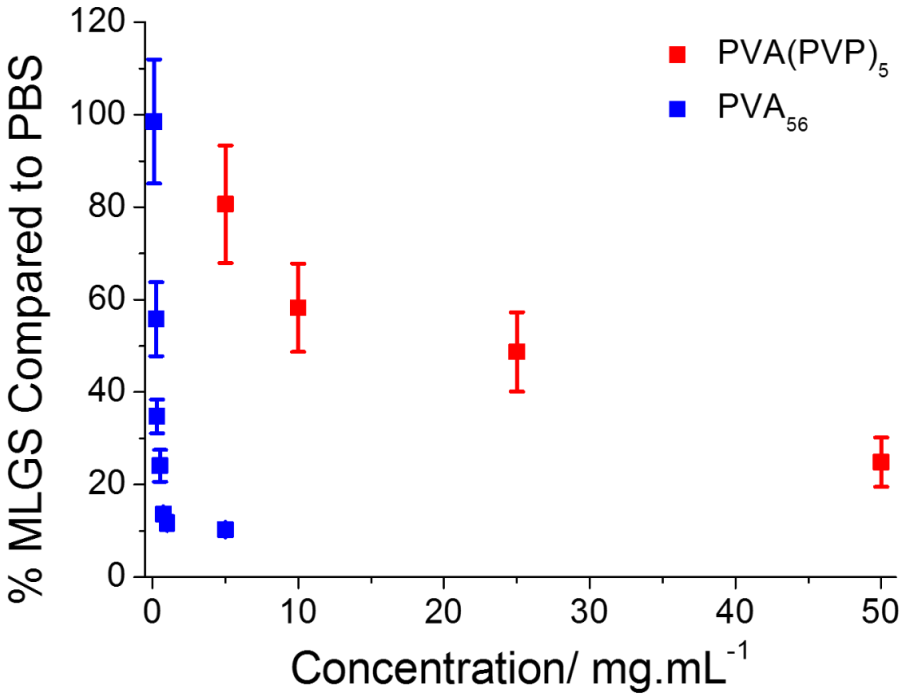

Figure 2.17 The concentration dependent ice recrystallisation inhibition activity of **PVA(PVP)$_5$**, a statistical co-polymer of PVA-*co*-PVP. **PVA$_{56}$** has been included for reference as a homopolymer with a similar number of hydroxyl groups.

Despite the loss of activity above 20 % PVP, very low concentrations of PVP do appear to be tolerated. PVA suffers from reduced aqueous solubility as the molecular weight increases, but it also has increased IRI activity. Therefore, the controlled inclusion of small amounts of comonomers may enable the application of the more active, higher molecular weight polymers.

2.3vi Main Chain Hydrophobic Modifications

The results so far suggest that addition of either hydrophobic or hydrophilic co-monomers into PVA leads to a significant decrease in its IRI activity above 20 mol % inclusion of PVAc or PVP; approximately one in five hydroxyl groups were blocked. As discussed, this could be interpreted as an unbroken sequence of hydroxyl groups being essential for direct interaction with the growing ice crystal

face and hence the inhibition. The above hypothesis is supported by the observations that as the length of the PVA chain increases from 10 to 19 units the IRI activity increases dramatically, compared to subsequent increases in chain length. Therefore the effect of modulating polymer properties without disrupting hydroxyl group sequence needed to be tested. Due to the important role that hydrophobic surfaces play in antifreeze proteins, and the increase in IRI activity observed in small molecule inhibitors with hydrophobic components, it seemed prudent to follow this trend and design a polymer that maintained the hydroxyl sequence of homo-PVA, but included specific hydrophobic functionality.

In order to increase the hydrophobicity of the polymer, but maintain an unbroken sequence of hydroxyl groups, a co-polymer was synthesised with isopropenyl acetate (iPA) as the co-monomer (Scheme 2.6).

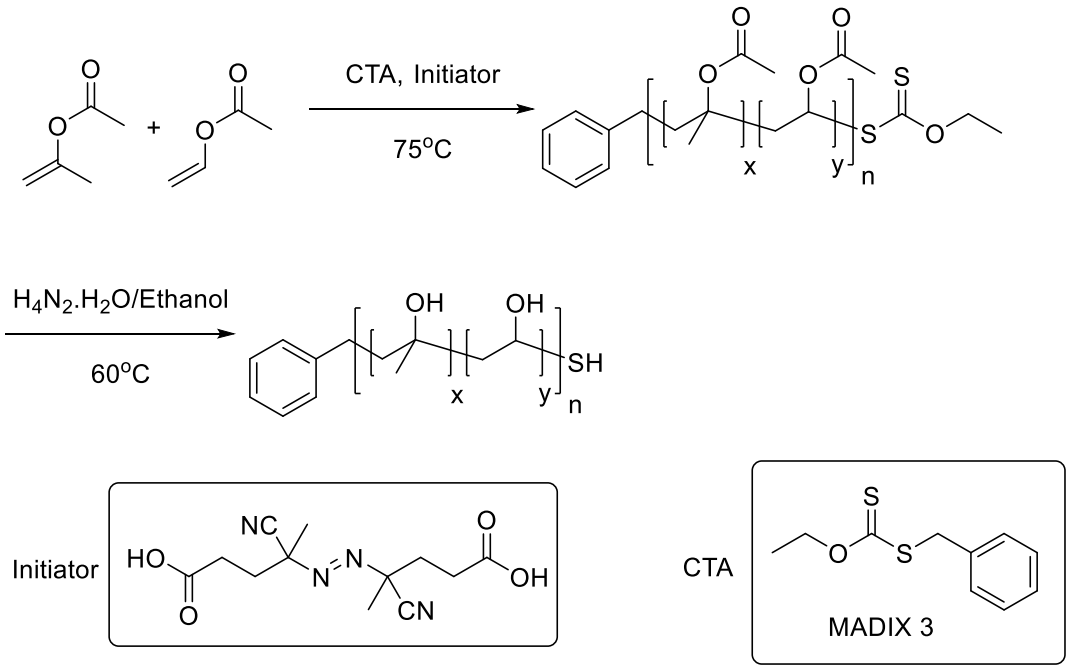

Scheme 2.6 Co-polymerisation of vinyl acetate and isopropenyl acetate *via* MADIX in dioxane, and subsequent hydrolysis using hydrazine hydrate solution to form a random co-polymer of vinyl alcohol and isopropenyl alcohol.

Isopropenyl acetate has a pendant α-methyl group, but will maintain the spacing of hydroxyls along the backbone. There are very few reports in the literature of the successful polymerisation of isopropenyl acetate,[32,33] and no reports using the MADIX methodology used here to polymerise vinyl acetate and *N*-vinyl pyrrolidone. Nevertheless polymerisations were successful, albeit with low conversion, which can be attributed to high degrees of termination, due to the α-methyl protons on the monomer being susceptible to causing termination by disproportionation.[32] Low conversion could also be due to the MADIX agent being less compatible with the isopropenyl acetate monomer. Isopropenyl acetate could also be co-polymerised with vinyl acetate. Low conversions were observed but dispersity remained narrow (Table 2.5). These polymers were subsequently characterised by SEC and ^{1}H NMR spectroscopy (Figure 2.18)

Table 2.5 Random PVAc.PiPAc co-polymers.

Polymer	[VAc]/[iPAc]/ [CTA]	conv.[a] %	$M_{n,NMR}$[c] g.mol^{-1}	$M_{n,SEC}$[d] g.mol^{-1}	M_w/M_n[d]	PiPA[e] mol %
PVA(PIPA)$_1$	500/50/1	11	4800	4200	1.28	10

A Determined by ^{1}H NMR spectroscopy, theoretical M_n determined from monomer to RAFT agent ratio. **C** Determined by ^{1}H NMR spectroscopic of the co-polymers after precipitation and drying. **D** Determined by SEC in DMF using PMMA standards. **E** Determined by ^{1}H NMR spectroscopy.

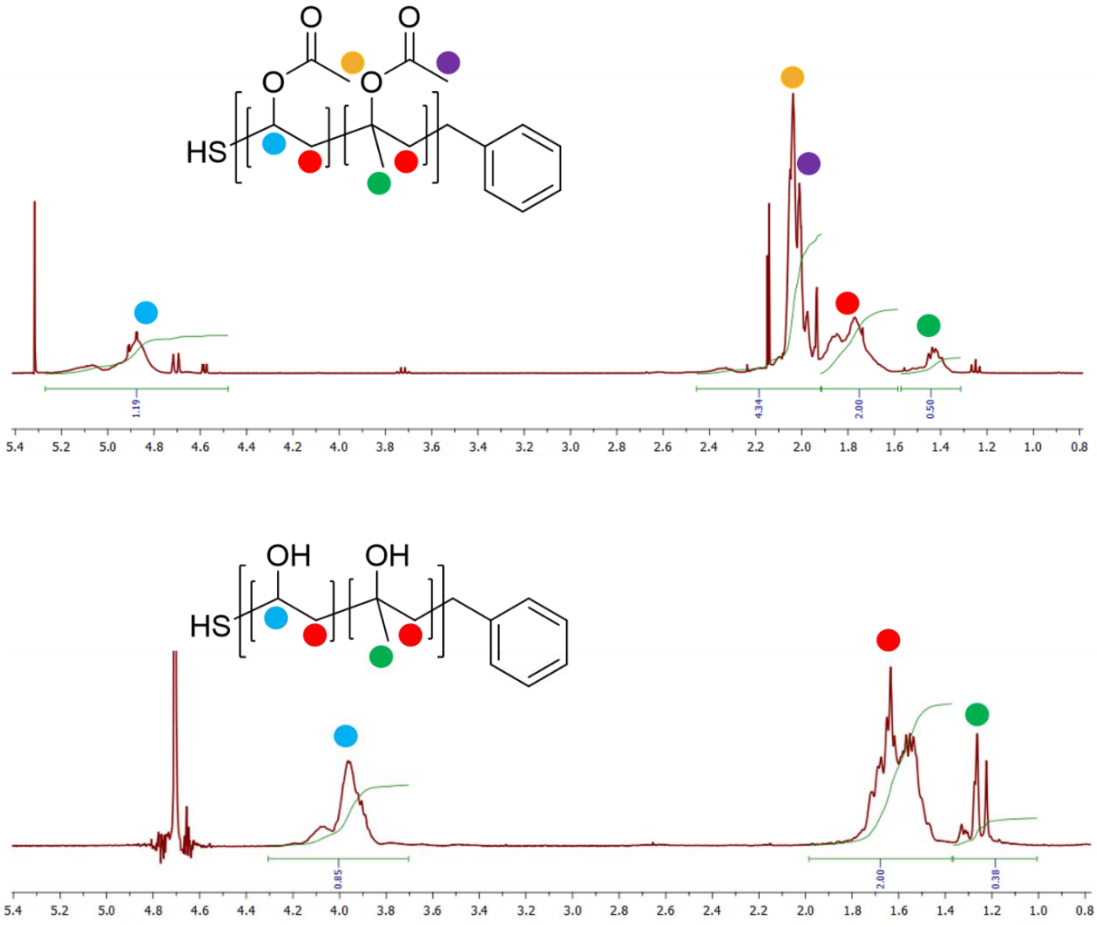

Figure 2.18 ^{1}H NMR of PVAc-*co*-PiPAc and PVA-*co*-PiPA. Residual DCM at δ = 5.3 ppm and residual H_2O at δ = 4.7 ppm.

Initial investigations using poly(isopropenyl alcohol) (PiPA) revealed that, as reported, it is not water soluble so could not be tested as a homopolymer and hence only a co-polymer was used. Solubility of the co-polymers in water was also extremely poor, to the extent that only a polymer with a maximum 10 mol % PiPA could be solubilised for IRI testing (Figure 2.19).

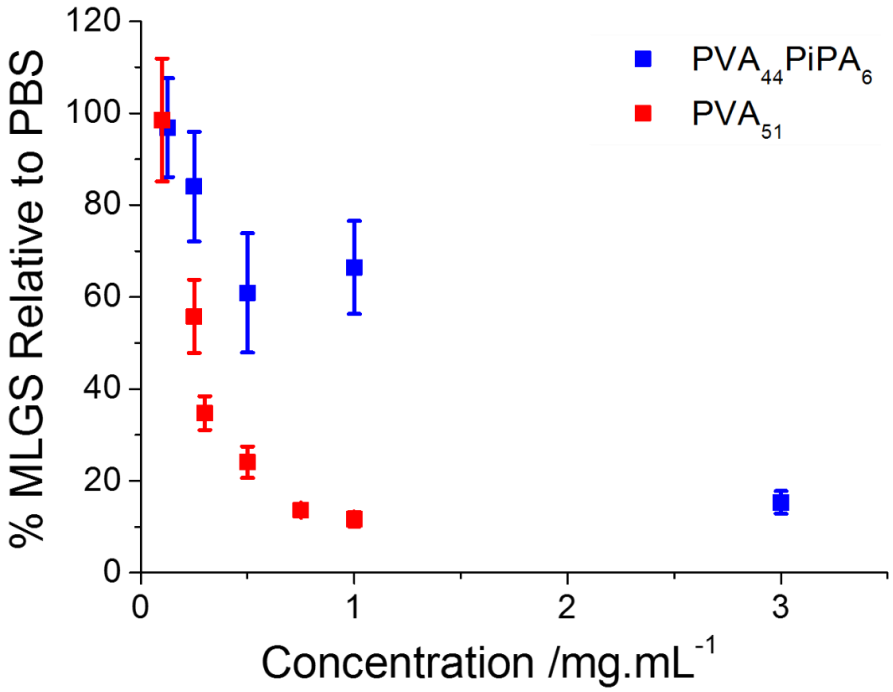

Figure 2.19 The Concentration-dependent ice recrystallisation inhibition activity of **PVA(PIPA)$_1$** compared to homo-PVA with a similar degree of polymerisation.

While **PVA(PIPA)$_1$** maintains its IRI activity to a greater extent than either the acetylated or PVP co-polymers, it still shows less activity than homo-PVA, particularly as the concentration is lowered below 1 mg.mL^{-1}. Nevertheless, high IRI activity is observed at 3 mg.mL^{-1}, comparable to homo-PVA of the same length, which lends credence to the supposition that an unbroken sequence of hydroxyl groups is essential to activity. Due to solubility issues, the effect on IRI of a range of PiPA functionalities could not be tested to the same degree as with acetate or *N*-vinyl pyrrolidone.

2.3vii Discussion

This data shows that main chain substitutions are tolerated more than modifying or 'blocking' hydroxyl groups, but that it still results in decreased activity relative to homo-PVA. This confirms that simply appending increasingly hydrophobic groups onto the polymer chain does not result in an increase in IRI activity. On the surface, this appears to disagree with the expected contributions of hydrophobicity on IRI activity; previous studies have shown native AFGPs and synthetic inhibitors must display hydrophobic faces, but here the addition of acetate groups or pendant methyl groups decreases activity. The flexibility of a polymer chain compared to a rigid protein held together by secondary structures or discrete small molecules may explain this. It could well be the case that the large methyl group is causing a conformational strain in the polymer chain and affecting how the hydroxyl groups are presented, compared to homo-PVA. Therefore the conformation (either solution or ice-bound) of the polymer chains could be disrupted by the co-monomers, and hence, activity is modulated.

Hydrophobic residues are likely to associate into the core of the polymer coil to reduce unfavourable interactions with the solvent (water). It is important to note however that no aggregation of the polymers was observed, so micellisation was not occurring. The second point of discussion is that AFGPs have a polyhydroxylated disaccharide unit with different spacing between hydroxyl groups compared to PVA. Octyl-galactose has been shown to be a potent IRI agent despite it having a different carbohydrate to AFGP and different hydroxyl spacing to PVA, but octyl glucoside has negligible activity. Oligosaccharides, such as dextran, have relatively little or no IRI,[24] ruling out a polyhydroxylated structure being the universally active template.

De novo peptides with potent IRI, which were designed by matching hydroxyl spacing to an ordered ice-lattice, suggest that precision matching to an ice surface at a molecular level can be important.[34] Specific ice-face matching has been shown to provide the underlying mechanism for the separate (and undesirable) properties of thermal hysteresis (TH) and dynamic ice shaping (DIS): attempts to measure these did not reveal any noticeable TH gap or ice shaping in PVA, but that does not necessarily rule out any ice-face matching. Previous work by Inada *et al.* showed PVA had a TH of 0.03 °C at 50 mg.mL^{-1}, which is about 100 times less than that seen for a native AFGP.[35] Therefore, at the moment we cannot rule out any crystal face-binding, but we can state it is significantly weaker than that found in native antifreeze proteins. The importance of backbone–side chain linker length has also been found to be crucial to IRI but is outside of the scope of this study.[16] These apparently contradictory observations imply that multiple structural features (hydroxyl group spacing, hydrophobicity, conformation) contribute to IRI activity, which itself may have more than one mechanistic feature. Ben *et al.* have suggested that IRI agents function by disrupting the quasi-liquid layer (QLL) at the ice/water interface,[18] without any direct interaction with the ice crystal which may explain anomalous activity of non-peptide IRI active compounds. No conclusive evidence exists as yet to prove if both (specific face-matching or disrupting of QLL) of these mechanisms occur simultaneously for a given inhibitor, or are mutually exclusive.

2.4 Conclusion

This chapter describes a detailed study into the structural basis of the inhibition of ice crystal growth by poly(vinyl alcohol). MADIX polymerisation allowed access to a range of well-defined polymers with variable molecular weights and hydrophilic/hydrophobic comonomers. It was observed that the critical chain length at which PVA exhibits IRI activity was between 10 and 20 repeat units, implying a minimum repeat sequence is essential for strong interactions with the ice surface. Increasing the chain length further gave rise to increased activity, which was maintained at concentrations as low as 0.05 mg.mL^{-1} for **PVA$_{351}$**. Addition of either vinyl acetate or *N*-vinyl pyrrolidone comonomers both led to a reduction in activity above approximately 20 mol % incorporation, showing that only very small quantities of additional functional groups can be tolerated in the main-chain structure if activity is to be maintained. Modifications to the polymer backbone using isopropenyl acetate to maintain a hydroxyl group functionality were hindered by solubility issues, but the resulting polymers displayed IRI activity. These co-polymers however were not as potent as homo-PVA of a similar size. This intolerance to functional groups raises questions about the mechanism of IRI, particularly the role of hydrophobicity. Hydrophobic domains are crucial in AFPs, but here, inclusion of these domains removed IRI activity. This suggests that sequence, not composition, is essential to activity, and that the solution (or surface-absorbed) conformation of the inhibitor is crucial to the IRI activity of PVA. The use of controlled radical polymerisation did indeed provide new insight into the underlying mechanisms, and the next chapters will explore the importance of hydroxyl sequence and overall morphology.

2.5 Experimental

Materials and Methods

For general materials and methods details, see the Appendix. Phosphate-buffered saline (PBS) solutions were prepared using pre-formulated tablets (Sigma-Aldrich) in 200 mL of Milli-Q water (>18.2 Ω mean resistivity) to give [NaCl] = 0.138 M, [KCl] = 0.0027 M, and pH 7.4. Isopropenyl acetate, Vinyl acetate and *N*-vinyl pyrrolidone were purchased from Sigma-Aldrich and were filtered through a plug of basic alumina to remove inhibitors prior to their use. 4,4′-Azobis(4-cyanovaleric acid) was recrystallised from methanol and stored at - 8 °C in the dark. Acetic acid (glacial, 99.5 %) was purchased from Fisher Scientific. Hydrazine hydrate solution (approximately 80 %) was purchased from Sigma Aldrich. All solvents were purchased from VWR or Sigma-Aldrich and used without further purification, except for 1,4-dioxane, which was filtered through a plug of alumina prior to use.

Synthesis of Methyl (isoproxy carbonothioyl) sulfanyl acetate (MADIX 1)

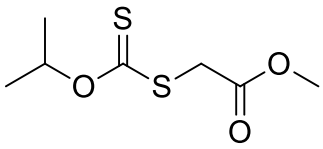

2-Propanol (25 mL) was added to a round bottom flask equipped with a stir bar. Potassium hydroxide (3.913 g, 0.07 mol) was added and left to dissolve overnight. Carbon disulfide (12.5 mL, 0.2 mol) was added drop-wise over 5 mins, forming a yellow slurry. The mixture was left to stir at for 5 h. Methyl bromoacetate (6.55 mL 0.07 moles) was added, dissolving the solid. The reaction was left to stir overnight. The solution was filtered and the solid washed with cold isopropanol. The solution

was then concentrated *in vacuo* and then purified on a column of neutral alumina using 5:1 pet ether:ethyl acetate as the eluent, Rf = 0.3. The fractions were concentrated *in vacuo* and the resultant yellow oil dried under vacuum. Yield 8.34 g 57.3 % ^{1}H NMR ($CDCl_3$): δ = 1.39 (6H, d, J = 6 Hz (CH_3)$_2$CH), 3.77 (3H, s, CH_3O), 3.90 (2H, s, CH_2S), 5.73 (1H, septet, J = 6.2 Hz (CH_3)$_2$C*H*). ^{13}C NMR ($CDCl_3$): δ = 21.1 (CH(*C*H_3)$_2$), 37.3 (*C*H_2), 52.6(CO_2*C*H_3), 78.6 (*C*H(CH_3)$_2$), 168.3 (*C*=O), 211.4 (*C*=S).

Synthesis of methyl (ethoxy carbonothioyl) sulfanyl acetate (MADIX 2)

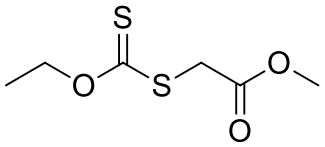

Ethanol (70 mL) was added to a round bottom flask equipped with a stir bar. Potassium hydroxide (11.45 g, 0.2 mol) was added and left to dissolve for 1 h. Carbon disulphide (12.1 mL, 0.2 mol) was added drop-wise, forming a yellow solution, which was left for 5 h. Methyl bromoacetate (6.5 mL, 0.06 moles) was added drop-wise and the solution left to stir overnight. The solution was filtered and washed with cold ethanol and concentrated *in vacuo*. The crude product was partitioned in DCM and sat. brine solution and the organic fraction concentrated *in vacuo*. The residue was washed through a column of basic alumina using pure ethyl acetate as the eluent. The fractions were concentrated *in vacuo* and then dried under vacuum. Yield 5.25 g 46 %. ^{1}H NMR ($CDCl_3$): δ = 1.42 (3H, t, J=7.2, CH_3CH_2), 3.76 (3H, s, CH_3O), 3.92 (2H, d, J=7, SCH_2), 4.64 (2H, q, J=7.2, CH_3CH_2). ^{13}C NMR ($CDCl_3$): δ = 14.0 (CH_2–CH_3), 37.7 (*C*H_2), 61.0 (CO_2*C*H_3), 70.4 (*C*H_2–CH_3), 167.7 (C=O), 212.4 (C=S).

Synthesis of methyl (ethoxy carbonothioyl) sulfanyl benzene (MADIX 3)

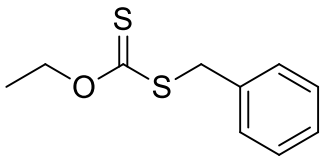

Ethanol (70 mL) was added to a round bottom flask equipped with a stir bar. Potassium hydroxide (3.00 g, 0.054 mol) was added and stirred until dissolved. Carbon disulfide (3.02 mL, 0.05 mol) was added drop-wise and the reaction stirred for 5 h. Benzyl bromide (6.00 mL, 0.05 mol) was added, and the reaction stirred at 50 °C for 18 h. The solution was filtered and washed with acetone, then concentrated *in vacuo.* The residue was purified on a column of silica with 99:1 hexane:methanol as the eluent. Yield 3.25 g 30 % ^{1}H NMR ($CDCl_3$): δ = 1.36 (3H, t, J=7.2, C*H*$_3$CH$_2$), 4.33 (2H, s, SC*H*$_2$), 4.61 (2H, q, J=7.2, OC*H*$_2$CH$_3$) 7.25 (5H, m, benzyl protons); ^{13}C NMR ($CDCl_3$): δ = 13.91 (CH$_2$–*C*H$_3$), 40.54 (*C*H$_2$), 70.16 (*C*H$_2$CH$_3$), 212.4 (C=S), 127.56 (*para C*H), 128.72 (*meta C*H), 129.19 (*ortho C*H).

Alternative synthesis of methyl (ethoxy carbonothioyl) sulfanyl benzene (MADIX 3)

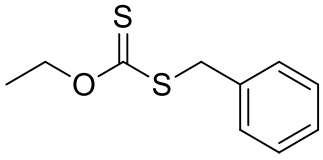

Acetone (70 mL) was added to a round bottom flask equipped with a stir bar. Potassium ethyl xanthate (2.97 g, 0.017 mol) was added and stirred until the solid had dissolved. Benzyl bromide (2.08 mL, 0.017 mol) was added, the flask stoppered and the reaction stirred at 50 °C for 18 h. The solution was then filtered and washed

with acetone, then concentrated *in vacuo.* The residue was purified on a column of silica with DCM as the eluent. Yield 3.25 g 54 % ^{1}H NMR ($CDCl_3$): δ = 1.36 (3H, t, J=7.2, C*H*$_3$CH$_2$), 4.33 (2H, s, SC*H*$_2$), 4.61 (2H, q, J=7.2, OC*H*$_2$CH$_3$) 7.25 (5H, m, benzyl protons); ^{13}C NMR ($CDCl_3$): δ = 13.91 (CH$_2$–*C*H$_3$), 40.54 (*C*H$_2$), 70.16 (*C*H$_2$CH$_3$), 212.4 (C=S), 127.56 (*para C*H), 128.72 (*meta C*H), 129.19 (*ortho C*H).

Polymerisation of Vinyl Acetate Using MADIX 2

As a representative example, MADIX 2 (0.21 g, 0.99 mmol), vinyl acetate (4.67 g, 2.64 mmol), and ACVA (4,4′-azobis(4-cyanovaleric acid); 0.013 g, 0.1 mol) were added to a stoppered vial. The solution was thoroughly degassed by bubbling N_2 through the solution for 20 min, and the reaction mixture was then allowed to polymerise at 68 °C for typically 15 h. The yellow solutions were then cooled to room temperature. Poly(vinyl acetate) was then recovered as a yellow sticky solid after precipitation into hexane. The hexane was then decanted and the poly(vinyl acetate) was re-dissolved in THF, which was then concentrated *in vacuo* and thoroughly dried under vacuum at 40 °C for 24 h, forming a pale yellow solid. Representative characterisation data for **PVAc$_{56}$**: ^{1}H NMR (400 MHz, D_2O) δ 4.61 (−C*H*O–CH$_2$, br, 1H), 1.74 (−CO–C*H*$_3$, br, 3H), 1.53 (−C*H*$_2$–, br, 2H); M_n^{SEC}(THF) = 5100 Da, M_w/M_n = 1.23.

Hydrazinolysis of Poly(vinyl acetate) to Poly(vinyl alcohol)

As a representative example, poly(vinyl acetate) (1.5 g, 3300 Da, M_w/M_n = 1.22) was dissolved in a methanol (20 mL) and hydrazine hydrate solution (15 mL, 80% in water) in a round-bottom flask. The reaction mixture was stirred at 30 °C for 2 h. The reaction mixture was then dialyzed using distilled water and poly(vinyl alcohol)

was recovered as a spongy white solid by freeze-drying the dialysis solution. Hydrazinolysis was determined by ^{1}H NMR. Representative characterisation data for **PVA$_{56}$**: ^{1}H NMR (400 MHz, $CDCl_3$) δ 4.00 (−C*H*OH–, br, 1H), 1.68–1.60 (−C*H*$_2$–, br, 2H).

Acetylation of Poly(vinyl alcohol)

As a representative example, poly(vinyl alcohol) (0.5 g, 29 kDa, M_n/M_w = 1.28) was dissolved in water (2.4 mL), acetic acid (7.6 mL), and HCl (0.1 mL, 3 M solution in water) in a vial equipped with a stir bar. The reaction mixture was stirred at 40 °C for 4 days. The reaction mixture was then dialyzed, and partially acetylated poly(vinyl alcohol) was recovered by freeze-drying the dialysis solution. Conversion was determined by ^{1}H NMR integration of the acetate methyl protons (δ = 2.08) and the −CH_2– backbone protons (δ = 1.93–1.50). Representative characterisation data for pure **PVA(Ac)$_6$**: ^{1}H NMR (400 MHz, D_2O) δ 4.61 (-C*H*O-CH_2-) 4.00 (-C*H*OH-, br, 1H), 2.08 (-CO-CH_3, br, 3H), 1.93–1.50 (-C*H*$_2$-, br, 2H).

Polymerisation of *N*-Vinyl Pyrrolidone Using MADIX 3

As a representative example, *N*-vinyl pyrrolidone (2.09 g, 18.78 mmol), CTA 1 (0.037 g, 0.17 mmol), and ACVA (0.005 g, 0.02 mmol) were dissolved in dioxane (4 mL) in a stoppered vial equipped with a stir bar. The reaction mixture was thoroughly degassed by bubbling N_2 through the solution for 20 min and the reaction mixture was allowed to polymerise at 70 °C for, typically, 5 h. The dark yellow solutions were then cooled to room temperature and the random co-polymer was recovered as white flakes by several precipitations into diethyl ether. The bulk of the solvent was carefully decanted and the solid collected by centrifugation. The product

was thoroughly dried under vacuum at 40 °C for 24 h, forming a yellow solid. Representative characterisation data for **PVP$_{62}$**: ^{1}H NMR (400 MHz, $CDCl_3$) δ 3.74 (-C*H*N-, br, 1H), 3.19 (-NC*H*$_2$CH$_2$-, br, 2H), 2.38 (-NCOC*H*$_2$-, br, 2H), 2.21(-NCH$_2$C*H*$_2$CH$_2$-, br, 2H), 1.81–1.53 (-C*H*$_2$-, br, 2H); M_n^{SEC} (DMF) = 2700 Da; M_w/M_n = 1.59.

Co-polymerisation of Vinyl Acetate and *N*-Vinyl Pyrrolidone using MADIX 3

As a representative example, vinyl acetate (0.68 g, 7.98 mmol), *N*-vinyl pyrrolidone (0.944 g, 8.83 mmol), CTA 1 (0.035 g, 0.17 mmol), and ACVA (4.7 mg, 0.02 mmol) were dissolved in dioxane (8.41 mL) in a stoppered vial equipped with a stir bar. The reaction mixture was thoroughly degassed by bubbling N_2 through the solution for 20 min, and the reaction mixture was allowed to polymerise at 70 °C for 7 h. The dark yellow solutions were then cooled to room temperature and the random co-polymer was recovered as a sticky yellow solid by several precipitations into diethyl ether or hexane, depending on the composition of the polymer. The solvent was carefully decanted and the product thoroughly dried under vacuum at 40 °C for 24 h, forming a yellow solid. The polymer was then hydrolysed using hydrazine hydrate solution (15 mL, 80% in water) in a round-bottom flask. The reaction mixture was stirred at 30 °C for 2 h, then dialysed using distilled water. Poly(vinyl alcohol)-co-poly(vinyl pyrrolidone) was recovered as a spongy white solid by freeze-drying the dialysis solution. Hydrazinolysis was determined by ^{1}H NMR spectroscopy. Representative characterisation data for **PVA(PVP)$_3$**: ^{1}H NMR (400 MHz, D_2O) δ 3.52 (−C*H*N–, br, 1H), 3.26 (−C*H*O–, br, 1H), 3.12 (−NC*H*$_2$CH$_2$–, br, 2H), 2.49 (−NCOC*H*$_2$–, br, 2H), 2.13 (−NCH$_2$C*H*$_2$CH$_2$–, br, 2H), 1.97 (−COC*H*$_3$–, br, 3H), 1.80–1.50 (−C*H*$_2$–, br, 2H);M_n^{NMR}(D_2O) = 8400 Da; M_n^{SEC}(DMF) = 2700 Da; M_w/M_n = 1.30.

Co-polymerisation of Vinyl Acetate and Isopropenyl Acetate Using MADIX 3

As a representative example, **MADIX 3** (0.032 g, 0.99 mmol), vinyl acetate (7.96 g, 92.45 mmol), isopropenyl acetate (0.83 g, 8.26 mmol), and ACVA (4,4′-azobis(4-cyanovaleric acid); 0.003 g, 0.012 mmol) were added to a stoppered vial. The solution was thoroughly degassed by bubbling N_2 through the solution for 20 min and the reaction mixture was then allowed to polymerise at 75 °C for 14 h. The yellow solutions were then cooled to room temperature. The polymer was then recovered as a yellow sticky solid after precipitation into hexane. The hexane was then decanted and the polymer was re-dissolved in DCM, which was then concentrated in vacuo, forming a yellow solid. Representative characterisation data for **PVA(PiPA)$_1$** ^{1}H NMR (400 MHz, $CDCl_3$) δ 4.85 (−C*H*O–CH_2, br, 1H), 2.59 (−C(CH_3)–C*H*$_2$–, br, 2H), 2.02 (−CO–C*H*$_3$, br, 6H), 1.75 (−C*H*$_2$–, br, 2H), 1.56 (−C(C*H*$_3$)–CH_2–, br, 3H); M_n^{SEC}(THF) = 4200 Da; M_w/M_n = 1.28.

Hydrazinolysis of Poly(vinyl acetate)-*co*-poly(isopropenyl acetate)

Poly(vinyl acetate)-*co*-poly(isopropenyl acetate) (1.50 g, M_n = 4200 Da, M_w/M_n = 1.28) was dissolved in ethanol (40 mL) and heated to 60 °C. Hydrazine hydrate (80 % solution, 30 mL) was then added carefully with stirring. The solution was stirred at 60 °C for 6 h. The solution was then concentrated *in vacuo* leaving a clear solution. The solution was dialysed using 1000 Da MWCO dialyzed tubing and distilled water. The dialysed solution was then freeze-dried and the polymer recovered as white powder. ^{1}H NMR (400 MHz, D_2O) δ 3.95 (−C*H*OH, br, 1H), 1.75–1.40 (−C*H*$_2$–, br, 4H), 1.28 (−C(C*H*$_3$), br, 3H).

Ice Recrystallisation Inhibition ‘Splat’ Assay

A droplet of polymer containing PBS solution is dropped from 1.4 m onto a glass microscope coverslip, which is on top of an aluminium plate cooled to -78 °C using dry ice. The droplet freezes instantly upon impact with the plate, spreading out and forming a thin wafer of ice. This wafer is then placed on a liquid nitrogen cooled cryostage held at - 8 °C. Photographs of the wafer at 20× zoom under cross polarisers are taken and then the wafer is left to anneal for 30 minutes at - 8 °C. Three photographs are taken of the wafer and a final photograph at 4× zoom is taken. These photographs are then analysed using ImageJ, a free image analysis software program, to determine crystal size, using a standard of 100 μm wide gold tracks printed on a glass slide. The largest 4 crystals from three 20× photographs are measured and then averaged, and this average is then divided by the MLGS for PBS solution (138 μm). This gives as a percentage of growth compared to PBS, or the % MLGS.

2.6 References

1. Deller, R. C.; Vatish, M.; Mitchell, D. A.; Gibson, M. I., Synthetic polymers enable non-vitreous cellular cryopreservation by reducing ice crystal growth during thawing. *Nature Communications* **2014,** *5*, DOI:10.1038/ncomms4244.

2. Li, B.; Sun, D.-W., Novel methods for rapid freezing and thawing of foods – a review. *Journal of Food Engineering* **2002,** *54* (3), 175-182; Lv, J.; Song, Y.; Jiang, L.; Wang, J., Bio-Inspired Strategies for Anti-Icing. *ACS Nano* **2014,** *8* (4), 3152-3169.

3. Knight, C. A.; Wen, D.; Laursen, R. A., Nonequilibrium Antifreeze Peptides and the Recrystallization of Ice. *Cryobiology* **1995,** *32* (1), 23-34.

4. Gibson, M. I., Slowing the growth of ice with synthetic macromolecules: beyond antifreeze(glyco) proteins. *Polymer Chemistry* **2010,** *1* (8), 1141-1152.

5. Chao, H.; Davies, P. L.; Carpenter, J. F., Effects of antifreeze proteins on red blood cell survival during cryopreservation. *The Journal of experimental biology* **1996,** *199* (9), 2071-2076.

6. Lu, S. S.; Inada, T.; Yabe, A.; Zhang, X.; Grandum, S., Microscale study of poly(vinyl alcohol) as an effective additive for inhibiting recrystallization in ice slurries. *International Journal of Refrigeration-Revue Internationale Du Froid* **2002,** *25* (5), 562-568.

7. Baker, M. I.; Walsh, S. P.; Schwartz, Z.; Boyan, B. D., A review of polyvinyl alcohol and its uses in cartilage and orthopedic applications. *Journal of Biomedical Materials Research Part B: Applied Biomaterials* **2012,** *100* (5), 1451-1457.

8. Alves, M. H.; Jensen, B. E. B.; Smith, A. A. A.; Zelikin, A. N., Poly (vinyl alcohol) physical hydrogels: new vista on a long serving biomaterial. *Macromolecular bioscience* **2011,** *11* (10), 1293-1313.

9. Deller, R. C.; Congdon, T.; Sahid, M. A.; Morgan, M.; Vatish, M.; Mitchell, D. A.; Notman, R.; Gibson, M. I., Ice recrystallisation inhibition by polyols:

comparison of molecular and macromolecular inhibitors and role of hydrophobic units. *Biomaterials Science* **2013,** *1* (5), 478-485.

10. Budke, C.; Koop, T., Ice recrystallization inhibition and molecular recognition of ice faces by poly(vinyl alcohol). *Chemphyschem* **2006,** *7* (12), 2601-2606.

11. Wang, H.-Y.; Inada, T.; Funakoshi, K.; Lu, S.-S., Inhibition of nucleation and growth of ice by poly(vinyl alcohol) in vitrification solution. *Cryobiology* **2009,** *59* (1), 83-89.

12. Stenzel, M. H.; Cummins, L.; Roberts, G. E.; Davis, T. P.; Vana, P.; Barner-Kowollik, C., Xanthate mediated living polymerization of vinyl acetate: A systematic variation in MADIX/RAFT agent structure. *Macromolecular Chemistry and Physics* **2003,** *204* (9), 1160-1168.

13. Paik, H.-j.; Teodorescu, M.; Xia, J.; Matyjaszewski, K., Block Copolymerizations of Vinyl Acetate by Combination of Conventional and Atom Transfer Radical Polymerization. *Macromolecules* **1999,** *32* (21), 7023-7031.

14. Debuigne, A.; Willet, N.; Jérôme, R.; Detrembleur, C., Amphiphilic poly (vinyl acetate)-b-poly (N-vinylpyrrolidone) and novel double hydrophilic poly (vinyl alcohol)-b-poly (N-vinylpyrrolidone) block copolymers prepared by cobalt-mediated radical polymerization. *Macromolecules* **2007,** *40* (20), 7111-7118.

15. Eniade, A.; Purushotham, M.; Ben, R. N.; Wang, J. B.; Horwath, K., A serendipitous discovery of antifreeze protein-specific activity in C-linked antifreeze glycoprotein analogs. *Cell Biochemistry and Biophysics* **2003,** *38* (2), 115-124.

16. Liu, S. H.; Ben, R. N., C-linked galactosyl serine AFGP analogues as potent recrystallization inhibitors. *Organic Letters* **2005,** *7* (12), 2385-2388.

17. Budke, C.; Koop, T., Ice recrystallization inhibition and molecular recognition of ice faces by poly(vinyl alcohol). *Chemphyschem* **2006,** *7* (12).

18. Tam, R. Y.; Ferreira, S. S.; Czechura, P.; Chaytor, J. L.; Ben, R. N., Hydration Index—A Better Parameter for Explaining Small Molecule Hydration in

Inhibition of Ice Recrystallization. *Journal of the American Chemical Society* **2008,** *130* (51), 17494-17501.

19. Zhao, F.; Mahdavian, A.; Teimouri, M.; Daniels, E.; Klein, A.; El-Aasser, M., RAFT-mediated emulsion polymerization of vinyl acetate: a challenge towards producing high molecular weight poly(vinyl acetate). *Colloid and Polymer Science* **2012,** *290* (13), 1247-1255.

20. Congdon, T.; Notman, R.; Gibson, M. I., Antifreeze (Glyco)protein Mimetic Behavior of Poly(vinyl alcohol): Detailed Structure Ice Recrystallization Inhibition Activity Study. *Biomacromolecules* **2013,** *14* (5), 1578-1586.

21. Balcerzak, A. K.; Febbraro, M.; Ben, R. N., The importance of hydrophobic moieties in ice recrystallization inhibitors. *RSC Advances* **2013,** *3* (10), 3232-3236.

22. Inada, T.; Lu, S. S., Inhibition of recrystallization of ice grains by adsorption of poly(vinyl alcohol) onto ice surfaces. *Crystal Growth & Design* **2003,** *3* (5), 747-752.

23. Ahmed, A. I.; Osuga, D. T.; Feeney, R. E., Antifreeze Glycoprotein from an Antarctic Fish: Effects of Chemical Modifications of Carbohydrate Residues on Antifreeze and Antilectin Activities. *Journal of Biological Chemistry* **1973,** *248* (24), 8524-8527.

24. Capicciotti, C. J.; Leclere, M.; Perras, F. A.; Bryce, D. L.; Paulin, H.; Harden, J.; Liu, Y.; Ben, R. N., Potent inhibition of ice recrystallization by low molecular weight carbohydrate-based surfactants and hydrogelators. *Chemical Science* **2012,** *3* (5), 1408-1416.

25. Stejskal, J.; Kratochvíl, P.; Helmstedt, M., Polyaniline Dispersions. 5. Poly(vinyl alcohol) and Poly(N-vinylpyrrolidone) as Steric Stabilizers. *Langmuir* **1996,** *12* (14), 3389-3392.

26. Nguyen, T. L. U.; Eagles, K.; Davis, T. P.; Barner-Kowollik, C.; Stenzel, M. H., Investigation of the influence of the architectures of poly(vinyl pyrrolidone) polymers made via the reversible addition–fragmentation chain transfer/macromolecular design via the interchange of xanthates mechanism on the

stabilization of suspension polymerizations. *Journal of Polymer Science Part A: Polymer Chemistry* **2006,** *44* (15), 4372-4383.

27. Wu, C.-S., *Handbook Of Size Exclusion Chromatography And Related Techniques: Revised And Expanded*. CRC Press: 2003; Vol. 91.

28. Ieong, N. S.; Redhead, M.; Bosquillon, C.; Alexander, C.; Kelland, M.; O'Reilly, R. K., The Missing Lactam-Thermoresponsive and Biocompatible Poly(N-vinylpiperidone) Polymers by Xanthate-Mediated RAFT Polymerization. *Macromolecules* **2011,** *44* (4), 886-893.

29. Ieong, N. S.; Brebis, K.; Daniel, L. E.; O'Reilly, R. K.; Gibson, M. I., The critical importance of size on thermoresponsive nanoparticle transition temperatures: gold and micelle-based polymer nanoparticles. *Chemical Communications* **2011,** *47* (42), 11627-11629.

30. Gibson, M. I.; Barker, C. A.; Spain, S. G.; Albertin, L.; Cameron, N. R., Inhibition of Ice Crystal Growth by Synthetic Glycopolymers: Implications for the Rational Design of Antifreeze Glycoprotein Mimics. *Biomacromolecules* **2009,** *10* (2), 328-333.

31. Bork, J. F.; Coleman, L. E., Nitrogen-containing monomers. II. Reactivity ratios of n-vinyloxazolidone and N-vinylpyrrolidone with vinyl monomers. *Journal of Polymer Science* **1960,** *43* (142), 413-421.

32. Nishino, T.; Kitamura, N.; Murotani, K., High-Pressure-Synthesis of Poly(isopropenyl alcohol) and Its Biocompatibilities. *Journal of Polymer Science Part a-Polymer Chemistry* **2009,** *47* (3), 754-761.

33. Ma, W. Y.; Wu, Y. X.; Feng, L.; Xu, R. W., Synthesis of poly(styrene-co-isopropenyl acetate) -g-polyisobutylene graft copolymers via combination of radical polymerization with cationic polymerization. *Polymer* **2012,** *53* (15), 3185-3193.

34. Kuiper, M. J.; Fecondo, J. V.; Wong, M. G., Rational design of α-helical antifreeze peptides. *The Journal of Peptide Research* **2002,** *59* (1), 1-8.

35. Inada, T.; Lu, S. S., Thermal hysteresis caused by non-equilibrium antifreeze activity of poly(vinyl alcohol). *Chemical Physics Letters* **2004,** *394* (4-6), 361-365.

Chapter 3

Synthesis and Ice Recrystallisation Inhibition Activity of PVA-*block*-PVP Co-polymers

---

3.1 Chapter Overview

The aim of this chapter is to further investigate the influence of the structural features of PVA on its IRI activity. A brief review of the literature is presented, highlighting the key points of preparing PVA-*b*-PVP co-polymers. PVP and PVAc macroCTAs were prepared and chain extended with vinyl acetate and vinyl pyrrolidone respectively, in order to determine the most efficient synthetic pathway with which to prepare these block co-polymers. By combining analysis from size exclusion chromatography and ^{1}H NMR spectroscopy these polymers could be characterised. Using the IRI 'splat' assay the ice growth inhibition activity of these polymers was assessed. These results showed that when an uninterrupted hydroxyl sequence is preserved these PVA-*b*-PVP co-polymers are far more effective inhibitors than random copolymers of similar monomer distribution, and it appears that when PVP is presented in a block there is no effect on the IRI activity of PVA.

3.2 Chapter Introduction

Proteins of all types, sizes and function employ not only their primary structure – the sequence of amino acids comprising the protein – but also their secondary and tertiary structures to achieve function. The secondary structure (the shape of the protein that forms due to the nature of the interactions and conformations of the component amino acids) is as, if not more, vital than the functionality of the primary structure, as it allows the protein to interact with entities far larger than itself. This is the case for many antifreeze proteins (AFPs) and antifreeze glycoproteins (AFGPs). Davies and co-workers showed that *Marinomonas primoryensis*, an Antarctic bacterium, produces a large antifreeze protein that absorbs clathrate waters onto the protein surface that act as a binding motif, aiding the protein adsorption onto growing ice crystals and inhibiting ice growth.[1] This interaction would of course be impossible without a rigid secondary structure.

There is much less structural diversity, and hence less diversity of secondary structures, in antifreeze glycoproteins. AFGPs are comprised of alternating alanine-alanine threonine tripeptide units with disaccharide residues,[2] and most reports agree that AFGPs exist as 3-fold helices, a highly unconventional structure.[3,4] Through NMR spectroscopic analysis it also appears that the disaccharide is held against the backbone *via* the amine hydrogen bonding to the Thr residue, stabilising the structure and affording a stationary binding surface.[5]

A simple method of introducing 'secondary structure' type functionality into polymers is through block co-polymerisation of monomers with different solubility, or making blocks that can aggregate. The most common examples of block co-polymer self-assembly produce large ordered sheets, bilayers or micelles.[6] Does the importance of

hierarchal structures also apply to antifreeze protein mimics? Tam *et al.* have shown that the activity of AFGP mimics is highly dependent on secondary structure; both in sequence length, and the distance at which the disaccharide is held from the chain.[7] In this case the linker length needs to be exact, as MD simulations show that IRI active species are capable of folding the disaccharide onto the backbone, very similar to the proposed conformation of AFGPs.[8] The importance of the secondary structure of IRI active synthetic macromolecules has not been examined in detail, in part due to the lack of IRI active candidates, beyond PVA. The secondary structure (in this case the solution conformation) of PVA is mostly likely one of the major reasons for its activity; PVA is widely employed as a surfactant and stabilizer, both applications highly dependent on solution conformation.

There are two reports on IRI active block co-polymers. Mastai and Baruch used branched poly(ethylene oxide)-poly(ethyleneimine) block co-polymers with polyglycidol side chains, but only analysed antifreeze activity using differential scanning calorimetry, making it difficult to compare IRI activity.[9] The second, by Antonietti and co-workers, is very interesting as it is comprised of partially phosphorylated poly(ethylene oxide)-*block*-poly[2-(2-hydroxyethyl) ethylene]; essentially an IRI active block with a non-active PEG block.[10] The polymer was tested using a range of methods and displays IRI activity, but only at high concentrations (~30 $mg.mL^{-1}$). Nevertheless, the non-active block does not appear to be adversely affecting activity.

Controlled radical polymerisation affords many straightforward routes to preparing block co-polymers,[11] as due the inherent living nature of the reaction, polymerisations are never terminated and new monomers can be incorporated. Using the MADIX methodology employed previously, and by keeping the selection of monomers the

same (vinyl acetate and *N*-vinyl pyrrolidone), effects of block co-polymer morphology can be examined and compared to the random co-polymer prepared previously. Preparing block co-polymers would also allow the testing of the minimum hydroxyl sequence hypothesis put forward in Chapter 2.

Reports using a MADIX methodology to prepare block copolymers of PVAc generally focus on chain extension of macro chain transfer agents (mCTAs) using vinyl acetate, to prove living character. For example, Stenzel and co-workers conducted several studies into the MADIX mediated polymerisation of *N*-vinyl pyrrolidone (NVP), examining chain extension using vinyl acetate, and accessing NVP star polymers in order to determine the effect of these water soluble polymers on suspension polymerisation.[12] The MADIX polymerisation of NVP was first reported by Okamoto and co-workers,[13] using a benzyl and *o*-ethoxy functional MADIX agent in fluoroalcohols to control the molecular weight and tacticity of the polymer. At low conversion good dispersities and high end group fidelity were reported, but no further evidence of living character, particularly chain extension, was reported. Since then there have been several reports on the MADIX mediated living polymerisation of *N*-vinyl pyrrolidone. Destarac and co-workers reported the ambient temperature polymerisation of *N*-vinyl pyrrolidone in dioxane as a way to bypass issues associated with using acid or ester functional MADIX agents, such as end group hydrolysis or elimination caused by acid catalysed side reactions, which were reported by Pound *et al.*[14, 15] Klumperman, and co-workers also published several reports on the preparation of NVP-containing block co-polymers.[16, 17]

While there are several reports on the controlled radical polymerisation of NVP and other lesser activated monomers - namely vinyl acetate - and the use of macroCTAs of PVP to prepare block co-polymers of PVP and PVA, there is currently no research into their IRI activity. The preparation and study of these block co-polymers is important as it will inform ideas about the structural properties necessary for ice growth inhibition, as well as determining whether the IRI activity of PVA is tolerant to functionality introduced separately, as opposed to randomly.

3.3 Results

3.3i The Synthesis of Block Co-polymers *via* Controlled Radical Polymerisation

In order to prepare well-defined block co-polymers using a RAFT/MADIX methodology, macroCTAs (polymers with a terminal chain transfer functional group) with a high degree of end-group fidelity are required in order to control the composition of the block co-polymer. If the end-group fidelity is low, the final polymer will be a disperse mix of the homopolymer of both components, and a poorly defined block co-polymer with an unpredictable molecular weight.

This problem can be addressed by prematurely quenching the controlled/living polymerisation of the macroCTA, halting the polymerisation at low conversion and improving the end group fidelity, compared to high conversion polymerisations. Using a CTA compatible with both the polymerisation of vinyl acetate and *N*-vinyl pyrrolidone, macroCTAs of both monomers were prepared and chain extended, in order to determine the most effective strategy for preparing these block co-polymers.

3.3ii The Polymerisation and Chain Extension of PVP Macroinitiators

Most reports of the MADIX mediated polymerisation of PVA-*b*-PVP start with the formation of a PVP macroCTA and then subsequently chain extend with vinyl acetate. This is in part because many of the reports focus on showing the controlled living radical polymerisation of vinyl pyrrolidone, which can be proven by a successful chain extension. Following previous literature reports,[16, 18] PVP macroCTA was prepared, using methyl(ethoxycarbonothioyl)sulfanyl benzene CTA to mediate the polymerisation (Scheme 3.1).

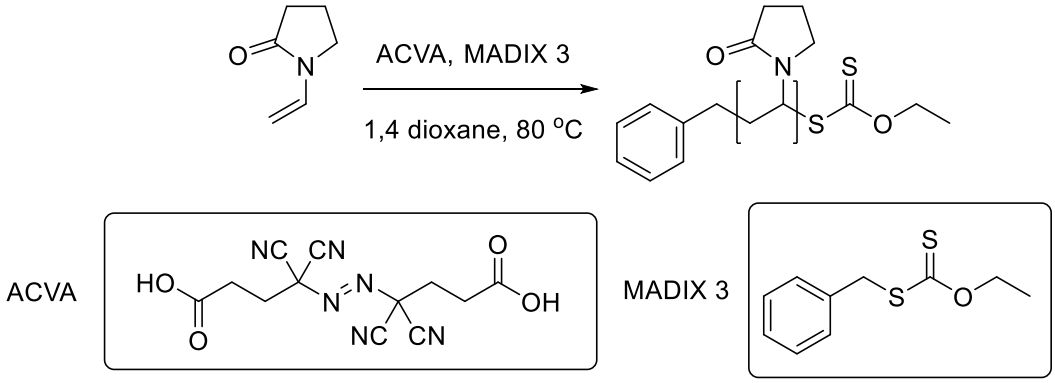

Scheme 3.1 Preparation of PVP macroCTA.

The polymerisations were quenched 3 hours after initiation by rapid cooling in liquid nitrogen followed by exposure to air, to ensure good end-group fidelity. The above method afforded a small library of PVP macroCTA, (Table 3.1) which was characterised using SEC in DMF (Figure 3.1) and ^{1}H NMR spectroscopy (Figure 3.2). Low molecular weights were chosen in order to prepare PVA-*b*-PVP co-polymers with similar molecular weight ranges as the random PVA.PVP co-polymers outlined in Chapter 2, so that morphological effects could be directly compared.

Table 3.1 PVP macroCTAs prepared for this study.

Macro CTA	[M]/ [CTA][a]	Conv.[b] %	$M_{n,NMR}$[d] g.mol^{-1}	$M_{n,GPC}$ [e] g.mol^{-1}	M_w/M_n [e]	DP_n [f] (−)	DP_n [g] (−)
PVP_{30}	50	60	3350	1700	1.46	15	30
PVP_{55}	100	30	6110	3350	1.42	30	55
PVP_{70}	100	38	7780	3840	1.42	35	70

A Monomer to RAFT agent ratio. The polymerisation was conducted in a 2 M solution of monomer in 1,4-dioxane. **B** Determined by ^{1}H NMR spectroscopy. **C** Theoretical M_n determined from [M]/[CTA] and conversion. **D** Determined by ^{1}H NMR of PVP after precipitation and drying. **E** Determined by SEC in DMF using PMMA standards. **F** Number-average degree of polymerisation from SEC analysis. **G** Number-average degree of polymerisation from ^{1}H NMR spectroscopic analysis of the integrals of the benzyl end group protons at δ = 7.23 ppm and the N-CH_2 functional group protons at δ = 3.26 ppm.

Reported $Đ$ values are still high for a controlled system, especially one with low molecular weight ranges, but this can be attributed to the issues of analysing these materials in a DMF SEC system.[19] ^{1}H NMR spectroscopic end-group analysis shows that, as expected, SEC analysis substantially underestimates the molecular weight distribution of these polymers (Figure 3.2).[18] Given the strong molecular weight dependence of the IRI activity of PVA, it is important to be as accurate as possible in regards to molecular weight.

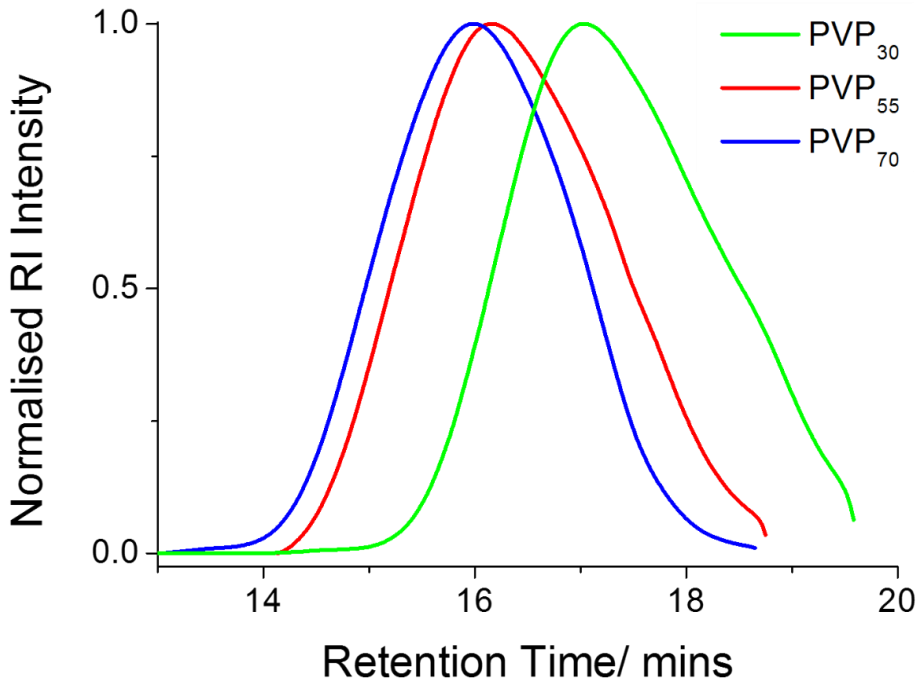

Figure 3.1 SEC traces of poly(vinyl pyrrolidone) prepared for this study.

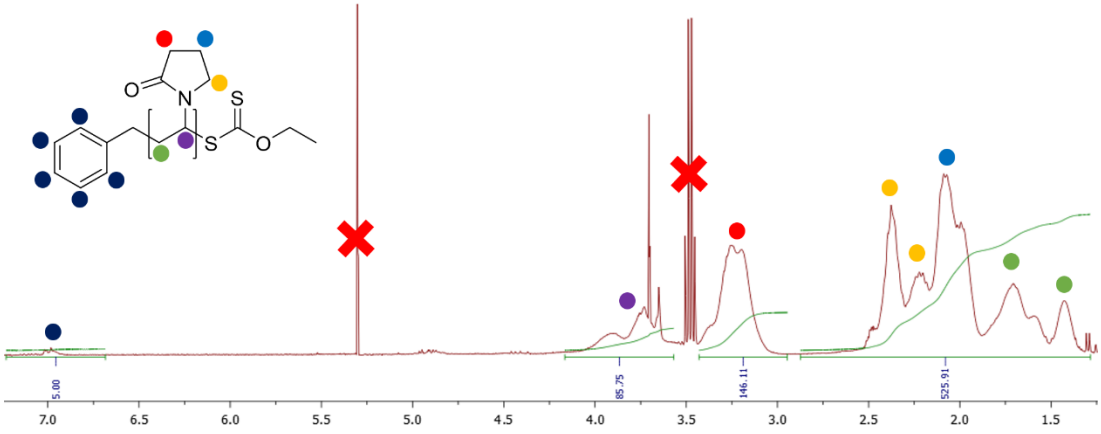

Figure 3.2 ^{1}H NMR spectrum of **PVP$_{70}$**. Residual solvent peaks at δ = 5.3 ppm and 3.5 ppm can be attributed to DCM and diethyl ether, respectively.

The PVP macroCTAs above were chain extended using vinyl acetate in dioxane, in order to prepare PVAc-*b*-PVP co-polymers (Scheme 3.2). This reaction can prove difficult, due to the size and solubility of the mCTA, and the different fragmentation and propagation kinetics. The concentration of azo initiator also needs to be sufficient

for initiation and propagation to occur, but low enough to prevent uncontrolled free radical polymerisation.

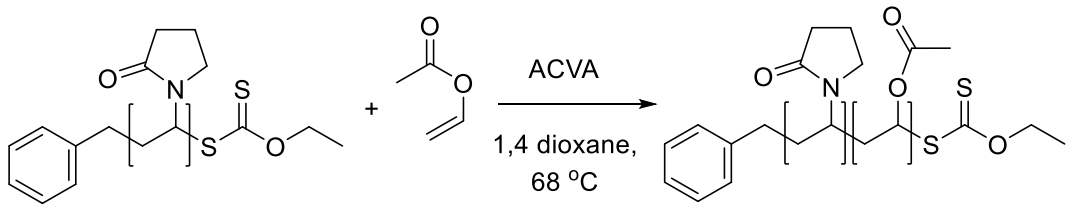

Scheme 3.2 Preparation of PVAc-*b*-PVP block co-polymer.

MacroCTA solubility in the 1,4-dioxane/monomer solution was not an issue, but initial results showed no chain extension, suggesting a low propagation rate. Increasing initiator concentration would lead to formation of PVAc homopolymer, so this problem was circumvented by using high [M]/[mCTA] ratios (Table 3.2). These block co-polymers were precipitated into cold diethyl ether to maximise recovery of the chain extended polymer. The polymers were analysed using DMF SEC, (Figure 3.3), and chain extension confirmed by comparing SEC traces of macroCTA and the subsequent chain extended product, (Figure 3.4). These polymers were then converted to PVA-*b*-PVP using hydrazinolysis with hydrazine hydrate solution, dialysed and freeze dried, furnishing PVA-*b*-PVP co-polymers as white solids. ^{1}H NMR spectroscopy was then used to determine block length. The hydrolysed versions of the block co-polymers retain the benzyl end group, but have less overlapping chemical shifts, making characterisation simpler (Figure 3.5).

Table 3.2 PVA-*b*-PVP block co-polymers prepared for this chapter.

PVAc-*b*-PVP	[M]/ [mCTA]	Conv.[b] %	$M_{n,NMR}$[c] g·mol^{-1}	$M_{n,SEC}$[d] g·mol^{-1}	M_w/M_n[d]	PVAc[e] DP
PVAc$_{20}$-*b*-PVP$_{30}$	20	96.8	5050	3400	1.47	20
PVAc$_{18}$-*b*-PVP$_{55}$	500	15.6	7650	5400	1.35	18
PVAc$_{32}$-*b*-PVP$_{70}$	1000	11.2	10520	9130	1.36	32
PVAc$_{37}$-*b*-PVP$_{70}$	2000	6.1	10950	9650	1.38	37

A [total monomer]/[RAFT agent] ratio; Polymerisations conducted in 2 M monomer solutions in dioxane. **B** Determined by ^{1}H NMR spectroscopy. Theoretical M_n determined from monomer to RAFT agent ratio. **C** Determined by ^{1}H NMR of the co-polymers after precipitation and drying. **D** Determined by SEC in DMF using PMMA standards. **E** Determined by ^{1}H NMR spectroscopy of the PVP-*b*-PVA block co-polymers.

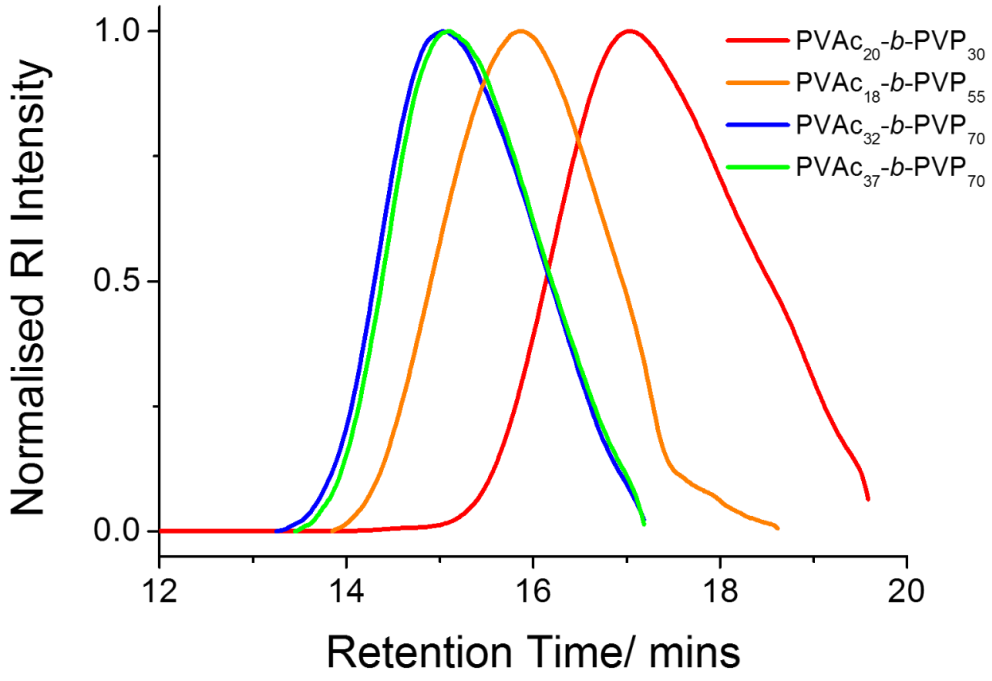

Figure 3.3 SEC traces of PVAc-*b*-PVP prepared for this study.

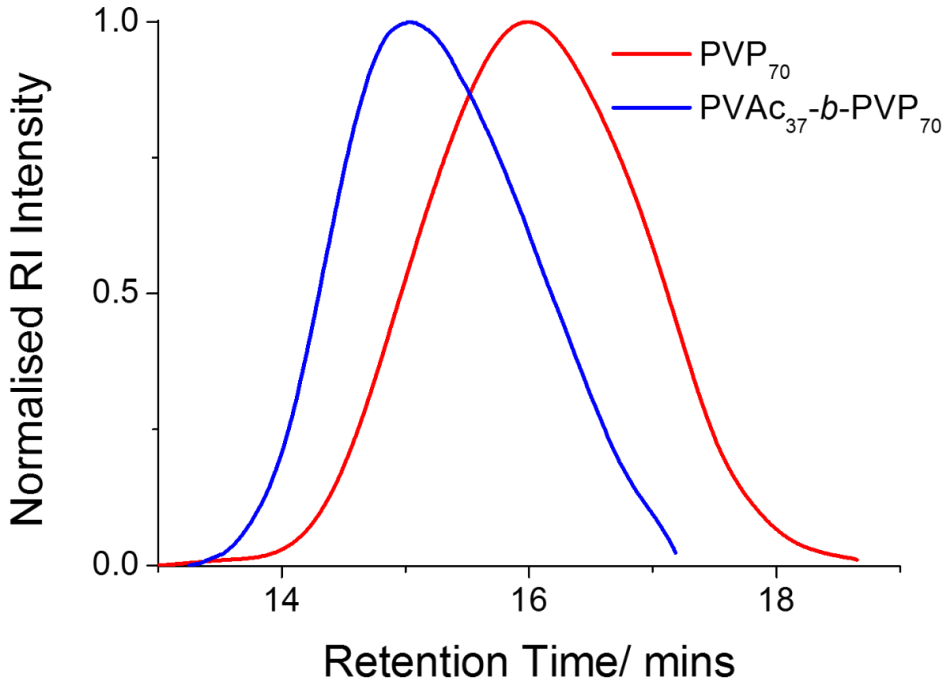

Figure 3.4 DMF SEC traces showing successful chain extension of **PVP_{70}** with vinyl acetate.

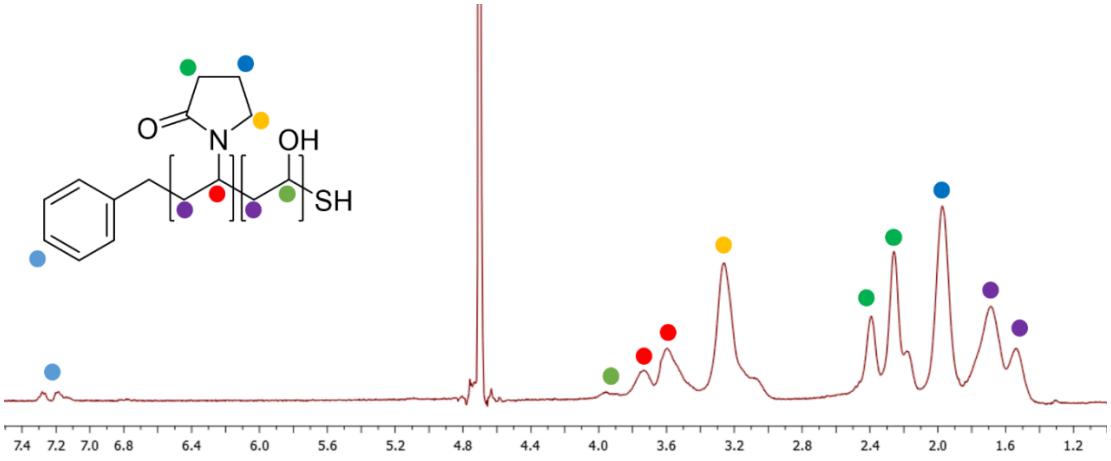

Figure 3.5 ^{1}H NMR spectrum of **$PVAc_{18}$-b-PVP_{55}**.

With these PVA-*b*-PVP co-polymers prepared and characterised, splat assays could be conducted to evaluate the IRI activity, and compare the results to the PVA homopolymers and random co-polymers tested in Chapter 2.

3.3iii The IRI Activity of PVA-*b*-PVP Co-polymers

The PVA-*b*-PVP co-polymers were dissolved in PBS solution and their IRI activity examined using the splat assay. The polymers were tested with increasing dilution until any indication of inhibition had disappeared (Figure 3.6).

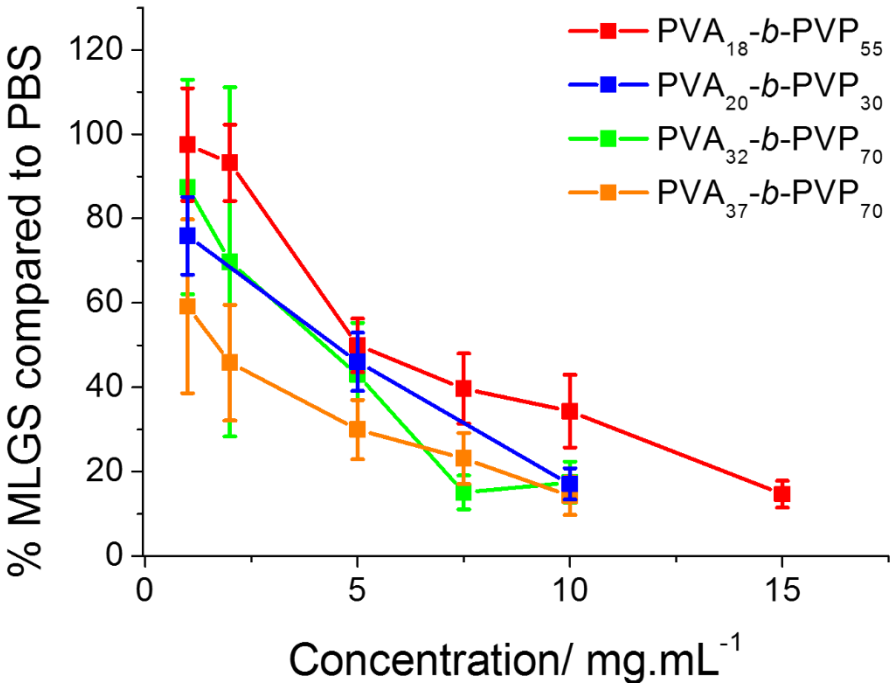

Figure 3.6 The IRI activity of PVA-*b*-PVP co-polymers prepared from PVP macroCTA.

At high concentrations (15 mg.mL^{-1} to 7.5 mg.mL^{-1}) of block co-polymer, very efficient inhibition of ice crystal growth was observed. Activity at this concentration alone shows that these block co-polymers are far more active than any of the PVP co-polymers tested in Chapter 2. This demonstrates that sequence, not composition, is crucial to IRI activity. As the polymer concentration was diluted, ice crystal growth increased linearly, and at 1.0 mg.mL^{-1} there is almost no inhibition of ice growth observed. **PVA$_{18}$-*b*-PVP$_{55}$** displays the weakest activity and **PVA$_{37}$-*b*-PVP$_{70}$** the

strongest, and block co-polymers with larger PVA blocks display greater IRI activity. **PVA$_{20}$-*b*-PVP$_{30}$** displays marginally better activity than **PVA$_{18}$-*b*-PVP$_{55}$**, which could be attributed to the larger PVA block.

In Chapter 2, PVP was shown to have no IRI activity. Therefore the IRI differences in the PVA blocks cannot be quantitatively assessed using a polymer mass scale, and it is necessary to examine the activity based on the active component – the effective PVA concentration. This will show if the activity is affected by the PVP block, and will give a fair comparison. When these results are analysed purely on the concentration of PVA, a different picture appears. When the % MLGS is replotted against the weight % of PVA in solution, (Figure 3.7, Figure 3.8) it can be seen that the IRI activity is maintained in dilute concentration, to the point where activity is unaffected by the PVP block.

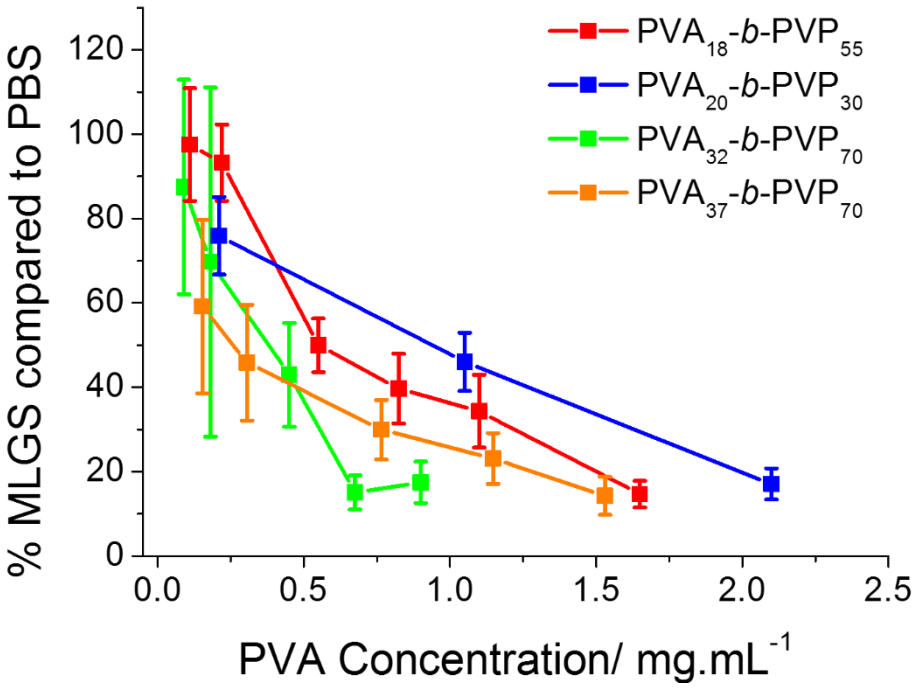

Figure 3.7 The PVA wt % dependent IRI activity of PVA-*b*-PVP co-polymers prepared from PVP macroCTA.

Pleasingly, when the % MLGS is considered as a function of PVA concentration, **PVA$_{32}$-*b*-PVP$_{70}$** and **PVA$_{37}$-*b*-PVP$_{70}$** display the strongest IRI activity, showing total inhibition of ice growth at 1 mg.mL^{-1} to 1.5 mg.mL^{-1}. This potent IRI activity is in line with PVA homopolymers tested in Chapter 2 that contained similar numbers of hydroxyl groups. The overall weakest activity is displayed by **PVA$_{20}$-*b*-PVP$_{30}$**, which gives a % MLGS of 50 at 1.0 mg.mL^{-1}. This is still comparable to **PVA$_{20}$** homopolymer, showing that activity is essentially preserved in the dilute concentration range (Figure 3.9). **PVA$_{20}$-*b*-PVP$_{30}$** is also far more active on a mol % OH scale than **PVA$_{70}$-*rand*-PVP$_{20}$**, the most active random co-polymer testing in Chapter 2. Due to the similar sizes of PVA blocks, these results suggests that the activity of PVA block may in fact be increased by a larger PVP block (Figure 3.8), and highlights the need for a systematic approach to studying the effect of the PVP block on IRI (section 3.3iv).

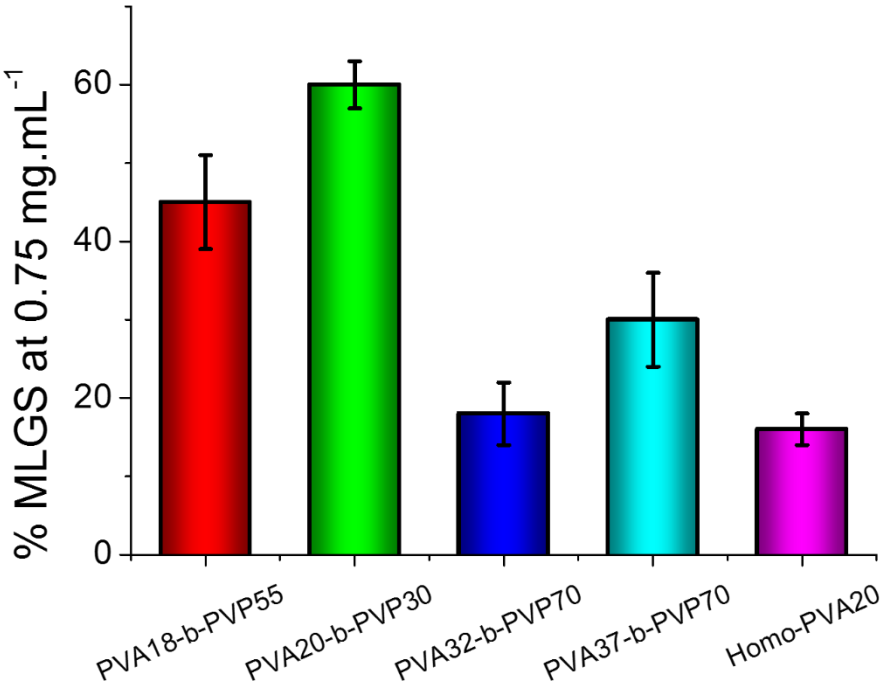

Figure 3.8 Bar chart showing differences in IRI activity. Y-axis gives % MLGS at 0.75 mg.mL^{-1} PVA concentration.

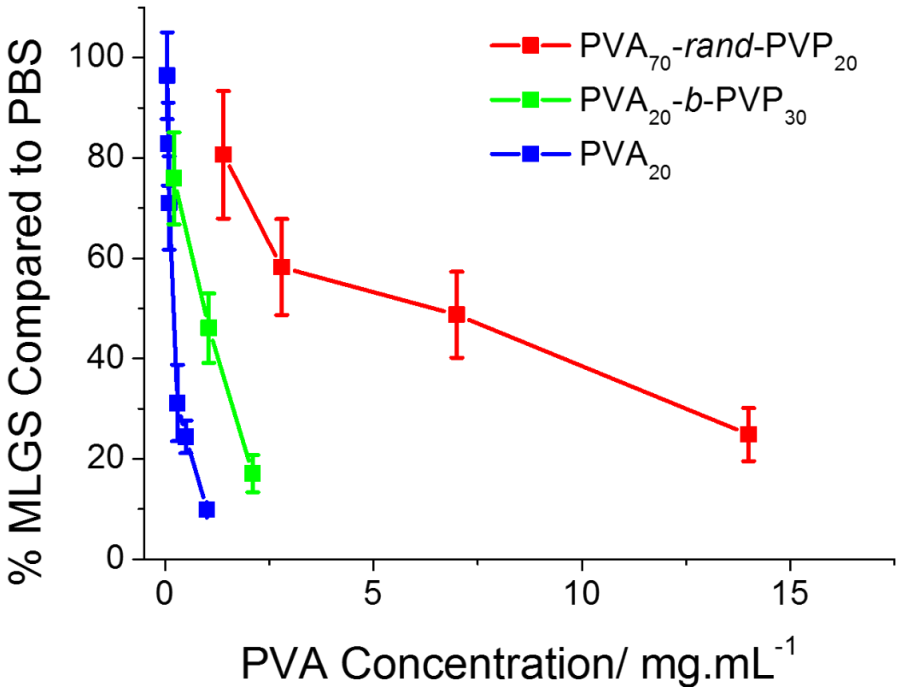

Figure 3.9 The PVA wt % dependent IRI activity of **PVA_{20}-*b*-PVP_{30}** block co-polymer, **PVA_{20}** homopolymer, and the **PVA_{70}-*rand*-PVP_{20}** random co-polymer; detailed in Chapter 2 (M_n = 4320, Đ 1.33, PVA = 48 wt %,).

Figure 3.10 shows that the activity of **PVA_{32}-*b*-PVP_{70}**, which gives a % MLGS of 18 at 0.75 $mg.mL^{-1}$, is comparable with many of the PVA homopolymers tested in Chapter 2. This is especially intriguing considering it comprises of 54 % non-active units by composition, and 85% non-active units by mass.

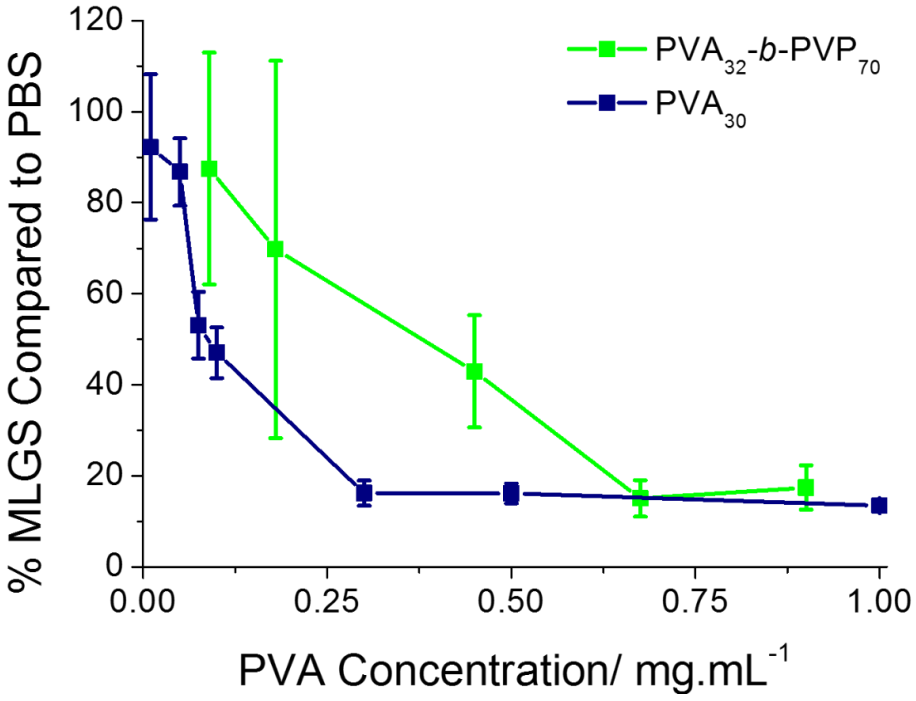

Figure 3.10 The PVA wt % dependent IRI activity of **PVA_{32}-*b*-PVP_{70}** block co-polymer and **PVA_{30}** homopolymer.

Figure 3.10 shows that even in dilute concentration (< 1 $mg.mL^{-1}$) this polymer still has comparable activity to a homo-PVA with the same IRI active chain length, especially when considering that the calculated concentration (x-axis) is only an estimate based on the M_n of the polymer by SEC and ^1H NMR spectroscopy. These results show that when arranged in blocks the IRI activity of PVA is preserved. This opens up a strategy for the addition of polymer functionality onto blocks of PVA, without drastically compromising the IRI behaviour of the polymer. These results also highlight the need for a more systematic analysis of the effect of the size of the PVP block, and any effect it may be having, beyond being a non-active water soluble component of the block co-polymer.

3.3iv Polymerisation and Chain Extension of PVAc MacroCTAs

In the literature PVP macroCTAs are polymerised with VAc to afford PVAc.PVP block co-polymers.[16, 12] This was done to show that under a MADIX scheme PVP can be chain extended, proving its living character and viable end-group fidelity. This method worked well for preparing block co-polymers (Table 3.2), but further examination into the effect that the PVP block was having on IRI activity was required. To achieve this, well-defined, living PVAc needed to be prepared and the same sample chain extended with a range of different molecular weights of PVP. This would afford a small library of PVA.PVP block copolymers with identical PVA blocks.

PVAc macroCTAs were prepared and then chain extended with PVP to give a range of block co-polymers with the same size PVA block. In order to test the efficacy of this method, vinyl acetate was polymerised using **MADIX 3** (Scheme 3.3) and allowed to polymerise to approximately 20% conversion, affording PVAc macroCTA with high degrees of end group fidelity.

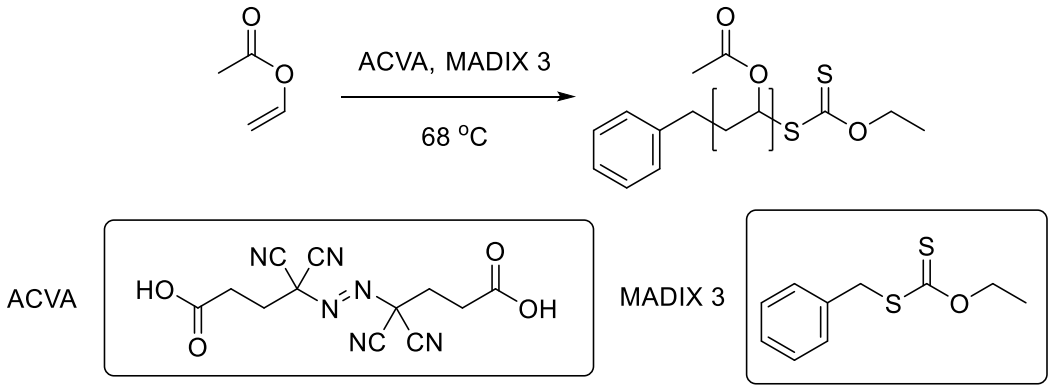

Scheme 3.3 Preparation of PVAc macroCTA.

The polymerisation was quenched using liquid nitrogen and then exposure to air. This reaction afforded polymer with very low dispersity, (Table 3.3).

Table 3.3 Initial PVAc homopolymer prepared for this study.

Entry	[M]/ [CTA][a]	Conv [b] %	$M_{n,}^{theo}$ [c] $g{\cdot}mol^{-1}$	$M_{n,}^{NMR}$ [d] $g{\cdot}mol^{-1}$	$M_{n,}^{SEC}$ [e] $g{\cdot}mol^{-1}$	$Đ$ [e]	DP_n [f]
$PVAc_{30}$	100	24.2	8610	2670	2640	1.12	30

A Monomer to RAFT agent ratio. **B** Determined by ^{1}H NMR spectroscopy. **C** Theoretical M_n determined from monomer to RAFT agent ratio. **D** Determined by ^{1}H NMR spectroscopy. **E** Determined by SEC in THF using PMMA standards. **F** Number-average degree of polymerisation.

Although several reports of PVAc-containing block co-polymers exist,[20, 21] no one has reported using a MADIX scheme to chain extend PVAc with PVP. The most applicable report uses a cobalt-mediated system.[11] The PVAc macroCTA detailed in Table 3.3 was taken on and chain extended with *N*-vinyl pyrrolidone in dioxane, with a high targeted degree of polymerisation. The resultant polymer was recovered *via* precipitation into diethyl ether and then dried thoroughly under vacuum. Pleasingly this trial polymerisation afforded chain extended polymer with narrow dispersity, showing the viability of this synthetic method (Table 3.4).

Table 3.4 Details of **$PVAc_{30}$-*b*-PVP_{60}** block co-polymer prepared for this study.

PVAc-*b*-PVP	[M]/ [mCTA]	conv.[b] %	$M_{n,theo}$[c] $g{\cdot}mol^{-1}$	$M_{n,NMR}$[d] $g{\cdot}mol^{-1}$	$M_{n,SEC}$[e] $g{\cdot}mol^{-1}$	M_w/M_n[e]	PVP[f] DP
$PVAc_{30}$–PVP_{60}	240	18.3	29300	4730	5380	1.16	24

A [total monomer]/[RAFT agent] ratio = 100:1; Polymerisation conducted in 3 mL VP and 0.5 mL 1,4-dioxane. **B** Determined by ^{1}H NMR spectroscopy. **C** Theoretical M_n determined from monomer to RAFT agent ratio. **D** Determined by ^{1}H NMR spectroscopy of the co-polymers after precipitation and drying. **E** Determined by SEC in THF using PMMA standards. **F** Determined by ^{1}H NMR spectroscopy of the PVAc-*b*-PVP block co-polymers.

Mono-modal chain extension was confirmed by SEC in THF (Figure 3.11). The polymer was then hydrolysed using hydrazine hydrate solution, dialysed and freeze dried, affording the PVA-*b*-PVP block co-polymer **PVA$_{30}$-*b*-PVP$_{60}$**, which was characterised using ^{1}H NMR spectroscopy, (Figure 3.12).

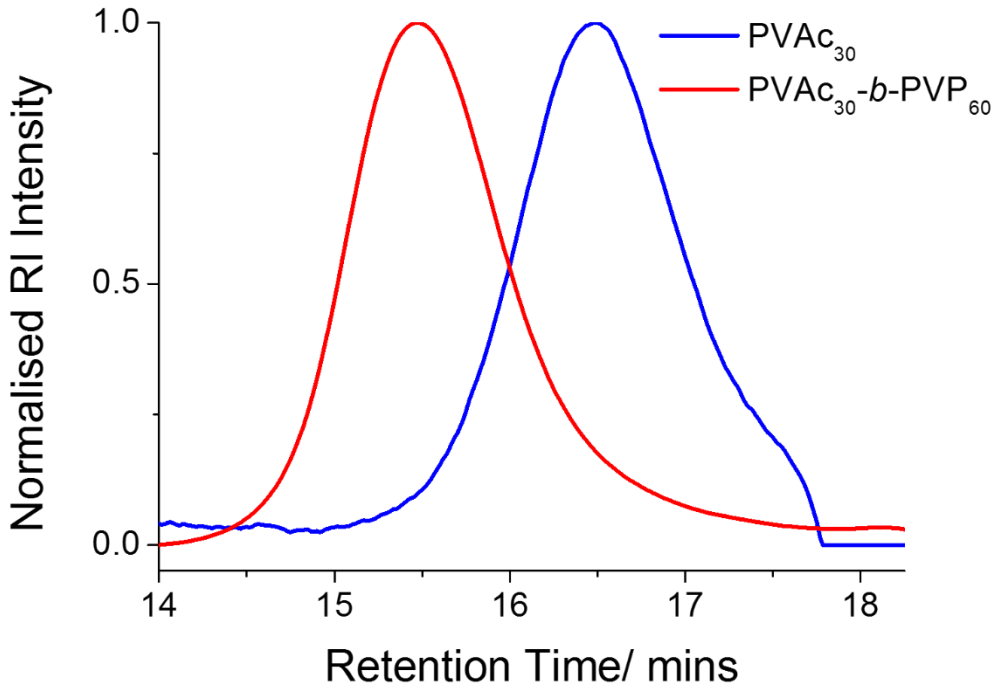

Figure 3.11 SEC in THF using PMMA standards, showing increase in molecular weight of PVAc chain extended with NVP.

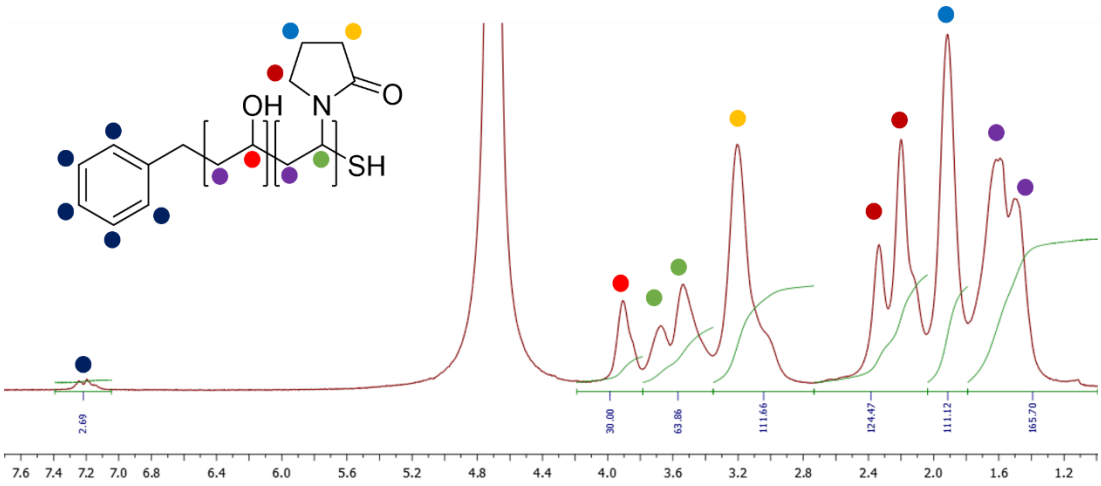

Figure 3.12 ^{1}H NMR spectroscopic analysis of **PVA$_{30}$-*b*-PVP$_{60}$**.

This strategy of chain extending PVAc macroCTA is a more effective way of preparing block co-polymers than using PVP macro CTAs, due to the greater control over the polymerisation and the more accurate characterisation of both the initial PVAc polymer the resultant block co-polymers.

Using this methodology, low molecular weight DP$_n$ 10 PVAc was prepared and then chain extended with NVP to afford a small library of block co-polymers with an identical PVA block but different sizes of PVP block. Such a small polymer was chosen due to its weak IRI compared to other PVA polymers; any changes in IRI activity caused by the PVP block would be easier to observe.

PVA$_{10}$ was prepared in a similar fashion as before, polymerising VAc in 1,4 dioxane using a suitable MADIX agent, in this case **MADIX 2,** as this CTA was slightly better suited to mediating the polymerisation of vinyl acetate at low conversion. Terminating the reaction at low conversion after approximately 10 minutes afforded a DP 9 PVAc oligomer, (Table 3.5). These polymers were then characterised using ^{1}H NMR spectroscopic analysis of the reaction mixture and the precipitated polymer, (Figure

3.13, Figure 3.14) SEC in THF using PMMA standards, (Figure 3.15) and electrospray ionisation mass spectroscopy (ESI-MS) (Figure 3.16).

Table 3.5 $PVAc_{10}$ homopolymer prepared for this study.

Entry	[M]/ [CTA][a]	Conv [b] %	$M_{n,}^{theo}$ [c] $g{\cdot}mol^{-1}$	$M_{n,}^{NMR}$ [d] $g{\cdot}mol^{-1}$	$M_{n,}^{SEC}$ [e] $g{\cdot}mol^{-1}$	$Đ$ [e]	DP_n [f]
$PVAc_{10}$	100	10	1056	780	920	1.32	9

A Monomer to RAFT agent ratio. **B** Determined by ^{1}H NMR spectroscopy. **C** Theoretical M_n determined from monomer to RAFT agent ratio. **D** Determined by ^{1}H NMR Spectroscopy. **E** Determined by SEC in THF using PMMA standards. **F** Number-average degree of polymerisation.

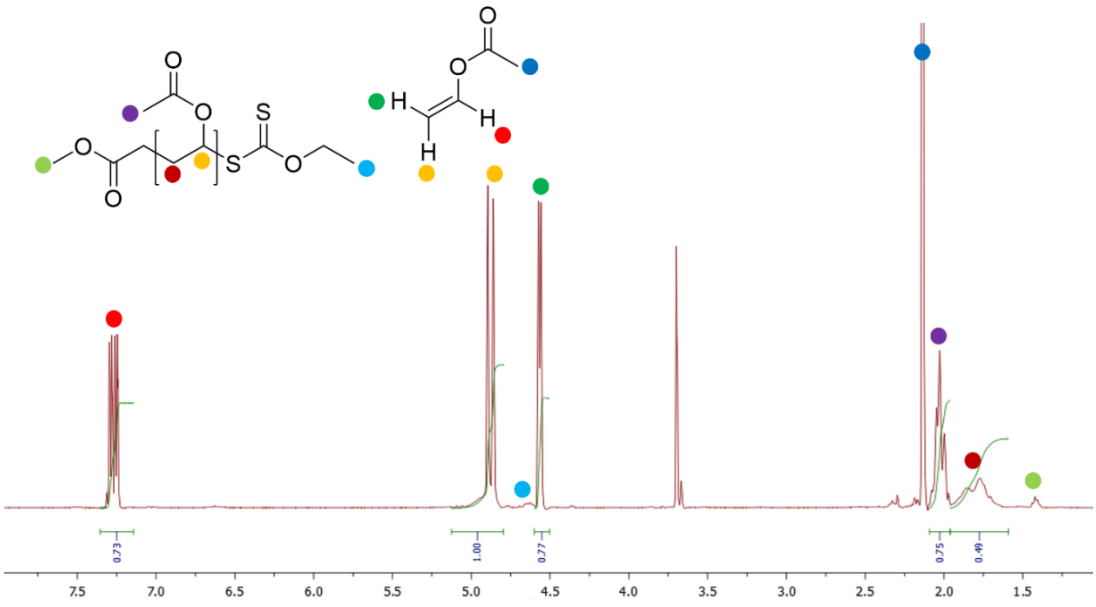

Figure 3.13 ^{1}H NMR spectrum of **$PVAc_{10}$** reaction mixture.

Figure 3.14 shows that precipitation of the polymers is not effective at recovering polymer due to the low molecular weight, but was sufficient for end-group analysis..

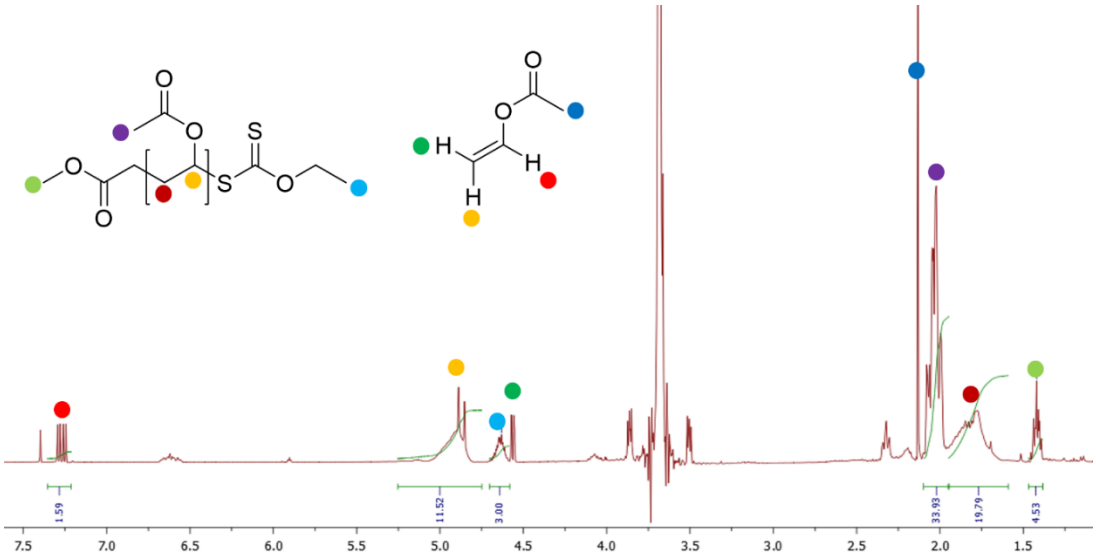

Figure 3.14 ^{1}H NMR spectrum of **PVAc$_{10}$** after precipitation.

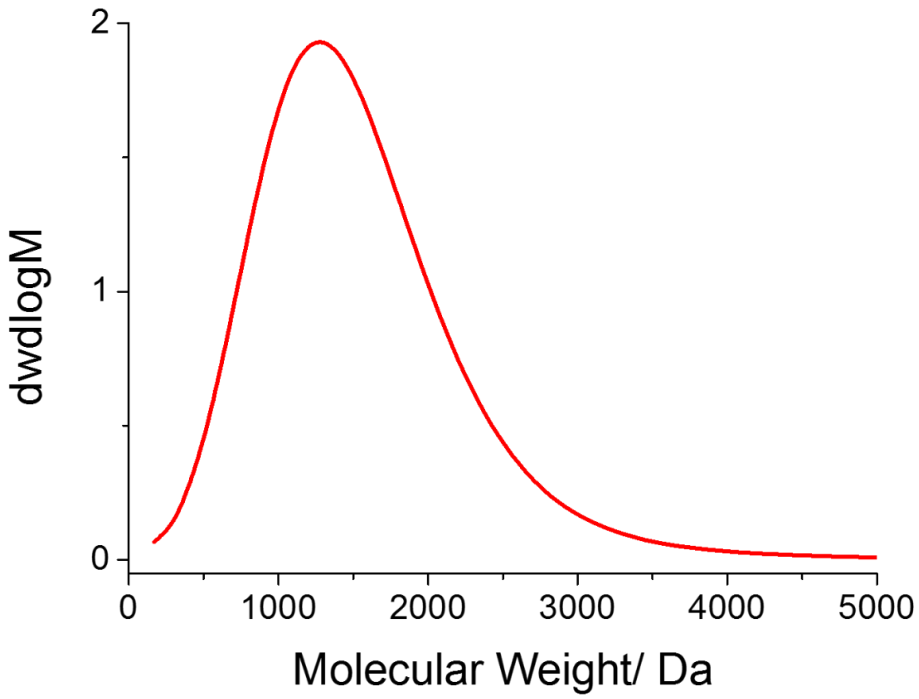

Figure 3.15 SEC analysis of **PVAc$_{10}$** in THF using PMMA standards.

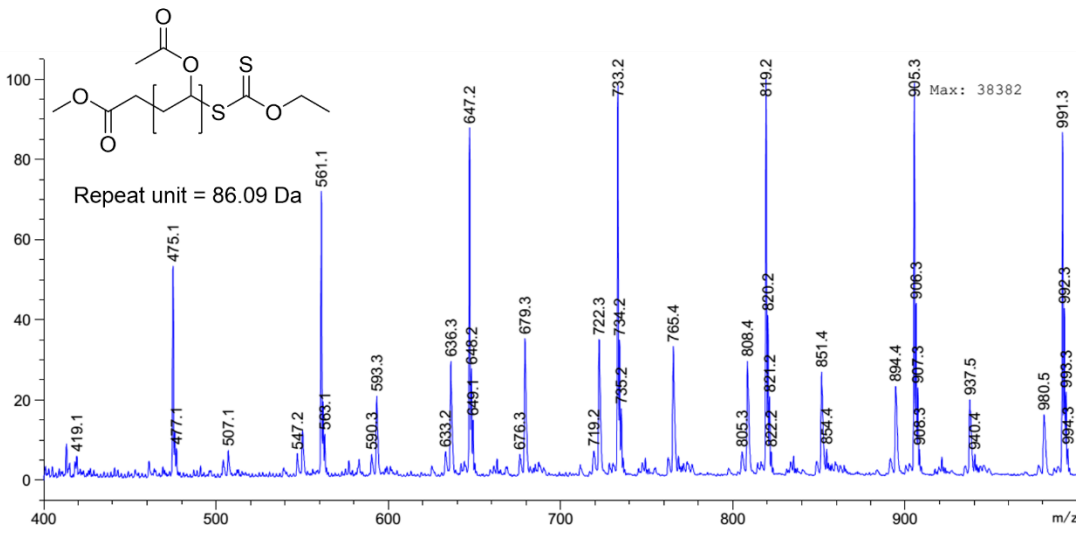

Figure 3.16 ESI-MS of **$PVAc_{10}$**, major peaks correspond to each different length of PVAc with a Na counter-ion.

Due to the low molecular weight of these polymers it was easier to remove excess monomer *in vacuo* rather than precipitate the polymers, which tended to be soluble in the precipitation solvent. Mass spectrometry shows the formation of a small amount of side product with a different mass peak pattern, which is most likely PVAc with differing end-group functionality. Due to the low conversion used, this is essentially unavoidable. At such low degrees of polymerisation, the concentration of radicals is higher than average for most the polymerisation. This can be seen in kinetic experiments, where the polydispersity initially broadens before narrowing as the reaction proceeds. Interestingly the mass difference in these minor peaks is half of the vinyl acetate monomer, which suggests the presence of a doubly charged species.

Samples of $PVAc_{10}$ polymer were chain extended with NVP, using different ratios of mCTA to monomer to give different molecular weights of PVP in the final block co-polymers (Table 3.6).

Table 3.6 $PVAc_{10}$-*b*-PVP block co-polymer prepared for this study.

PVAc-*b*-PVP	[M]/ [CTA]	NVP/ mL	Conv.[b] %	$M_{n,NMR}$[c] g.mol^{-1}	$M_{n,DMF}$[d] g.mol^{-1}	$M_{n,THF}$[e] g.mol^{-1}	M_w/M_n [d]
$PVAc_{10}$-*b*-PVP_{20}	10	0.75	18.3	1970	3080	570	1.37
$PVAc_{10}$-*b*-PVP_{34}	30	1.90	100	4190	4600	740	1.59
$PVAc_{10}$-*b*-PVP_{60}	50	3.79	56.8	3640	7479	760	1.76
$PVAc_{10}$-*b*-PVP_{83}	75	5.78	43.2	3970	10060	690	1.99

A [total monomer]/[RAFT agent] ratio; Polymerisation conducted in 5 mL 1,4-dioxane and varying **B** Determined by ^{1}H NMR spectroscopy. **C** Determined by ^{1}H NMR of the co-polymers after precipitation and drying. **D** Determined by SEC in THF using PMMA standards. **E** Determined by ^{1}H NMR spectroscopy of the PVAc-*b*-PVP block co-polymers.

The polymers detailed above displayed higher degrees of conversion than the trial polymerisation in Table 3.6. DMF SEC showed polymers with broad Đ, which is expected for SEC of PVP. These traces are bimodal, with a peak at approximately 1 kDa appearing in every spectra, (Figure 3.17). These are most likely dormant PVAc chains that lacked the correct end-group functionality to chain extend, as seen in the mass spectrometry analysis above.

THF SEC corroborates this, showing low molecular weight peaks around M_n 700, (Figure 3.18). In order to see if there was any chain extension the polymers were hydrolysed in hydrazine hydrate solution, dialysed and freeze dried, then analysed by ^{1}H NMR spectroscopy, to see if the purified polymers contained any PVA functionality.

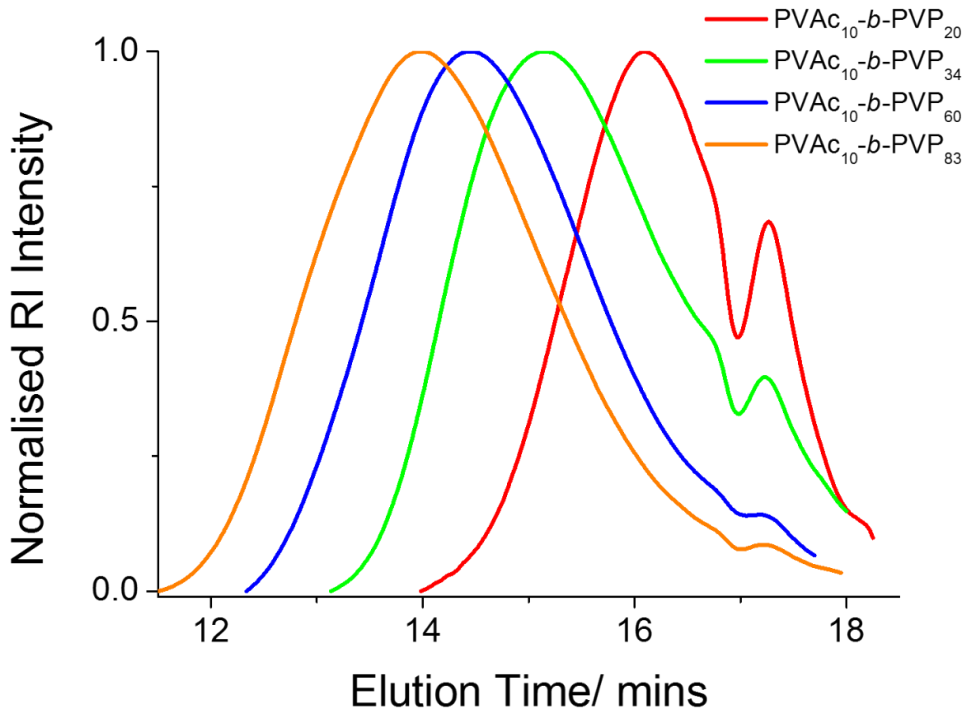

Figure 3.17 SEC analysis of **PVAc$_{10}$-*b*-PVP** in DMF.

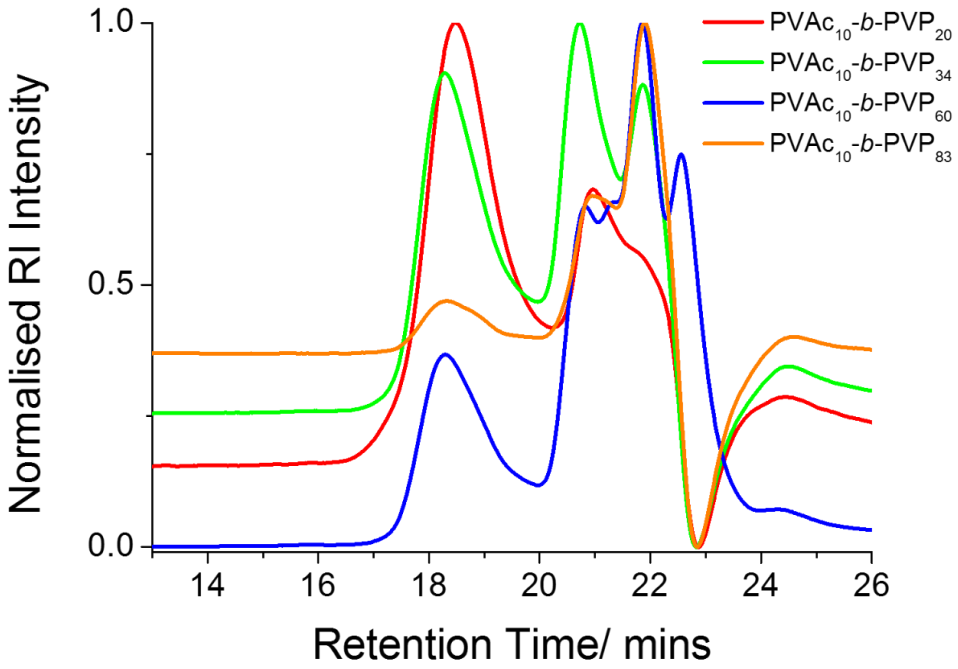

Figure 3.18 SEC analysis of **PVAc$_{10}$-*b*-PVP** in THF. Peaks at 18 mins are PVAc, peaks between 20 – 22 minutes can be attributed to residual solvent and monomer.

Table 3.7 Comparison of ^{1}H NMR spectroscopic analysis and SEC data collected for PVAc-*b*-PVP block co-polymers.

PVAc-*b*-PVP[b]	$M_{n,NMR}$[a] **g.mol^{-1}**	$M_{n,DMF}$[b] **g.mol^{-1}**	$M_{n,THF}$[c] **g.mol^{-1}**	M_w/M_n[b]	**PVA-*b*-PVP** [a]
PVAc$_{10}$-*b*-PVP$_{20}$	1150	3080	570	1.37	**PVA$_{10}$-*b*-PVP$_{27}$**
PVAc$_{10}$-*b*-PVP$_{34}$	3370	4600	740	1.59	**PVA$_{10}$-*b*-PVP$_{90}$**
PVAc$_{10}$-*b*-PVP$_{60}$	3220	7479	760	1.76	**PVA$_{10}$-*b*-PVP$_{85}$**
PVAc$_{10}$-*b*-PVP$_{83}$	3550	10060	690	1.99	**PVA$_{10}$-*b*-PVP$_{72}$**

A Determined by ^{1}H NMR spectroscopic analysis of the co-polymers after hydrolysis and purification. **B** Determined by SEC in DMF using PMMA standards. **C** Determined by SEC in THF using PMMA standards.

^{1}H NMR spectroscopic analysis was in agreement with the above DMF SEC analysis (Table 3.7); similar molecular weight values were calculated for each of the blocks, by integration of the methine -C*H* protons for the PVA and PVP blocks, at δ = 4.0 ppm and δ = 3.8 - 3.6 ppm respectively (Figure 3.19).

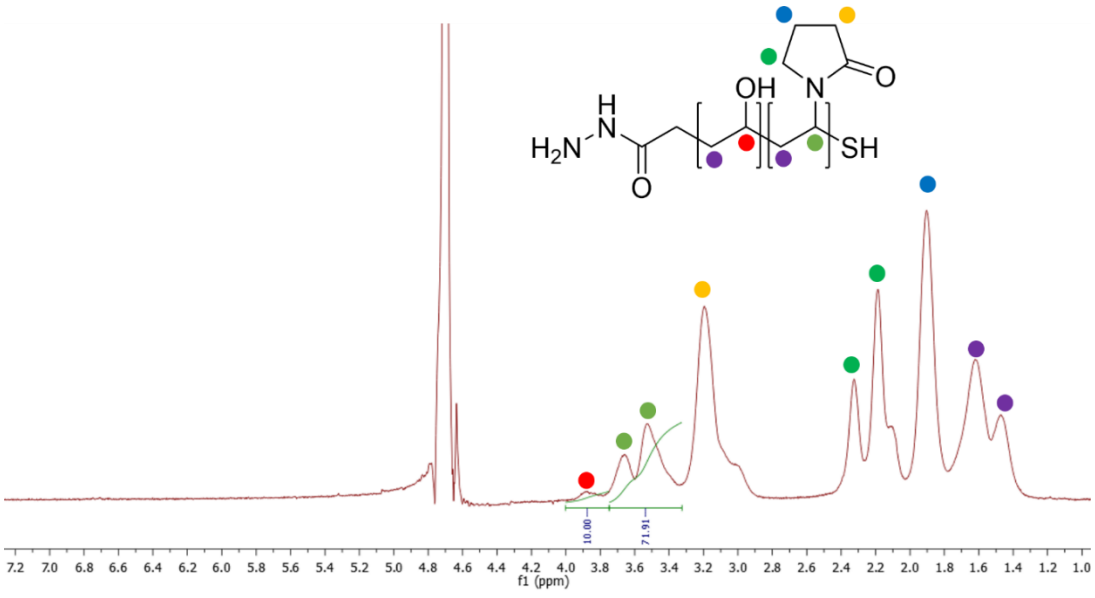

Figure 3.19 ^{1}H NMR spectrum of **PVA$_{10}$-*b*-PVP$_{72}$**.

3.3v The IRI Activity of PVA_{10}-*b*-PVP_n Block Co-polymers

Firstly, the IRI activity of **PVA_{30}-*b*-PVP_{60}** was assessed to determine that there were no major changes in IRI activity arising from the alternate synthetic method applied to prepare these polymers, (Figure 3.20, Figure 3.21).

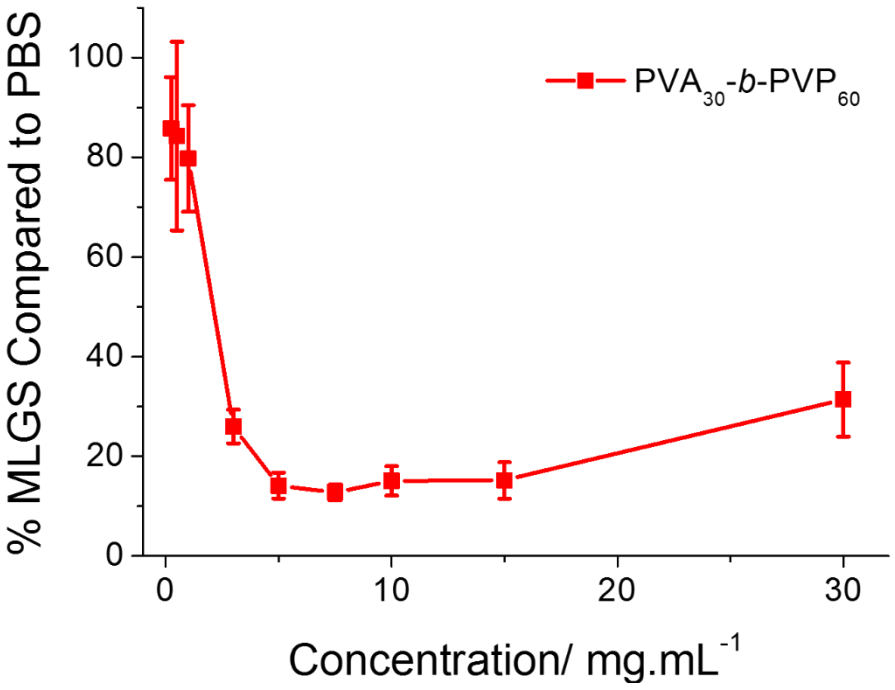

Figure 3.20 IRI activity of **PVA_{30}-*b*-PVP_{60}** block copolymer.

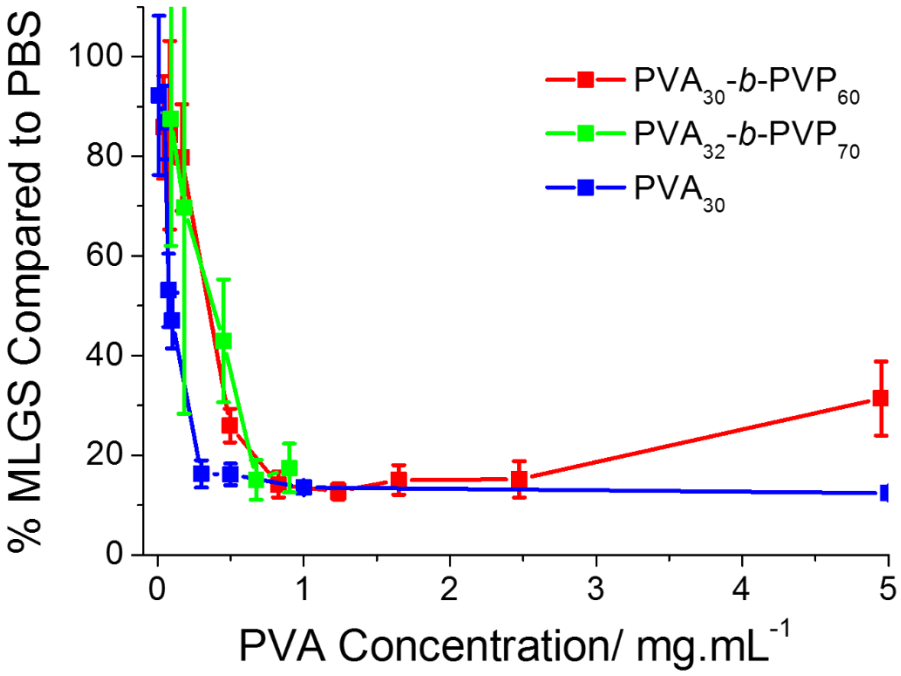

Figure 3.21 The PVA weight % dependent IRI activity of **PVA$_{30}$-*b*-PVP$_{60}$** block co-polymer.

As would be expected, the synthetic pathway used to prepare PVA-*b*-PVP co-polymers had no effect on the IRI activity, as Figure 3.21 shows. Pleasingly the IRI activity of **PVA$_{30}$-*b*-PVP$_{60}$** is almost identical to both the PVP derived block co-polymer **PVA$_{32}$-*b*-PVP$_{70}$** and **PVA$_{30}$** homo-polymer. Also there is the characteristic 'switching' of ice growth over a small PVA concentration range, which was observed for the highly IRI active PVA homopolymers tested in Chapter 2.

Next the IRI activity of the **PVA$_{10}$-*b*-PVP** co-polymers was determined. Polymers were dissolved in PBS solution and their IRI activity determined using the splat assay. The polymers were tested with increasing dilution until any indication of inhibition had disappeared, (Figure 3.22).

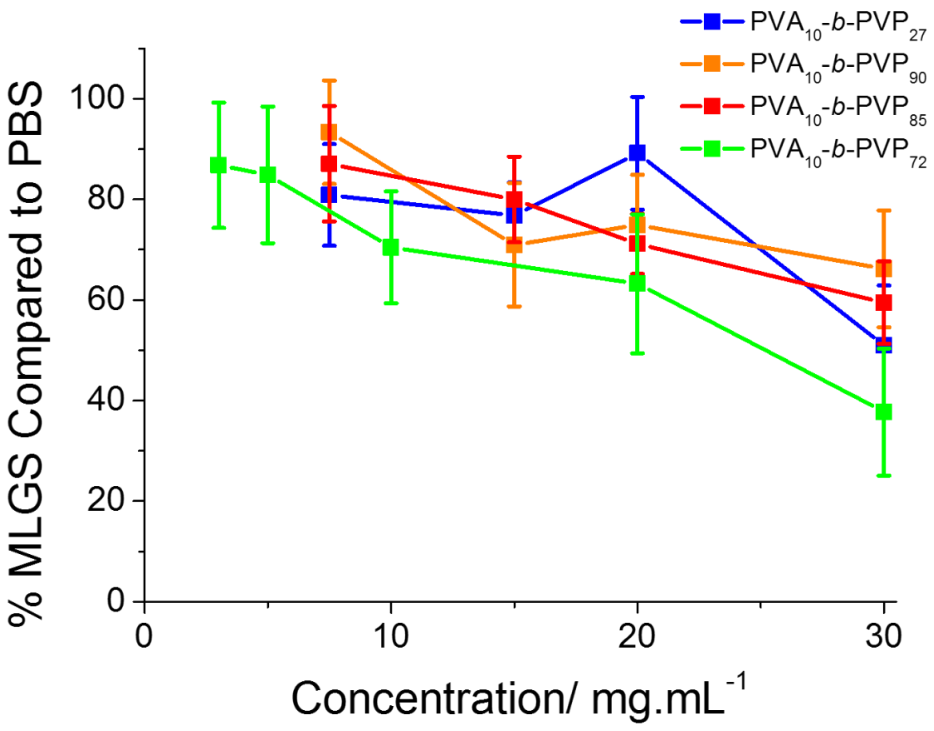

Figure 3.22 IRI activity of PVA_{10}-*b*-PVP block co-polymers.

As expected, these block co-polymers showed little activity across the concentration range tested. This is in line with the weak IRI activity of **PVA_{10}** seen in Chapter 2. A general trend of increasing crystal size is seen as the concentration of polymer in PBS solution is reduced, but there seems to be no observable trend in molecular weight dependence of each of the polymers. The size of the crystals, and the range of largest crystal sizes (given by the error bars) shows that there is a large amount of crystal growth over the 30 minute annealing time of the splat assay. When the MLGS is plotted against PVA concentration, (Figure 3.23) it can be seen that at dilute concentrations (>1 $mg.mL^{-1}$) there is some inhibition of crystal growth, which is surprising as DP 10 PVA is almost inactive at 1 $mg.mL^{-1}$.

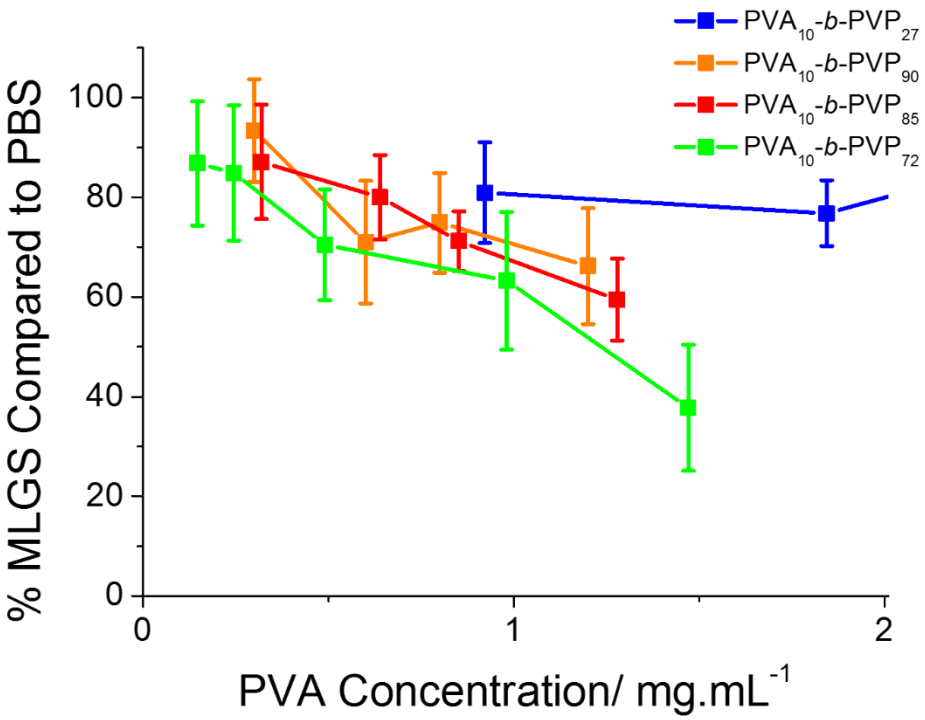

Figure 3.23 The PVA weight % dependent IRI activity of PVA_{10}-*b*-PVP block co-polymers.

When the PVA-concentration dependent activity of these PVA_{10}-*b*-PVP co-polymers is compared to PVA_{10} homopolymer, it can be seen that for all the samples tested block co-polymer activity closely matches that of homopolymer (Figure 3.24). Again, it can been seen that the non-active chain is having no detrimental effect on IRI activity. In fact, **PVA_{10}-*b*-PVP_{72}** is consistently more active than **PVA_{10}** over the concentration range tested, giving a % MLGS of 38 at 1.5 $mg.mL^{-1}$, which PVA_{10} cannot achieve below 7 $mg.mL^{-1}$, a dramatic increase in activity that can only be attributed the inclusion of the 'non-active' PVP block.

Figure 3.24 it shows that even at this high degree of chain extension and very low active block weight fraction, PVA activity is entirely unhindered by these large non-active PVP blocks.

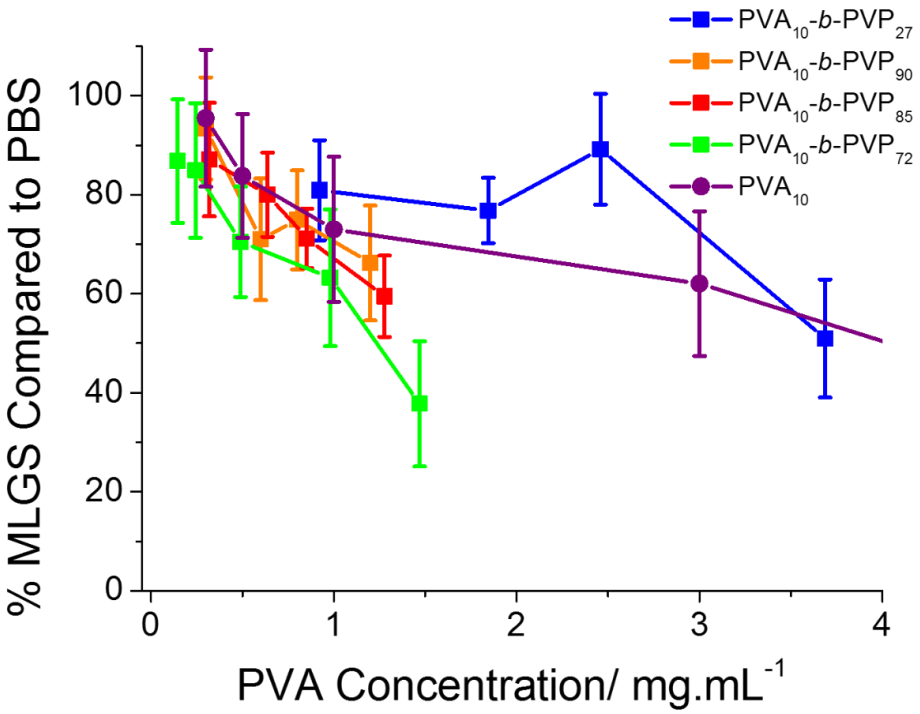

Figure 3.24 The PVA weight % dependent IRI activity of PVA_{10}-*b*-PVP block co-polymers compared to **PVA_{10}** (M_n = 440, Đ = 1.18).

It must be stressed that 10 repeat units of PVA is barely IRI active, and while at high concentrations (10 $mg.mL^{-1}$) it does show ice growth inhibition, **PVA_{10}** can be classified as on the borderline between IRI active and inactive. The fact that the addition of such large percentages of PVP does not affect activity, and it some cases measurably improve it, is fascinating when compared to the small molecule analogues prepared by Ben *et al.*[22] and the work into poly-ols conducted by Gibson *et al.*[23] (Figure 3.25).

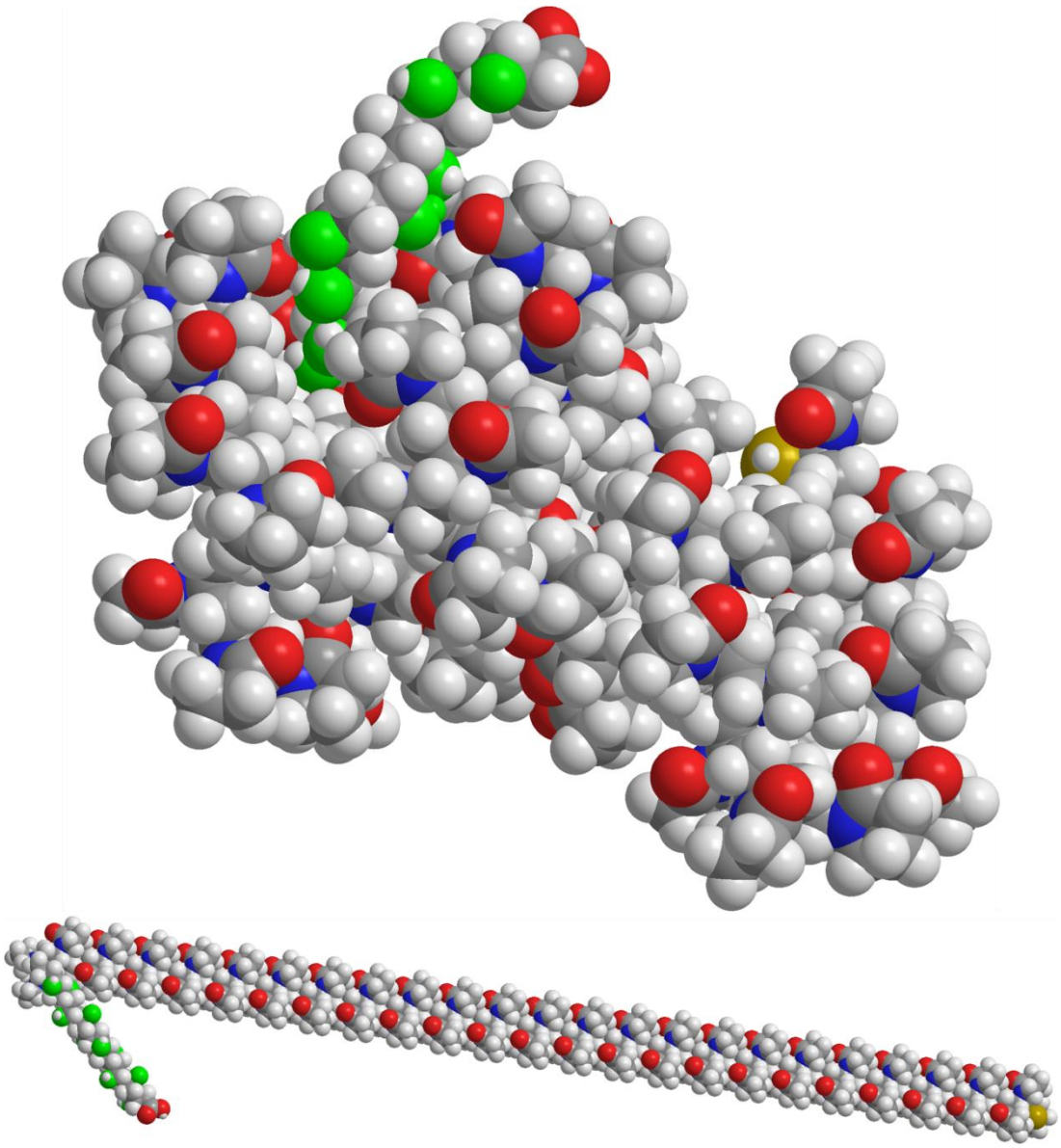

Figure 3.25 Space-fill graphical illustrations of **PVA_{10}-*b*-PVP_{72}**, green = alcohol groups of the PVA block, blue = nitrogen, red = carbonyl oxygen, yellow = sulfur. The polymer is presented in both a globular and linear forms, and neither represent the actual structure or conformation, and are intended merely to highlight the small percentage of IRI-active material in the polymer.

The IRI activity of those molecules was dependent on small changes in the length of hydrophobic groups or enantiomeric configurations. The above results clearly show the potency of PVA-based IRI agents and the potential of these polymers in more advanced antifreeze technologies.

3.4 Conclusion

In this chapter the synthesis, polymerisation, and IRI activity of PVA-*b*-PVP co-polymers was studied. First the MADIX mediated polymerisation of NVP was used to prepare a range of low molecular weight mCTA agents. This polymer was then chain extended with PVAc to prepare block co-polymers, which were characterised through a combination of ^{1}H NMR spectroscopy and SEC in DMF and THF. These polymers were then hydrolysed *via* hydrazinolysis, dialysed and freeze dried to afford pure PVA-*b*-PVP co-polymers. These polymers were tested for IRI activity using the splat assay, and when compared in terms of the concentration of hydroxyl group functionality, it was seen that there is no loss of IRI activity at all due to the 'non-active' PVP block. In some cases the PVP block may in fact be increasing the potency of the IRI agent. Next, in order to systematically probe the effect of the PVP group, a range of PVA-*b*-PVP co-polymers were prepared from the same DP_n 10 PVAc macroCTA. To the author's knowledge this is the first time PVAc has been chain extended with PVP, using a MADIX-based system. Trial polymerisations were very positive and showed that the PVAc mCTAs were highly effective at controlling the polymerisation of NVP, and the resultant polymers possessed narrow molecular weight dispersity. After hydrazinolysis and dialysis the resultant polymer, **PVA_{30}-*b*-PVP_{60}** was tested using the splat assay and showed excellent retention of IRI activity. Finally the idea of activity retention by block copolymers was taken to its logical extreme, and using the same PVAc mCTA method a small library PVA_{10}-*b*-PVP block copolymers were prepared from the same DP_n 10 mCTA precursor. The borderline inactive PVA_{10} block, coupled with very large PVP blocks, displayed equal and sometimes greater IRI activity than a comparable homopolymer.

These findings, in the context of the results presented in chapter 2, and recent reports on the IRI activity of small molecules, show that the mechanism by which these polymers inhibit ice growth is perhaps more complex than previously thought. Nevertheless these results show that by presenting the hydroxyls groups in a continuous sequence activity is preserved, and that when designing IRI active co-polymers, sequence is more important than composition.

3.5 Experimental

For general materials and methods details, see the Appendix. Phosphate-buffered saline (PBS) solutions were prepared using pre-formulated tablets (Sigma-Aldrich) in 200 mL of Milli-Q water (>18.2 Ω mean resistivity) to give [NaCl] = 0.138 M, [KCl] = 0.0027 M, and pH 7.4. Vinyl acetate and *N*-vinyl pyrrolidone were purchased from Sigma-Aldrich and were filtered through a plug of basic alumina to remove inhibitors prior to their use. 4,4′-Azobis(4-cyanovaleric acid) was recrystallised from methanol and stored at - 8 °C in the dark. Hydrazine hydrate solution (approximately 80%) was purchased from Sigma Aldrich. All solvents were purchased from VWR or Sigma-Aldrich and used without further purification, except for 1,4-dioxane, which was filtered through a plug on alumina prior to use.

Synthesis of methyl (ethoxycarbonothioyl) sulfanyl acetate (MADIX 2)

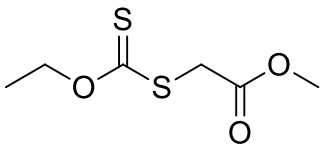

Acetone (70 mL) was added to a round bottom flask equipped with a stir bar. Potassium ethyl xanthate (2.97 g, 0.017 moles) was added and stirred until the solid had dissolved. Methyl bromoacetate (6.5 mL, 0.06 moles) was added dropwise and the solution left to stir overnight. The solution was filtered and washed with cold ethanol and concentrated *in vacuo*. The crude product was partitioned in DCM and sat. brine solution and the organic fraction concentrated *in vacuo*. The residue was washed through a column of basic alumina using pure ethyl acetate as the elutant. The fractions were concentrated *in vacuo* and then dried under vacuum. Yield 5.25 g 46 %. ^{1}H NMR ($CDCl_3$): δ = 1.42 (2H, t, J=7.2, CH_3CH_2), 3.76 (3H, s, CH_3O), 3.92 (2H,

d, J=7, SCH_2), 4.64 (3H, q, J=7.2, CH_3CH_2). ^{13}C NMR ($CDCl_3$): δ = 14.0 (CH_2–CH$_3$), 37.7 (CH$_2$), 61.0(CO$_2$$CH_3$), 70.4 ($CH_2$–CH$_3$), 167.7 (C=O), 212.4 (C=S).

Synthesis of methyl (ethoxycarbonothioyl) sulfanyl benzene (MADIX 3)

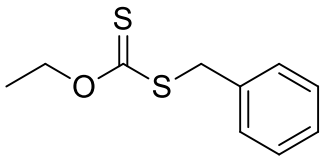

Acetone (70 mL) was added to a round bottom flask equipped with a stir bar. Potassium ethyl xanthate (2.97 g, 0.017 mol) was added and stirred until the solid had dissolved. Benzyl bromide (2.08 mL, 0.017 mol) was added, the flask stoppered and the reaction stirred at 50 °C for 18 h. The solution was then filtered and washed with acetone, then concentrated *in vacuo*. The residue was purified on a column of silica with DCM as the eluent, R_f = 0.2. Yield 3.25 g 54 % ^{1}H NMR ($CDCl_3$): δ = 1.36 (3H, t, J=7.2, CH_3CH_2), 4.33 (2H, s, SCH_2), 4.61 (2H, q, J=7.2, OCH_2CH_3) 7.25 (5H, m, benzyl protons); ^{13}C NMR ($CDCl_3$): δ = 13.91 (CH_2–CH$_3$), 40.54 (CH$_2$), 70.16 (CH$_2$CH$_3$), 212.4 (C=S), 127.56 (*para C*H), 128.72 (*meta C*H), 129.19 (*ortho C*H).

Polymerisation of *N*-vinyl Pyrrolidone using MADIX 3

As a representative example, *N*-vinyl-pyrrolidone (2.09 g, 18.78 mmol), CTA 1 (0.037 g, 0.17 mmol), and ACVA (0.005 g, 0.02 mmol) were dissolved in dioxane (4 mL) in a stoppered vial equipped with a stir bar. The reaction mixture was thoroughly degassed by bubbling N_2 through the solution for 20 min and the reaction mixture was allowed to polymerise at 70 °C for typically 3 h. The dark yellow solutions were then cooled to room temperature and the block co-polymer was recovered as white flakes by precipitation into cold diethyl ether held under ice. The bulk of the solvent was

carefully decanted and the solid collected by centrifugation. The product was thoroughly dried under vacuum at 40 °C for 24 h, forming a yellow solid. Representative characterisation data for PVP_{55}: ^{1}H NMR (400 MHz, $CDCl_3$) ^{1}H NMR (400 MHz, $CDCl_3$) δ 3.74 (−C*H*N–, br, 1H), 3.19 (−NC*H*$_2$CH_2–, br, 2H), 2.38 (−NCOC*H*$_2$–, br, 2H), 2.21(-NCH$_2$C*H*$_2$CH_2–, br, 2H), 1.81–1.53 (−C*H*$_2$–, br, 2H); M_n^{SEC}(THF) = 3350 Da, M_w/M_n = 1.42.

Chain Extension of Poly(vinyl pyrrolidone) macroCTA with Vinyl Acetate

As a representative example, PVP macroCTA (0.158 g, 2.6 × 10^{-5} mol), vinyl acetate (1.12 g, 13 × 10^{-3} mol), dioxane (2.6 mL) and ACVA (4,4′-azobis(4-cyanovaleric acid); 0.001 g, 4.2 × 10^{-6} mol) were added to a stoppered vial. The solution was thoroughly degassed by bubbling N_2 through the solution for 20 min, and the reaction mixture was then allowed to polymerise at 68 °C for 12 h. The yellow solutions were then cooled and opened to air. The block co-polymer was then recovered as a yellow sticky solid after precipitation into diethyl ether. The diethyl ether was then decanted and the block co-polymer was re-dissolved in THF, which was then concentrated *in vacuo* and thoroughly dried under vacuum at 40 °C for 24 h, forming a yellow solid. Representative characterisation data for **$PVAc_{18}$-*b*-PVP_{55}**: ^{1}H NMR (400 MHz, $CDCl_3$) δ 4.61 (−C*H*OAc–, br, 1H), δ 3.74 (−C*H*N–, br, 1H), 3.19 (−NC*H*$_2$CH_2–, br, 2H), 2.38 (−NCOC*H*$_2$–, br, 2H), 2.21(-NCH$_2$C*H*$_2$CH_2–, br, 2H), δ 2.00 (−C*H*$_3$, t, 3H), 1.81–1.53 (−C*H*$_2$–, br, 2H); M_n^{SEC} (DMF) = 9130 Da; M_w/M_n = 1.36.

Polymerisation of Vinyl Acetate using MADIX 2

As a representative example, MADIX 2 (5.2 mg, 2.6×10^{-5} mol), vinyl acetate (4.67 g, 2.6×10^{-3} mol), and ACVA (4,4′-azobis(4-cyanovaleric acid); 0.0013 g, 4.6×10^{-6} mol) were added to a stoppered vial. The reaction mixture was thoroughly degassed by bubbling N_2 through the solution for 20 min, and the reaction mixture was then allowed to polymerise at 68 °C for 10 to 30 minutes, depending on the desired degree of conversion (at 1/100 [CTA]/[Monomer] conversion = 1 % /min). The yellow solutions were then quenched in liquid nitrogen and exposed to air. The polymer was then recovered as a yellow sticky solid after precipitation into hexane. The hexane was then decanted and the poly(vinyl acetate) redissolved in THF, which was then concentrated *in vacuo* and thoroughly dried under vacuum at 40 °C for 24 h, forming a yellow solid. Representative characterisation data for $PVAc_{30}$: ^{1}H NMR (400 MHz, $CDCl_3$) δ 4.61 (−C*H*O–CH_2, br, 1H), 1.74 (−CO–C*H*$_3$, br, 3H), 1.53 (−C*H*$_2$–, br, 2H); M_n^{SEC}(THF) = 2642 Da, M_w/M_n = 1.12.

Chain Extension of Poly(vinyl acetate) macroCTA with *N*-vinyl Pyrrolidone

As a representative example, PVAc macroCTA (0.307 g, 1.16×10^{-3} mol), *N*-vinyl pyrrolidone (3 g, 28.2 mmol), dioxane (0.5 mL) and ACVA (4,4′-azobis(4-cyanovaleric acid); 0.028 g, 1×10^{-4} mol) were added to a stoppered vial. The reaction mixture was thoroughly degassed by bubbling N_2 through the solution for 20 min, and the reaction mixture was then allowed to polymerise at 70 °C for 12 h. The yellow solutions were then cooled and opened to air. The block co-polymer was then recovered as a yellow sticky solid after precipitation into diethyl ether. The diethyl ether was then decanted and the block co-polymer re-dissolved in THF, which was

then concentrated *in vacuo* and thoroughly dried under vacuum for 24 h, forming a pale yellow solid. Representative characterisation data for **PVAc$_{30}$-*b*-PVP$_{24}$**: ^{1}H NMR (400 MHz, $CDCl_3$) δ 4.61 (−C*H*OAc–, br, 1H), δ 3.74 (−C*H*N–, br, 1H), 3.19 (−NC*H*$_2$CH$_2$–, br, 2H), 2.38 (−NCOC*H*$_2$–, br, 2H), 2.21(-NCH$_2$C*H*$_2$CH$_2$–, br, 2H), δ 2.00 (−C*H*$_3$, t, 3H), 1.81–1.53 (−C*H*$_2$–, br, 2H); M_n^{SEC} (THF) = 5376 Da; M_w/M_n = 1.16.

Hydrolysis of PVAc-*b*-PVP Block Co-polymers

As a representative example, **PVAc$_{30}$-*b*-PVP$_{24}$** (0.3 g, 5376 Da, M_n/M_w = 1.16) was dissolved in a methanol (2 mL) and hydrazine hydrate solution (5 mL, 80 % in water) in a stoppered vial. The reaction mixture was stirred at 60 °C for 5 h. The reaction mixture was then dialysed using distilled water and **PVA$_{30}$-*b*-PVP$_{24}$** was recovered as a spongy white solid by freeze drying the dialysis solution. Complete hydrolysis was confirmed by ^{1}H NMR. Representative characterisation data for **PVA$_{30}$-*b*-PVP$_{24}$**: ^{1}H NMR (400 MHz, D_2O): δ=3.52 (-C*H*N- br d 1H), δ=4.00 (-C*H*O- br 1H), δ=3.12 (-NC*H*$_2$CH$_2$- br d 2H), δ=2.49 (-NCOCH$_2$- br 2H), δ=2.13 (-NCH$_2$C*H*$_2$CH$_2$- br d 2H), δ=1.80-1.50 (-C*H*$_2$- br 2H),

3.6 References

1. Garnham, C. P.; Campbell, R. L.; Davies, P. L., Anchored clathrate waters bind antifreeze proteins to ice. *Proceedings of the National Academy of Sciences* **2011,** *108* (18), 7363-7367.

2. Harding, M. M.; Anderberg, P. I.; Haymet, A. D. J., 'Antifreeze' glycoproteins from polar fish. *European Journal of Biochemistry* **2003,** *270* (7), 1381-1392.

3. Lane, A. N.; Hays, L. M.; Feeney, R. E.; Crowe, L. M.; Crowe, J. H., Conformational and dynamic properties of a 14 residue antifreeze glycopeptide from Antarctic cod. *Protein Science : A Publication of the Protein Society* **1998,** *7* (7), 1555-1563.

4. Nguyen, D. H.; Colvin, M. E.; Yeh, Y.; Feeney, R. E.; Fink, W. H., The dynamics, structure, and conformational free energy of proline-containing antifreeze glycoprotein. *Biophysical Journal* **2002,** *82* (6), 2892-2905.

5. Yeh, Y.; Feeney, R. E., Antifreeze proteins: Structures and mechanisms of function. *Chemical Reviews* **1996,** *96* (2).

6. Mai, Y.; Eisenberg, A., Self-assembly of block copolymers. *Chemical Society Reviews* **2012,** *41* (18), 5969-5985.

7. Tam, R. Y.; Rowley, C. N.; Petrov, I.; Zhang, T.; Afagh, N. A.; Woo, T. K.; Ben, R. N., Solution Conformation of C-Linked Antifreeze Glycoprotein Analogues and Modulation of Ice Recrystallization. *Journal of the American Chemical Society* **2009,** *131* (43), 15745-15753.

8. Yeh, Y.; Feeney, R. E., Antifreeze proteins: Structures and mechanisms of function. *Chemical Reviews* **1996,** *96* (2), 601-618.

9. Baruch, E.; Mastai, Y., Antifreeze Properties of Polyglycidol Block Copolymers. *Macromolecular Rapid Communications* **2007,** *28* (23), 2256-2261.

10. Mastai, Y.; Rudloff, J.; Cölfen, H.; Antonietti, M., Control over the Structure of Ice and Water by Block Copolymer Additives. *ChemPhysChem* **2002,** *3* (1), 119-123.

11. Debuigne, A.; Willet, N.; Jérôme, R.; Detrembleur, C., Amphiphilic poly (vinyl acetate)-b-poly (N-vinylpyrrolidone) and novel double hydrophilic poly (vinyl alcohol)-b-poly (N-vinylpyrrolidone) block copolymers prepared by cobalt-mediated radical polymerization. *Macromolecules* **2007,** *40* (20), 7111-7118.

12. Nguyen, T. L. U.; Eagles, K.; Davis, T. P.; Barner-Kowollik, C.; Stenzel, M. H., Investigation of the influence of the architectures of poly(vinyl pyrrolidone) polymers made via the reversible addition–fragmentation chain transfer/macromolecular design via the interchange of xanthates mechanism on the stabilization of suspension polymerizations. *Journal of Polymer Science Part A: Polymer Chemistry* **2006,** *44* (15), 4372-4383.

13. Wan, D.; Satoh, K.; Kamigaito, M.; Okamoto, Y., Xanthate-Mediated Radical Polymerization of N-Vinylpyrrolidone in Fluoroalcohols for Simultaneous Control of Molecular Weight and Tacticity. *Macromolecules* **2005,** *38* (25), 10397-10405.

14. Pound, G.; Eksteen, Z.; Pfukwa, R.; McKenzie, J. M.; Lange, R. F. M.; Klumperman, B., Unexpected reactions associated with the xanthate-mediated polymerization of N-vinylpyrrolidone. *Journal of Polymer Science Part A: Polymer Chemistry* **2008,** *46* (19), 6575-6593.

15. Pound, G.; McKenzie, J. M.; Lange, R. F. M.; Klumperman, B., Polymer-protein conjugates from [small omega]-aldehyde endfunctional poly(N-vinylpyrrolidone) synthesised via xanthate-mediated living radical polymerisation. *Chemical Communications* **2008,** (27), 3193-3195.

16. Bailly, N.; Pound-Lana, G.; Klumperman, B., Synthesis, Characterization, and Self-Assembly of Poly(N-vinylpyrrolidone)-block-poly(vinyl acetate). *Australian Journal of Chemistry* **2012,** *65* (8), 1124-1131.

17. Bailly, N.; Thomas, M.; Klumperman, B., Poly(N-vinylpyrrolidone)-block-poly(vinyl acetate) as a Drug Delivery Vehicle for Hydrophobic Drugs. *Biomacromolecules* **2012,** *13* (12), 4109-4117.

18. Ieong, N. S.; Redhead, M.; Bosquillon, C.; Alexander, C.; Kelland, M.; O'Reilly, R. K., The Missing Lactam-Thermoresponsive and Biocompatible Poly(N-vinylpiperidone) Polymers by Xanthate-Mediated RAFT Polymerization. *Macromolecules* **2011,** *44* (4), 886-893.

19. Wu, C.-S., *Handbook Of Size Exclusion Chromatography And Related Techniques: Revised And Expanded*. CRC Press: 2003; Vol. 91.

20. Pound, G.; Aguesse, F.; McLeary, J. B.; Lange, R. F. M.; Klumperman, B., Xanthate-mediated copolymerization of vinyl monomers for Amphiphilic and double-hydrophilic block copolymers with poly(ethylene glycol). *Macromolecules* **2007,** *40* (25), 8861-8871.

21. Debuigne, A.; Caille, J.-R.; Willet, N.; Jérôme, R., Synthesis of Poly(vinyl acetate) and Poly(vinyl alcohol) Containing Block Copolymers by Combination of Cobalt-Mediated Radical Polymerization and ATRP. *Macromolecules* **2005,** *38* (23), 9488-9496.

22. Balcerzak, A. K.; Capicciotti, C. J.; Briard, J. G.; Ben, R. N., Designing ice recrystallization inhibitors: from antifreeze (glyco)proteins to small molecules. *RSC Advances* **2014,** *4* (80), 42682-42696.

23. Deller, R. C.; Congdon, T.; Sahid, M. A.; Morgan, M.; Vatish, M.; Mitchell, D. A.; Notman, R.; Gibson, M. I., Ice recrystallisation inhibition by polyols: comparison of molecular and macromolecular inhibitors and role of hydrophobic units. *Biomaterials Science* **2013,** *1* (5), 478-485.

Chapter 4

Synthesis and Ice Recrystallisation Inhibition Activity of Three-Arm *Star*-PVA

4.1 Chapter Overview

In this chapter, 3-arm *star*-PVAcs are prepared *via* a MADIX methodology and then hydrolysed to give *star*-PVAs. These polymers are then tested for IRI activity using the splat assay and the results compared to linear PVAs of similar molecular weight and chain length, in order to determine relative activities and assess the ability of these star polymers to inhibit ice crystal growth.

The design philosophy behind making efficient multifunctional MADIX agents is discussed and a novel MADIX agent is prepared incorporating these ideas. This agent's ability to control the polymerisation of vinyl acetate and its ability to prepare star polymers is trialled, with excellent results. Using this, a library of well-defined PVA star polymers is prepared and their IRI activity tested. Pleasingly these polymers displayed extremely efficient IRI activity, and the results were comparable to some of the most efficient PVA IRI agents tested.

4.2 Chapter Introduction

Star polymers comprise of a number of linear polymer chains arranged around a single core, so that the resultant structures resemble a star or, perhaps more accurately, a starfish.[1] There are many methods available to prepare these polymers, and the multi-armed structural motif finds use in anti-adhesion therapies targeting bacterial toxins.[2] A large amount of interest in multi-arm star polymers stems from the fact that the intrinsic viscosity of these polymers is lower in bulk and in solution than linear polymers of the same molecular weight.[3, 4] Star polymers also contain a greater amount of end-group functionality than linear polymers. For these reasons star polymers are promising tools for use in thermoplastics,[5] biomedical applications,[6] drug delivery,[7] and microelectronic devices.[8] Star polymers based on polyamides were first prepared by Florey,[9] and later in a controlled fashion using anionic polymerisation.[10] More recently star polymers have been prepared by ATRP,[11] NMP,[12] and RAFT.[13] The utility of RAFT agent synthesis means that preparation of multifunctional RAFT agents is straightforward and requires little change to the synthetic protocol. Based on their previous work into MADIX agent optimisation,[14] Stenzel and co-workers reported the synthesis and application of multifunctional MADIX agents for the polymerisation of *N*-vinyl pyrrolidone and vinyl acetate.[15] This report examined the morphological effect of these polymers as stabilisers in suspension polymerisation, and it was found that star polymers led to smaller particle sizes, due to differences in interfacial tension and overall viscosity. While PVP is not IRI active it finds use commercially as a kinetic hydrate inhibitor in oil pipelines, where it will stop the growth of clathrate hydrates[16] – crystalline solids comprised of non-polar molecules trapped in ‘cages’ of hydrogen-bonded, frozen water molecules.

If the morphology of the polymer affects its interfacial properties and solution behaviour, then it is logical that PVA star polymers may have different IRI effects compared to linear PVA. If the polymer is interacting with the ice crystal face, then star functionality would afford greater binding affinity, similar to the chelate or co-operative effects seen in a range of natural and synthetic mechanisms. For example, glyco-polymers have been shown to competitively bind bacterial toxins using the multivalency of the polymer to increase potency well above the predicted linear response.[17]

However, if IRI activity is due to interactions in the quasi-liquid layer, or in bulk solution, then the lower viscosity and interfacial tension may cause a change in the IRI activity, in line with the results reported by Gibson and co-workers[18] and Ben and co-workers,[19] where hydration and viscosity have been shown to play an important role. Either way, the IRI activity of star polymers of PVA would inform these theories on mechanism.

4.3 Results

4.3i The Synthesis of Multi-Arm MADIX Agents

In order to probe the effects of multi-arm stars of PVA on IRI, a multifunctional MADIX agent was required. Several of these have been prepared before by Stenzel and co-workers, who found that MADIX agents which fragmented from the core (X functionalised CTAs, Figure 4.1 A) were more suitable for the polymerisation of vinyl acetate than MADIX agents which would fragment from the arm (R functionalised CTAs, Figure 4.1 B).[20, 21, 22]

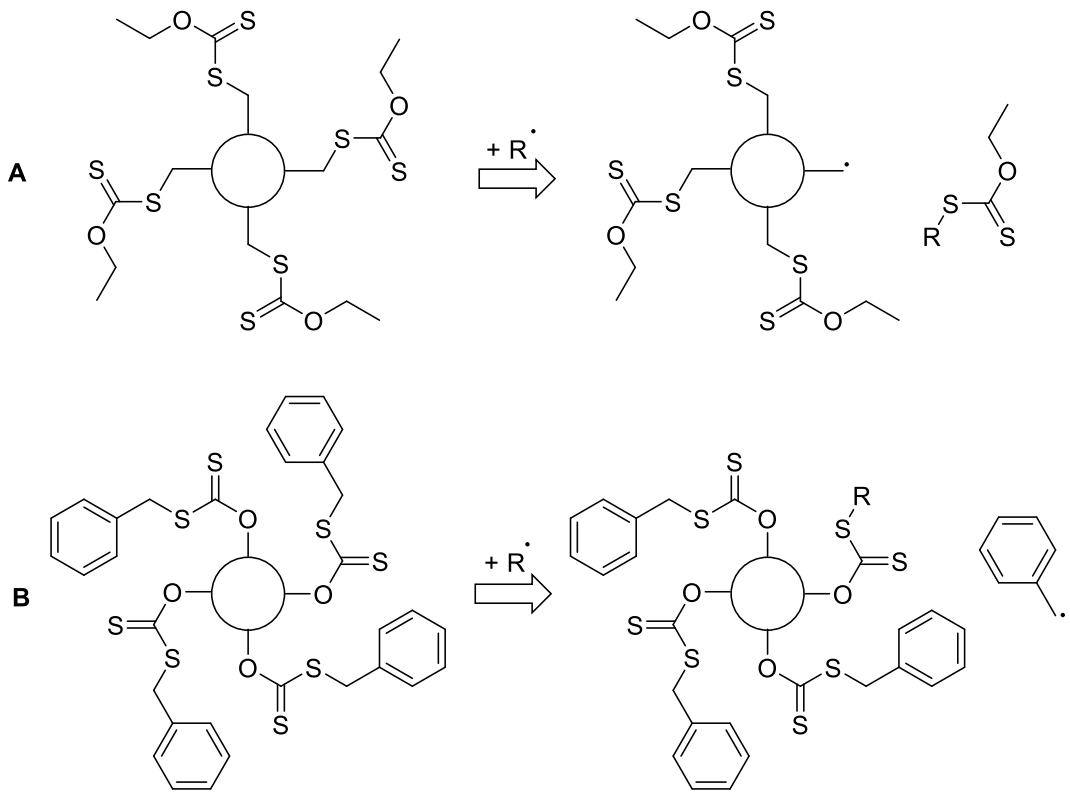

Figure 4.1 Different possible designs for multifunctional MADIX agents and their predicted fragmentation products in a radical polymerisation reaction.

At first it would appear that the R-group functionalised MADIX agents would be more suitable, since radical activity is sequestered only in the propagating fragment of the MADIX agent, away from the star, and would hence minimise star-star coupling. However this is not the case, as Stenzel reports in a paper comparing both methods that the X-group functionalised MADIX agent gave lower dispersity, and mono-modal SEC traces, signifiers that star-star coupling was not occurring.[22] It is not certain why this is. It could be that confining all radical activity in the system to a single core affords better control, due to propagating chains undergoing chain transfer with neighbouring MADIX groups in an intramolecular process. Compared to R-group MADIX agents, where the propagating radical species is separated from the core, and the core concentration is (in the example above) ¼ of the potential radical

concentration. This would make events such as termination by combination much more likely.

However, if the final product desired is PVA then the choice becomes somewhat elementary; a carbon-carbon bond from the core to the arm is required (X-group MADIX agents), otherwise during hydrazinolysis single polymer chains would be hydrolysed off the stars.

The next step was to choose a suitable core. Between 2001 and 2008 several reports were published focussing on several types of cores suitable for MADIX mediated polymerisation of lesser activated monomers, namely vinyl acetate and *N*-vinyl pyrrolidone. It was known that R-groups in the MADIX agent are a major factor in controlling the polymerisation of *N*-vinyl pyrrolidone, but are less important for vinyl acetate.

Stenzel and co-workers reported two classes of multifunctional MADIX agents for vinyl acetate and *N*-vinyl pyrrolidone, based around quaternary hydroxyl functionalised alkyl chains,[20] and substituted benzene rings,[15] respectively. For the purposes of preparing star polymers, and because the benzyl protons are such a convenient marker for ^{1}H NMR spectroscopic end-group analysis, a tri-functional benzyl group was chosen and prepared, (Scheme 4.1). While the 3-arm MADIX agent below is novel, the strategy has been used previously by Stenzel and co-workers, first to prepare a 6-arm multifunctional RAFT agent,[22] and later a 4-armed MADIX agent.[15] Polymerisations of styrene conducted utilising the 6-arm RAFT agent yielded a mixture of well controlled star and linear polymers. Control over the polymerisation was attributed to the significant steric hindrance within the initial stages of propagation and chain transfer. Polymerisations conducted using the 4-armed MADIX agent (the

synthesis of which is essentially the same as that outlined in Scheme 4.1) resulted in improved performance when compared to the 6-armed agent.

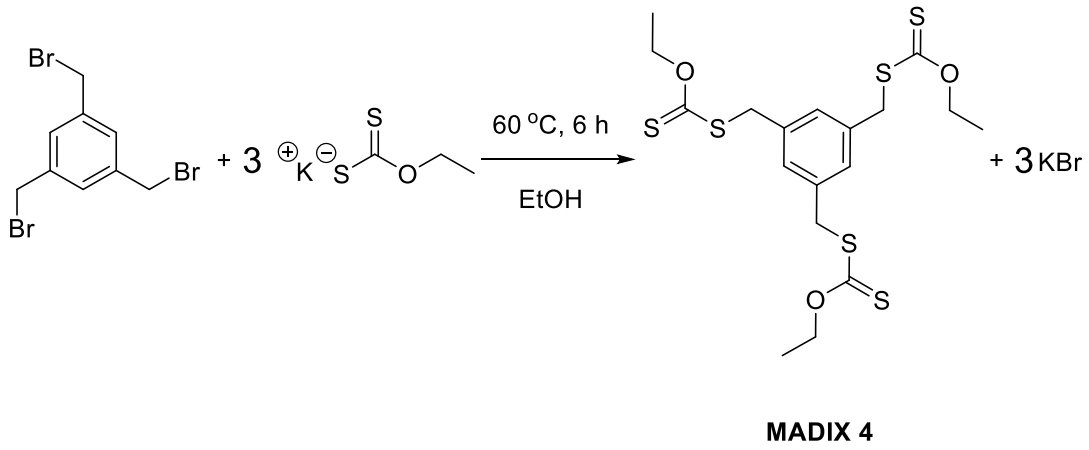

MADIX 4

Scheme 4.1 Preparation of the 3 arm multifunctional MADIX agent.

This is an efficient reaction that proceeds in good yield, with minimal work up required to afford the product as a powdery white solid as opposed to the yellow oils of the monofunctional MADIX agents prepared in previous chapters. After removing ethanol *in vacuo* the product can be extracted from DCM and water. The product (**MADIX 4**) was characterised using ^{1}H NMR spectroscopy (Figure 4.2), ^{13}C NMR spectroscopy (Figure 4.3) and ESI mass spectrometry (Figure 4.4).

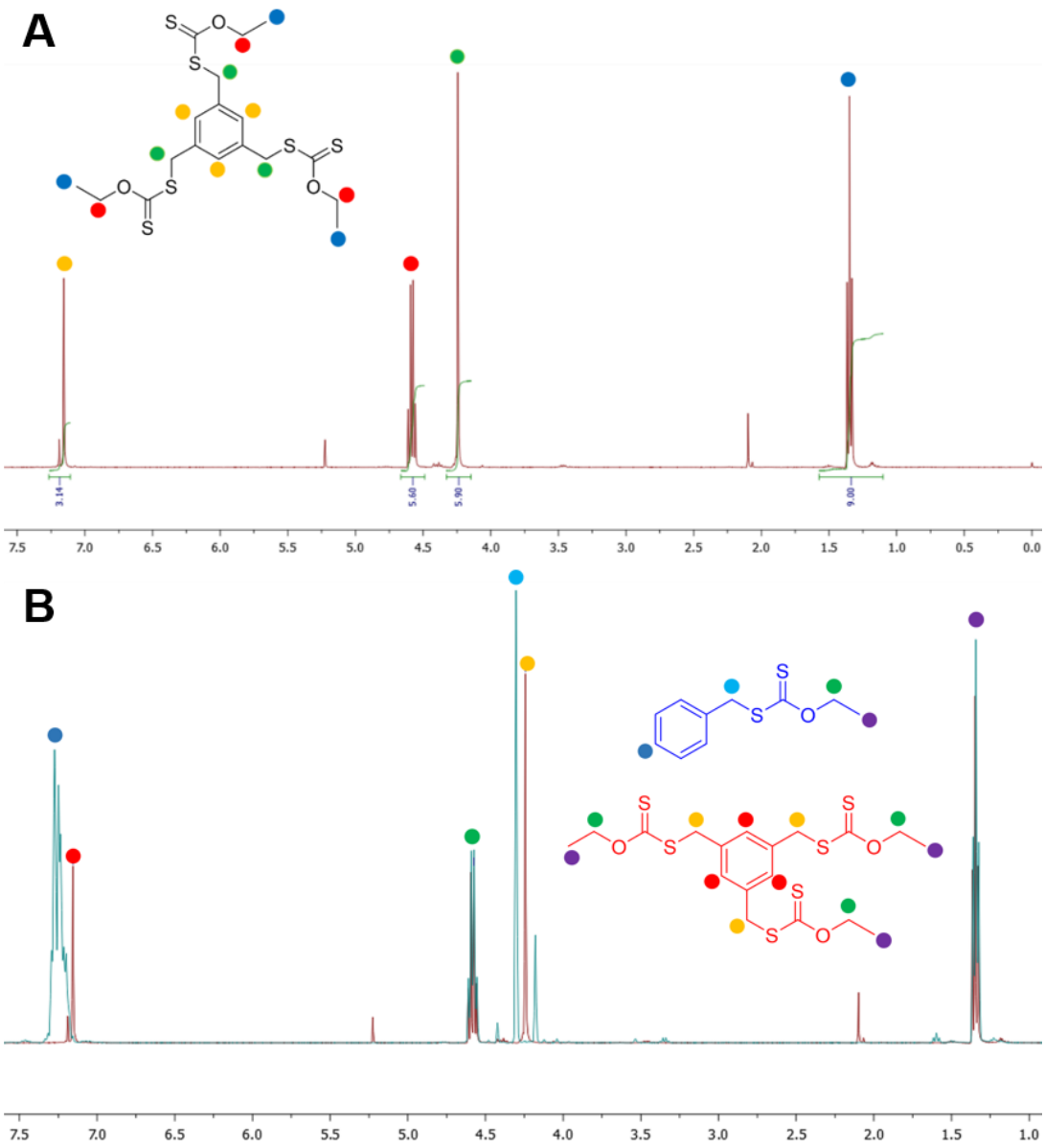

Figure 4.2 A ^{1}H NMR spectrum of **MADIX 4**. **B** Comparison ^{1}H NMR spectra of **MADIX 4** and its one arm analogue, **MADIX 3**.

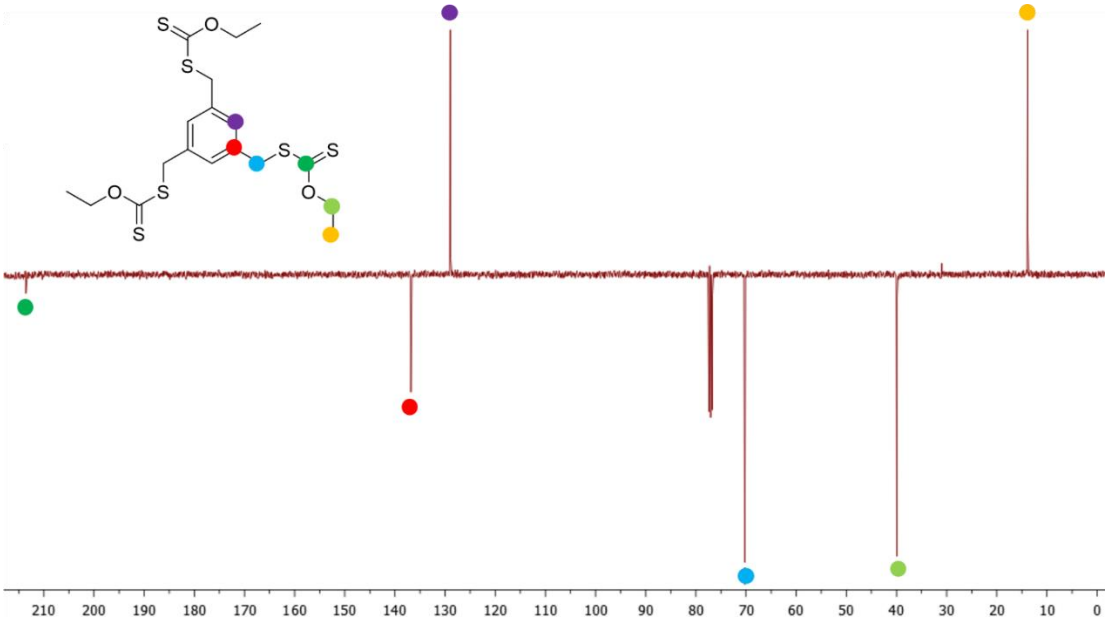

Figure 4.3 ^{13}C NMR spectrum of **MADIX 4**.

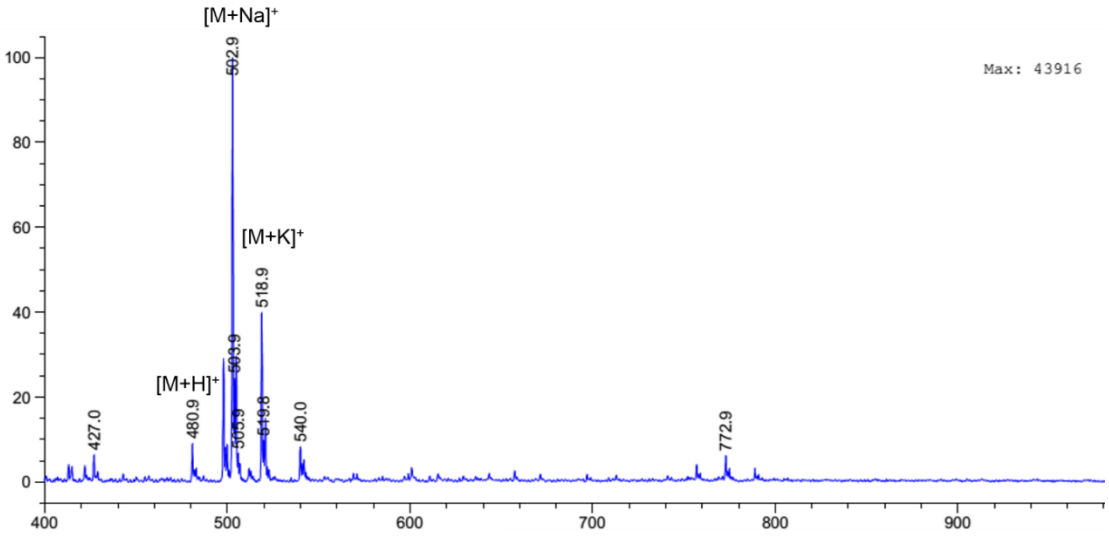

Figure 4.4 ESI MS (positive mode) Mass Spectrum of **MADIX 4**.

With **MADIX 4** characterised, testing of this new multifunctional MADIX agent could be conducted. A library of 3-arm PVAc stars was prepared by polymerising vinyl acetate, and then subsequent hydrazinolysis to afford *star*-PVA. IRI activities of the PVA stars were analysed using the splat assay and compared to other PVA based IRI agents discussed in previous chapters.

4.3ii The Polymerisation of Vinyl Acetate Using a Trifunctional MADIX Agent

In order to prepare well defined PVA stars, a polymerisation procedure had to be optimised and then the polymers tested to determine if the reaction proceeded in a controlled and living fashion, in line with what is expected from MADIX agents and controlled radical polymerisations.

Initial results polymerising in bulk with 10 mol % azo initiator to MADIX agent concentration showed that the polymerisation was indeed controlled, but the conversion was very low, (Table 4.1). Also, the number average molecular weight (M_n) from SEC in THF and ^{1}H NMR spectroscopic end-group analysis were not in good agreement with one another. Employing increasing amounts of initiator (optimal initiator concentration appearing to be 30 mol % to account for the trifunctional MADIX agent) and higher ratios of **MADIX 4** with respect to vinyl acetate, yielded better conversions whilst maintaining control of molecular weight and dispersity.

Polymerisations appeared to proceed in a controlled fashion, affording good conversions and narrow Đ values, but ^{1}H NMR spectroscopic analysis cannot provide enough evidence to conclusively show that each arm has polymerised at similar rates, *i.e.* that these polymers are actual stars as opposed to a single chain on a trifunctional agent. Using a SEC machine equipped with a viscometer, the intrinsic viscosity of star PVAc samples can be measured and compared to linear PVAc of the same molecular weight. Star or branched polymers will have a lower viscosity in solution compared to their linear counterparts, due to their lower hydrodynamic radius which is caused by the compact nature of the stars.

Table 4.1 Trial polymerisations and optimisation for PVAc star polymers.

Entry	[M]/ [CTA]/[INI] [a]	Conv[b] %	$M_{n,}^{NMR}$ [c] $g{\cdot}mol^{-1}$	$M_{n,}^{SEC}$ [d] $g{\cdot}mol^{-1}$	$Đ$ [d]	DP_n [e]	DP_A [f]
1	200/1/0.1	28	1290	4700	1.25	54	18
2	30/1/0.3	39	1030	1560	1.11	18	6
3	120/1/0.3	78	6040	7420	1.18	86	29
4	150/1/1	86	10300	14900	1.48	173	57

A Monomer to **MADIX 4** agent ratio. **B** Determined by ^{1}H NMR spectroscopy, theoretical M_n determined from monomer to RAFT agent ratio. **C** Determined by ^{1}H NMR spectroscopy. **D** Determined by SEC in THF using PMMA standards. **E** Number-average degree of polymerisation. **F** Number-average degree of polymerisation per arm.

This method of analysis is more suitable for higher molecular weight star polymers with more arms,[23] but results show a decrease in intrinsic viscosity characteristic to star polymers, (Figure 4.5).

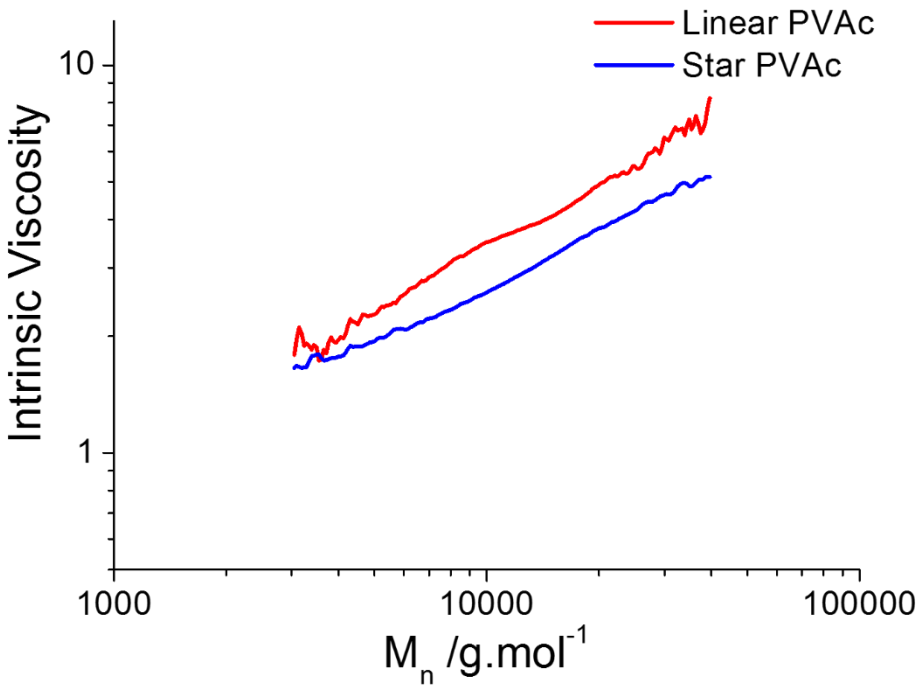

Figure 4.5 Mark-Houwink plot showing the intrinsic viscosity of 3-arm star PVAc and linear PVAc with almost identical M_n and similar Đ. Linear PVAc (DP_n 81, M_n = 7010, Đ = 1.19). Star PVAc (DP_n 81, DP_A = 27, M_n = 7060 Đ = 1.29).

^{1}H NMR spectroscopic analysis also shows high degrees of end-group fidelity in the purified polymer which closely match the SEC results (Figure 4.6, Figure 4.7). This shows that high degrees of both the 'R' and 'X' components of **MADIX 4** are incorporated into the polymer. Due to the way that chains are held around the core, entanglement occurs in the star polymer, compacting the structure, and reducing the overall viscosity, compared to linear polymers, which tend to entangle with other chains, increasing solution viscosity.

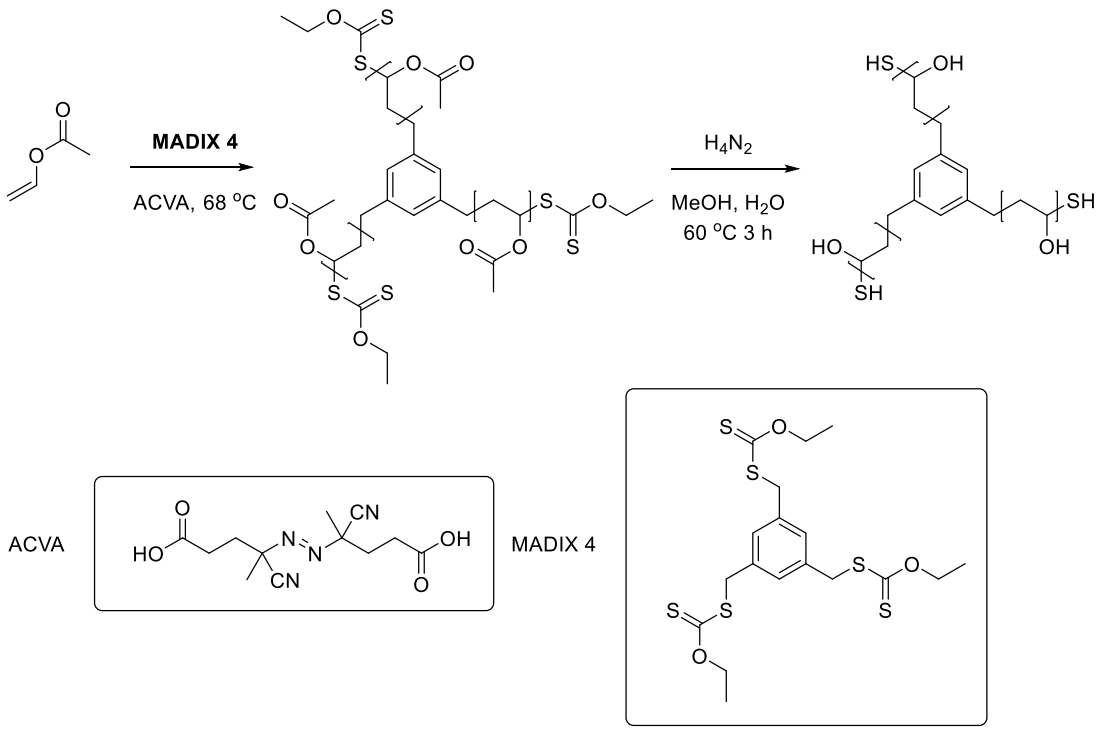

Scheme 4.2 MADIX 4 mediated polymerisation of vinyl acetate to poly(vinyl acetate), and the subsequent hydrazinolysis to poly(vinyl alcohol) using hydrazine hydrate solution.

With an efficient polymerisation protocol in place, (Scheme 4.2) and confirmation of the 3-arm star morphology present, a library of PVAc polymers using **MADIX 4** were prepared and hydrolysed to afford 3-arm PVA stars, (Table 4.2).

These star polymers were then characterised by size exclusion chromatography in THF (Figure 4.6). Pleasingly, all the proton environments in the polymers could be assigned to ^{1}H NMR spectroscopic shifts in both the *star*-PVAc and *star*-PVA spectra. ^{1}H NMR spectroscopy (Figure 4.7). Hydrazinolysis using concentrated hydrazine hydrate solution removed the acetate functionality affording *star*-PVA, with no evidence of chain scission from the core, as evidenced by ^{1}H NMR spectroscopic end-group analysis of the *star*-PVA (Figure 4.8).

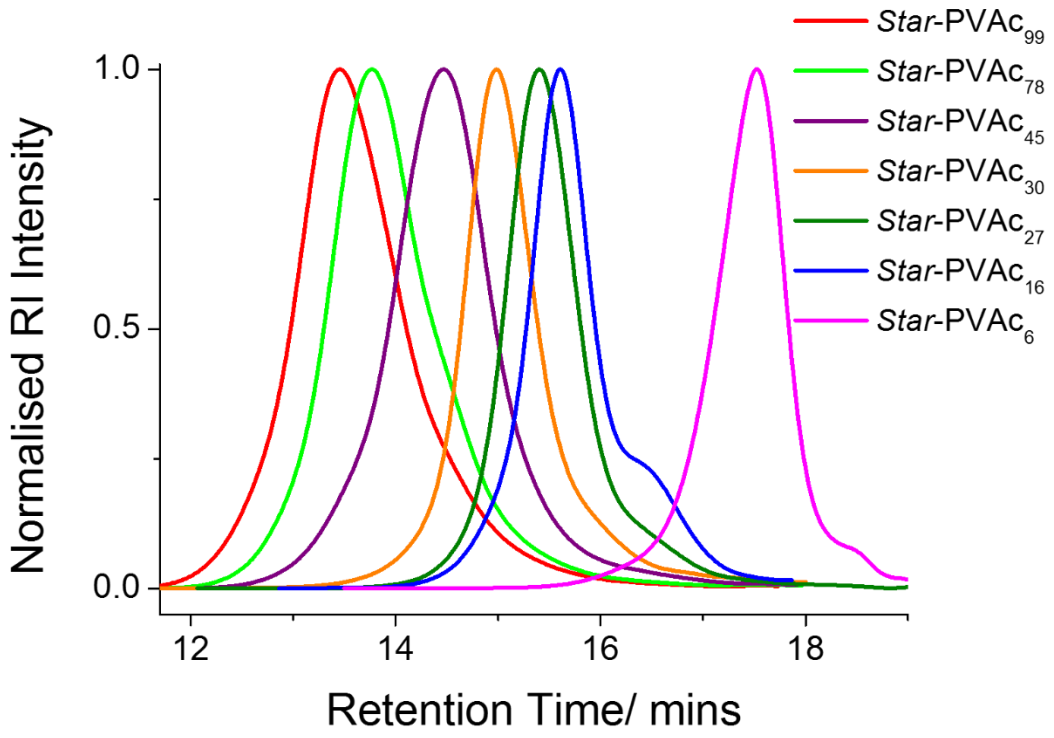

Figure 4.6 A selection of SEC traces for 3-arm *star*-poly(vinyl acetate) polymers prepared for this study.

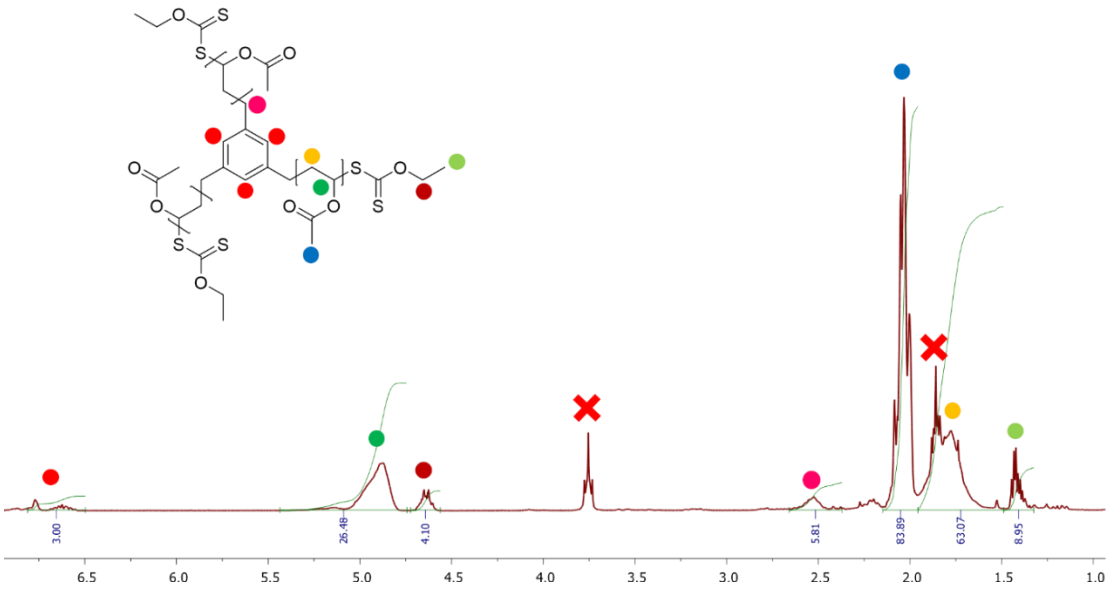

Figure 4.7 ^{1}H NMR spectrum of 3-arm star poly(vinyl acetate) polymer, ***Star*-PVAc$_{27}$**. Signals arising due to residual THF solvent are marked with an **x**.

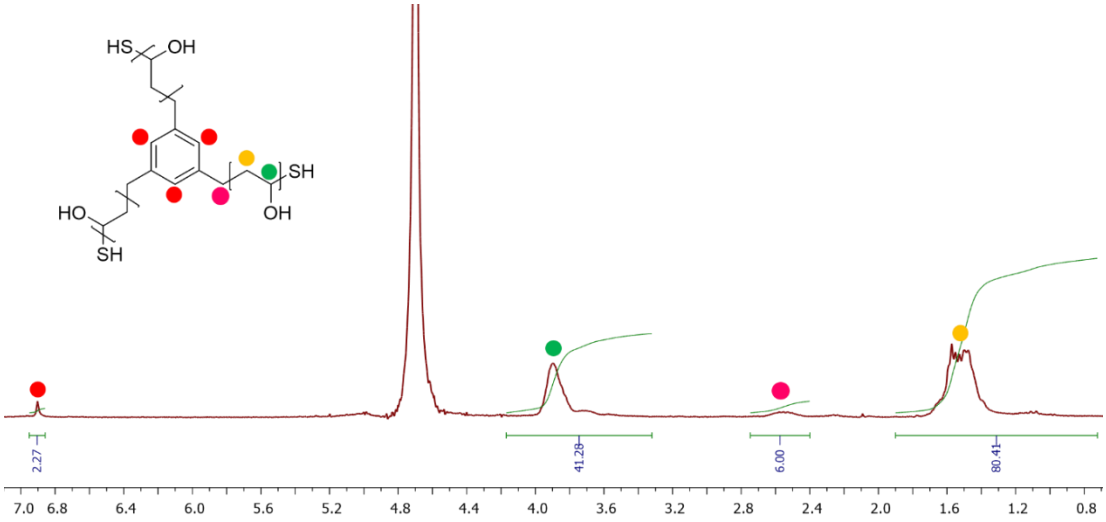

Figure 4.8 ^{1}H NMR spectrum of 3-arm star poly(vinyl alcohol) polymer, ***Star*-PVA$_{27}$** prepared for this study.

Table 4.2 3-arm PVAc star polymers prepared for this study.

***Star*-PVAc**	**[M]/[CTA]** [a]	**Conv** [b] **%**	$M_{n,}^{NMR}$ [b] ***g·mol*$^{-1}$**	$M_{n,}^{SEC}$ [c] ***g·mol*$^{-1}$**	***Đ*** [c]	**DP$_n$** [d]	**DP$_A$** [e]	***Star*-PVA** [f]
***Star*-PVAc$_6$**	30	36	1290	1560	1.12	18	6	***Star*-PVA$_6$**
***Star*-PVAc$_{16}$**	48	94	4050	4300	1.34	48	16	***Star*-PVA$_{16}$**
***Star*-PVAc$_{17}$**	120	76	5940	4450	1.25	51	17	***Star*-PVA$_{17}$**
***Star*-PVAc$_{21}$**	220	30	5680	5490	1.35	63	21	***Star*-PVA$_{21}$**
***Star*-PVAc$_{27}$**	58	95	6460	7060	1.28	81	27	***Star*-PVA$_{27}$**
***Star*-PVAc$_{30}$**	120	78	6200	7420	1.18	87	30	***Star*-PVA$_{30}$**
***Star*-PVAc$_{45}$**	180	82	13300	11800	1.41	138	45	***Star*-PVA$_{45}$**
***Star*-PVAc$_{78}$**	270	94	21900	20200	1.38	234	78	***Star*-PVA$_{78}$**
***Star*-PVAc$_{99}$**	330	94	26700	25700	1.42	299	99	***Star*-PVA$_{99}$**

A Monomer to RAFT agent ratio. **B** Determined by ^{1}H NMR spectroscopy. **C** Determined by SEC in THF using PMMA standards. **D** Number-average degree of polymerisation. **E** Number-average degree of polymerisation per arm. **F** Corresponding PVA prepared by hydrolysis of the respective PVAc star polymer.

4.3iii The IRI Activity of Well-Defined 3-Arm *Star*-PVA

With these *star*-PVAs in hand, a cross-section of the different molecular weights was selected and their IRI activities measured using the splat assay, (Figure 4.9). All of these polymers were active in the dilute (< 1 $mg.mL^{-1}$) concentration range, (Figure 4.10) and IRI activity showed a strong molecular weight dependence. Note that star polymers have been assigned labels denoting the length of each arm, to aid the analysis when comparing these polymers to other morphologies on the basis of continuous hydroxyl sequences (*vide infra)*.

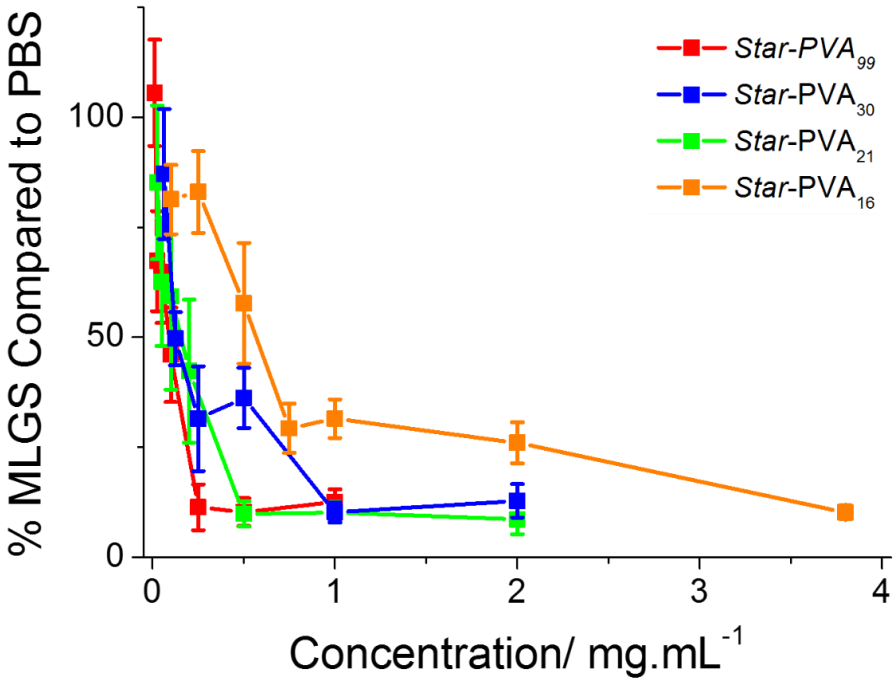

Figure 4.9 Ice recrystallisation inhibition activity of *star*-PVA polymers as measured by the splat assay.

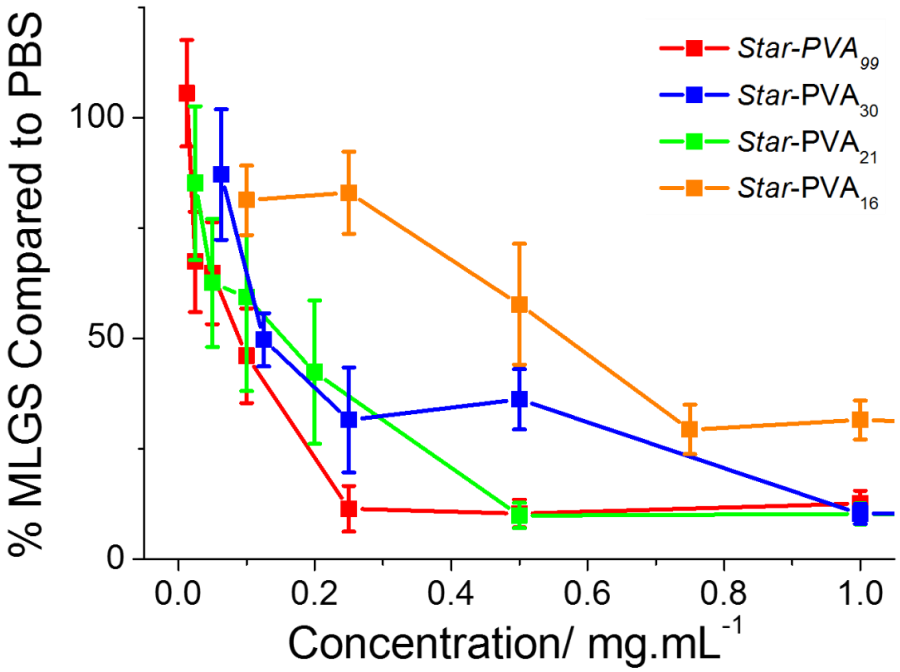

Figure 4.10 Ice recrystallisation inhibition activity of star-PVA polymers at low concentration, as measured by the splat assay.

These results show that in this 3-arm star conformation PVA is still highly effective at inhibiting the growth of ice crystals. Total inhibition of ice growth (where the % MLGS is less than 20 %, meaning that after 30 minutes at - 8 °C the crystal size is essentially the same as when the ice crystals were initially nucleated) was observed for every star polymer tested. This is akin to the IRI behaviour seen with the PVA homopolymers, but not for many of the random or block copolymers tested earlier. This demonstrates that the 3-arm morphology does not adversely affect activity in any way, as expected given the uninterrupted hydroxyl sequence. However it does appear that there is a slight difference in activity when these polymers are compared to their linear PVA homopolymer analogues.

***Star*-PVA$_{21}$** has an approximate (based on M_n) total of 63 hydroxyl groups, split into 21 hydroxyl groups per chain, or arm, of the 3-arm star polymer. It appears that ***Star*-PVA$_{21}$** is as effective an inhibitor as its 1-arm and 3-arm linear analogues (**PVA$_{20}$** and **PVA$_{50}$**). There is a difference in activity between stars and linear PVAs at very low polymer concentrations (0.25 mg.mL^{-1}) (Figure 4.11).

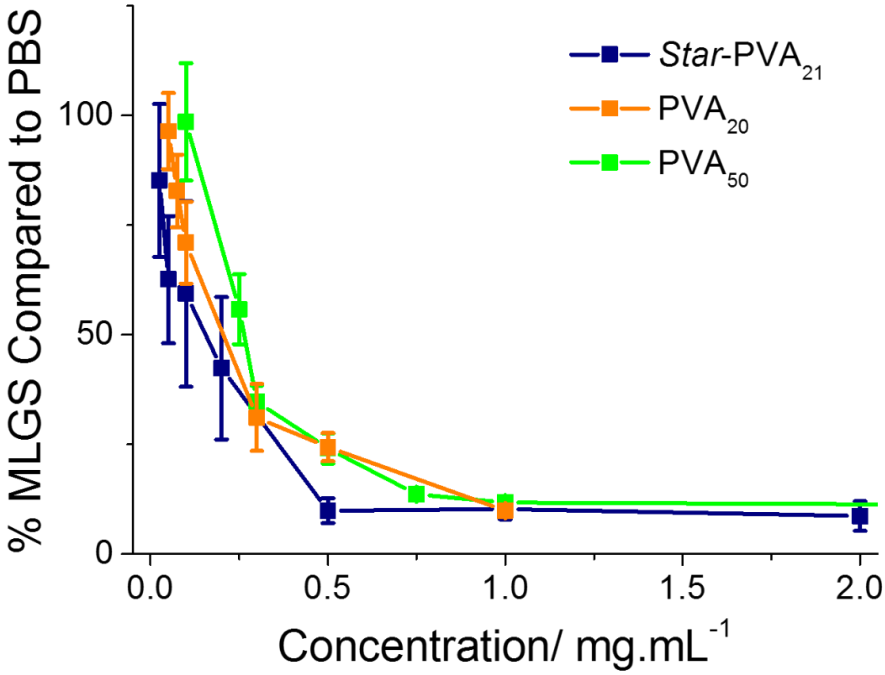

Figure 4.11 Ice recrystallisation inhibition activity of ***Star*-PVA$_{63}$** and its 1-arm and 3-arm linear analogues.

Figure 4.12 shows that the activity of ***Star*-PVA$_{30}$** closely mirrors its 1-arm and 3-arm linear analogues until it is diluted to below 0.5 mg.mL^{-1}. Below this ***Star*-PVA$_{30}$** displays a similar loss in activity to **PVA$_{30}$**, while **PVA$_{150}$** maintains high activity until approximately 0.3 mg.mL^{-1}. **PVA$_{150}$** was the closest comparison available, but the molecular weight dependence of the IRI activity of PVA is not a linear trend, so in this instance it is difficult to compare relative potencies.

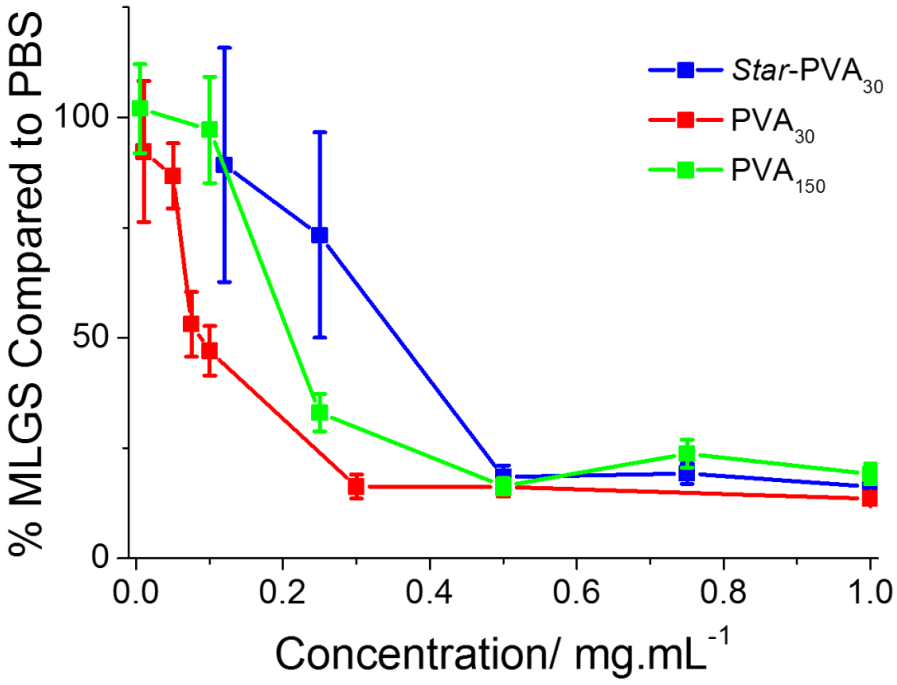

Figure 4.12 Ice recrystallisation inhibition activity of ***Star*-PVA$_{30}$** and its 1-arm and 3-arm linear analogues.

***Star*-PVA$_{16}$** is an interesting case as its arm length lies at the boundary of the minimum hydroxyl sequence length seen in the difference in activity between DP_n 10 and DP_n 20 linear PVA homopolymer (Chapter 2). The total number of hydroxyl groups is approximately 48, more than enough to display high activity (Figure 4.13). From these results it can be seen that, on a *per arm* basis, this small polymer maintains activity better than expected for such a short sequence length, but when compared to very similar arm size and total size PVAs (**PVA$_{20}$** and **PVA$_{50}$** respectively) the activity is definitely reduced.

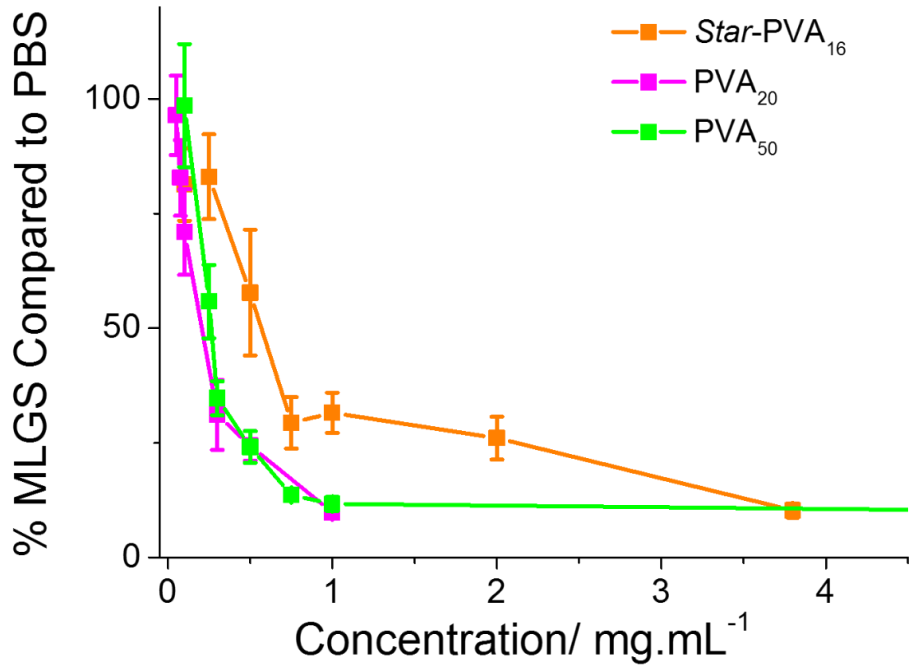

Figure 4.13 Ice recrystallisation inhibition activity of ***Star*-PVA$_{16}$** and its 1-arm and 3-arm linear analogues.

These results show that while *star*-PVAs can display strong IRI activity across a range of molecular weight distributions, activity is weaker on a *per* hydroxyl group basis than linear polymers. High activity at low concentrations means that it is harder to draw conclusions as the changes are across small differences in concentration, but these results show that the total length of the polymer chain is playing a role in IRI activity, beyond what has been seen or reported before.

These results indicate it is highly unlikely that any ice-binding is occurring; if it was, 3 linked arms would have a better binding affinity than 3 single polymer chains, and would give a corresponding increase in IRI activity. This was not seen. Another explanation for PVA IRI activity could be that the polymer is interacting in the QLL or the bulk water layer. This is similar to the idea that viscosity or gelation could be responsible for IRI activity, but the interaction is more specific. PVA can induce the

long-range ordering of water molecules, which in theory could be increasing the energetic cost of adding water into the QLL (Figure 4.14). Ice growth can only occur through the QLL so any change to QLL formation would have corresponding effects on the rate of crystal growth.

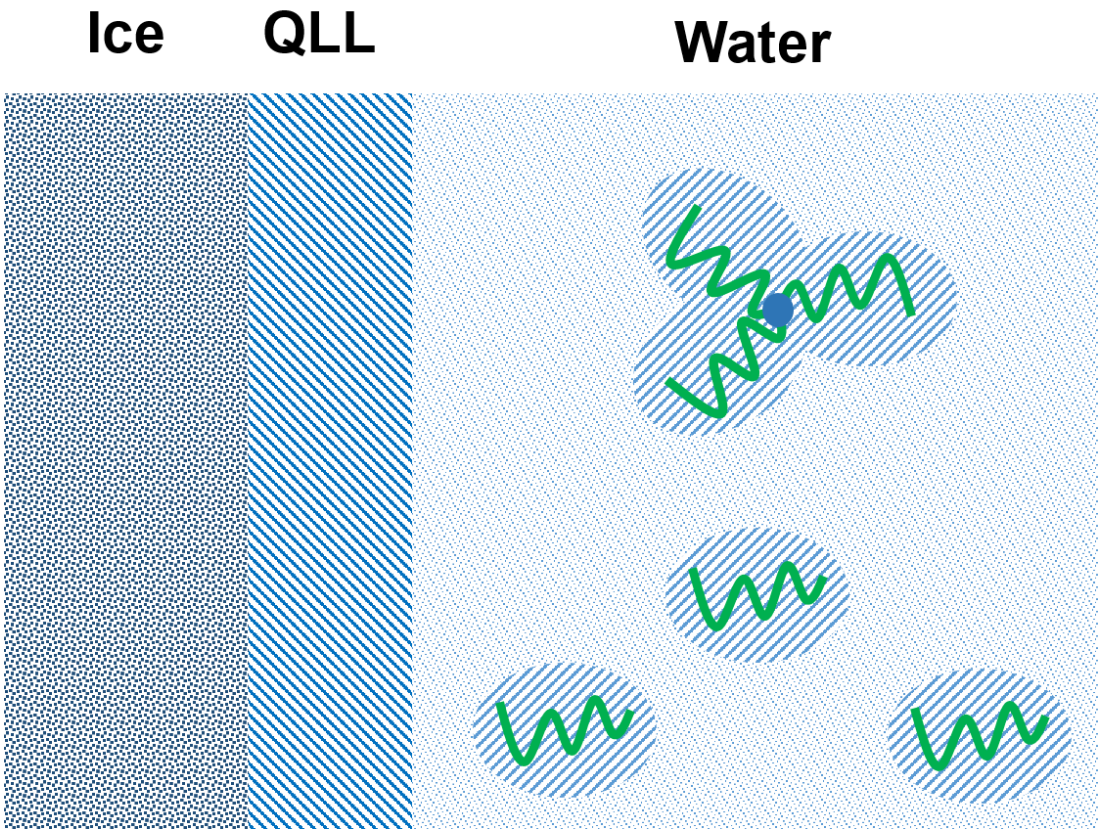

Figure 4.14 Illustration of *star*-PVA and linear PVA in frozen solution, showing the proposed long-range ordering of water that inhibits addition of water molecules into the QLL.

4.4 Conclusion

Based on a proven synthetic protocol a novel trifunctional CTA, **MADIX 4**, was synthesised and purified in good yield without the need for purification *via* column chromatography. Through tailoring the MADIX agent to fragment from the core of the molecule instead of the arm, propagating radicals were confined to the trifunctional RAFT agent, and no low molecular weight single-arm polymers were observed. The MADIX agent also afforded polymers with narrow degrees of dispersity and predictable molecular weights. S*tar*-PVAs were prepared from S*tar*-PVAc *via* hydrazinolysis using concentrated hydrazine hydrate solution, then purified using dialysis. The resultant star polymers were analysed using ^{1}H NMR spectroscopy, which was used to confirm the SEC analysis and pleasingly showed excellent retention of end-group functionality after polymerisation.

This library of star polymers was then tested for IRI activity using the splat assay. This analysis showed that PVA stars are highly efficient inhibitors of ice crystal growth, capable of complete inhibition of ice growth at concentrations below 1 mg.mL^{-1}. These 3-arm star polymers displayed comparable activity to their linear analogues across the range of molecular weights tested. It appears that while single chain PVA may be a more potent inhibitor of ice crystal growth overall, these polymers are more efficient than block and random co-polymers of PVA, not to mention almost any other synthetic agent, macromolecule or otherwise, to be tested for IRI activity.

4.5 Experimental

Synthesis of 3-arm MADIX agent 1,3,5 *tris*-(ethoxycarbonothioyl sulfanyl) benzene

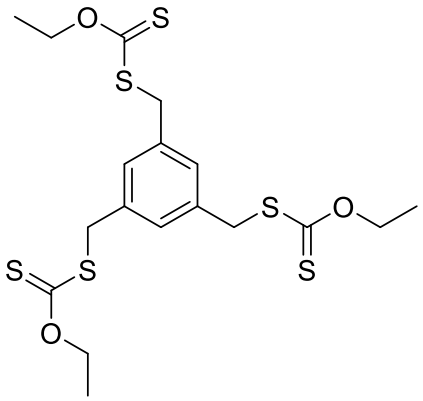

Potassium ethyl xanthate (5.00 g, 0.031 mol, 3.0 eq) was added ethanol (120 mL) in a round bottom flask and stirred at 60 °C until the solid had fully dissolved. 1,3,5 *tris*-(bromomethyl)benzene (3.71 g, 0.01 moles, 1.0 eq) was added to the stirred solution in a single portion and the reaction stirred at 60 °C for 6 h, forming a pale yellow solution and a white precipitate. The mixture was filtered to remove the salt and then Ethanol was removed *in vacuo* leaving a yellow oil and a white solid. The mixture was dissolved in DCM (150 mL) and the product precipitated upon the addition of small amounts of water (10 mL). The product was filtered leaving a white solid, which was then thoroughly dried under vacuum using a schlenk line apparatus, furnishing the product as a white solid. Yield 2.69 g 56 %, ^{1}H NMR ($CDCl_3$): δ = 7.23 (3H, s, benzyl ring), 4.65 (6H, q, *J* = 6.8 Hz, O*CH*$_2$), 4.31 (6H, s, S*H*$_2$), 1.42 (9H, t, *J* = 8 Hz, C*H*$_3$). ^{13}C NMR ($CDCl_3$): δ = 212.4 (C=S), 136.0 (*ipso* C), 128.0 (benzyl *C*H), 70.2 (S*C*H$_2$), 39.9 (O*C*H$_2$), 13.8 (*C*H$_3$). ESI MS; 480.9 Da $[M+H]^+$, 502.9 Da $[M + Na]^+$, 518.9 Da $[M + K]^+$.

Polymerisation of Vinyl Acetate Using a 3-arm MADIX Agent

As a representative example, **MADIX 4** (0.137 g, 0.27 mmol), vinyl acetate (2.814 g, 0.33 mol), and ACVA (4,4′-azobis(4-cyanovaleric acid); 0.082 g, 33 mol%) were added to a stoppered vial equipped with a stir bar. The solution was thoroughly degassed by bubbling N_2 through the solution for 20 min, and the reaction mixture was then allowed to polymerise at 68 °C for typically 15 h. The yellow solutions were then cooled to room temperature. Poly(vinyl acetate) was then recovered as a yellow sticky solid after precipitation into hexane. The hexane was then decanted and the poly(vinyl acetate) was re-dissolved in THF, which was then concentrated *in vacuo* and thoroughly dried under vacuum at 40 °C for 24 h, forming a white solid. Representative characterisation data for ***Star*-PVAc$_{87}$**: ^{1}H NMR (400 MHz, $CDCl_3$) δ = 7.16 (benzyl *H*, s, 3H), 4.61 (-C*H*O-CH_2, br, 90H), 4.42 (-C*H*$_2$CH$_3$, q, 6H), 4.24 (-C*H*$_2$S-, s, 6H), 1.74 (-CO-C*H*$_3$, br, 270H), 1.53 (-C*H*$_2$-, br, 180H); M_n^{SEC}(THF) = 7420 Da, M_w/M_n = 1.18.

Hydrazinolysis of 3-Arm Star Poly(vinyl acetate)

As a representative example, 3-arm *star*-poly(vinyl acetate) (1.0 g, 7420 Da, M_n/M_w = 1.18) was dissolved in a methanol (5 mL) and hydrazine hydrate solution (10 mL, 80% in water) in a round-bottom flask. The reaction mixture was stirred at 30 °C for 4 h. The reaction mixture was then dialyzed using distilled water and 3-arm *star*-poly(vinyl alcohol) was recovered as a spongy white solid by freeze-drying the dialysis solution. Hydrazinolysis was determined by ^{1}H NMR Spectroscopy. Representative

characterisation data for ***Star*-PVA$_{87}$**: ^{1}H NMR (400 MHz, $CDCl_3$) δ = 7.16 (benzyl *H*, s, 3H), 4.00 (−C*H*OH–, br, 90), 1.68–1.60 (−CH_2–, br, 180H).

4.6 References

1. Hadjichristidis, N.; Pitsikalis, M.; Iatrou, H.; Driva, P.; Sakellariou, G.; Chatzichristidi, M., 6.03 - Polymers with Star-Related Structures: Synthesis, Properties, and Applications. In *Polymer Science: A Comprehensive Reference*, Möller, K. M., Ed. Elsevier: Amsterdam, 2012; pp 29-111.

2. Mattarella, M.; Garcia-Hartjes, J.; Wennekes, T.; Zuilhof, H.; Siegel, J. S., Nanomolar cholera toxininhibitors based on symmetrical pentavalent ganglioside GM1os-sym-corannulenes. *Organic & Biomolecular Chemistry* **2013,** *11* (26), 4333-4339.

3. Fetters, L. J.; Kiss, A. D.; Pearson, D. S.; Quack, G. F.; Vitus, F. J., Rheological behavior of star-shaped polymers. *Macromolecules* **1993,** *26* (4), 647-654.

4. Lapienis, G., Star-shaped polymers having PEO arms. *Progress in Polymer Science* **2009,** *34* (9), 852-892.

5. Knoll, K.; Nießner, N., Styrolux+ and styroflex+ - from transparent high impact polystyrene to new thermoplastic elastomers: Syntheses, applications and blends with other styrene based polymers. *Macromolecular Symposia* **1998,** *132* (1), 231-243.

6. Liu, X.; Jin, X.; Ma, P. X., Nanofibrous hollow microspheres self-assembled from star-shaped polymers as injectable cell carriers for knee repair. *Nature Materials* **2011,** *10* (5), 398-406.

7. Zhu, W.; Ling, J.; Shen, Z., Synthesis and Characterization of Amphiphilic Star-Shaped Polymers With Calix[6]arene Cores. *Macromolecular Chemistry and Physics* **2006,** *207* (9), 844-849.

8. Forman, D. C.; Wieberger, F.; Gröschel, A.; Müller, A. H. E.; Schmidt, H.-W.; Ober, C. K. In *Comparison of Star and Linear ArF Resists*, 2010; pp 76390 - 76390.

9. Schaefgen, J. R.; Flory, P. J., Synthesis of Multichain Polymers and Investigation of their Viscosities. *Journal of the American Chemical Society* **1948,** *70* (8), 2709-2718.

10. Hadjichristidis, N.; Pitsikalis, M.; Pispas, S.; Iatrou, H., Polymers with Complex Architecture by Living Anionic Polymerization. *Chemical Reviews* **2001,** *101* (12), 3747-3792.

11. Gao, H.; Matyjaszewski, K., Synthesis of functional polymers with controlled architecture by CRP of monomers in the presence of cross-linkers: From stars to gels. *Progress in Polymer Science* **2009,** *34* (4), 317-350.

12. Hawker, C. J., Architectural Control in "Living" Free Radical Polymerizations: Preparation of Star and Graft Polymers. *Angewandte Chemie International Edition in English* **1995,** *34* (13-14), 1456-1459.

13. Mayadunne, R. T. A.; Jeffery, J.; Moad, G.; Rizzardo, E., Living Free Radical Polymerization with Reversible Addition−Fragmentation Chain Transfer (RAFT Polymerization): Approaches to Star Polymers. *Macromolecules* **2003,** *36* (5), 1505-1513.

14. Stenzel, M. H.; Cummins, L.; Roberts, G. E.; Davis, T. P.; Vana, P.; Barner-Kowollik, C., Xanthate mediated living polymerization of vinyl acetate: A systematic variation in MADIX/RAFT agent structure. *Macromolecular Chemistry and Physics* **2003,** *204* (9), 1160-1168.

15. Nguyen, T. L. U.; Eagles, K.; Davis, T. P.; Barner-Kowollik, C.; Stenzel, M. H., Investigation of the influence of the architectures of poly(vinyl pyrrolidone) polymers made via the reversible addition–fragmentation chain transfer/macromolecular design via the interchange of xanthates mechanism on the stabilization of suspension polymerizations. *Journal of Polymer Science Part A: Polymer Chemistry* **2006,** *44* (15), 4372-4383.

16. Lederhos, J. P.; Long, J. P.; Sum, A.; Christiansen, R. L.; Sloan Jr, E. D., Effective kinetic inhibitors for natural gas hydrates. *Chemical Engineering Science* **1996,** *51* (8), 1221-1229.

17. Jones, M. W.; Otten, L.; Richards, S. J.; Lowery, R.; Phillips, D. J.; Haddleton, D. M.; Gibson, M. I., Glycopolymers with secondary binding motifs mimic glycan branching and display bacterial lectin selectivity in addition to affinity. *Chemical Science* **2014,** *5* (4), 1611-1616.

18. Deller, R. C.; Congdon, T.; Sahid, M. A.; Morgan, M.; Vatish, M.; Mitchell, D. A.; Notman, R.; Gibson, M. I., Ice recrystallisation inhibition by polyols: comparison of molecular and macromolecular inhibitors and role of hydrophobic units. *Biomaterials Science* **2013,** *1* (5), 478-485.

19. Balcerzak, A. K.; Capicciotti, C. J.; Briard, J. G.; Ben, R. N., Designing ice recrystallization inhibitors: from antifreeze (glyco)proteins to small molecules. *RSC Advances* **2014,** *4* (80), 42682-42696.

20. Stenzel, M. H.; Davis, T. P.; Barner-Kowollik, C., Poly(vinyl alcohol) star polymers prepared via MADIX/RAFT polymerisation. *Chemical Communications* **2004,** (13), 1546-1547.

21. Bernard, J.; Favier, A.; Zhang, L.; Nilasaroya, A.; Davis, T. P.; Barner-Kowollik, C.; Stenzel, M. H., Poly(vinyl ester) star polymers via xanthate-mediated living radical polymerization: From poly(vinyl alcohol) to glycopolymer stars. *Macromolecules* **2005,** *38* (13), 5475-5484.

22. Barner-Kowollik, C.; Davis, T. P.; Stenzel, M. H., Synthesis of Star Polymers using RAFT Polymerization: What is Possible? *Australian Journal of Chemistry* **2006,** *59* (10), 719-727.

23. James, A. B.; David, M. H.; Becer, C. R., Synthesis and SEC Characterization of Poly(methyl methacrylate) Star Polymers. In *Progress in Controlled Radical Polymerization: Materials and Applications*, American Chemical Society: 2012; Vol. 1101, pp 81-98.

Chapter 5

Synthesis and Cloud Point Behaviour of Thermoresponsive PVA Co-polymers

---

5.1 Chapter Overview

The aim of this chapter was to investigate the thermoresponsive behaviour of a range of co-polymers of PVA. Thermoresponsive polymers are an emerging topic of study for use in smart medical devices, and PVA has yet to be investigated for thermoresponsivity using a controlled radical polymerisation methodology. Using a MADIX methodology a library of poly(vinyl acetate) polymers was prepared, hydrolysed to poly(vinyl alcohol), and then using an acid catalysed acetylation reaction, acetate functionality was reintroduced randomly along the polymer chain. The cloud point of these polymers was determined to investigate the effect of degree of acetylation, polymer size, and the end-group effects of short-chain PVA. Inclusion of benzyl end-groups affected the observed cloud point drastically and led some initially contradictory results. Hydrophobic dye inclusion assays showed that there was no ordering or micellisation of the polymer chains prior to the thermally induced phase change. The effect of increasingly hydrophobic functionality was examined by randomly introducing butanoate and propanoate functional groups onto PVA using the same acid catalysed acetylation reaction. These polymers displayed predictably lower temperature thermal phase transitions, at much lower degrees of functionalisation compared to the PVA.PVAc co-polymers. Finally the effect of enzymatic degradation

on these polymers was examined, by using porcine liver esterase to hydrolyse acetate groups. Over four days the cloud point increased linearly with increasing degree of hydrolysis.

5.2 Chapter Introduction

Thermoresponsive polymers have attracted huge interest as adaptable biomaterials based on their reversible solubility behaviour which can be exploited for controlled drug delivery or cellular uptake. Poly(ethylene glycol) (PEG) and poly(*N*-isoprpylacrylamide) (PNiPAM) see the most widespread application, but for PEG the thermal transition temperatures that are practically accessible are not physiologically useful. There are some notable examples of synthetic responsive polymers that are highly tunable over a physiologically relevant range, but there is still a need for these to be clinically validated in terms of toxicology and immunogenicity for *in vivo* usage, in addition to their widely used *in vitro* applications. The biocompatibility of poly(vinyl alcohol), (PVA) is well known and the polymer is already used for a huge range of biomedical applications. What is less well known is that, when hydrophobic functionality is present on the polymer chain, PVA can undergo thermally induced phase transitions in line with Lower Critical Solution Temperature (LCST)-like cloud point behaviour as described by Flory-Huggins solution theory.

The first report on the thermoresponsive behaviour of PVA was published by Timasheff *et al.*[1] Miya *et al.* reported that fractionated, butanoated PVA displayed both LCST and Upper Critical Solution Temperature (UCST) thermal transitions.[2] Tagawa *et al.* reported that 88kDa PVA with 20 mol % residual acetate groups

displayed LCST type cloud point transitions that showed a strong concentration dependence.[3] Later reports by Crowther *et al.* examined the effect that the molar mass of PVA,[4] and the size and sequence of acetate and hydroxyl functionality has on the thermoresponsive behaviour,[5] surmising that random regions of hydroxyl/acetate groups would contribute less to the thermodynamic drive towards de-mixing compared to the blocky regions of either group. Both of these reports used high molecular weight PVA with degrees of acetylation ranging from 6 - 20 mol %. Ivanova *et al.* prepared and tested a range of acetal functionalised PVAs that displayed thermoresponsive behaviour.[6] More recently Chen *et al.* reported that the incorporation of small amounts of glycine, alanine and valine along a PVA chain afforded thermoresponsive behaviour, dependent on the amino acid installed.[7]

More commonly PVA is incorporated into materials, usually hydrogels, alongside more well-known thermoresponsive polymers.[8] Often the reason cited is to exploit the water solubility or another favourable property of PVA. Few examples exist using just PVA as the thermoresponsive component. For example, Xiao *et al.* utilised glutaraldehyde cross-linked PVA as a thermoresponsive hydrogel.[9]

However, despite its biocompatible nature, PVA has not been widely explored for application as a stimuli-responsive biomaterial and there are few established studies detailing structure-property relationships on its transition temperatures. In part this is due to the previous difficulties in synthesising PVA in a controlled manner, which have recently been overcome by advances in controlled radical polymerisation. Therefore, it was decided to conduct a detailed study into this thermoresponsive behaviour.

5.3 Results

5.3i The Synthesis of PVA-*rand*-PVAc Co-polymers

In order to probe the cloud point behaviour of PVA/PVAc a range of co-polymers with different molecular weights and degrees of acetylation were required. Previous studies on the responsive behaviour of PVAs have been limited to high molecular weight polymers with broad molecular weight dispersity, derived from free radical polymerisation. Due to the deactivated nature of vinyl acetate, xanthates (rather than the more commonly used dithioesters or trithiocarbonates) were required to enable MADIX polymerisation. The MADIX agent methyl(ethoxycarbonothioyl)sulfanyl benzene (**MADIX 3**) was chosen as it has been reported to control the radical polymerisation of vinyl acetate (Scheme 5.1),[10] and because it incorporates a benzyl end group into the polymer, which is easily distinguishable by ^{1}H NMR spectroscopy.

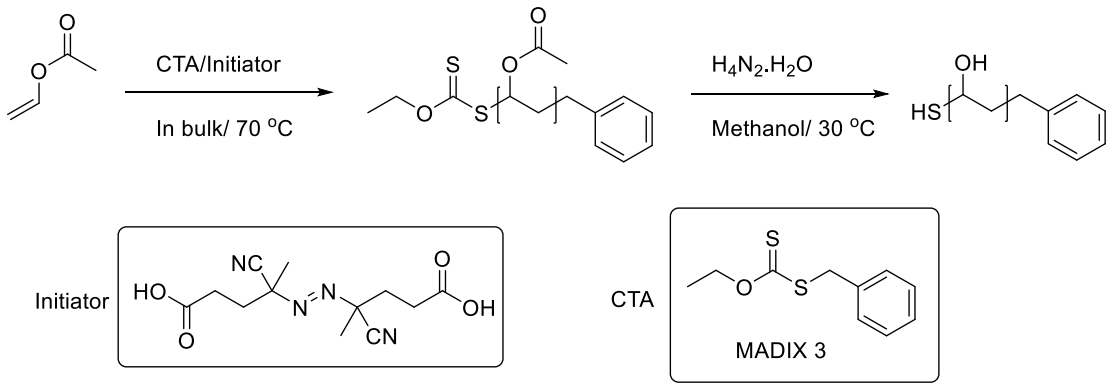

Scheme 5.1 MADIX controlled polymerisation of vinyl acetate and its subsequent conversion to PVA using hydrazine hydrate solution.

Vinyl acetate was polymerised in bulk (Figure 5.1) and then subsequently hydrolysed using hydrazine hydrate, followed by dialysis to afford well defined PVA with no residual acetate groups, as seen in Chapter 2.

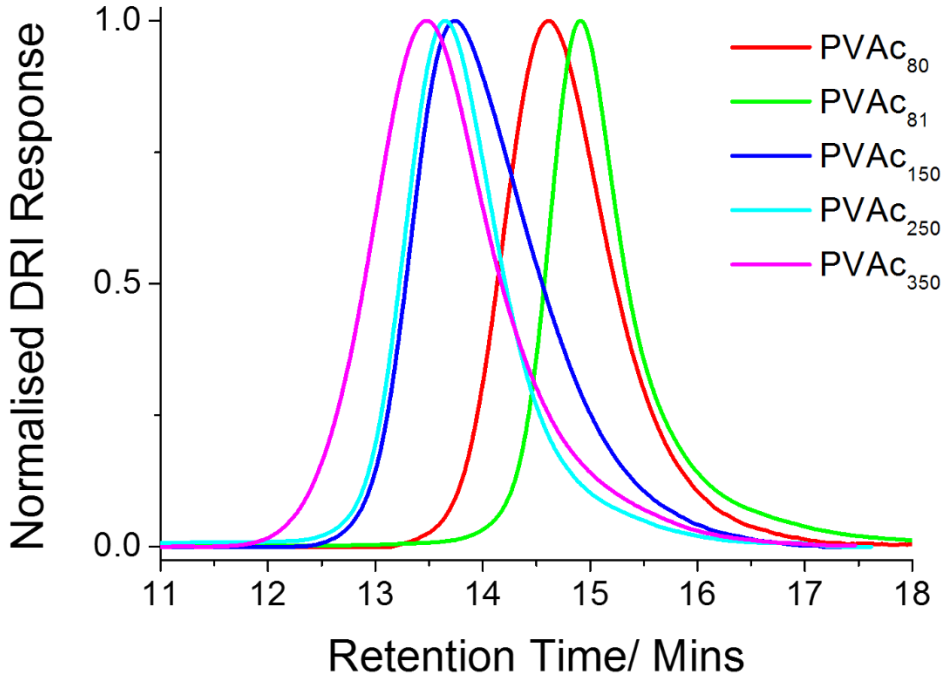

Figure 5.1 Size exclusion chromatography (SEC) traces of poly(vinyl acetate) polymers. The discrepancy between DP80 and DP 81 is due to the polymers being analysed on different THF SEC machines, using different eluting columns.

SEC analysis showed that the polymers prepared had low dispersity and predictable molecular weights, and PVAc with higher molecular weight ranges displayed correspondingly higher dispersity - expected for a MADIX polymerisation of deactivated monomers (Table 5.1).

Table 5.1 PVAc and corresponding PVA polymers prepared for this study.

Entry	[M]/ [CTA]	Conv. [a]	M_n(SEC) [b] ($g.mol^{-1}$)	Đ [b] (-)	DP_n [c]	PVA [d]
$PVAc_{80}$	100	82.9	7100	1.17	83	**PVA_{80}**
$PVAc_{81}$ [e]	100	81.4	7000	1.18	81	**PVA_{80}***
$PVAc_{150}$	200	73.8	12700	1.45	148	**PVA_{150}**
$PVAc_{250}$	300	80.1	20700	1.21	240	**PVA_{250}**
$PVAc_{350}$	500	68.8	29600	1.39	344	**PVA_{350}**

A Determined by ^{1}H NMR spectroscopy of the reaction mixture, theoretical M_n assuming 100% conversion. **B** Determined by SEC in THF using PMMA polymer standards. **C** Number average degree of polymerisation, determined from conversion of monomer to polymer by ^{1}H NMR spectroscopy. **D** Corresponding PVA prepared by complete hydrolysis of the PVAc, determined by ^{1}H NMR spectroscopy. **E** Prepared using MADIX agent **MADIX 2** to afford a carboxylic acid functionalised end group, required for determining end group effects. All other entries prepared using **MADIX 3**. * Denotes carboxylic acid functional end-group on the PVA polymer afforded using MADIX 2.

Typically PVA/PVAc co-polymers would be obtained by partial basic (NaOH) hydrolysis of PVAc, but this has been shown to give rise to 'blocky' polymers rather than true random distribution of the acetate groups.[11] Arrangement of acetate groups along the PVA chain has been shown to be important to cloud point transitions; 'blockier' polymers will have lower cloud points than their randomised counterparts,[5] but actual 'degree of blockiness' is hard to control. By utilising a procedure that randomly distributes acetate functionality this variable is removed. As before (Chapter 2), hydrazine hydrate was used as a strong nucleophile to completely hydrolyse the acetate groups, without affecting the chain length. Acetic acid/HCl solutions were then used to re-introduce acetate groups in a statistical and controlled fashion, due to the

inherent reversibility of the reaction, as has been previously demonstrated in Chapter 2 (Scheme 5.2).[12] The degree of acetylation was quantified by ^{1}H NMR spectroscopy (Figure 5.2).

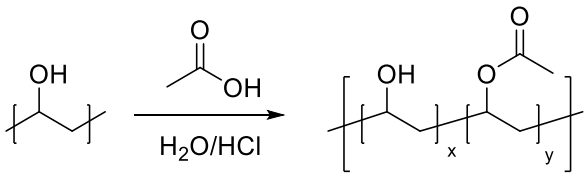

Scheme 5.2 Reaction scheme showing PVA reacetylation using acetic acid/water mixtures.

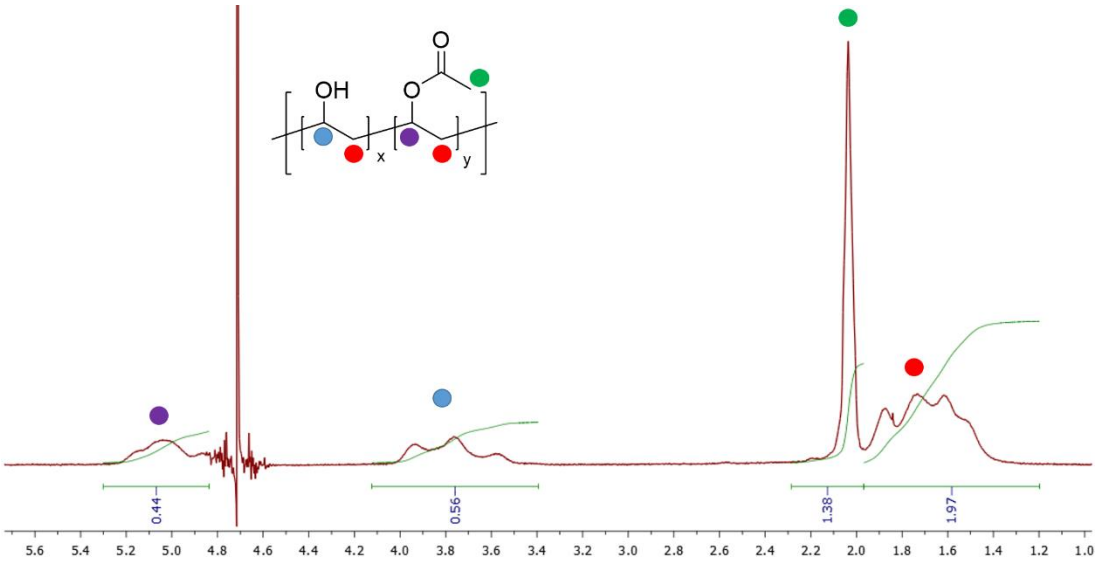

Figure 5.2 Representative ^{1}H NMR spectrum of $\mathbf{P_{350}Ac_{0.44}}$ in D_2O. Degree of reacetylation determined by ^{1}H NMR, by comparing the integrals of the PVA α-H (δ = 4.10 – 3.30 ppm), PVAc α-H (δ = 5.50 - 4.80), and PVAc–CH_3 (δ = 2.10 ppm) shifts of the purified co-polymer.

^{1}H NMR spectroscopy was used to also examine the dyad and triad peaks from methine and methylene proton shifts, in order to determine the arrangement of hydroxyl and acetate groups on the polymer (Figure 5.3). It was necessary to determine this as previous reports have shown that this 'degree of blockiness' (whether the acetate groups are arranged at random, or in contiguous sequences) plays an important

factor in many of the physical and solution properties of PVA. This is important, particularly in its use as a surfactant,[13] but also in its thermal transition temperatures.[4]

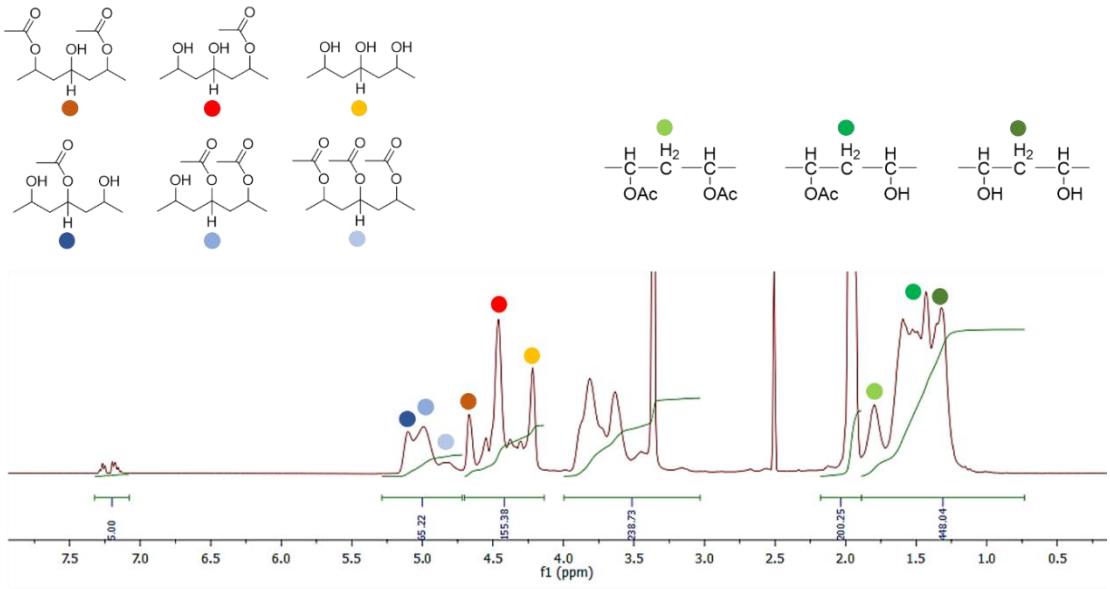

Figure 5.3 ^{1}H NMR spectrum of $\mathbf{P_{250}Ac_{0.25}}$ in deuterated DMSO d6, showing the dyads and triads from methine and methylene proton shifts.

Blockiness arises during hydrolysis of acetate groups. Hydroxyl groups adjacent to acetate groups will catalyse the hydrolysis reaction, leading to blocks of hydroxyl groups if the polymer is not completely hydrolysed. It was expected that complete removal of hydroxyl groups, followed by reversible acid catalysed reacetylation, would introduce acetate functionality randomly. Mean sequence length and the blockiness index, η can be determined by using the integrals of the methylene proton shifts, and the percentages of acetate and hydroxyl groups on the polymer, (Equation 5.1). Blockiness index, (η) can be defined as the percentage of alternating substituents (OH, Ac), divided by the percentage of polymer which can be blocks. $0 \leq \eta < 1$ indicates blocky distributions, $\eta = 1$ a random distribution, and $1 < \eta \leq 2$ for alternate-like polymers. A useful graphical representation was reported by Fujiwara and Moritani,[14] (Figure 5.4).

$$l_{OH} = \frac{2(OH)}{(OH, OAc)}$$

$$l_{OAc} = \frac{2(OAc)}{(OH, OAc)}$$

$$\eta = \frac{(OH, OAc)}{2(OH)(OAc)}$$

Equation 5.1 Mean sequence length, l_x and the blockiness index, η.

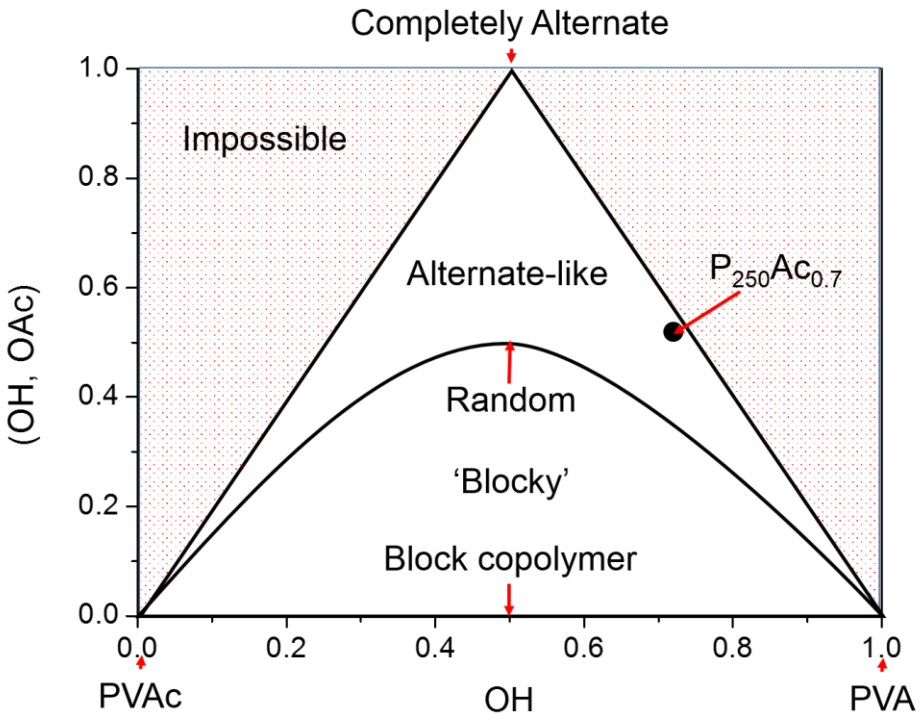

Figure 5.4 Graphical representation of blockiness index.

Using the above equations, the average sequence length of hydroxyl groups, acetate groups, and the 'blockiness index' for **$P_{250}Ac_{0.25}$** were calculated to be l_{OH} = 2.81, l_{OAc} = 1.05, and η = 1.28. For reference most PVA.PVAc co-polymers prepared by hydrolysis or alcoholysis have blockiness values of η = 0.4 - 0.6. This shows that the

polymer is highly alternating, and that substitution is almost statistical, with almost no blocks of acetate functionality occurring along the polymer chain. This means that the random reacetylation reaction was highly successful, and that degree of blockiness would not be a variable factor in thermal phase transitions. Using **PVA$_{350}$** a library of eight sequentially acetylated polymers were obtained with degrees of acetylation ranging from 0 - 70 mol % (Table 5.2).

Table 5.2 Acetylated PVA prepared for this study.

Entry[a]	**[H_2O]:[Acetic acid]:[HCl]**[b]	**Acetylation /mol%**[c]	**DP**
$P_{350}Ac_{0.7}$	17:83:10	70	350
$P_{350}Ac_{0.44}$	32:68:10	44	350
$P_{350}Ac_{0.27}$	50:50:10	27	350
$P_{350}Ac_{0.22}$	45:55:10	22	350
$P_{80}Ac_{0.29}$	25:75:1	29	80
$P_{150}Ac_{0.27}$	25:75:1	27	150
$P_{250}Ac_{0.25}$	25:75:1	25	250
$P_{80}Ac_{0.33}$*	19:67:12	33	80

A For simplicity and ease of cross-referencing, polymers are denoted firstly their size, then by the degree of alkylation as a fraction. **B** Ratios given as v:v:v; 1 mL to 0.1 g PVA. 3M HCl solution. **C** Determined by ^{1}H NMR spectroscopy, by comparing the integrals of the PVA α-H (δ = 4.00 ppm) and PVAc –CH_3 (δ = 1.74 ppm) shifts of the purified co-polymer. * Denotes carboxylic acid functional end group on the PVA/PVAc polymer afforded by using MADIX 2.

5.3ii The Thermoresponsive Behaviour of PVA-*rand*-PVAc Co-polymers

With this library of polymers to hand, the thermoresponsivity of the polymers was evaluated by turbidimetry, using a UV/Vis spectrometer equipped with a temperature control unit. All experiments were conducted at 10 mg.mL^{-1} (to remove concentration associated effects).[15] The cloud point was defined as being the point where absorbance (or strictly, scattering) is 50 % of the maximum measured intensity at 650 nm. It should be noted that this method gives the cloud point only. The LCST is the lowest temperature at which a binary system will de-mix into two separate phases, and is governed by the ratio of the two components in that system.

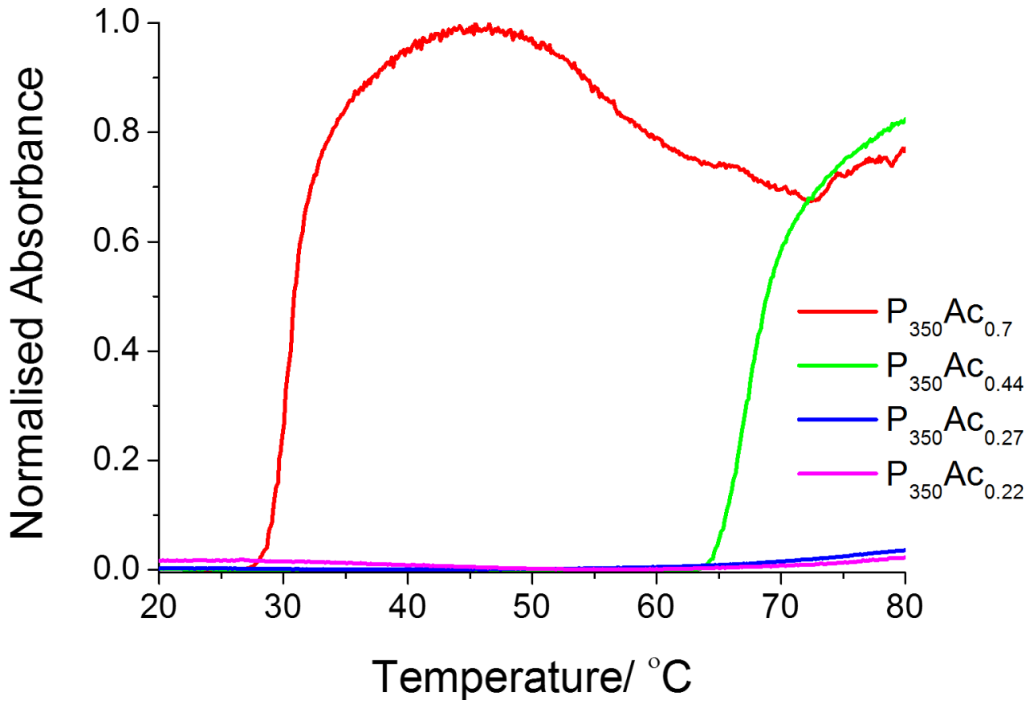

Figure 5.5 Turbidimetry curves of **P_{350}**, with different degrees of acetylation. Measurements were carried out using 10 mg.mL^{-1} solutions of each polymer.

At degrees of acetylation below 40 % there is no thermally induced de-mixing and no cloud point is observed at this temperature range in distilled water (Figure 5.5). This slight increase seen in **$P_{350}Ac_{0.27}$** and **$P_{350}Ac_{0.22}$** is likely due to the solution coming close to boiling point and the formation of bubbles in the solution. **$P_{350}Ac_{0.44}$** shows a clear transition between 63 - 80 °C, with a cloud point of 69 °C. **$P_{350}Ac_{0.7}$** has a much higher degree of acetylation, and hydrophobicity, hence a comparably lower cloud point transition.

$P_{350}Ac_{0.7}$ was further investigated as a function of concentration. As expected, the cloud point transition temperature increased with a corresponding decrease in concentration. However this increase only became apparent below 2.5 mg.mL^{-1}, (Figure 5.6).

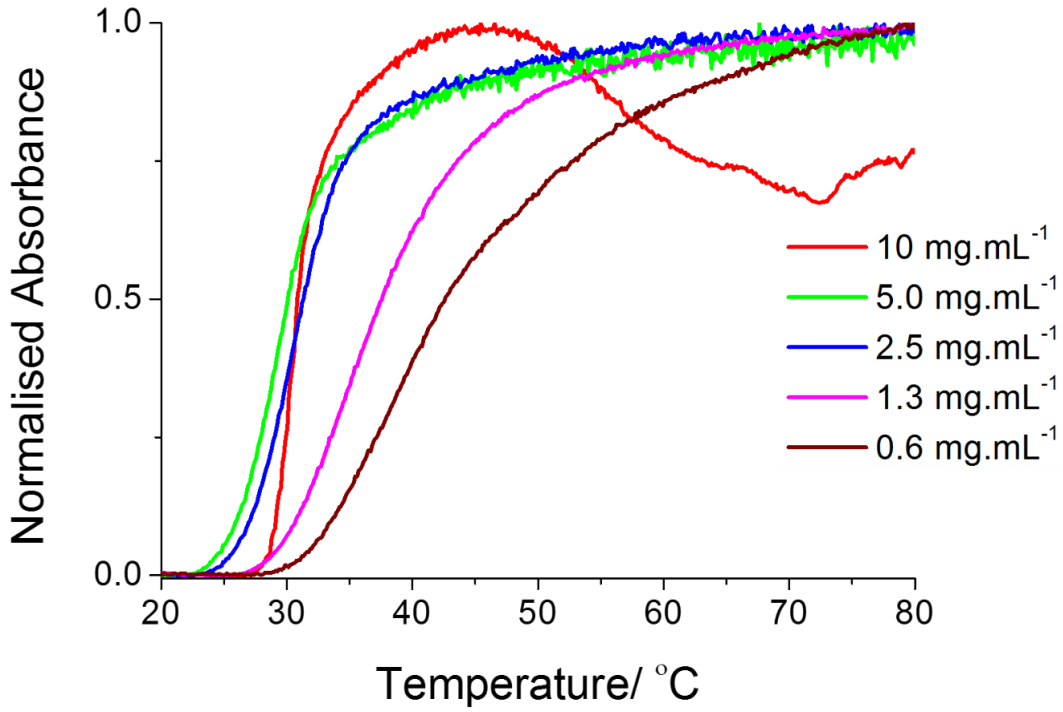

Figure 5.6 The concentration dependent behaviour of **$P_{350}Ac_{0.7}$**.

Flory-Huggins solution theory postulates that longer polymers will have lower transition temperatures, due to the volume fraction of the polymer being larger and hence driving the energetics of the system towards de-mixing. A series of polymers with degrees of polymerisation ranging from 80 to 350 with a fixed degree of acetylation of ~ 30 % were evaluated. These results show that at this low degree of acetylation, and high concentration of 30 mg.mL^{-1}, the cloud point actually increased with chain length, seemingly the opposite of what Flory-Huggins theory predicts (Figure 5.7).

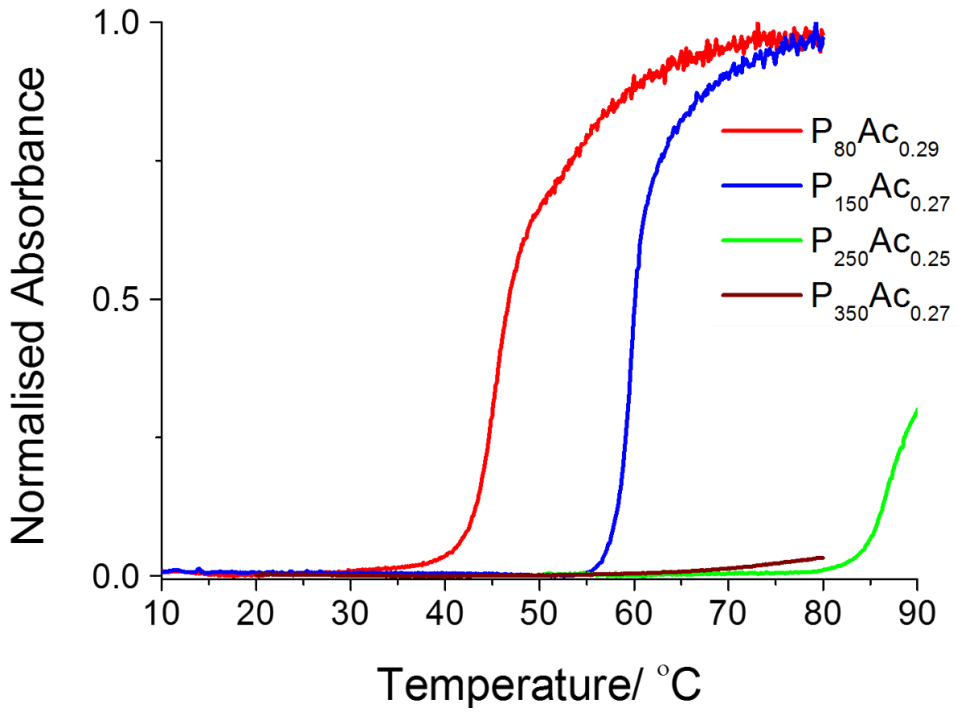

Figure 5.7 Turbidimetry curves showing the cloud point behaviour of PVA(Ac) statistical co-polymers with 30 mol % acetylation at 30 mg.mL^{-1}.

P$_{80}$Ac$_{0.29}$, with a DP of 80, has a cloud point of 47 °C whereas **P$_{150}$Ac$_{0.27}$**, with a DP of 150, has a cloud point of 59 °C. This trend holds at lower concentrations, where the cloud point for each polymer is correspondingly higher but the difference in temperature is roughly the same, (Figure 5.8) The initial hypothesis was that this was

due to the formation of 'pseudo' micelles; a rearrangement of hydrophilic and hydrophobic regions in the polymer, a property which makes PVA(Ac) co-polymers so useful as stabilisers and emulsifiers in water based paints.

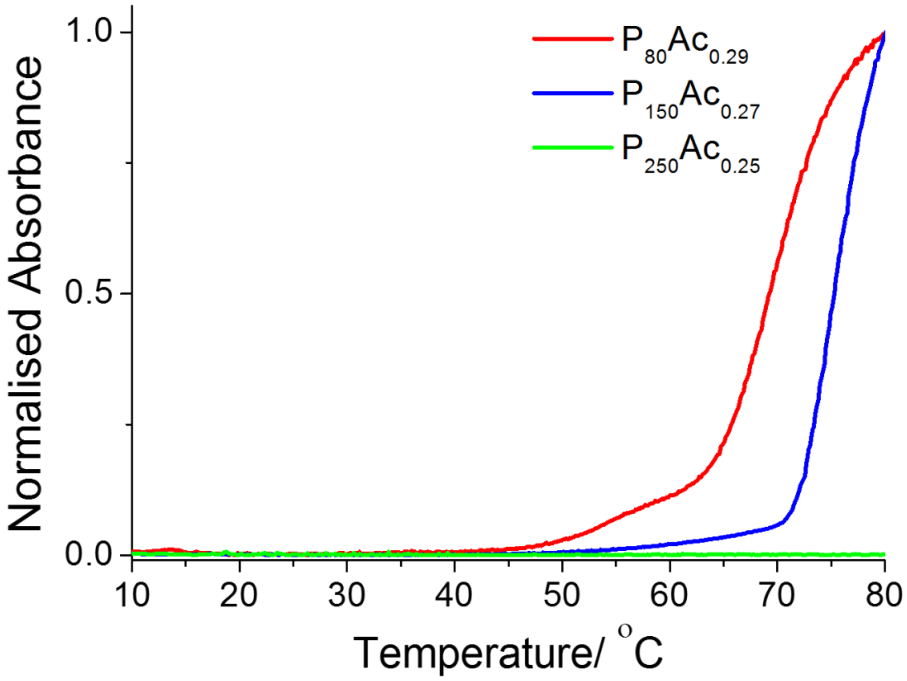

Figure 5.8 Cloud point behaviour of PVA(Ac) statistical co-polymers with 30 mol % acetylation at 10 mg.mL^{-1}.

The ability of PVA to form hydrophobic domains can be probed using a fluorescent hydrophobic dye assay. This assay is commonly used to determine block co-polymer self-assembly in water. The dye, diphenylhexatriene, will fluoresce only in hydrophobic environments, and is sparingly soluble in water. Briefly, diphenylhexatriene was dissolved in water to a concentration of approximately 0.01 mg.mL^{-1}. PVA was then dissolved in this solution to a range of concentrations. Using a microplate reader the samples was excited at 360 nm and the emission at 460 nm was measured.

For PVA, a linear increase in fluorescence is observed as the concentration is increased. This was reported by Deller *et al.* using the same dye assay, (Figure 5.9) indicating that PVA does form hydrophobic domains in water.[16] Deller also reported that Dynamic Light Scattering (DLS) shows no aggregates or micelles forming, and this suggests that PVA has local hydrophobic regions and will reorient its structure in response to guest molecules.

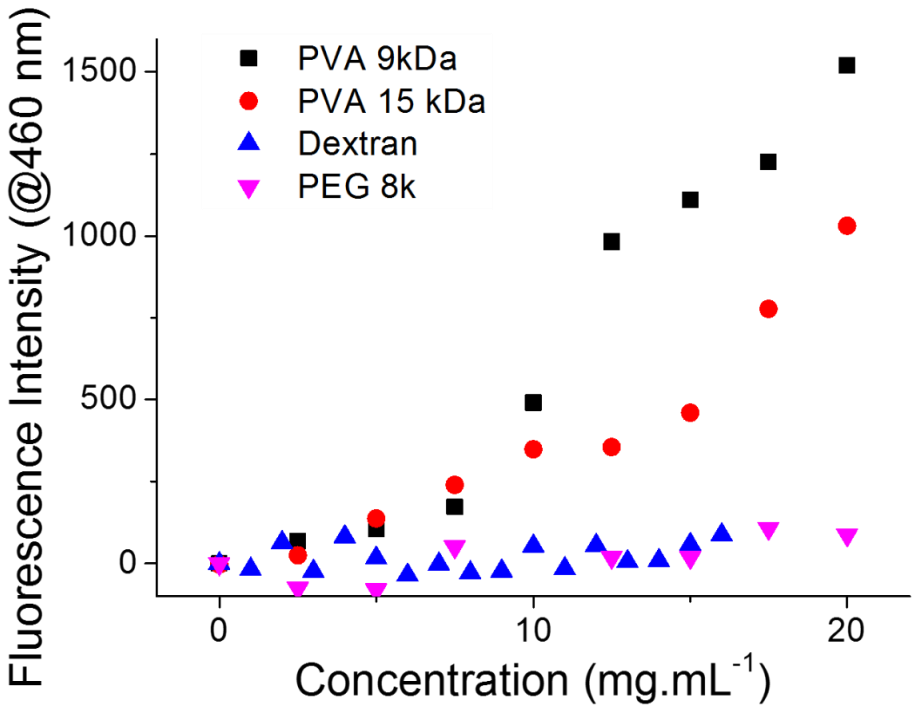

Figure 5.9 Fluorescence at 460 nm of triphenyl hexatriene solutions containing commercial 9 kDa and 15 kDa PVA, compared to dextran and PEG, as reported by Deller *et al.*

The above assay was conducted for $\mathbf{P_{80}Ac_{0.29}}$ and $\mathbf{P_{250}Ac_{0.25}}$, over a range of concentrations and temperatures. For almost all the polymers tested a linear increase in fluorescence is observed, and no discernible trend with respect to temperature is seen (Figure 5.10, Figure 5.11). This strongly indicates that there is no micelle formation caused by increases in temperature.

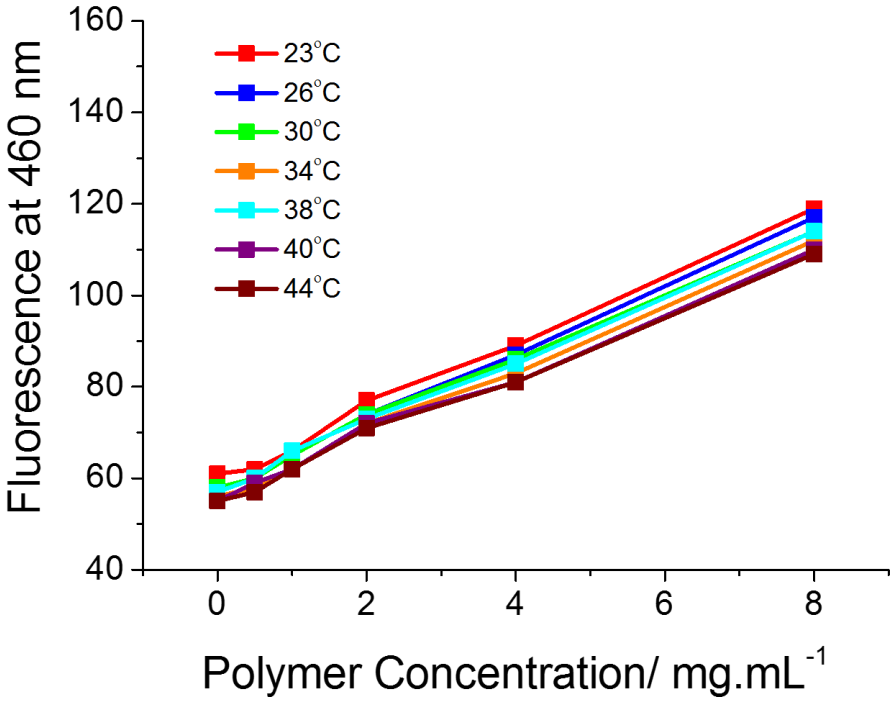

Figure 5.10 Graph showing fluorescence at 460 nm of a solution of $\mathbf{P_{80}Ac_{0.29}}$.

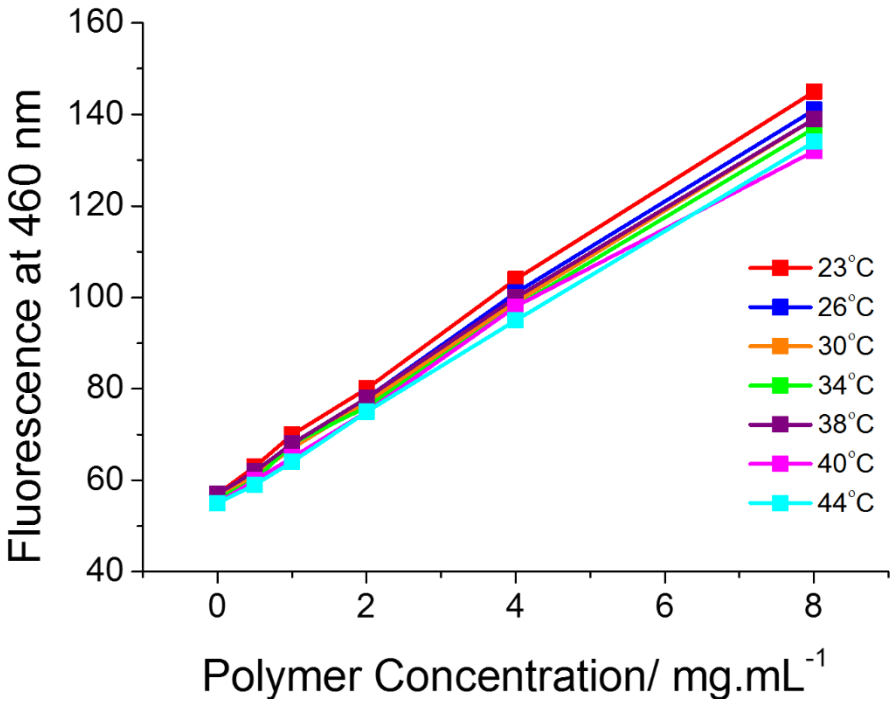

Figure 5.11 Graph showing fluorescence at 460 nm of a solution of $\mathbf{P_{250}Ac_{0.25}}$.

Dye fluorescence intensity and trend closely matches that of the commercial PVA solutions. The larger $\mathbf{P_{250}Ac_{0.25}}$ shows greater fluorescence as concentration is increased, in line with previous reports. The temperature is inducing no noticeable effect to the hydrophobic environment PVA is capable of presenting, so no rearrangement on the scale of aggregation or micellisation is occurring.

It was hypothesised that the above phenomenon could be attributed to the larger effect the end-groups would have on shorter polymers compared to larger polymers. It has been shown previously how the hydrophibicity of end-groups will affect the thermal transitions of poly(*N*-isopropylacrylamide) (pNIPAM).[17] Stöver *et al.* observed that the thermal phase transition of oligomeric pNIPAM appeared to be influenced by more hydrophobic end groups,[18] and this observation was confirmed by Huh *et al.*[19]

To test this a different MADIX agent, MADIX 2 was used to incorporate a carboxylic acid end group in to a PVA(Ac) co-polymer with the same degree of polymerisation and degree of acetylation. This polymer $\mathbf{P_{80}Ac_{0.33}}^{*}$ showed no detectable cloud point, with turbidity slightly decreasing with temperature (Figure 5.12), compared to the benzyl-terminated polymers which showed cloud points in this range. Note that the carboxylic acid end-group of the polymer in Figure 5.12 arises due to the hydrolysis and reacetylation of $\mathbf{P_{80}Ac_{0.33}}$.

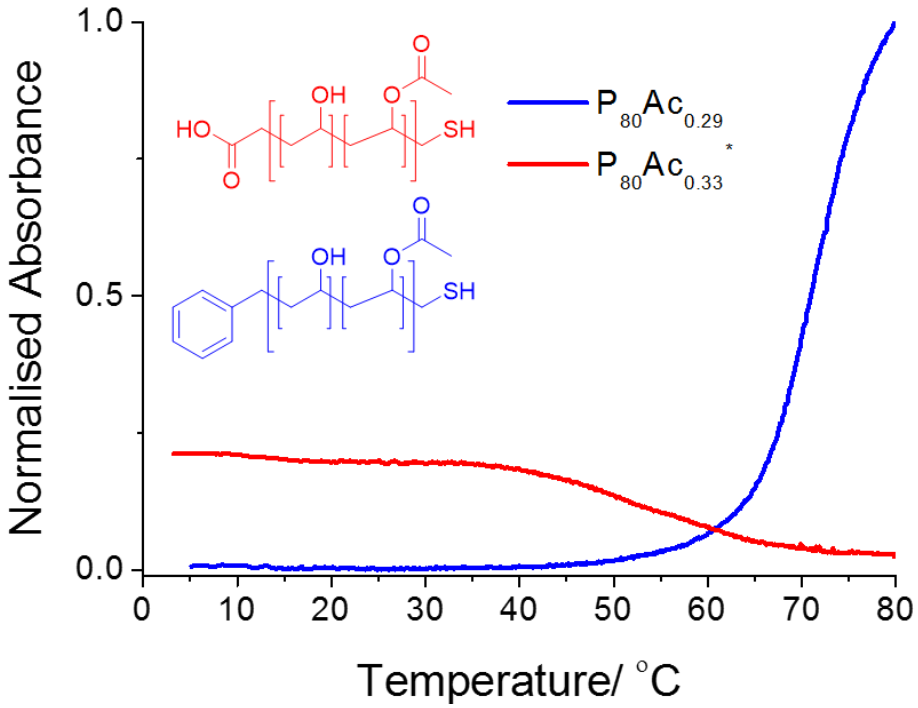

Figure 5.12 Turbidimetry curves showing the cloud point behaviour of **$P_{80}Ac_{29}$** and **$P_{80}Ac_{0.33}^{*}$** with hydrophobic and hydrophilic end groups at 10 mg.mL^{-1}. Absorbance normalised to **$P_{80}Ac_{29}$**

These results, and the literature precedent for the role of end groups affecting thermal phase transitions, explain the initial anomalous activity of these co-polymers. The magnitude of the effect observed here has not been seen before, and suggests that the thermodynamics and kinetics of thermally induced phase transitions for these PVA.PVAc co-polymers, and the nature of solubility of PVA in water, is perhaps more complex than first thought.

5.3iii The Synthesis of PVA-*rand*-PVProp and PVA-*rand*-PVBu Co-polymers

The above data showed that chain length and degree of acetylation enabled control over transition temperature, and highlighted the importance of end group selection. To provide a wider 'toolbox' of transitions and to potentially reduce the degree of substitution which is required, the effect of incorporating increasingly hydrophobic side chains was studied. Using a similar method as for acetate modification PVA was modified using water/propanoic acid or butanoic acid mixtures (Scheme 5.3).

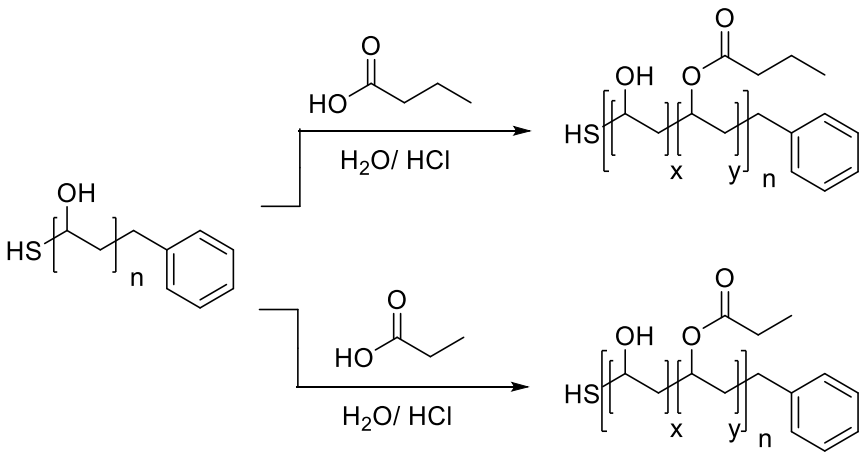

Scheme 5.3 Modification of PVA to form random PVA.Alkyl co-polymers.

As with the preparation of PVA.PVAc co-polymers, different ratios of alkyl acid:water gave different degrees of functionalisation. Higher concentrations of propanoic acid and butanoic acid in the reaction mixture were less able to solubilise PVA, but this could be circumvented by using lower ratios of alkyl acid:water in conjunction with the addition of more catalytic hydrochloric acid (Table 5.3). After alkoxylation, the polymer solutions were dialysed and freeze dried, then characterised by ^{1}H NMR spectroscopy (Figure 5.13, Figure 5.14).

Table 5.3 Alkoxylated PVA prepared for use in this study.

Entry	[H_2O]:[Alkanoic acid] :[HCl] [a]	Alkylation (NMR)/ mol% [b]	DP	Cloud Point/ °C
$P_{250}Pr_{0.25}$	15:85:1	25	**250**	29.51
$P_{250}Pr_{0.20}$	40:60:1	20	**250**	34.18
$P_{250}Pr_{0.10}$	50:50:3	10	**250**	None
$P_{350}Bu_{0.10}$	60:40:2	10	**350**	44.3
$P_{350}Bu_{0.08}$	70:30:2	8	**350**	48.9
$P_{350}Bu_{0.03}$	80:20:2	3	**350**	None

A Ratios given as v:v:v; 1 mL to 0.1 g PVA to 3M HCl solution. Alkanoic acid is either propanoic or butanoic acid, depending on entry. **B** Determined by ^{1}H NMR spectroscopy, by comparing the integrals of the PVA α-*H* (δ = 4.00 ppm) and –C*H*$_3$ (δ = 1.74 ppm) shifts of the purified co-polymers.

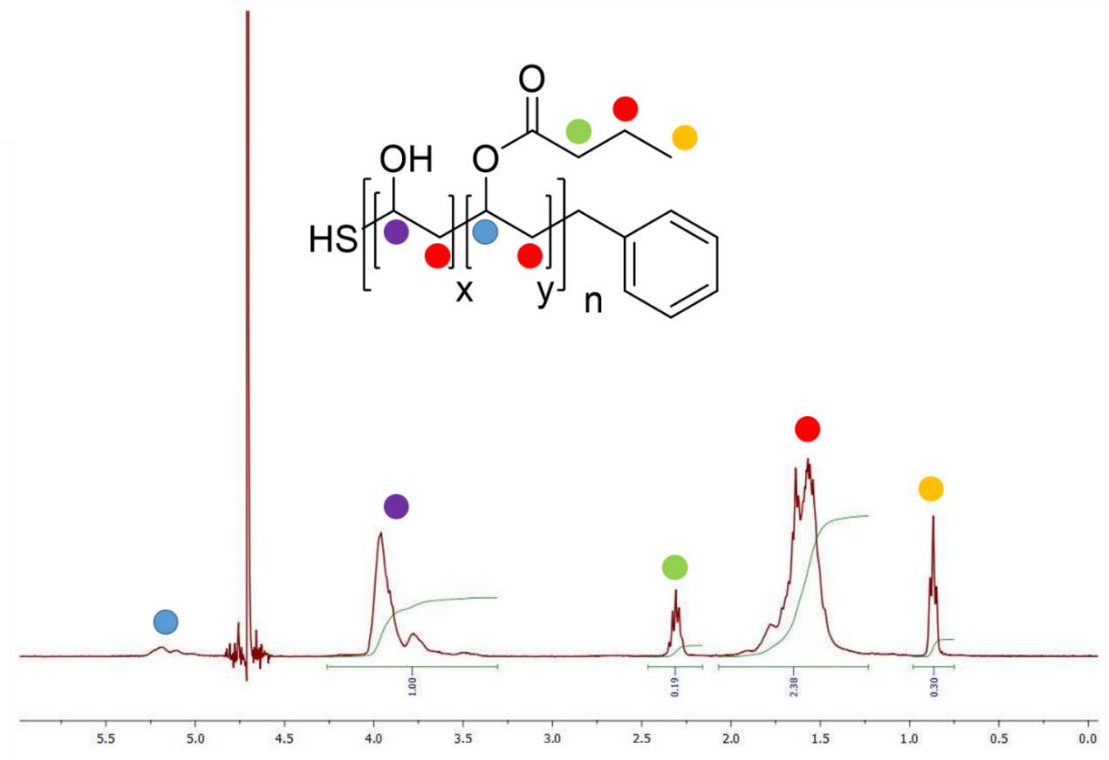

Figure 5.13 ^{1}H NMR spectrum for butanoate functionalised co-polymer **$P_{350}Bu_{0.03}$**.

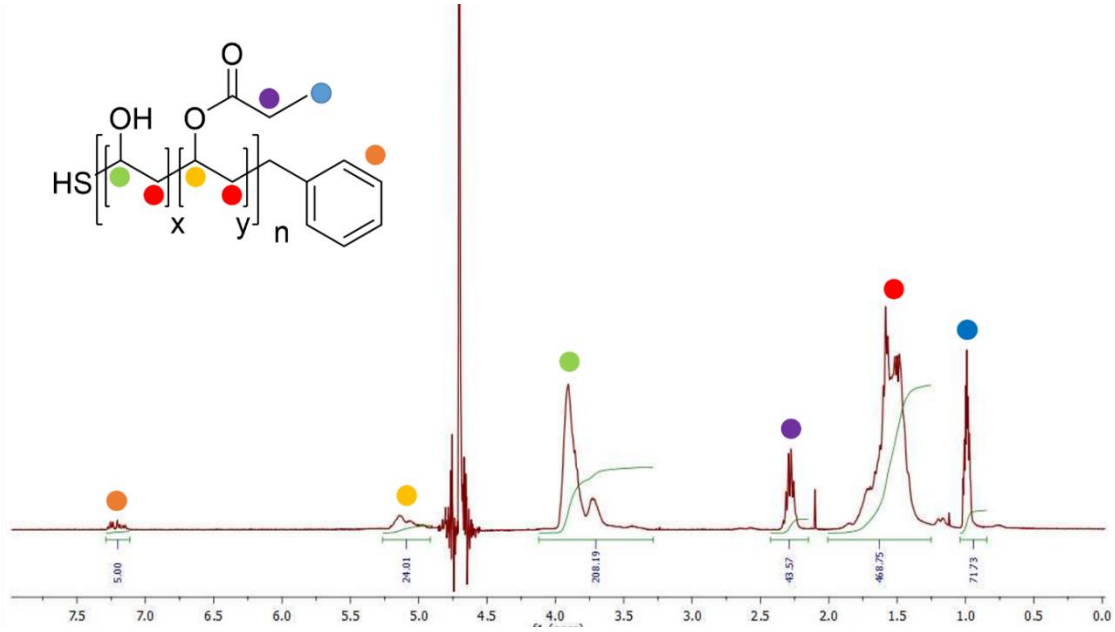

Figure 5.14 ^{1}H NMR spectrum for propanoate functionalised co-polymer **$P_{250}Pr_{0.10}$**.

5.3iv The Thermoresponsive Behaviour of PVA-*rand*-PVProp and PVA-*rand*-PVBu Co-polymers

The solubility of the resultant PVA.Alkyl co-polymers in water was (predictably) lower than corresponding PVA/PVAc co-polymers, meaning only low degrees of functionalisation could be tested for thermoresponsive behaviour.

These co-polymers showed sharp cloud point transitions between 25 – 35 °C for the propyl functionalised PVA (Figure 5.15) and 40 - 50 °C for the butyl functionalised PVA (Figure 5.16). Interestingly **$P_{350}Bu_{0.10}$**, with 10 mol % butyl functional groups displayed a cloud point of 50 °C, whereas **$P_{250}Pr_{0.10}$** displayed no observable cloud point at the same concentration, indicating that lower degrees of substitution are needed for the butyl functionalised PVAs (Figure 5.17).

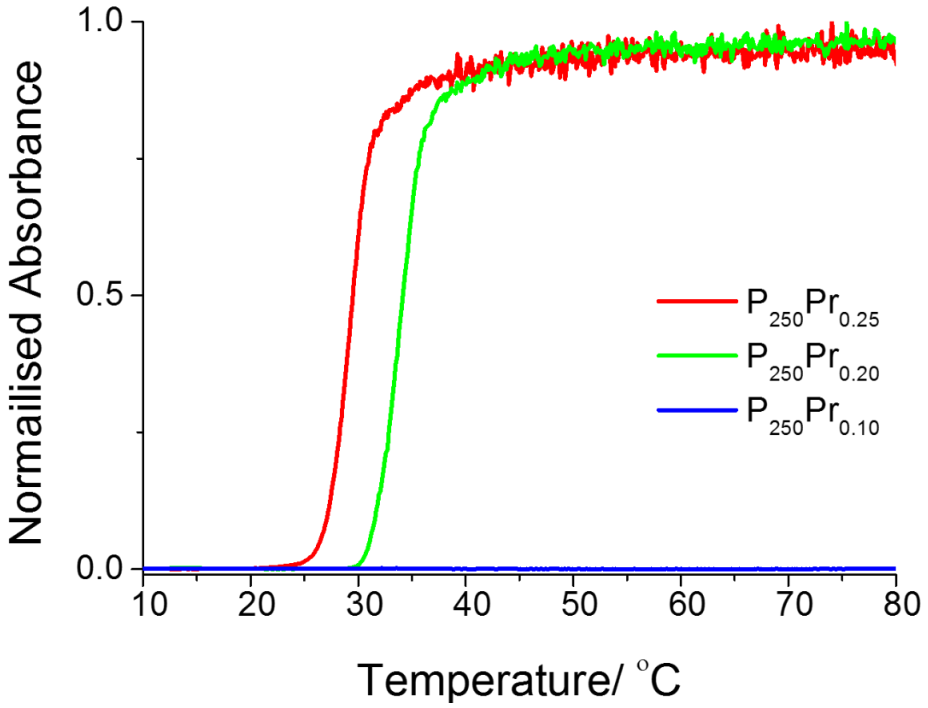

Figure 5.15 Turbidimetry curves showing the cloud point behaviour of PVA.Propyl statistical co-polymers at 10 mg.mL^{-1}.

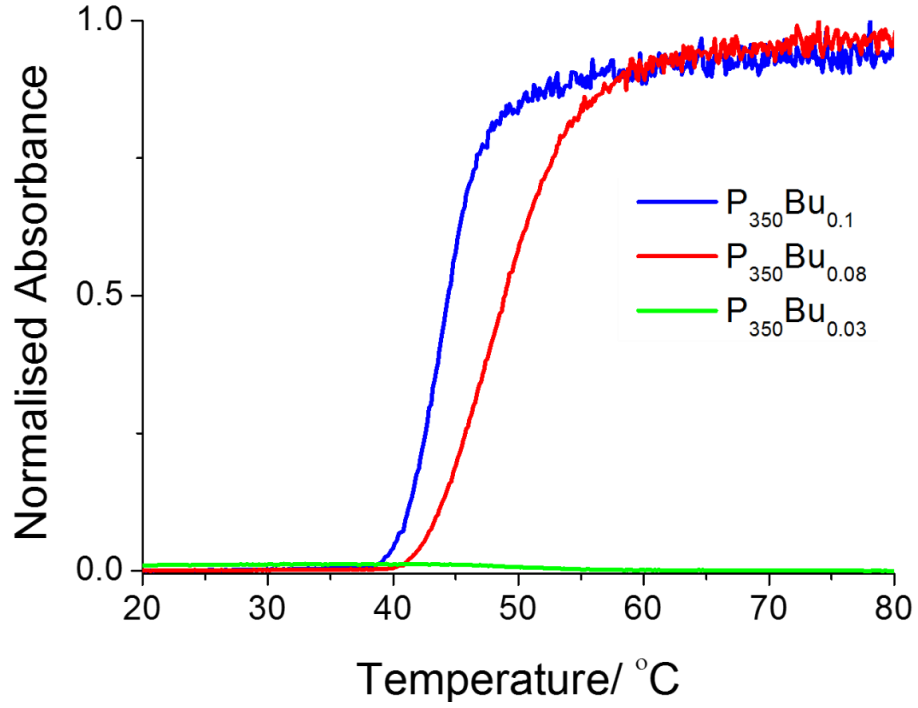

Figure 5.16 The cloud point behaviour of PVA.Bu co-polymers at 10 mg.mL^{-1}.

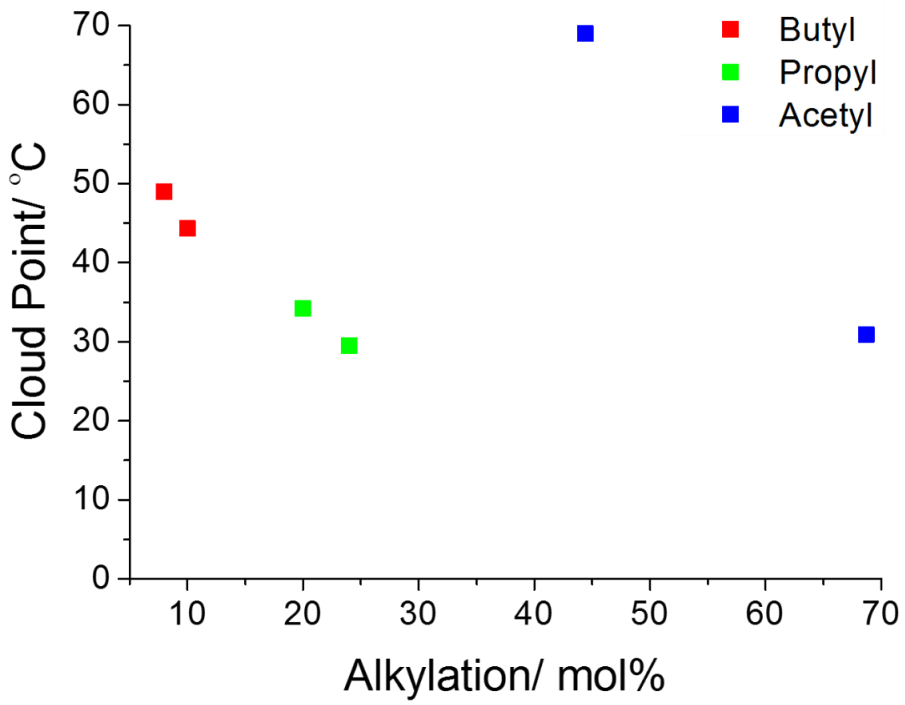

Figure 5.17 Comparison of cloud points (the temperature at 50 % of normalised absorbance) of differently alkanoylated PVA co-polymers.

5.3v The Enzymatically-Triggered Isothermal Cloud Point Behaviour of PVA-*rand*-PVAc Co-polymers

As another demonstration of the utility of PVA as a scaffold for a responsive polymer its susceptibility to enzymatic degradation was studied, to make the polymers 'doubly' responsive and enable the LCST behaviour to be isothermally 'switched off'. **$P_{350}Ac_{0.7}$** was prepared to a dilution of 10 mg.mL^{-1} in Phosphate-Buffered Saline (PBS) solution to which was added porcine liver esterase, an enzyme that will cleave ester linkages, (Scheme 5.4). The solutions were stirred vigorously at 37 °C for 6 days, with aliquots taken and the cloud point determined every 24 hours (Figure 5.18, Figure 5.19).

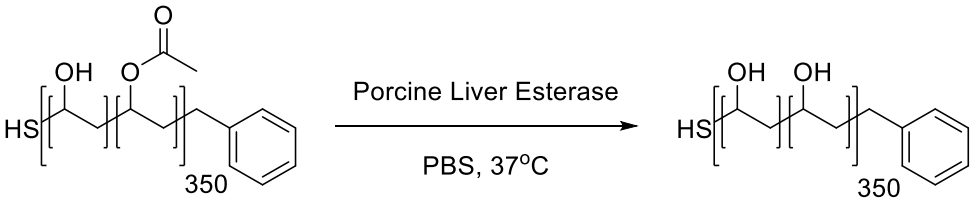

Scheme 5.4 Hydrolysis of acetate functionality of $\mathbf{P_{350}Ac_{0.7}}$ using Porcine Liver Esterase in PBS solution.

A linear increase in the observable cloud point was seen, as acetate groups were removed by the esterase and the solubility of the polymer increased at higher temperatures, without any change in the total polymer concentration. Without the enzyme, no significant hydrolysis was observed over the same time period.

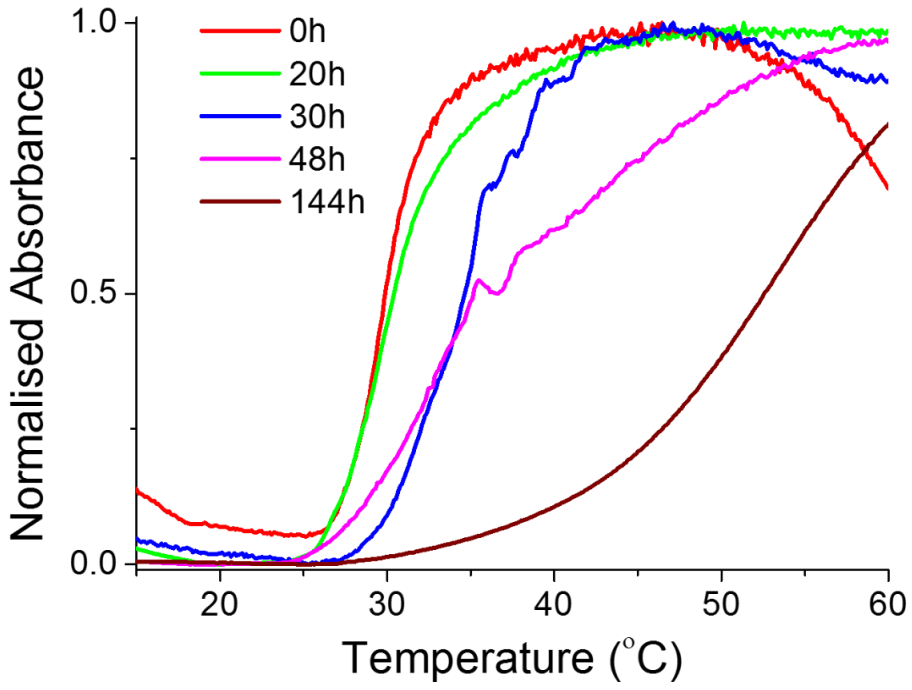

Figure 5.18 The thermally induced phase transition behaviour of $\mathbf{P_{350}Ac_{0.7}}$ after addition of porcine liver esterase.

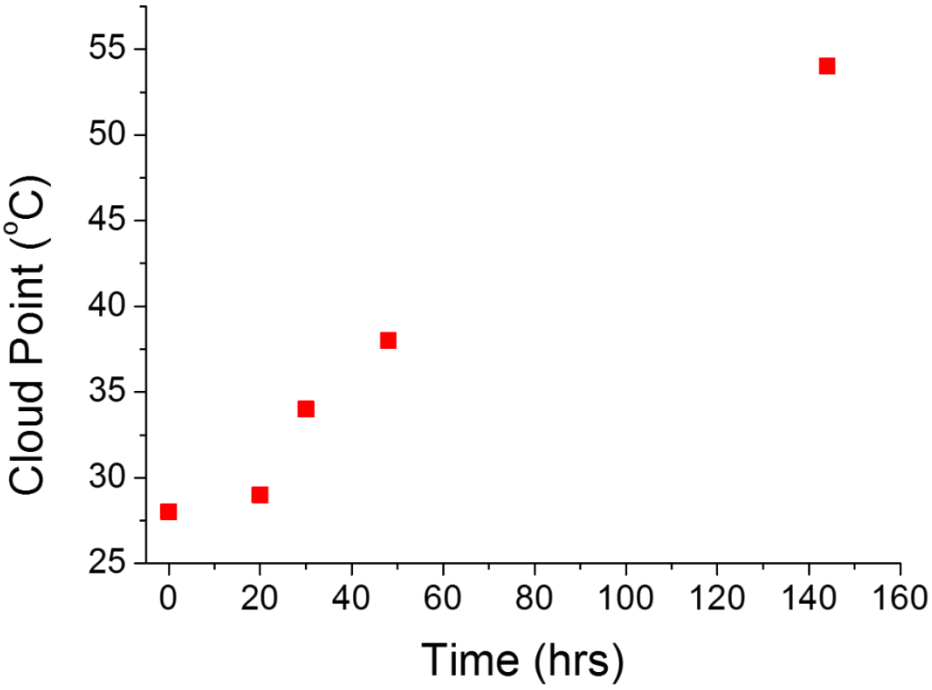

Figure 5.19 The cloud point behaviour of $\mathbf{P_{350}Ac_{0.7}}$ after addition of porcine liver esterase, showing increase in cloud point over time as acetate groups are enzymatically hydrolysed.

5.4 Conclusion

Alkoxylated poly(vinyl alcohol) as a tunable thermoresponsive polymer scaffold was studied in detail. Using MADIX polymerisation it was possible to obtain polymers with chain lengths between 80 and 350 units and low dispersities. Statistical co-polymers were obtained by first removing the acetates from PVAc and then incorporating either acetyl, propanoyl or butanoyl esters. This diverse library was evaluated to show that longer PVAs have an inverse relationship between cloud point (LCST) and chain length. Several formulations were shown to have transitions temperatures in the ambient and physiological temperature range, with the more

hydrophobic side groups (butanoic) only requiring 10 mol % functionalisation compared to 60 mol % for acetate. The importance of end groups was also studied, with hydrophobic end-groups shown to dominate the phase transition such that shorter polymers appeared to give lower LCST than longer, which must be considered when investigating such properties. Finally, the ability of an esterase to selectively remove the acetate groups, to enable the LCST to be 'switched' off was demonstrated. In the context of the thesis, this work highlights the utility of PVA as a smart polymer with a range of applications in emerging technologies, and highlights the complex physical properties affecting solution conformation in water.

5.5 Experimental

Materials and Methods

For general materials and methods details, see the Appendix. Phosphate-buffered saline solutions were prepared using pre-formulated tablets (Sigma-Aldrich) in 200 mL of MilliQ water (>18 Ω mean resistivity) to give a buffered pH of 7.4. Acetic Acid (glacial), 4,4'-Azobis(4-cyanovaleric acid), Butanoic Acid, Hydrazine Hydrate solution (78 - 82 %), lyophilised porcine liver esterase, Propionic Acid and Vinyl Acetate were all purchased from Sigma Aldrich.

Synthesis of methyl(ethoxycarbonothioyl) sulfanyl benzene (MADIX 2)

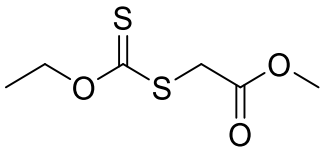

Acetone (70 mL) was added to a round bottom flask equipped with a stir bar. Potassium ethyl xanthate (2.97 g, 0.017 mol) was added and stirred until the solid had dissolved. Methyl bromoacetate (1.88 mL, 0.017 mol) was added, the flask stoppered and the reaction stirred at 50 ^{o}C for 18 h. The solution was then filtered and washed with acetone, then concentrated *in vacuo.* The residue was purified on a column of silica with DCM as the eluent. Yield 3.25 g 54 %. ^{1}H NMR ($CDCl_3$): δ = 1.42 (2H, t, J=7.2, $CH_3C\mathit{H}_2$), 3.76 (3H, s, $C\mathit{H}_3O$), 3.92 (2H, d, J=7, $SC\mathit{H}_2$), 4.64 (3H, q, J=7.2, $C\mathit{H}_3CH_2$). ^{13}C NMR ($CDCl_3$): δ = 14.0 ($CH_2–\mathit{C}H_3$), 37.7 ($\mathit{C}H_2$), 61.0($CO_2\mathit{C}H_3$), 70.4 ($\mathit{C}H_2–CH_3$), 167.7 (C=O), 212.4 (C=S).

Synthesis of methyl(ethoxycarbonothioyl) sulfanyl benzene (MADIX 3)

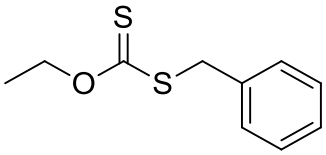

Acetone (70 mL) was added to a round bottom flask equipped with a stir bar. Potassium ethyl xanthate (2.97 g, 0.017 mol) was added and stirred until the solid had dissolved. Benzyl bromide (2.08 mL, 0.017 mol) was added, the flask stoppered and the reaction stirred at 50 °C for 18 h. The solution was then filtered and washed with acetone, then concentrated *in vacuo.* The residue was purified on a column of silica with DCM as the eluent, R_f = 0.2. Yield 3.25 g 54 % ^{1}H NMR ($CDCl_3$): δ = 1.36 (3H,

t, J=7.2, C*H*$_3$CH$_2$), 4.33 (2H, s, SC*H*$_2$), 4.61 (2H, q, J=7.2, OC*H*$_2$CH$_3$) 7.25 (5H, m, benzyl protons); ^{13}C NMR ($CDCl_3$): δ = 13.91 (CH$_2$–*C*H$_3$), 40.54 (*C*H$_2$), 70.16 (*C*H$_2$CH$_3$), 212.4 (C=S), 127.56 (*para C*H), 128.72 (*meta C*H), 129.19 (*ortho C*H).

Polymerisation of Vinyl Acetate Using MADIX 3

As a representative example MADIX 3 (0.21 g, 0.99 mmol), vinyl acetate (4.67 g, 2.64 mmol) and ACVA (4,4'-azobis(4-cyanovaleric acid)) (0.013 g, 0.046 mmol) were added to a stoppered vial. The solution was thoroughly degassed by bubbling N_2 through the reaction mixture for 20 mins and then allowed to polymerise at 68 ^{o}C for typically 15 h. The yellow solutions were then cooled to room temperature. Poly(vinyl acetate) was then recovered as a yellow sticky solid after precipitation into hexane. The hexane was decanted and the poly(vinyl acetate) was re-dissolved in THF, which was then concentrated *in vacuo* and thoroughly dried under vacuum at 40 ^{o}C for 24 h, forming a white crystalline solid. Representative characterisation data for **PVAc$_{80}$**: ^{1}H NMR (400 MHz, $CDCl_3$): δ=4.61 (-C*H*O-CH$_2$ br 1H), δ=1.74 (-CO-C*H*$_3$ br 3H), 1.53 (-C*H*$_2$- br 2H), M_n^{SEC}(THF) = 6900 Da, M_w/M_n = 1.17.

Hydrazinolysis of Poly(vinyl acetate)

As a representative example, Poly(vinyl alcohol) (0.5 g, M_n 29 kDa, Đ = 1.28) was dissolved in water (2.4 mL), acetic acid (7.6 mL) and HCl (0.1 mL, 3M solution in water) in a vial equipped with a stir bar. The reaction mixture was stirred at 40 °C for 4 days. The reaction mixture was then dialysed and partially acetylated poly(vinyl alcohol) was recovered by freeze drying the dialysis solution. Conversion was determined by ^{1}H NMR spectroscopic analysis by integration of the acetate methyl protons (δ=2.08) and the –CH$_2$- backbone protons (δ = 1.93 - 1.50) and IR by

examining the -OH stretch at 3340 cm^{-1} and the –C=O stretch at 1738 cm^{-1}. Representative characterisation data for **$P_{350}Ac_{0.7}$**: ^{1}H NMR (400 MHz, D_2O): δ = 4.00 (-C*H*OH- br 1H), 3.82 (-C*H*O-CH_2 br 1H), 2.08 (-CO-C*H*$_3$ br 3H), δ=1.93-1.50 (-C*H*$_2$- br 2H).

Post Polymerisation Modification of PVA to PVA.PVButanoate Co-polymers

As a representative example, Poly(vinyl alcohol) (0.1 g, M_n 29 kDa, Đ = 1.28) was dissolved in water (3.0 mL), butanoic acid (2.0 mL) and HCl (0.1 mL, 3M solution in water) in a vial equipped with a stir bar. The reaction mixture was stirred at 40 °C for 4 days. The reaction mixture was then dialysed and partially butanoated poly(vinyl alcohol) was recovered by freeze drying the dialysis solution. Conversion was determined by ^{1}H NMR spectroscopy by integration of the butyl -CH_3 protons (δ=0.93, t) and the -CH- backbone protons (δ=4.1-3.4), and IR by examining the -OH stretch at 3340 cm^{-1} and the -C=O stretch at 1738 cm^{-1}. Representative characterisation data for **$P_{350}Bu_{0.03}$**: ^{1}H NMR (400 MHz, D_2O): δ=4.00 (-C*H*O- br m 1H), δ=2.31 (-C*H*$_2$-CH_3 t 2H), δ=1.93-1.50 (-C*H*$_2$- and CH_2-C*H*$_2$-CH_3 br m 4H,), δ=0.93 (-CH_2-C*H*$_3$ t 3H).

Post Polymerisation Modification of PVA to PVA.PVPropanoate Co-polymers

As a representative example, Poly(vinyl alcohol) (0.1 g, M_n 11.1 kDa, Đ = 1.21) was dissolved in water (1.5 mL), propanoic acid (1.5 mL) and HCl (0.1 mL, 3M solution in water) in a vial equipped with a stir bar. The reaction mixture was stirred at 40 °C for 4 days. The reaction mixture was then dialysed and partially propanoated

poly(vinyl alcohol) was recovered by freeze drying the dialysis solution. Conversion was determined by ^{1}H NMR spectroscopy by integration of the propyl -CH_2 protons (δ=2.27, t) and the -CH- backbone proton (δ=4.1-3.4), and IR by examining the -OH stretch at 3340 cm^{-1} and the -C=O stretch at 1738 cm^{-1}. Representative characterisation data for $P_{250}Pr_{0.10}$: ^{1}H NMR (400 MHz, D_2O): δ=4.00 (-C*H*O- br m 1H), δ=2.27 (-CH_2-CH_3 t 2H), δ=1.93-1.50 (-CH_2- br 2H).

Enzymatic Degradation of Co-polymers

$P_{350}Ac_{0.7}$ (30 mg, M_n 29 kDa, Đ 1.39) was dissolved in PBS solution (5 mL) in a stoppered vial equipped with a stir bar, to make up a final solution of 10 $mg.mL^{-1}$ of polymer. Lypholysed porcine liver esterase (5 mg) was added and the mixture was stirred vigorously for 7 days at 37 °C. Aliquots were taken and the turbidimetry curves were recorded using a Cary60 UV/Vis spectrometer.

Hydrophobic Dye Inclusion Assay

Fluorescence intensity of polymer solutions was determined by fluorescence spectrometry using a Synergy HT multi-mode microplate reader (BioTek UK, Bedfordshire, UK). Aqueous 80 μL aliquots of polymer, ranging from 0 - 8.0 $mg.mL^{-1}$ and 20 μL of 0.01 mg mL^{-1} DPH were added to a clear flat-bottom 96-well plate and samples incubated at 25 °C for a minimum of 3 minutes. The fluorescence of each sample was then measured with excitation at 360 nm and emission at 460 nm.

5.6 References

1. Nord, F. F.; Bier, M.; Timasheff, S. N., Investigations on Proteins and Polymers. IV.1 Critical Phenomena in Polyvinyl Alcohol-Acetate Copolymer Solutions. *Journal of the American Chemical Society* **1951,** *73* (1), 289-293.

2. Shiomi, T.; Imai, K.; Watanabe, C.; Miya, M., Thermodynamic and conformational properties of partially butyralized poly(vinyl alcohol) in aqueous solution. *Journal of Polymer Science: Polymer Physics Edition* **1984,** *22* (7), 1305-1312.

3. Furusawa, K.; Tagawa, T., Adsorption behavior of water soluble polymers with lower critical solution temperature. *Colloid Polymer Science* **1985,** *263* (5), 353-360.

4. Eagland, D.; Crowther, N. J., Influence of composition and segment distribution upon lower critical demixing of aqueous poly(vinyl alcohol-stat-vinyl acetate) solutions. *European Polymer Journal* **1991,** *27* (3), 299-301.

5. Crowther, N. J.; Eagland, D.; Vercauteren, F. F.; Donners, W. A. B., The temperature dependent contributions of component dyads to the partial molal volumes of a series of poly(vinyl alcohol-vinyl acetate) copolymers in aqueous solution. *European Polymer Journal* **1993,** *29* (12), 1553-1561.

6. Christova, D.; Ivanova, S.; Ivanova, G., Water-soluble temperature-responsive poly(vinyl alcohol-co-vinyl acetal)s. *Polymer Bulletin* **2003,** *50* (5-6), 367-372.

7. Wang, R.-C.; Liu, H.-J.; Tong, J.-G.; Chen, Y., Thermoresponsive poly(vinyl alcohol) derivatives: preparation, characterization and their capability of dispersing gold nanoparticles. *Polymer Chemistry* **2014,** *5* (7), 2417-2424.

8. Wei, L.; Cai, C.; Lin, J.; Chen, T., Dual-drug delivery system based on hydrogel/micelle composites. *Biomaterials* **2009,** *30* (13), 2606-2613.

9. An, Q.; Beh, C.; Xiao, H., Preparation and characterization of thermo-sensitive poly(vinyl alcohol)-based hydrogel as drug carrier. *Journal of Applied Polymer Science* **2014,** *131* (1), DOI: 10.1002/app.39720.

10. Stenzel, M. H.; Cummins, L.; Roberts, G. E.; Davis, T. P.; Vana, P.; Barner-Kowollik, C., Xanthate mediated living polymerization of vinyl acetate: A systematic variation in MADIX/RAFT agent structure. *Macromolecular Chemistry and Physics* **2003,** *204* (9), 1160-1168.

11. Piirma, I., *Polymeric surfactants*. M. Dekker: New York, N.Y., 1992.

12. Congdon, T.; Notman, R.; Gibson, M. I., Antifreeze (Glyco)protein Mimetic Behavior of Poly(vinyl alcohol): Detailed Structure Ice Recrystallization Inhibition Activity Study. *Biomacromolecules* **2013,** *14* (5), 1578-1586.

13. Budhlall, B. M.; Sudol, E. D.; Dimonie, V. L.; Klein, A.; El-Aasser, M. S., Role of grafting in the emulsion polymerization of vinyl acetate with poly(vinyl alcohol) as an emulsifier. I. Effect of the degree of blockiness on the kinetics and mechanism of grafting. *Journal of Polymer Science Part A: Polymer Chemistry* **2001,** *39* (20), 3633-3654.

14. Moritani, T.; Fujiwara, Y., 13C- and 1H-NMR Investigations of Sequence Distribution in Vinyl Alcohol-Vinyl Acetate Copolymers. *Macromolecules* **1977,** *10* (3), 532-535.

15. Ieong, N. S.; Hasan, M.; Phillips, D. J.; Saaka, Y.; O'Reilly, R. K.; Gibson, M. I., Polymers with molecular weight dependent LCSTs are essential for cooperative behaviour. *Polymer Chemistry* **2012,** *3* (3), 794-799.

16. Deller, R. C.; Congdon, T.; Sahid, M. A.; Morgan, M.; Vatish, M.; Mitchell, D. A.; Notman, R.; Gibson, M. I., Ice recrystallisation inhibition by polyols: comparison of molecular and macromolecular inhibitors and role of hydrophobic units. *Biomaterials Science* **2013,** *1* (5), 478-485.

17. Phillips, D. J.; Gibson, M. I., Degradable thermoresponsive polymers which display redox-responsive LCST Behaviour. *Chemical Communications* **2012,** *48* (7), 1054-1056.

18. Xia, Y.; Yin, X.; Burke, N. A. D.; Stöver, H. D. H., Thermal Response of Narrow-Disperse Poly(N-isopropylacrylamide) Prepared by Atom Transfer Radical Polymerization. *Macromolecules* **2005,** *38* (14), 5937-5943.

19. Li, Z.; Kim, Y.-H.; Min, H. S.; Han, C.-K.; Huh, K. M., Molecular weight and end group effects on the thermo-responsive property of oligomeric N-isopropylacrylamide. *Macromolecular Research* **2010,** *18* (6), 618-621.

Chapter 6

Conclusion

This work has shown that the difficulties of preparing well-defined PVA are worth overcoming, as this polymer displays potent IRI activity and highly tunable thermoresponsive properties.

To summarise the thermoresponsive work, what initially started out as a small side project quickly grew into a fully-fledged investigation into PVA thermoresponsivity. Using a MADIX meditated polymerisation scheme and a reliable post-polymerisation modification strategy, PVA-PVAc co-polymers were prepared and their cloud point behaviour was assessed. These results showed that PVA-PVAc cloud point phase transitions were highly tunable across the entire temperature range of liquid water. Different hydrophobic functionality could be easily introduced, and much lower degrees of functionalisation could be used to access transition temperatures between 10 °C and 50 °C. The acetate ester linkage was exploited to introduce an isothermal cloud point change, through the inclusion of different hydrophobic functionalities. Hopefully these results will inspire some new interesting thermoresponsive technologies, considering how easy vinyl acetate and butanoic acid are to obtain.

To summarise the antifreeze work, a MADIX controlled radical polymerisation scheme was employed to prepare poly(vinyl acetate) in a predictable fashion, with good control over the molecular weight and narrow dispersity. A library of discrete molecular weights of PVAc were then hydrolysed to PVA, and tested for IRI activity.

These results showed that activity is highly molecular weight and concentration dependent, with large variances in ice crystal size occurring over small concentration ranges, and a substantial decrease in activity if the chain size was smaller than 20 repeat units. Modifying functional groups completely removed activity once the degree of hydroxyl groups on the polymer backbone was less than 80 %, equivalent to 1 in 5 hydroxyl groups being 'blocked'. The relative hydrophobicity or hydrophilicity of the functional substituent did not matter and also led to dramatic decreases in activity. These results reinforced the theory of a minimum hydroxyl group sequence. Using a monomer that could install methyl groups into the PVA backbone proved difficult, but activity was essentially unaffected. Polymerisation of isopropenyl acetate was also a bit of a coup, and remains the only successful report of PiPAc co-polymerisation today, and led to that report being highlighted in a recent high-impact review of vinyl ester polymerisation.

From these results it was clear that an uninterrupted sequence of hydroxyl groups is vital to PVA IRI activity. The work into PVA-*b*-PVP co-polymers confirmed this. Almost no loss of activity was seen over a range of differently sized block co-polymers. These results could be interpreted in 1 of 3 ways. 1) Ice-binding was *irreversibly* occurring at the ice/QLL interface, 2) Ice-binding was *reversibly* occurring at the ice/QLL interface, or 3) the ice/QLL is not involved. The first two mechanisms are known to occur with AFPs and AFGPs, and there is still contention over which mechanism dominates, but that is another debate entirely. The third possible interpretation is that PVA does not interact with growing ice crystals at all, but is affecting the bulk water and/or the quasi liquid layer properties. Certain IRI-only antifreeze agents, such as *syn*-AFGP mimics and some IRI active small molecules, are theorised to function in the same way. Further to this, more potent IRI

active small molecules are better able to arrange or order water molecules around themselves. It is well known that PVA in solution will form a long-ranged shell of ordered water molecules around itself, compared to PEG, which displays no such long-range ordering. Ordered water molecules would be less able to reorient and add to the quasi-liquid layer. Could this ordering be affecting IRI activity? To test this, *star*-PVAs were prepared using a novel trifunctional MADIX agent. This polymer was able to test several of these theories; the multiple arms would afford much stronger binding to ice, if any ice binding was occurring, and in solution *star*-PVAs have a different conformation and lower overall viscosity compared to polymers of the same weight, essentially meaning that they are less able to order water. IRI analysis conclusively shows no increase in activity, which would be expected if PVA was, reversibly or otherwise, binding to the ice crystal. When considered alongside all other results in this thesis, PVA ice-binding can be effectively ruled out, although some form of microscopy to confirm this would be required to conclusively show this. Therefore IRI activity must be linked to interactions with the QLL/bulk water. *Star*-PVA is still a potent ice growth inhibitor, but is systematically less IRI active than linear PVA of similar arm lengths and overall molecular weights. While there is not enough of a difference to confirm that conformational differences are affecting water-ordering in *star*-PVA, these results are tantalisingly close to providing a complete picture of the mechanisms that govern the IRI activity of PVA. The one major difference between *star* and linear PVA is the ease with which each polymer can entangle, which would translate to differences in solution viscosity. Obviously, to confirm this more detailed studies into PVA solution conformation are required, but this was not the experimental focus of this work.

These results represent a substantial leap forward in understanding the mechanism by which PVA inhibits ice growth. Conclusive evidence is shown for a minimum hydroxyl sequence. Strategies are also detailed for adding secondary functionality to PVA, or changing the morphology, without reducing activity. I hope that one day soon the full mechanism can be elucidated and proven, and a range of PVA-based functional antifreeze agents will be employed in new cryopreservation strategies.

Appendices

Appendix 1 – Materials and Methods

Size Exclusion Chromatography (SEC)

DMF SEC data was obtained in HPLC grade DMF containing 1 $mg.mL^{-1}$ lithium bromide at 323 K, with a flow rate of 1.0 $mL.min^{-1}$, using a Varian 390-LC MDS system equipped with a PL-AS RT/MT autosampler, a set of two Varian PLgel 5 µm Mixed-D columns (7.5 mm diameter), with a guard column, and equipped with a differential refractive index analyser. THF SEC data was obtained in HPLC grade THF containing 2 % trimethylamine at 293 K, with a flow rate of 1.0 $mL.min^{-1}$, using a Varian 390-LC MDS system equipped with a PL-AS RT/MT autosampler, a set of two Varian PLgel 5 µm Mixed-D columns (7.5 mm diameter), with a guard column and equipped with a differential refractive index analyser, Light Scattering detectors at 90° and 135°, and a differential viscometer. SEC data was analysed using Cirrus SEC software and was calibrated using poly(methyl methacrylate standards (690-271400 Da).

NMR Spectroscopy

^{1}H (400 MHz) and ^{13}C (100 MHz) NMR spectra were recorded on a Bruker DPX-400 spectrometer at 293 K. Chemical shifts are reported as δ in parts per million (ppm) and referenced to the residual solvent resonances ($CDCl_3$ ^{1}H: δ = 7.26 ppm, ^{13}C δ = 77.16 ppm. D_2O ^{1}H: δ = 4.79 ppm. d_6-DMSO ^{1}H: δ = 2.50 ppm.) The spectra were analysed using MestreNova.

Mass Spectrometry

ESI mass spectra were collected on a Bruker Esquire2000 ESI-MS TOF machine in positive mode using either Methanol or Water as the sample solvent, depending on sample solubility.

UV/Vis Spectroscopy

Thermal transitions were measured using an Agilent Technologies Cary60 UV/Vis spectrometer equipped with a Quantum Northwest TC1 temperature controller. Samples were heated from 10 °C to 90 °C at 2 °C/min, and absorbance was measured at 650 nm.

Ice Recrystallisation Inhibition 'Splat' Assay

A droplet of polymer containing PBS solution is dropped from 1.4 m onto a glass microscope coverslip, which is on top of an aluminium plate cooled to -78 °C using dry ice. The droplet freezes instantly upon impact with the plate, spreading out and forming a thin wafer of ice. This wafer is then placed on a liquid nitrogen cooled cryostage held at - 8 °C. Photographs of the wafer at 20 x zoom under cross polarisers are taken and then the wafer is left to anneal for 30 minutes at - 8 °C. Three photographs are taken of the wafer and a final photograph at 4x zoom is taken. These photographs are then analysed using ImageJ, a free image analysis software program, to determine crystal size, using a standard of 100 μm wide gold tracks printed on a glass slide. The largest 4 crystals from three 20 x photographs are measured and then averaged, and this average is then divided by the MLGS for PBS solution (138 μm). This gives as a percentage of growth compared to PBS, or the % MLGS.

Hydrophobic Dye Inclusion Assay

Fluorescence intensity of polymer solutions was determined by fluorescence spectrometry using a Synergy HT multi-mode microplate reader (BioTek UK, Bedfordshire, UK). Aqueous 80 μL aliquots of polymer, ranging from 0 - 8.0 mg.mL^{-1} and 20 μL of 0.01 mg mL^{-1} DPH were added to a clear flat-bottom 96-well plate and samples incubated at 25 °C for a minimum of 3 minutes. The fluorescence of each sample was then measured with excitation at 360 nm and emission at 460 nm.

Appendix 2 - Publications

During the course of this work I collaborated with a number of other researchers in topics related to my topic of study. Some of the findings from these papers have been referenced in Chapters 1 – 5, but were not included as in several cases I supervised the work, or it was not pertinent to the topic of this thesis. A list of publications and my contributions to them are included below, and the work on methacryalted sugars is included in its entirety.

1) Deller, R.C., Congdon, T., Sahid, M., Morgan, M., Vatish, M., Mitchell, D.A., Notman, R., Gibson, M.I., *Biomater. Sci*., **2013**, 1, 478 - 485 "Ice recrystallisation inhibition by polyols: comparison of molecular and macromolecular inhibitors and role of hydrophobic units" *Top 10 Most accessed Articles Jan and Feb 2013*

- In this work I supervised M. Sahid, and carried out some of the hydrophobic dye inclusion assays, and prepared PVA materials.

2) Al-Zhrani, A, Yeo, B., Skelhon, T.S., Deller, RC., Congdon, TC, Gibson, M.I., Bon, SAF *In Revision.*

- This manuscript was submitted to *Science*. In this work I conducted the IRI 'splat assays'.

3) Congdon, T, Notman, R., Gibson, MI, *Biomacromolecules*, **2013**, 14, 1578 - 1586 "Antifreeze (Glyco)Protein Mimetic Behaviour of Poly(vinyl alcohol): Detailed Structure-Ice Recrystallisation Inhibition Activity Study".

- As the first author in this manuscript I carried out all experimental work and contributed equally with R. Notman and M. I. Gibson in the writing and

preparation of the manuscript. The results of this paper form the bulk of Chapter 2.

4) Congdon, T, Wilmet, C., Williams, R., Polt, J., Lilliman, M., and Gibson, M.I., *Eur. Polym. J.*, **2015**, 62, 352 - 362, "Functionalised Carbohydrate-Centred Oligomers and Polymers. Thermoresponsivity, Lectin Binding and Degradability" *Special issue on Precision Polymer Materials*

- In this work I supervised C. Wilmet, R. Williams, J. Polt and M. Lilliman during their Masters/Erasmus projects, prepared diethylene glycol thiol and maltotriose methacrylate and carried out some degradation assays. I also prepared the bulk of the manuscript. The complete paper is included below as it represents a significant amount of time and effort invested over the course of my studies, but due to the number of collaborators and the subject matter it would not be appropriate to be submitted as a results chapter.

5) Congdon, T., Shaw P., Gibson, MI., *Polym. Chem.*, **2015**, 6, 4749 – 4757, "Thermoresponsive, Well-Defined, Poly(vinyl alcohol) Co-polymers"

- For this manuscript I carried out all the experimental work and prepared the manuscript equally with M.I. Gibson.

6) Mitchell, D E., Congdon, T., Rodger, A., Gibson, MI. *In Revision*

- In this work I prepared a range of PVA samples for testing.

7) Dean, B. T., Congdon T., Gibson, MI, *Submitted*

- In this work I supervised B. Dean during her URSS summer placement project.

European Polymer Journal 62 (2015) 352–362

Contents lists available at ScienceDirect

European Polymer Journal

journal homepage: www.elsevier.com/locate/europolj

Diversely functionalised carbohydrate-centered oligomers and polymers. Thermoresponsivity, lectin binding and degradability

Thomas Congdon, Charline Wilmet, Rebecca Williams, Julia Polt, Mary Lilliman, Matthew I. Gibson *

Department of Chemistry, University of Warwick, Coventry CV4 7AL, UK

ARTICLE INFO

Article history:
Received 10 April 2014
Received in revised form 28 May 2014
Accepted 2 June 2014
Available online 17 June 2014

Keywords:
Star polymer
Glycopolymer
Thermoresponse
Lectin binding
Biodegradable polymer
Thiol-ene click

ABSTRACT

Nature is capable of synthesizing perfectly defined, sequence-controlled oligomers and polymers, whereas synthetic polymerization methods inherently give rise to dispersity and limited reproducibility. This inherent dispersity provides a barrier to translation into biomedical applications and for probing material-biology interactions. Templating of polymers based upon biosynthesized cores offers a route to reproducible oligo/polymers if the template itself is readily available and highly tunable. Here oligosaccharides are employed as monodisperse scaffolds for the synthesis of highly functional biomaterials. The pendant hydroxyl units are converted to reactive methacrylates, which are themselves amenable for thiol-ene ('click') functionalization. Using this strategy, extremely well defined ($M_W/M_N < 1.05$) polymers are prepared bearing thermoresponsive or lectin-binding moieties. The templatation strategy ensures identical polymers are obtained from each synthesis. Their thermoresponsive behavior and multivalent interactions with a bacterial lectin are studied as a function of the discrete number of functional groups. Due to the ester linkage, these polymers are also shown to be inherently degradable.

1. Introduction

The development of biomaterials that are capable of interacting with and inducing a beneficial responsive from biological systems is providing new routes to treat human disease, infection and aging. For example, scaffolds for tissue or bone repair/re-growth [1], slow release formations [2], polymer–protein conjugation, nanoparticle delivery [3,4], gene delivery [5], sensing [6], diabetes treatment [7], cryopreservation [8] and nanomedicine [9].

The introduction of functionality that can enable 'smart' responses to biological cues [10], such as temperature, pH [11], biochemical gradients [12,13], light [14] or enzymes [15] is being used to enhance the complexity of materials. This enables dynamic interactions with biology to trigger cellular uptake [16,17], drug release, protein purification [18] or stem-cell differentiation [19]. Another approach focuses on incorporating biological binding motifs such as peptides [20], DNA [21], or carbohydrates [22] that trigger responses or highly specific binding events. In the development of all the above-mentioned materials, the key requirement is precise and reproducible synthesis; both to obtain structure–activity relationships, but also to meet regulatory requirements to ensure predictable pharmacokinetics, degradability and cellular trafficking.

The highly functional polymers described above are routinely accessible using controlled radical polymerization (RAFT, ATRP, SET and NMP) that allow the routine

* Corresponding author. Tel.: +44 247 652 4803; fax: +44 247 652 4112.
E-mail address: m.i.gibson@warwick.ac.uk (M.I. Gibson).

http://dx.doi.org/10.1016/j.eurpolymj.2014.06.001
0014-3057/

synthesis of highly functional polymers with excellent control over molecular weight and molecular weight distributions, and have been widely reviewed for biomedical applications [23,24]. The key challenge remains that these polymers are inherently non-biodegradable due to them being derived from vinyl monomers, with the rare exceptions of cyanoacrylates or copolymers made from radical-ring opening polymerizations [25]. Alternatively the use of ring-opening polymerization (ROP) of cyclic esters/amides [1,26] enables the introduction of a degradable backbone, but is limited in terms of functional group compatibility, requiring post-polymerization modification to access functional (e.g. hydroxyl) polymers [27]. (Bio)orthogonal (click) chemistries have revolutionized this synthetic approach, with particular attention paid to the [3+2] cycloadditions of azides/alkynes and either nucleophilic or radical additions of thiols onto alkenes. Despite these synthetic tools both ROP and radical polymerizations are limited by their statistical nature resulting in a distribution of molecular weights ($Đ < 1.3$ typically) even for the best single electron transfer (SET) processes [28]. This presents an additional challenge when it comes to the precision study of polymer–biological interactions where small differences in degree of polymerization (valency) and dispersity can have a significant influence on the observed biological outcome. This is a particular problem in the glycosciences where the binding affinity between multivalent scaffolds and their target proteins increases dramatically with valency. For example, Lee et al. observed a 10^5 fold reduction in the minimum inhibitory concentration upon changing from mono- to tetra-antennary lactosides against a hepatic lectin [29]. Many glycopolymer antagonists for pathogenic proteins with exceptionally high affinity/activity have been reported and the roles of polymer composition, architecture and length have been shown to be crucial [30,31]. Therefore there still exists huge chemical space to be explored to translate new anti-adhesive therapies as alternatives to traditional antibiotics [32,33], but this is somewhat constrained by the limitations of controlled radical polymerizations.

For these reasons dendrimers, perfectly branched macromolecules, have been extensively explored as biomaterials [34]. Due to their step-wise synthetic protocols, dendrimers or peptides (from solid phase synthesis) can be obtained with narrow dispersity and be constructed out of biodegradable units [35]. Detailed mass spectrometry and chromatographic analysis by Banaszak-Holl and co-workers has quantified the presence of generational defects in PAMAM dendrimers which increase their heterogeneity [36]. Perhaps the biggest constraint on the use of dendrimers is their high cost and relatively low availability compared to linear polymers. Nature is capable of synthesizing perfectly monodisperse macromolecules, in the form of proteins and DNA, and these have been studied extensively as templates for polymer synthesis [37,38]. Synthetic machines capable of assembling peptides have also been created [39]. (Pseudo) site-specific functionality can also be introduced at predetermined sites within the backbone of CRP derived polymers, based on differential reactivity of maleimides with other monomers [40].

Oligosaccharides are usually thought of as polymers of monosaccharides, but they could also be considered to be monodisperse multifunctional poly(ols) and are therefore ideal template molecules. STARFISH like multivalent glycoclusters [30], or PAMAM dendrimers around trehalose ('Octopus glycosides') are examples of these materials [41,42]. Gao et al. have made propargyl-functional galactose that was suitable for 'click' cycloaddition to make small (tetravalent) glycosylated clusters that displayed a 400-fold affinity enhancement relative to the carbohydrate alone [43] In particular, this functionalizable/clickable core is an appealing scaffold to generate libraries of monodisperse/polymers oligomers, and materials other than glycoconjugates.

Here we explore the synthesis and extend the application of carbohydrate-centered polymers *via* a thiol-ene modification strategy. This method is used to obtain stimuli responsive polymers, anti-adhesive pathogen inhibitors and also demonstrate their biodegradability.

2. Experimental

2.1. General procedures

Phosphate-buffered saline solutions were prepared using preformulated tablets (Sigma–Aldrich) in 200 mL of MilliQ water (>18 Ω mean resistivity) to give a buffered pH of 7.4. Cellobiose was purchased from Acros Organics. Benzylamine, Bovine serum albumen (BSA), FITC labeled Cholera Toxin B subunit, 2-(2-methoxyethoxy)ethanethiol, galactose, glucose, 2-[4-(2-hydroxyethyl)piperazin-1-yl]ethanesulfonic acid (HEPES), mannose, maltotriose, methacrylic anhydride, lactose, raffinose and tributyl phosphine were purchased from Sigma–Aldrich. Anhydrous pyridine was purchased from VWR. GM1 ganglioside, β-D-thiogalactose sodium salt and stachyose were purchased from Carbosynth (Berkshire, UK). Peanut Agglutinin-FITC was purchased from Vector Labs. Poly(diethylene glycol methacrylate) was prepared according to previous reported methods [47].

2.2. Physical and analytical methods

^{1}H and ^{13}C NMR spectra were recorded on Bruker DPX-300 and DPX-400 spectrometers using deuterated solvents purchased from Sigma–Aldrich. Chemical shifts are reported relative to residual non-deuterated solvent. Infrared spectra was recorded on a Bruker Vector 22 GI003097. Mass spectrometry analyses were obtained using Bruker MicroTOF or Bruker MaXis electrospray instruments using positive or negative electrospray mode. Thermal transitions were measured using an optimelt MPA100 system and an Agilent Technologies Cary60 UV/Vis spectrometer equipped with a Quantum Northwest TC1 temperature controller. Size exclusion chromatography (SEC) was used to examine and differentiate between the molecular weights and polydispersities of the synthesized carbohydrates. The DMF GPC system comprised of a Varian 390-LC-Multi detector suite fitted with a differential refractive index (DRI) detector equipped with a guard

column (Varian Polymer Laboratories PLGel 5 μm, 50 × 7.5 mm) and two mixed D columns of the same type. The mobile phase was DMF with 5nM NH_3BF_4 eluent at a flow of 1.0 mL/min, and samples were calibrated against Varian Polymer Laboratories Easi-Vials poly(methylmethacrylate) standards (162–2.4 × 105 g/mol) using Cirrus v3.3. The THF GPC system comprised of a Varian 390-LC-Multi detector suite fitted with differential refractive index (DRI), light scattering (LS) and ultra-violet (UV) detectors equipped with a guard column (Varian Polymer Laboratories PLGel 5 μm, 50 × 7.5 mm) and two mixed D columns of the same type. The mobile phase was THF with 5% triethylamine (TEA) eluent at a flow of 1.0 mL/min, and samples were calibrated against Varian Polymer Laboratories Easi0Vials linear poly(styrene) and poly(methylmethacrylate) standards (162–2.4 × 10^5 g/mol) using Cirrus v3.3.

2.3. General procedure for the methacrylation of carbohydrates

As a representative example, glucose (5.05 g, 27.75 mmol), methacrylic anhydride (21.52 g, 0.14 mol) and pyridine (125 mL) were added to a 250 mL round bottom flask equipped with a stir bar. The solution was stirred at room temperature for 15 h before being heated to 60 °C for 3 h. Upon cooling, dichloromethane (50 mL) was added and the product washed sequentially with hydrochloric acid (3M, 4 × 50 mL), water (2 × 50 mL), brine (50 mL) and saturated $NaHCO_3$ (2 × 50 mL) before being dried with $MgSO_4$. The solvent was then removed under vacuum to yield a clear viscous oil.

2.3.1. A-Meth$_5$

^{1}H NMR ($CDCl_3$, 400 MHz) δ (ppm): 6.27–6.03 (5H, m, C═CH_2 *cis*), 5.76–5.44 (5H, m, C═CH_2 *trans*), 5.39–5.09 (2H, m, CH_2OH), 4.44–4.15 (3H, m, CH_2), 2.01–1.84 (15H, m, CH_3); ^{13}C NMR ($CDCl_3$, 600 MHz, PENDANT) δ (ppm): 166.9–164.9 (*C*═O), 135.7–134.8 (*C*═CH_2), 128.2–126.4 (C═*C*H_2), 92.3–92.1 (β anomer), 89.8–89.7 (α anomer), 76.1–68.2 (*C*H), 62.8–62.0 (*C*H_2), 18.2–18.0 (*C*H_3); IR υ (cm^{-1}) 1721 (C═O), 1637 (C═C), 1453 (CH_2/CH_3 bend), 1317 (CH_3 bend), 1292 (alkyl C-H), 1140 (C—O stretch); MS (ESI) *m*/*z*: 475.0 [M(4mer)+Na]$^+$ $C_{22}H_{28}O_{10}$, *m*/*z* 543.2 [M(5mer)+Na]$^+$ $C_{26}H_{32}O_{11}$; M_N^{SEC}(THF) = 460, M_W/M_N = 1.03.

2.3.2. B-Meth$_5$

^{1}H NMR ($CDCl_3$, 400 MHz) δ (ppm): 6.27–6.03 (5H, m, C═CH_2 *cis*), 5.76–5.44 (5H, m, C═CH_2 *trans*), 5.39–5.09 (2H, m, CH_2OH), 4.44–4.15 (3H, m, C*H*), 2.01–1.84 (15H, m, CH_3); ^{13}C NMR ($CDCl_3$, 600 MHz, PENDANT) δ (ppm): 166.9–164.9 (*C*═O), 135.7–134.8 (*C*═CH_2), 128.2–126.4 (C═*C*H_2), 92.3–92.1 (β anomer), 89.8–89.7 (α anomer), 76.1–68.2 (*C*H), 62.8–62.0 (*C*H_2), 18.2–18.0 (*C*H_3); IR υ (cm^{-1}) 1721 (C═O), 1637 (C═C), 1453 (CH_2/CH_3 bend), 1317 (CH_3 bend), 1292 (alkyl C—H), 1140 (C—O stretch); MS (ESI) *m*/*z*: 475.1 [M(4mer)+Na]$^+$ $C_{22}H_{28}O_{10}$, *m*/*z* 543.2 [M(5mer)+Na]$^+$ $C_{26}H_{32}O_{11}$; M_N^{SEC}(THF) = 430, M_W/M_N = 1.02.

2.3.3. C-Meth$_5$

^{1}H NMR ($CDCl_3$, 400 MHz) δ (ppm): 6.24 (5H, d (*J* = 3.8 Hz), C═CH_2 *cis*), 5.68 (5H, d (*J* = 8.0 Hz), C═CH_2 *trans*), 4.47–3.92 (6H, m, ring protons), 2.04 (15H, t (*J* = 8.0 Hz), CH_3); ^{13}C NMR ($CDCl_3$, 600 MHz, PENDANT) δ (ppm): 166.9–164.9 (*C*═O), 135.7–134.8 (R_2*C*═CH_2), 128.2–126.4 (R_2C═*C*H_2), 92.3–92.1 (β anomer), 89.8–89.7 (α anomer), 76.1–68.2 (*C*H), 62.8–62.0 (*C*H_2), 18.2–18.0 (*C*H_3); IR υ (cm^{-1}) 1721 (C═O), 1637 (C═C), 1453 (CH_2/CH_3 bend), 1317 (CH_3 bend), 1292 (alkyl C—H), 1140 (C—O stretch); MS (ESI) *m*/*z*: 475.0 [M(4mer)+Na]$^+$ $C_{22}H_{28}O_{10}$, *m*/*z* 543.2 [M(5mer)+Na]$^+$ $C_{26}H_{32}O_{11}$; M_N^{SEC} (THF) = 448, M_W/M_N = 1.02.

2.3.4. D-Meth$_8$

^{1}H NMR ($CDCl_3$ 400 MHz) δ (ppm): 6.14 (8H, m, C═CH_2 *cis*), 5.55 (8H, m, C═CH_2 *trans*), 5.27–4.22 (14H, m, ring protons), 1.81 (15H, m, CH_3); IR υ (cm^{-1}): 1721 (C═O), 1637 (C═C), 1453 (CH_2/CH_3 bend), 1317 (CH_3 bend), 1292 (alkyl C—H), 1140 (C—O stretch); MS (ESI) *m*/*z*: 547 [Mtri+H] $^+$, 705 [Mpenta+Na]$^+$, 773 [Mhexa+Na]$^+$, 859 [Mhepta+Na]$^+$; M_N^{SEC}(THF) = 1300, M_W/M_N = 1.08.

2.3.5. E-Meth$_8$

^{1}H NMR ($CDCl_3$, 400 MHz) δ (ppm): 6.23–6.04 (8H, m, C═CH_2 *cis*), 5.75–5.54 (8H, m, C═CH_2 *trans*); 4.70–3.85 (14H, m, ring protons) 2.01–1.81 (24H, m, CH_3); ^{13}C NMR ($CDCl_3$, 600 MHz, PENDANT) δ (ppm): 167.2–165.1 (*C*═O), 135.8–134.7 (*C*═CH_2), 127.9–126.2 (C═*C*H_2), 101.8 (*C*H), 92.2 (β anomer), 82.2–81.8 (α anomer), 75.2–64.9 (*C*H), 63.2–62.1 (*C*H_2), 18.4–18.0 (*C*H_3); IR υ (cm^{-1}): 1721 (C═O ester), 1637 (C═C), 1453 (CH_2/CH_3 bend), 1317 (CH_3 bend), 1293 (C—H), 1140 (C—O stretch); MS (ESI) *m*/*z*: 637.2 [M(4mer)+Na]$^+$ $C_{28}H_{38}O_{15}$, *m*/*z* 705.2 [M(5mer)+Na]$^+$ $C_{32}H_{42}O_{16}$, *m*/*z* 773.2 [M(6mer)+Na]$^+$ $C_{36}H_{46}O_{17}$, *m*/*z* 841.3 [M(7mer)+Na]$^+$ $C_{40}H_{50}O_{18}$; M_N^{SEC} (THF) = 1170, M_W/M_N = 1.10.

2.3.6. F-Meth$_{11}$

^{1}H NMR ($CDCl_3$, 400 MHz), δ (ppm): 6.23 (11H, m, C═CH_2 *cis*), 5.82 (11H, m, C═CH_2 *trans*), 4.67–3.45 (20H, m, ring protons), 2.01 (33H, t (*J* = 8.0 Hz), CH_3); ^{13}C NMR ($CDCl_3$) 400 MHz, δ (ppm); 171.96 (*C*═O), 135.49 (*C*═CH_2), 127.43 (C═*C*H_2), 73.3 (*C*H), 53.23 (*C*H_2), 14.1 (*C*H_3); IR υ (cm^{-1}): 1721 (C═O ester), 1637 (C═C), 1453 (CH_2/CH_3 bend), 1317 (CH_3 bend), 1293 (alkyl C—H), 1140 (C—O stretch); MS (ESI) *m*/*z*: 951 [M(6mer)+K]$^+$, 1003 [M(7mer)+Na]$^+$, 1071 [M(8mer)+Na]$^+$, 1157 [M(9mer)+K]$^+$, 1225 [M(10mer)+K]$^+$, 1293 [M(11mer)+K]$^+$; M_N^{SEC} (THF) = 1600, M_W/M_N = 1.02.

2.3.7. G-Meth$_{11}$

^{1}H NMR ($CDCl_3$, 400 MHz) δ (ppm): 6.28–6.09 (11H, m, C═CH_2), 5.74–5.53 (11H, m, C═CH_2), 4.58–3.78 (16H, m, ring protons), 2.02–1.88 (33H, m, CH_3); ^{13}C NMR ($CDCl_3$, 600 MHz, PENDANT) δ (ppm): 167.6–165.7 (*C*═O), 136.0–134.9 (R_2*C*═CH_2), 128.5–126.1 (R_2C═*C*H_2), 99.5–89.5 (*C*H), 66.3–62.9 (*C*H_2), 18.4–18.0 (*C*H_3); IR υ (cm^{-1}): 1717 (C═O ester), 1636 (C═C), 1453 (CH_2/CH_3 bend), 1319 (CH_3 bend), 1295 (alkyl C—H), 1147 (C—O stretch); M_N^{SEC} (THF) = 1630, M_W/M_N = 1.04.

2.3.8. H-Meth$_{14}$

^{1}H NMR ($CDCl_3$, 400 MHz) δ (ppm): 6.28–6.05 (14H, m, C═CH_2 *cis*), 5.73–5.53 (14H, m, C═CH_2 *trans*), 5.24–4.08 (25H, m, ring protons), 2.01–1.81 (42H, m, CH_3); ^{13}C NMR ($CDCl_3$, 600 MHz, PENDANT) δ (ppm): 167.3–166.2 (*C*═O), 135.7–135.0 (R_2C═CH_2), 127.3–126.3 (R_2C═*C*H_2), 96.4–82.4 (*C*H), 68.0–64.9 (*C*H_2), 18.5–18.0 (*C*H_3); IR υ (cm^{-1}): 1715 (C═O ester), 1636 (C═C), 1454 (CH_2/CH_3 bend), 1318 (CH_3 bend), 1295 (alkyl C—H), 1146 (C—O stretch); M_N^{SEC}(THF) = 2312, M_W/M_N = 1.06.

2.4. General procedure for the Michael Addition of 2-(2-methoxyethoxy)ethanethiol to carbohydrate methacrylates

As a representative example methacrylated galactose (0.04 g, 33 μmoles) was dissolved in a mixture of ethanol and water (5:1 v/v, 3 mL) in a vial equipped with a suba seal, flushed with nitrogen and added dropwise under a flow of nitrogen to a nitrogen flushed solution of triethylamine (0.001 g, 10 μmoles) and 2-(2-methoxyethoxy)ethanethiol (0.5 g, 3.67 μmoles) in a mixture of ethanol and water (5:1, 3 mL) in a vial equipped with a suba seal and stir bar. The reaction was allowed to stir at room temperature for 12 h. The solution was then dialyzed using 1000 MWCO dialysis tubing and the product recovered by freeze drying.

2.4.1. A-DEG$_5$

^{1}H NMR ($CDCl_3$, 400 MHz) δ (ppm): 3.62 (24H, m, CH_2), 3.39 (15H, m, OCH_3), 2.90 (10H, m, SCH_2), 2.73 (10H, m, CHCH_2), 1.54 (7H, m, ring protons), 1.03 (15H, t (*J* = 8.0 Hz), CH_3); M_N^{SEC}(DMF) = 870, M_W/M_N = 1.08.

2.4.2. D-DEG$_8$

^{1}H NMR ($CDCl_3$) δ (ppm): 3.62 (64H, m, CH_2), 3.36 (24H, m, CH_2), 2.87 (16H, m, SCH_2), 2.71 (16H, m, CHCH_2), 1.55 (29H, m, ring protons), 1.03 (24H, m, CH_3); M_N^{SEC} (DMF) = 1240, M_W/M_N = 1.07.

2.4.3. E-DEG$_8$

^{1}H NMR ($CDCl_3$) δ (ppm): 3.59 (64H, m, CH_2), 3.36 (24H, m, CH_2), 2.86 (16H, m, SCH_2), 2.71 (16H, m, CHCH_2), 1.53 (29H, m, ring protons), 1.03 (24H, m, CH_3); M_N^{SEC} (DMF) = 1340, M_W/M_N = 1.07.

2.4.4. F-DEG$_{11}$

IR υ (cm^{-1}): 2962, 2956, 2875, 1735, 1600, 1463; M_N^{SEC} (DMF) = 1710, M_W/M_N = 1.04.

2.4.5. G-DEG$_{11}$

IR υ (cm^{-1}): 2954, 2929, 2866, 1734, 1597, 1454; M_N^{SEC} (DMF) = 2714, M_W/M_N = 1.03.

2.5. General procedure for the synthesis of galactosylated carbohydrates

Methacrylated raffinose (0.032 g, 24.7 μmol), β-D-thiogalactose sodium salt (0.06 g, 0.27 mmoles), benzylamine (0.01 mL, 9.1 μmoles) and tributyl phosphine (0.01 mL, 40 μmoles) were dissolved in a mixture of ethanol and water (1:1, 5 mL) before being stirred at 45 °C for 72 h at room temperature. Ethanol was removed *en vacuo* and the remaining solution dialyzed before the water was removed by freeze drying to yield a yellow sticky solid.

2.5.1. A-Gal$_5$

^{1}H NMR ($CDCl_3$, 400 MHz) δ (ppm): 3.88–3.48 (36H, m, ring protons), 3.36 (10H, m, S—CH_2), 3.21 (5H, m, C*H*), 2.11 (15H, t (*J* = 8.0 Hz), CH_3); ^{13}C NMR ($CDCl_3$ 500 MHz) δ (ppm): 215.3 (*C*═O), 120.3 (*C*H_2OH), 86.1 (*C*H), 84.0 (*C*H_2); M_N^{SEC}(DMF) = 1640, M_W/M_N = 1.03.

2.5.2. E-Gal$_8$

^{1}H NMR (D_2O, 400 MHz) δ (ppm): 3.91–2.65 (60H, m, ring protons), 3.14–3.10 (8H, m, C*H*), 1.84 (16H, d (*J* = 8.0 Hz), S—CH_2), 1.10 (24H, m, CH_3). ^{13}C NMR ($CDCl_3$, 500 MHz) δ (ppm): 184.3 (*C*═O), 120.2 (*C*H_2) 102.6 (α*C*H—C═O), 102.5(β*C*H—C═O), 96.0 (α*C*H—S), 91.9 (β*C*H—S) 86.4–86.9 (ring carbons), 60.8 (*C*H_2), 43.7 (*C*H), 34.3 (*C*H_2OH), 17.4 (*C*H_3); M_N^{SEC}(DMF) = 1940, M_W/M_N = 1.01.

2.5.3. G-Gal$_{11}$

^{1}H NMR (D_2O 400 MHz) δ (ppm): 4.27 (11H, m, C*H*C═O), 3.87 (11H, m, C*H*S), 3.72–3.34 (84H, m, ring protons), 3.50 (22H, m, SCH_2), 3.14–3.10 (11H, m, C*H*), 1.20 (33H, d (*J* = 8.0 Hz), CH_3); ^{13}C NMR ($CDCl_3$ 500 MHz) δ (ppm): 215.4 (*C*═O), 120.2 (*C*H_2) 102.6 (α*C*H—C═O), 102.5(β*C*H—C═O), 84.8–68.7 (ring carbons), 61.1 (*C*H_2), 46.7 (*C*H), 30.2 (*C*H_2OH), 11.5 (*C*H_3); M_N^{SEC}(DMF) = 3420, M_W/M_N = 1.01.

2.6. Degradation assay

Raffinose DEG (5 mg, 2 μmoles) was dissolved in sodium hydroxide solution (3 mL, 1M) in a stoppered vial and left for 5 days. The solution was then freeze dried and the residue taken up in DMF (2 mL), the insoluble parts filtered and the filtrate analyzed by size exclusion chromatography. The solvent was then removed *en vacuo* leaving a yellow viscous oil, which was analyzed by infrared spectroscopy.

2.7. Fluorescence-linked sorbent assay for inhibitory activity

Peanut Agglutinin (PNA) 96-well microtiter plates were incubated for 16 h with 150 μL of 100 μg mL^{-1} GM1 in PBS. Unbound GM1 was removed by washing extensively with water. 150 μL BSA solution (1% w/w) was added and incubated for 10 min, then unbound BSA was removed by washing extensively with water. Galactosylated carbohydrate solutions were made up as serial dilutions (up to 10 dilutions per sample from 0.1 mg mL^{-1} in water from a stock solution of 1 mg mL^{-1} in DMSO). 10 μL of 100 μg mL^{-1} PNA-FITC in 10 mM HEPES with 0.15M NaCl, 0.1 mM $CaCl_2$ and 0.01 mM Mn^{2+}(pH 7.5) was added to 90 μL of polymer solution to a final concentration of 11 μg mL^{-1}. 100 μL of the PNA/galactosylated carbohydrate solutions were then added to GM1 coated wells and incubated at 37 °C for 30 min. After this the wells were extensively washed with water and fluorescence was measured at excitation/emission wavelengths of 485/528 nm. All experiments were carried out in triplicate. Percentage inhibition was compared to relative to controls of pure PNA-FITC (with no galactosylated carbohydrate).

Cholera toxin B sub unit (CTxB) 96-well microtitre plates were incubated for 16 h with 150 μL of 100 μg mL^{-1} GM1 in PBS. Unbound GM1 was removed by washing extensively with water. 150 μL BSA solution (1% w/w) was added and incubated for 10 min, then unbound BSA was removed by washing extensively with water. Galactosylated polymer solutions were made up as serial dilutions (up to 10 dilutions per sample from either 0.1 mg mL^{-1} in water). 10 μL of 100 μg mL^{-1} CTxB in 10 mM Tris with 0.1 mM $CaCl_2$ and 0.5 mM NaCl (pH 8) was added to 90 μL of polymer solution to a final concentration of 11 μg mL^{-1}. 100 μL of the CTxB/galactosylated carbohydrate solutions was then added to GM1 coated wells and incubated at 37 °C for 30 min. After this the wells were extensively washed with water and fluorescence was measured at excitation/emission wavelengths of 485/528 nm. All experiments were carried out in triplicate. Percentage inhibition was compared to relative to controls of pure CTxB (with no galactosylated carbohydrate).

3. Results and discussion

Due to their monodisperse, but highly multifunctional nature, carbohydrates were identified as the ideal templates for monodisperse polymers. In order to exploit these we envisioned converting the hydroxyl groups into a (bio)orthogonal functionality which enables subsequent modification. Methacrylic anhydride was chosen for this as it is a cheap and readily available reagent and will install a conjugated alkene that is suitable for subsequent Michael Addition (often termed 'thiol-ene click'), which is a highly orthogonal and efficient reaction. Wagner and co-workers have previously reported the synthesis of methacrylated sugars using triethylamine as the base [44]. Initial screening found that the optimal conditions for the reaction were pyridine as the solvent followed by addition of methacrylic anhydride at 60 °C. Following the esterification reaction, the methacrylated oligosaccharides were isolated by washing between organic/aqueous layers, without the need for chromatography. Using this methodology a library of eight different (oligo)saccharides was functionalized covering monosaccharides to tetrasaccharides, Fig. 1.

SEC (size exclusion chromatography) analysis of the methacrylated sugars revealed monodisperse distributions with dispersity values between 1.02 and 1.10 which is comparable to (or indeed significantly better) than commercially available dendrimers and superior to most controlled radical polymerizations, especially at this relatively low molecular weight range, Fig. 2. The low molecular weight shoulders at high elution volumes are due to these oligomers being at the limit for SEC chromatography. Due to their branched structure and rigid backbones, the SEC elution behavior of the polymers was different to that of the poly(methylmethacrylate) (PMMA) standards used. However, the exact mass of the polymers can be calculated from the starting mass of the template sugar. This is a significant advantage of this method, in that there is no additional heterogeneity (unlike in controlled radical polymerization) along with reproducibility, as molecularly-identical cores can be utilized (see Tables 1 and 2).

Infrared (IR) analysis confirmed complete removal of the hydroxyl groups, by the disappearance of the O—H stretch at 3500 cm^{-1}, and also the appearance of (non-equivalent) carbonyl stretches between 1600 and 1800 cm^{-1}. ^1H NMR spectroscopy also confirmed the installation of the methacrylate groups with >90% efficiency. With these versatile, yet monodisperse, scaffolds at hand we were motivated to exploit thiol-ene chemistry to generate interesting and useful biomaterials, which is exemplified in two different biologically relevant applications, below.

3.1. Thermoresponsive biomaterials

We, and others, have demonstrated the utility of thermoresponsive polymers that can undergo externally triggered cellular interactions upon application of a stimulus

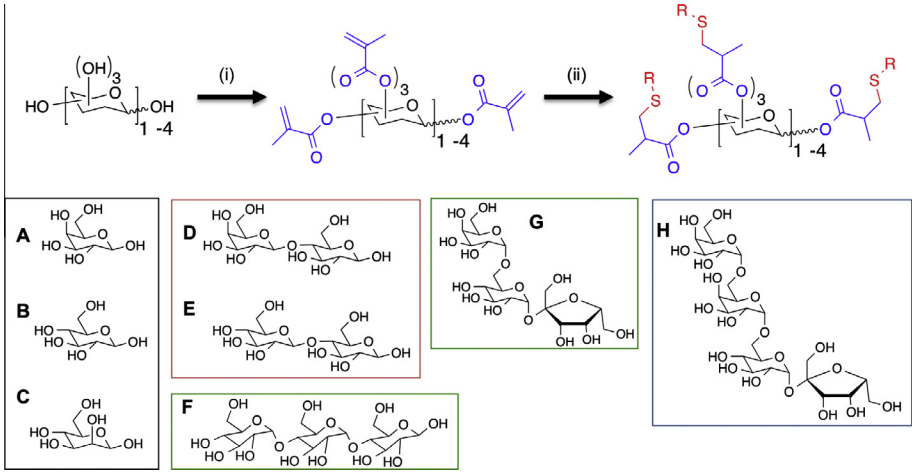

Fig. 1. General reaction scheme for the methacrylation and subsequent thiol Michael Addition functionalization and summary of carbohydrates used in this study as templates. Colored boxes indicate oligosaccharides with identical valency (equivalent to degree of polymerization). (i) Methacylic anhydride/pyridine/60 °C. (ii) R-SH (5 equivalents) in ethanol/water mixtures. Carbohydrates: A = Galactose; B = Glucose; C = Mannose; D = Lactose; E = Cellobiose; F = Maltotriose; G = Raffinose; H = Stachyose. Anomeric stereochemistry of reducing termini are not defined. (For interpretation of the references to colour in this figure legend, the reader is referred to the web version of this article.)

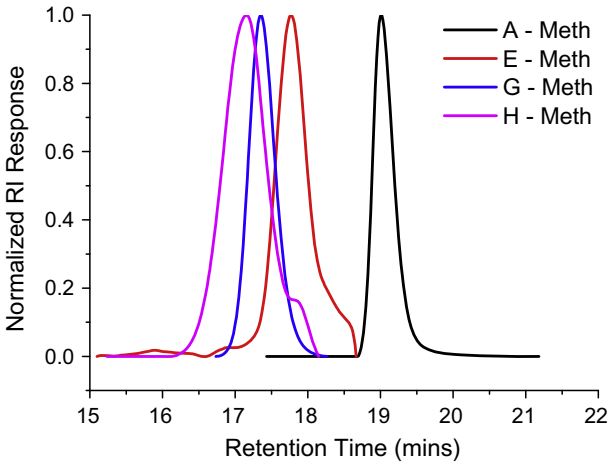

Fig. 2. SEC ($CHCl_3$) of methacrylated oligosaccharides.

Table 1
Characterization of methacrylated oligosaccharides.

Core	M_N (Theo)[a] (g mol^{-1})	M_N (SEC)[b] (g mol^{-1})	M_W/M_N[b] (–)	Product
A	520	460	1.03	**A-Meth$_5$**
B	520	430	1.02	**B-Meth$_5$**
C	520	450	1.02	**C-Meth$_5$**
D	886	1300	1.08	**D-Meth$_8$**
E	886	1200	1.1	**E-Meth$_8$**
F	1236	1600	1.02	**F-Meth$_{11}$**
G	1236	1800	1.04	**G-Meth$_{11}$**
H	1618	2300	1.06	**H-Meth$_{14}$**

[a] Theoretical number average degree of polymerization assuming 100% functionalization of the carbohydrate core. Numbers not rounded as these are theoretical value for 'perfect' cores.
[b] Number average degree of polymerization determined by SEC in THF against poly(styrene) standards.

Table 2
Characterization of DEG hybrid polymers by SEC.

Core	M_N (Theo)[a] (g mol^{-1})	M_N (SEC)[b] (g mol^{-1})	M_W/M_N[b] (–)	Product
A-Meth$_5$	1201	870	1.08	**A-DEG$_5$**
D-Meth$_8$	1976	1240	1.07	**D-DEG$_8$**
E-Meth$_8$	1976	1340	1.07	**E-DEG$_8$**
F-Meth$_{11}$	2751	1710	1.04	**F-DEG$_{11}$**
G-Meth$_{11}$	2751	2710	1.03	**G-DEG$_{11}$**

[a] Theoretical number average degree of polymerization assuming 100% functionalization of the carbohydrate core.
[b] Number average degree of polymerization determined by SEC, undertaken in DMF relative to poly(styrene) standards.

[45,46]. To synthesize carbohydrate-centered mimics of one of the most commonly used thermoresponsive vinyl-based polymers, poly(oligoethyleneglycol methacrylate) (POEGMA), thiolyated diethyleneglycol (DEG-SH) was conjugated to the methacrylated sugars. Using a two-fold excess of the DEG-SH and benzyl amine as the catalyst, four different carbohydrate cores were functionalized in a simple one-step procedure, Scheme 1. SEC analysis showed a clear increase in the observed molecular weight and retention of the narrow, monomodal distributions with dispersity values below 1.08. ^{1}H NMR spectroscopy indicated quantitative conversion after 12–15 h with no residual vinyl peaks detectable.

With these carbohydrate-based polymers in hand their utility as alternatives to poly(diethyleneglycolmethacrylate), PDEGMA, was investigated. Previous studies have demonstrated that degree of polymerization is a critical parameter in fine-tuning the observed transition temperatures of thermoresponsive polymers. The carbohydrate-centered polymers synthesized here have discrete molecular weights, and hence the importance of the precise number of responsive side chains on their cloud points (a macroscopic observation distinct from LCST, which is a single point on the phase diagram) was measured and compared to P(DEGMA) (DP = 50) prepared by conventional RAFT polymerization, Fig. 3. **A-DEG$_5$**, with only five DEG chains, had a cloud point of 50 °C, which decreased to 37 °C upon increasing the number of side-chains to eight (**D-DEG$_8$**), at fixed concentration. Increasing to eleven side chains (**E-DEG$_{11}$**) lead to a significant decrease in the cloud point to 18 °C, which is similar to what is observed for PDEGMA. This large decrease in cloud point upon addition of just three additional DEG chains could not have been determined by conventional CRP methods, which lack this level of precision. Concentration-dependent cloud point measurements of **E-DEG$_{11}$** (Fig. 3D) revealed a strong correlation. The cloud point increased to 40 °C from 18 °C upon dilution from 5 to 0.6 mg mL^{-1}, indicating that these materials can undergo transitions at physiologically relevant concentrations and temperatures. It should be noted that in the relatively dilute concentration range (<5 mg mL^{-1}) all thermoresponsive polymers show a strong concentration dependence and is not unique to this class [47,48]. Due to the degradable nature of these polymers (*vide infra*), they are ideal alternatives to the more commonly used poly(N-isopropyl acrylamide) and POEGMA, which require radical/ionic polymerization methods and are essentially non-biodegradable and hence limited in terms of their biological applications. Such low molecular weight responsive

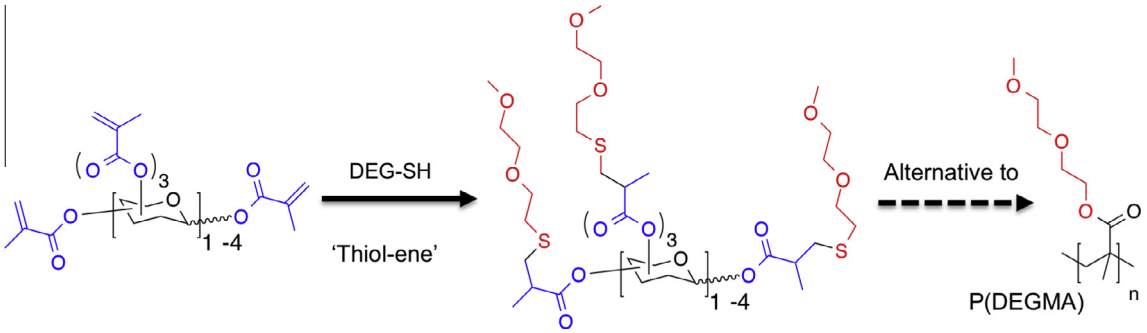

Scheme 1. Synthesis of thermoresponsive carbohydrate-centered polymers and comparison to poly(diethyleneglycol methacrylate).

polymers have also been shown to be useful to construct larger nanostructures through non-covalent nanoprecipitation above their LCST [49].

3.2. Glycosylated clusters as specific bacterial toxin inhibitors

Diethylene glycol was an interesting example of the utility of this synthetic method, but did not provide a challenge in terms of functional group tolerance. Therefore, a second class of functional biomaterial was targeted: glycopolymers with pendant carbohydrate groups, which can function as synthetic mimics of natural glycans/glycoproteins [22,50]. In addition to having multiple hydroxyl functional groups, carbohydrates are more sterically hindered than DEG-SH and hence provide a sterner challenge. 1-deoxy-1-thio-β-D-galactose (Gal-SH) was chosen as the carbohydrate to install on the carbohydrate scaffold, Scheme 2. We have demonstrated the application of

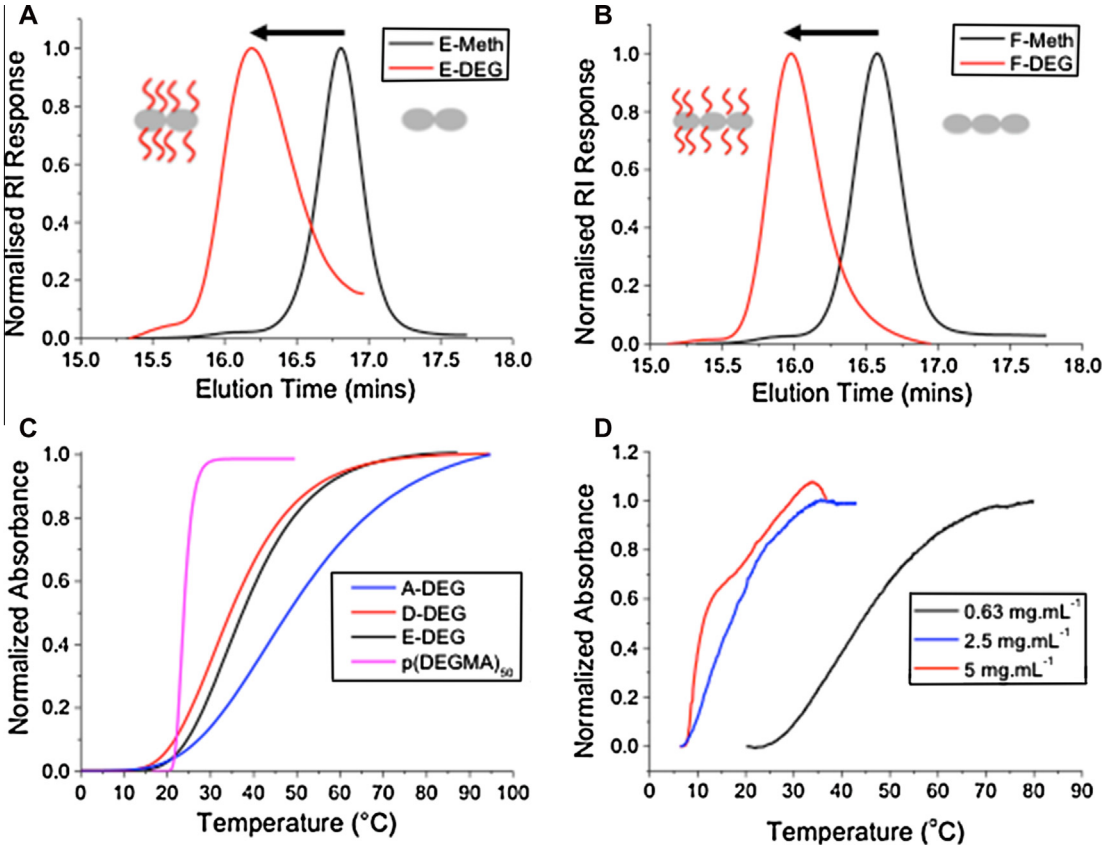

Fig. 3. Thermoresponsive carbohydrate-centered polymers. (A and B) show SEC analysis of thiol-ene click product of methacrylated sugars with DEG-SH showing clear increase in M_N but no change in dispersity. (C) Turbidimetry analysis of DEG-functional carbohydrates. Conditions, 12 mg mL^{-1}, PBS; (D) Turbidimetry analysis as a function of concentration for **G-DEG$_{11}$** in PBS.

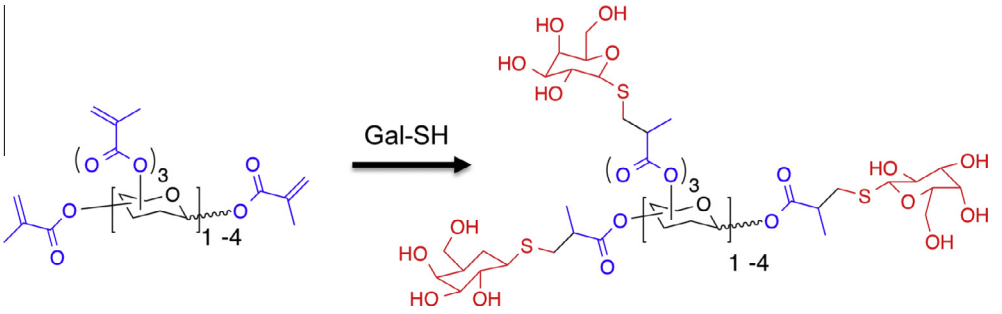

Scheme 2. Synthesis of galactosylated carbohydrate-centered polymers.

Table 3
Characterization of galactose conjugated hybrid polymers.

Core	M_N (Theo)[a] (g mol^{-1})	M_N (SEC)[b] (g mol^{-1})	M_W/M_N[b] (–)	Product
A-Meth$_5$	1500	1640	1.03	**A-Gal$_5$**
E-Meth$_8$	2454	1930	1.01	**E-Gal$_8$**
G-Meth$_{11}$	3197	3400	1.01	**G-Gal$_{11}$**
H-Meth$_{14}$	4363	3480	1.01	**H-Gal$_{14}$**

[a] Theoretical number average degree of polymerization assuming 100% functionalization of the carbohydrate core.
[b] Number average degree of polymerization determined by SEC in DMF against PMMA standards.

galacto-functional polymers as inhibitors of bacterial infection, and hence a bimolecular, degradable alternative to vinyl-based polymers could be of real practical use [33].

Initial attempts at the Michael Addition reaction of the Gal-SH onto **A-Meth$_5$** lead to low (<20%) conversion of the vinyl groups to thioethers. This was speculated to be due to a combination of disulfide formation between two Gal-SH molecules and the relative steric constraints imposed by placing several carbohydrates on a rigid scaffold that cannot reconfigure to reduce steric repulsions. This was also confirmed by SEC analysis (Supp. Info.), which showed significant broadening of the molecular weight distribution. This low conversion was overcome by the addition of a small amount of benzyl amine as catalyst, tributyl phosphine as an *in situ* reducing agent and heating the reaction mixture to 45 °C for 72 h. Under these conditions quantitative conversion of the vinyl groups was observed and monomodal distributions with dispersities below 1.03 were obtained, Table 3. Due to their branched structure, the molecular weight values obtained relative to linear standards underestimated the M_N, as is commonly seen for dendrimers or star-branched polymers.

The polymers in Table 3 represent an interesting set of glycopolymers which display a discrete number of carbohydrates. Using traditional (controlled) polymer chemistry it is challenging to precisely predict and control the degree of polymerization and dispersity. This is crucial in glycoscience, as small changes in valency lead to significant increases in avidity, and therefore even small fractions of higher (or lower) molecular weight fractions can significantly alter the observed binding affinity and preclude detailed structure activity relationships from being elucidated. To test the use of the glycopolymers, two different galactose binding lectins were chosen; Peanut Agglutinin (PNA) and the Cholera Toxin B-subunit (CTxB). Both these lectins have affinity for β-galactose, but differ in their exact

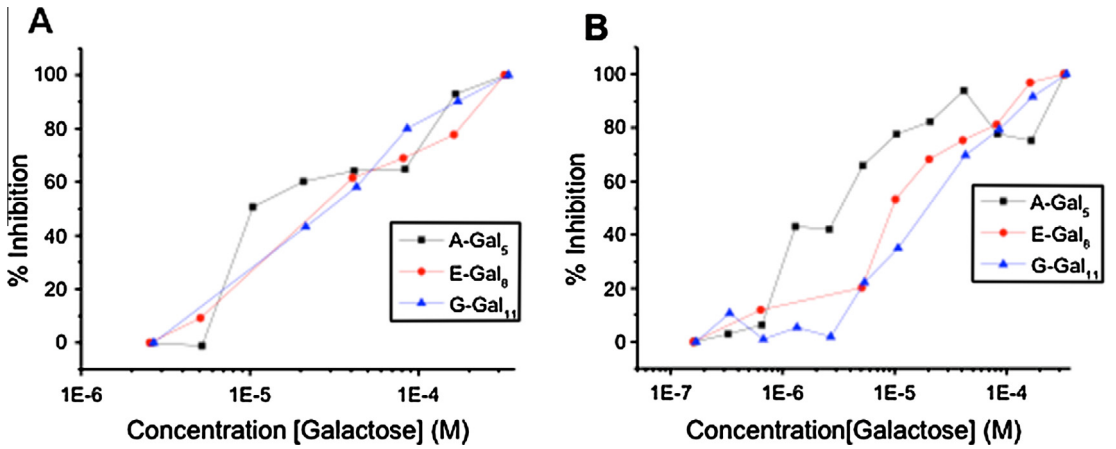

Fig. 4. Inhibition of lectin binding onto GM-1 functional surfaces by glycopolymers (in Table 3), determined by a fluorescence-linked sorbent assay. (A) PNA inhibition; (B) CTxB inhibition. Concentration is expressed in terms of total galactose concentration (not polymer concentration) to enable multivalent effects to be probed.

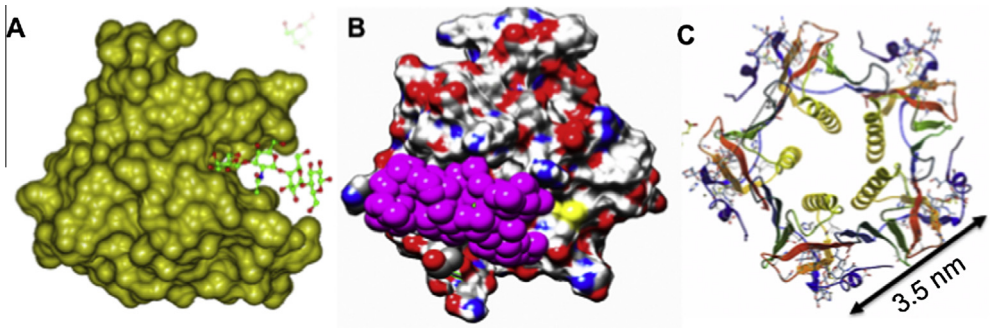

Fig. 5. Schematic showing CTxB binding domains. (A) Single binding site of CTxB with native ligand (GM-1) bound to show deep binding site; (B) Simulation of CTxB with **A-Gal$_5$** (pink) bound; (C) Crystal structure of CTxB showing distance between adjacent binding sites. Crystal structures obtained from the protein data bank [53]. (For interpretation of the references to colour in this figure legend, the reader is referred to the web version of this article.)

glycan specificity in line with their individual biological functions. The selective targeting and neutralization of pathogenic lectins (including CTxB) is particularly attractive for the development of prophylactic anti-adhesion therapies or non-antibody based diagnostics. To probe the binding affinity of the polymers to the lectins, a modified fluorescence-linked sorbent assay was used, as previously described [33]. Briefly, this assay probes the ability of the polymers to inhibit the lectins from binding a surface functionalized with galactose, by measuring lectin adhesion with fluorescence spectrometry. The three shortest polymers were selected to be evaluated for their inhibitory properties due to the amount isolated after purification and as these represent a set which would challenging to access by a traditional polymerization process (e.g. CRP). The results of this assay against PNA (A) and CTxB (B) are shown in Fig. 4.

As expected, all the polymers were capable of inhibiting the binding of the lectin to the surface at concentrations below 0.1 mg mL^{-1} (<0.1 mM Gal). This is significantly more active than free galactose, which only weakly inhibits the lectin binding (<20% inhibition at 5 mg mL^{-1}/25 mM)

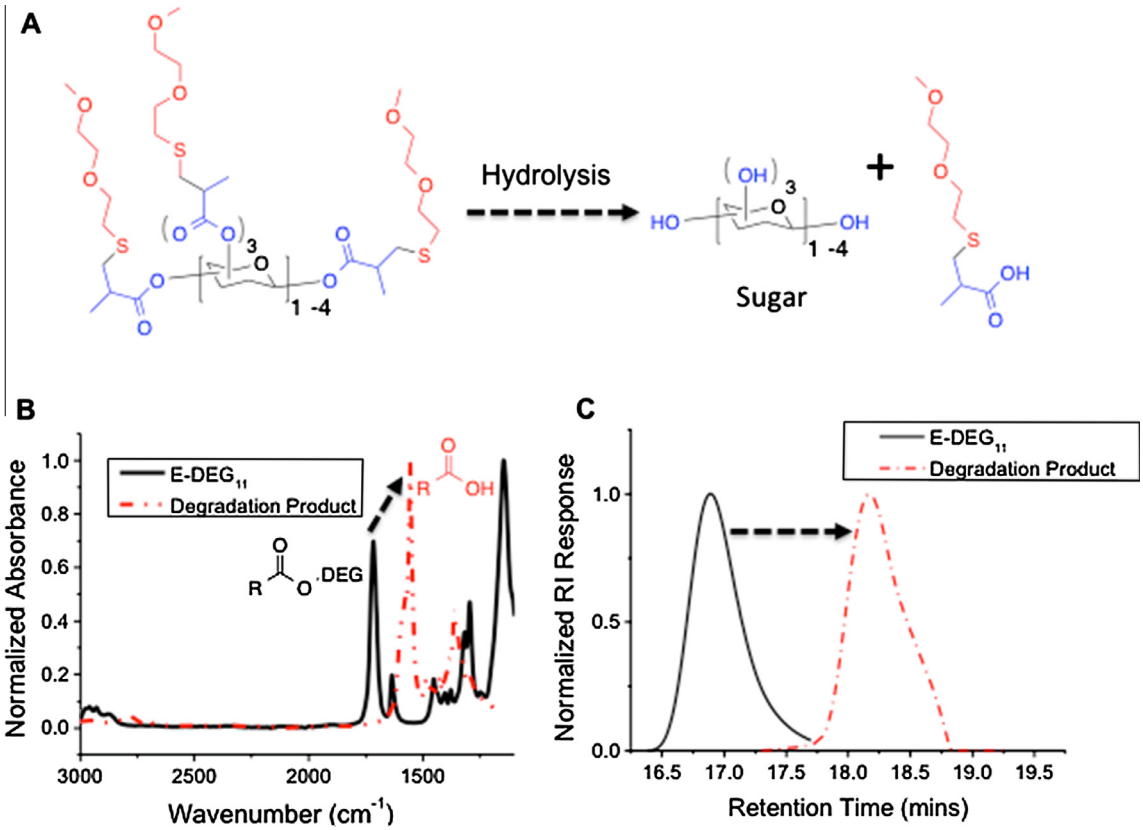

Fig. 6. Hydrolytic degradation of **G-DEG$_{11}$.** (A) Schematic of process assuming the carbohydrate core is released (omitting subsequent degradation processes); (B) Infrared analysis of hydrolysis product; (C) SEC analysis of hydrolysis (following isolation and dissolution in DMF).

demonstrating that these oligomers show significant cluster glycoside-linked affinity enhancement and that high molecular weight polymers are not always required. Pentameric GM-1 presenting multivalent scaffolds have been shown as the strongest CTx inhibitors yet reported [51], supporting this observation that very large valencies are not essential. Against PNA, all polymers showed essentially identical affinity on a per-carbohydrate basis, with a slight decrease in MIC_{50} (minimum concentration required to inhibit lectin binding by 50%) as the valency increases. Conversely, analysis of CTxB inhibition suggested that the smallest cluster (**A-Gal$_5$**) had higher activity than the larger versions. It should be noted that while the differences were relatively small compared to our previous studies on differential lectin binding by glycopolymers [33], it highlights the value of having precise control over the number of displayed binding ligands. The apparent lack of cluster glycoside enhancement with molecular weight is hypothesized to be due to the increased steric constraints of the larger, rigid polymers preventing access into the relatively deep binding pocket of CTxB (Fig. 5A) during statistical rebinding. These polymers are also too small to be able to span multiple binding sites which are approximately 3.5 nm apart in CTxB, Fig. 5C. Fig. 5B shows a simple model of **A-Gal$_5$** binding to a single unit of CTxB, to highlight the steric constraints imposed by a non-flexible scaffold. Accessibility has previously been shown by Gibson et al., and Kiick et al. to significantly affect glycopolymer-CTxB interactions [33,52]. As none of the polymers used here were sufficiently long to span multiple binding sites on the proteins the enhancement in affinity relative to free-galactose is likely due to statistical rebinding or cross-linking of multiple lectins by individual polymers, but more detailed studies are required to see if this is a significant effect. Nonetheless it does highlight that techniques which enable sequential control over valency may provide structural insight not available from even the best controlled radical polymerizations.

3.3. Polymer degradation

The polymers derived from the methacrylated carbohydrate cores all contain an ester linkage between side chain and carbohydrate, which should be prone to hydrolytic degradation in a similar manner to linear poly(esters), which find extensive use in biomedical applications. Rather than main chain scission, the mode of degradation here would be removal of the side chains; (Fig. 6A) which would release an oligosaccharide side product which itself can be degraded (or metabolized/excreted) by native glycosidases. As a proof-of-principle experiment, **G-DEG$_{11}$** was incubated in basic NaOH solution for 5 days and subsequently analyzed by SEC and IR. IR showed the hydrolysis of esters to carboxylic acids by the shift in the carbonyl stretch from 1750 cm^{-1} to 1600 cm^{-1}, Fig. 6B. Fig. 6C shows the reduction in molecular weight of the polymer by SEC after hydrolysis, giving a single peak at longer retention times (after filtration to remove any insoluble materials generated by degradation). No starting material was detected, indicating complete hydrolysis to the constituent and benign carbohydrate and DEG unit.

4. Conclusions

In this work we have demonstrated that simple and widely available oligosaccharides can be used as the cores to template the synthesis of monodisperse and highly functional biomaterials. The oligosaccharides were efficiently functionalized with methacrylate groups by a standard esterification procedure to generate the scaffolds with latent and orthogonal units for subsequent conjugation. These methacrylated scaffolds were monodisperse, and always give identical molecular weights on each synthesis, which is not possible with controlled radical polymerization methods. Addition of diethylene glycol units afforded thermo-responsive polymers and the impact of chain length on transition temperature was studied, enabling selection of polymers displaying responses in physiologically relevant ranges. It was discovered that increasing from five to eight diethylene glycol units caused significant shifts in the thermoresponsive behavior, which could not have been observed with controlled-radical derived polymers. Secondly, galactose units were incorporated onto the polymers to create monodisperse multivalent glycopolymers. The interaction of these glycopolymers, as a function of galactose valency against bacterial toxins and a plant lectin, were investigated. It was found that the larger glycopolymers do not show cluster glycoside enhancement against the cholera toxin, but do against peanut agglutinin. Finally, the polymers were shown to be hydrolytically degradable, indicating their potential application as functional, but reproducible biomaterials which may offer a simple and cheaper, but just as versatile alternative to classical dendrimers or radical-derived vinyl polymers.

Acknowledgements

Equipment used was supported by the Innovative Uses for Advanced Materials in the Modern World (AM2), with support from Advantage West Midlands (AWM) and part funded by the European Regional Development Fund (ERDF). MIG was a Birmingham Science City Interdisciplinary Research Fellow funded by the Higher Education Funding Council for England (HEFCE). This work was supported by a Research Project Grant from the Leverhulme Trust (RPG-144) and a Research Grant from the Royal Society. The ERASMUS scheme is acknowledged for funding C.W. and J.W.

Appendix A. Supplementary material

Supplementary data associated with this article can be found, in the online version, at http://dx.doi.org/10.1016/j.eurpolymj.2014.06.001.

References

[1] Pounder RJ, Dove AP. Polym Chem 2010;1:260–71.
[2] van der Ende AE, Sathiyakumar V, Diaz R, Hallahan DE, Harth E. Polym Chem 2010;1:93–6.
[3] Elsabahy M, Wooley KL. Chem Soc Rev 2012;41:2545–61.
[4] Freese C, Uboldi C, Gibson M, Unger R, Weksler B, Romero I, et al. Particle Fibre Toxicol 2012;9:23.

[5] Yang F, Cho S-W, Son SM, Bogatyrev SR, Singh D, Green JJ, et al. Proc Nat Acad Sci 2010;107:3317–22.
[6] Rodríguez-Lorenzo L, de la Rica R, Álvarez-Puebla RA, Liz-Marzán LM, Stevens MM. Nat Mater 2012;11:604–7.
[7] He P, Tang Z, Lin L, Deng M, Pang X, Zhuang X, et al. Macromol Biosci 2012;12:547–56.
[8] Gibson MI. Polym Chem 2010;1:1141–52.
[9] Duncan R. Nat Rev Drug Discov 2003;2:347–59.
[10] Gil ES, Hudson SM. Prog Polym Sci 2004;29:1173–222.
[11] Saeed AO, Magnusson JP, Moradi E, Soliman M, Wang W, Stolnik S, et al. Bioconj Chem 2011;22:156–68.
[12] Phillips DJ, Gibson MI. Chem Commun 2012;48:1054–6.
[13] Phillips DJ, Gibson MI. Biomacromolecules 2012;13:3200–8.
[14] Jochum FD, Theato P. Chem Soc Rev 2013;42:7468–83.
[15] Zelzer M, Todd SJ, Hirst AR, McDonald TO, Ulijn RV. Biomater Sci 2013;1:11–39.
[16] Salmaso S, Caliceti P, Amendola V, Meneghetti M, Magnusson JP, Pasparakis G, et al. J Mater Chem 2009;19:1608–15.
[17] Meyer DE, Shin BC, Kong GA, Dewhirst MW, Chilkoti A. J Control Rel 2001;74:213–24.
[18] Chang C-W, Nguyen TH, Maynard HD. Macromol Rapid Commun 2010;31:1691–5.
[19] Guvendiren M, Burdick JA. Curr Opin Biotech 2013;24:841–6.
[20] Singha NK, Gibson MI, Koiry BP, Danial M, Klok H-A. Biomacromolecules 2011;12:2908–13.
[21] Wilks TR, Bath J, de Vries JW, Raymond JE, Herrmann A, Turberfield AJ, et al. ACS Nano 2013;7:8561–72.
[22] Spain SG, Gibson MI, Cameron NR. J Polym Sci Part A: Polym Chem 2007;45:2059–72.
[23] Braunecker WA, Matyjaszewski K. Prog Polym Sci 2007;32:93–146.
[24] Boyer C, Bulmus V, Davis TP, Ladmiral V, Liu J, Perrier S. Chem Rev 2009;109:5402–36.
[25] Agarwal S. Polym Chem 2010;1:953–64.
[26] Gibson MI, Cameron NR. J Polym Sci A: Polym Chem 2009;47:2882–91.
[27] Gauthier MA, Gibson MI, Klok H-A. Angew Chem Int Ed 2009;48:48–58.
[28] Percec V, Guliashvili T, Ladislaw JS, Wistrand A, Stjerndahl A, Sienkowska MJ, et al. J Am Chem Soc 2006;128:14156–65.
[29] Lee YC, Townsend RR, Hardy MR, Lonngren J, Arnarp J, Haraldsson M, et al. J Biol Chem 1983;258:199–202.
[30] Kitov PI, Sadowska JM, Mulvey G, Armstrong GD, Ling H, Pannu NS, et al. Nature 2000;403:669–72.
[31] Garcia-Hartjes J, Bernardi S, Weijers CAGM, Wennekes T, Gilbert M, Sansone F, et al. Org Biomol Chem 2013;11:4340–9.
[32] Pieters RJ. Med Res Rev 2007;27:796–816.
[33] Richards S-J, Jones MW, Hunaban M, Haddleton DM, Gibson MI. Angew Chem Int Ed 2012;51:7812–6.
[34] Menjoge AR, Kannan RM, Tomalia DA. Drug Disc Today 2010;15:171–85.
[35] Malmstroem E, Johansson M, Hult A. Macromolecules 1995;28:1698–703.
[36] van Dongen MA, Desai A, Orr BG, Baker Jr JR, Banaszak Holl MM. Polymer 2013;54:4126–33.
[37] Kleiner RE, Brudno Y, Birnbaum ME, Liu DR. J Am Chem Soc 2008;130:4646–59.
[38] McHale R, Patterson JP, Zetterlund PB, O'Reilly RK. Nat Chem 2012;4:491–7.
[39] Lewandowski B, De Bo G, Ward JW, Papmeyer M, Kuschel S, Aldegunde MJ, et al. Science 2013;339:189–93.
[40] Lutz J-F, Ouchi M, Liu DR, Sawamoto M. Science 2013. http://dx.doi.org/10.1126/science.1238149.
[41] Dubber M, Lindhorst TK. Carbohydr Res 1998;310:35–41.
[42] Dubber M, Lindhorst TK. Org Lett 2001;3:4019–22.
[43] Gao Y, Eguchi A, Kakehi K, Lee YC. Bioorg Med Chem 2005;13:6151–7.
[44] Zandanel C, Mioskowski C, Baati R, Wagner A. Tetrahedron 2009;65:9395–402.
[45] Akimoto J, Nakayama M, Sakai K, Okano T. Mol Pharm 2010;7:926–35.
[46] Saaka Y, Deller RC, Rodger A, Gibson MI. Macromol Rapid Commun 2012;33:779–84.
[47] Bebis K, Jones MW, Haddleton DM, Gibson MI. Polym Chem 2011;2:975–82.
[48] Fujishige S, Kubota K, Ando I. J Phys Chem 1989;93:3311–3.
[49] Phillips DJ, Patterson J, O'Reilly RK, Gibson MI. Polym Chem 2014;5:126–31.
[50] Congdon T, Notman R, Gibson MI. Biomacromolecules 2013;14:1578–86.
[51] Mattarella M, Garcia-Hartjes J, Wennekes T, Zuilhof H, Siegel JS. Org Biomol Chem 2013;11:4333–9.
[52] Polizzotti BD, Maheshwari R, Vinkenborg J, Kiick KL. Macromolecules 2007;40:7103–10.
[53] Merritt EA, Kuhn P, Safaty S, Erbe JL, Holmes RK, Hol WG. J Mol Biol 1998;282:1043–59.